GALLIUM – CURCUMIN NANOPARTICLE CONJUGATE: A POTENT ALTERNATIVE TO ANTIBIOTICS AGAINST *PSEUDOMONAS* INFECTION

Gopika Ramesh

Ph.D. THESIS

2024

SREE CHITRA TIRUNAL INSTITUTE FOR MEDICAL SCIENCES AND TECHNOLOGY,

TRIVANDRUM

An Institution of National Importance established by an Act of the Indian Parliament (Act No.52 of 1980)
Dept. of Science and Technology, Govt. of India
www.sctimst.ac.in

GALLIUM – CURCUMIN NANOPARTICLE CONJUGATE: A POTENT ALTERNATIVE TO ANTIBIOTICS AGAINST *PSEUDOMONAS* INFECTION

A THESIS PRESENTED BY

GOPIKA RAMESH

TO

SREE CHITRA TIRUNAL INSTITUTE FOR

MEDICAL SCIENCES AND TECHNOLOGY

THIRUVANANTHAPURAM

INDIA

IN PARTIAL FULFILMENT OF THE

REQUIREMENTS FOR THE AWARD OF

DOCTOR OF PHILOSOPHY

2024

DECLARATION

I, **Gopika Ramesh**, hereby certify that I had personally carried out the work depicted in the thesis entitled, **"Gallium-Curcumin nanoparticle conjugate: A potent alternative to antibiotics against *Pseudomonas* infection",** except where due acknowledgment has been made in the text. No part of the thesis has been submitted for the award of any other degree or diploma before this date.

Thiruvananthapuram
Date: 23/4/2024

Gopika Ramesh
Reg no: 2017/PhD/03

Dr. Roy Joseph
Scientist 'G' (Senior Grade)
Division of Polymeric Medical Devices
Department of Medical Devices Engineering,
Biomedical Technology Wing, SCTIMST,
Poojappura -695012, Thiruvananthapuram, Kerala, India.
Email: rjoseph@sctimst.ac.in

This is to certify that **Ms. Gopika Ramesh,** in the Division of Polymeric Medical Devices/Department of Medical Devices Engineering, of this Institute has fulfilled the requirements prescribed for the PhD degree of the Sree Chitra Tirunal Institute for Medical Sciences and Technology, Thiruvananthapuram. The thesis entitled, **"Gallium-Curcumin nanoparticle conjugate: A potent alternative to antibiotics against *Pseudomonas* infection"** was carried out under my direct supervision. No part of the thesis was submitted for the award of any degree or diploma prior to this date.

* Clearance was obtained from the Institutional Ethics Committee for carrying out the study.

The thesis entitled

Gallium-curcumin nanoparticle conjugate: A potent alternative to antibiotics against *Pseudomonas* infection

Submitted by

Gopika Ramesh

for the degree of

Doctor of Philosophy

of

SREE CHITRA TIRUNAL INSTITUTE FOR MEDICAL SCIENCES AND TECHNOLOGY, TRIVANDRUM

Is evaluated and approved by

Name of Guide

Dr. Roy Joseph
Scientist G, Division of Polymeric Medical Devices
Biomedical Technology Wing,
Sree Chitra Tirunal Institute for Medical Sciences
and Technology, Poojapura, Trivandrum - 695012

Gopinath Packirisamy
Name of the thesis examiner

ACKNOWLEDGEMENT

I would like to express my sincere gratitude to all those who have contributed to the completion of this Ph.D. thesis.

First and foremost, I am deeply thankful to my supervisor, Dr. Roy Joseph, Scientist 'G' (Senior Grade), Division of Polymeric Medical Devices, Department of Medical Devices Engineering, BMT Wing, SCTIMST for his invaluable guidance and unwavering support, and insightful feedback throughout the entire research journey. His expertise and knowledge have been very instrumental in shaping the direction and quality of this work.

I am also indebted to my Doctoral Advisory Committee (DAC) members Dr. Maya Nandkumar (Division of Microbial Technology), Dr. Rekha M.R. (Division of Biosurface Technology), and Dr. Ruby John Anto (Division of Cancer Research, RGCB) for their time, expertise and constructive criticism. Their diverse perspectives have enriched the content and strengthened the overall quality of this thesis.

I wholeheartedly thank Dr. Jyothi E.K. (Department of Microbiology, Hospital Wing, SCTIMST) for her immense support and guidance. Her expertise, guidance, and unwavering support have been invaluable throughout the research process. I am grateful to Dr. Kavitha Raja (Head, Department of Microbiology, Hospital Wing, SCTIMST) for accommodating me in the lab and for the encouragement throughout my tenure. I extend my sincere appreciation to Dr. Dinoop K.P. for the overall positive impact he had on my research journey. I extend my sincere thanks

to Mr. Willi Paul and Dr. Renjith S. (Central Analytical Facility, BMT Wing) for all the technical inputs and intellectual discussions.

I extend my gratitude to the present and former Directors of SCTIMST. I am also thankful to the Head, BMT Wing, and the Head, Department of Medical Devices Engineering, for providing facilities to carry out this research work. I am grateful to the present and former Deputy Registrar, Registrar, Dean, Associate Dean (Ph.D. affairs), and all staff of the Academic division and Director's office for their assistance. I also thank the teaching faculty of my Ph.D. coursework.

I would like to acknowledge the Department of Science and Technology for the INSPIRE fellowship.

I extend my heartfelt gratitude to Ms. Cinta Rose, Ms. Reeja Rani, Ms. Soja Rani, Ms. Smitha, Ms. Sudha Chandran, and Mr. Renjith Kartha. I extend my thanks to all my labmates Dr. Dhanya C.S., Ms. Gopika Gopan, Dr. Resmi R, Ms. Jasmine Joseph, Ms. Prima, Dr. Medha, Ms. Theerdha, Ms. Prathyusha, Ms. Eliza, Dr. Chandrasekhar, and other PMD lab members.

I have no words to express my heartfelt gratitude and love to my family members. My academic journey would not have been possible without the love and support of my family. I would like to express my deepest gratitude to my parents, Mr.Ramesh K. and Mrs. Sindhulekhas S. for their belief in my abilities and the sacrifices they made so that I could navigate in my life with minimum difficulty. I am also eternally indebted to my brother, Mr. Gokul Ramesh for his love, support, and encouragement. I hereby express my deepest heartfelt gratitude to my grandmother Rajamma for her affection, love, and prayers. I am deeply grateful to my husband, Mr. Vishnu Raveendrakurup, for his love and affection and for being the most comforting presence in my

life. I thank my son Vasudev who has been the light that brightened my path. I also extend my sincere gratitude to my in-laws for their support, encouragement, understanding, and affection. I dedicate this work and all my achievements in life to my family. I am profoundly grateful to the Almighty for the strength, guidance, and inspiration bestowed upon me throughout this Ph.D. journey.

TABLE OF CONTENTS

LIST OF FIGURES

LIST OF TABLES

LIST OF ABBREVIATIONS

Antimicrobial resistance	AMR
Gallium-Curcumin nanoparticles	GaCurNPs
Pseudomonas aeruginosa	*P. aeruginosa*
Reverse Phase High-Pressure Liquid Chromatography	RP-HPLC
Liquid Chromatography- Mass spectrometry	LC-MS
Phosphate buffered saline	PBS
Fourier Transform - Infrared spectroscopy	FT-IR
Transmission Electron Microscopy	TEM
Field Emission- Scanning Electron Microscopy	FESEM
Principal component analysis	PCA
Quorum Sensing	QS
2'-7'- dichlorodihydroflourescien diacetate	DCFDA

LIST OF ANNOTATIONS

%	Percentage
*	Significance
~	Approximately
mg	Milligram
µg	Microgram
µL	Microlitre
mm	Millimeter
µm	Micrometer
min	Minutes

SYNOPSIS

Antimicrobial resistance (AMR) is a major threat to humankind in the present world. It has significantly increased the mortality rate and reduced the quality of life of patients and is a huge healthcare burden. According to Global Research on Antimicrobial Resistance (GRAM) (https://www.tropicalmedicine.ox.ac.uk/gram), 4.95 million people died due to drug-resistant infections in 2019 out of which 1.27 million deaths were directly caused by AMR. In India, 1,042,500 deaths were associated with AMR and 2,97,000 deaths were attributable to AMR in 2019. The number of AMR death tolls is more than the deaths from respiratory infections and tuberculosis, diabetes and kidney diseases, and maternal and neonatal disorders. WHO has declared antimicrobial resistance as a global emergency in the year 2019. WHO Country Office

for India in collaboration with the Department of Biotechnology, Government of India has recently published a list of pathogens, the 'Indian Priority Pathogen List', and has considered AMR as a national priority under the National Action Plan on AMR (NAP-AMR) endorsed by the Government of India. Among the critical priority pathogens is *Pseudomonas aeruginosa* (resistant to carbapenem and colistin) along with other species of *Enterobacteriacea* and *Acinetobacter baumannii*. *P. aeruginosa* is an intrinsically antibiotic-resistant bacterium that causes very serious infections in immunocompromised patients and is a major pathogen in nosocomial infections like ventilator-associated pneumonia and nosocomial urinary tract infections (UTIs), particularly catheter-associated UTIs. It is also a causative agent for many community-related infections like skin/soft tissue infections, green nail syndrome, toe web infection, hot tub folliculitis, and external otitis. *P. aeruginosa* biofilms were isolated from

almost all medical devices ranging from hip prostheses to catheters. Often these isolates are resistant to various antibiotics due to adaptive resistance as well.

The research and development of new antibiotics and antimicrobial agents have been prioritized in the last decade. Finding alternative antibacterial agents that can effectively control the growth of these resistant bacteria has become a clinical necessity. Curcumin is known for its excellent antibacterial as well as anti-biofilm properties but is known to have poor stability in physiological pH. After reviewing the literature, it was hypothesized that conjugating curcumin with a metal can improve its stability considerably without compromising its anti-bacterial properties. Gallium was chosen owing to its non-toxic nature. Additionally, citrate-buffered gallium nitrate used for the treatment of hypercalcemia post-chemotherapy is known to be well tolerated by patients. Also, nanoparticle formulations are known to have improved antibacterial properties compared to their bulk counterparts. Gallium-curcumin complexes reported by Mohammadi *et al* exhibited negligible antibacterial activity. In this work, gallium-curcumin nanoparticle conjugates (GaCurNP) are synthesized, and their antibacterial activity against the notorious pathogen *P. aeruginosa* was studied. Apart from the enhanced stability of curcumin, it was also hypothesized that the nanoparticle conjugate would have enhanced anti-bacterial activity and low cytotoxicity. The overall results were in agreement with the hypothesis.

The thesis is divided into 4 major chapters. Chapter 1 gives an introduction to antimicrobial resistance, the relevance of finding alternatives to antibiotics to fight AMR, and a brief introduction to curcumin. It also provides insight into *P. aeruginosa*, its characteristics, and clinical relevance. Quorum sensing of *P. aeruginosa* and its importance are also described. It also presents the overall contents of the thesis.

Chapter 2 gives a detailed review of the literature. It includes antibiotic resistance emphasizing *P. aeruginosa* and its resistance, the importance of alternatives to antibiotics for fighting AMR, and state-of-the-art research on antibacterial nanoparticles. It also provides a review of the work reported on curcumin as an antibacterial and antibiofilm agent and the advantages of nanoformulations of curcumin. Specific details of chemicals/materials used, physicochemical characterization techniques, and antibacterial and antibiofilm studies carried out are described in detail in Chapter 3 of the thesis. Chapter 4, the Result and Discussion section presents and interprets the key findings of the study. This chapter is divided into 4 sub-sections. The first sub-section deals with the results of the physicochemical characterization of GaCurNPs. It also deals with the stability study of curcumin in GaCurNPs using Reverse Phase - High-Performance Liquid Chromatography (RP-HPLC) and Liquid Chromatography-Mass spectrometry (LC-MS). The cytotoxicity of GaCurNPs was assayed by MTT assay as well as Alamar blue assay. The second sub-section deals with the results of the *in vitro* assays and experiments conducted to evaluate the antibacterial activity of GaCurNPs against *P. aeruginosa.* The activity of GaCurNPs was tested against an ATCC strain and a clinical strain and all the experiments were done on these two strains. The ATCC strain used was ATCC 27853 and the clinical strain was a patient isolate (IEC approval was obtained for the use of the strain). The identification and antibiotic sensitivity of both strains were done manually and by the Witec automated system (Biomeriux, France). Determination of MIC by microbroth dilution, growth curve study, live dead assay, and swarming motility test was explained. The effect of GaCurNPs on the production of pyocyanin and ROS by *P. aeruginosa* was also described in this sub-section. Additional evidence on the antibacterial activity of GaCurNPs elucidated using Raman spectroscopy and scanning electron

microscopy was also included in this sub-section. The third sub-section deals with the *in vitro* anti-biofilm studies of GaCurNPs against *P. aeruginosa* biofilm. Results of Crystal violet assay, Live dead assay, Scanning electron microscopy evidence, and confocal Raman microscopy are included in this sub-section. In this section, the potential of using confocal Raman microscopy along with PCA to study the effect of antibacterial nanoparticles on *P. aeruginosa* was explained.

In the 4th sub-section, the effect of GaCurNPs on 10 critical genes involved in *P. aeruginosa* biofilm formation and quorum sensing (QS) genes are explained. The expression of the following genes in both planktonic form and biofilm form were studied: *pelA, lecA, proC, algD, rpoS, exoS, lasI, lasR, rhlI, and rhlR.* Curcumin is known to downregulate the expression of biofilm formation and QS genes in *P. aeruginosa*. Therefore, this study was done to study whether GaCurNPs also have a similar effect on those genes. This was also aimed at studying the potential antimicrobial effect of GaCurNPs on the regulatory mechanism associated with quorum sensing and biofilm formation.

Chapter 5 succinctly summarises the results and conclusions drawn from the study. All the reference related to the work and literature was also added as a separate section.

CHAPTER 1

1. INTRODUCTION

1.1. Bacterial infections and antimicrobial resistance

Bacterial infections represent a significant facet of human health, stemming from the intrusion of pathogenic bacteria into the body's various systems. Antibiotics are the first class of antimicrobial medications that serve to combat bacterial infections. Antibiotics usually work on actively dividing bacteria by interfering with various cellular processes. The major mechanisms include inhibition of bacterial cell wall synthesis, inhibition of protein synthesis, inhibition of DNA synthesis, and inhibit metabolic pathways in bacteria. Antibiotics have revolutionized modern medicine by reducing morbidity and mortality associated with bacterial infections and enabled numerous medical procedures and treatments.

Antimicrobial resistance (AMR) is one of the major challenges faced by the human race in the 21st century. According to the World Health Organisation, AMR is a natural phenomenon that happens when bacteria become resistant to antibiotics that they were once sensitive to and that were previously effective in treating infections caused by them. Excessive use of antibiotics in humans and animals has resulted in the acceleration of AMR. As a result of AMR, infections become harder to treat, which increases the risk of spreading serious infectious diseases. Moreover, the spread of resistant bacteria in hospital settings and communities increases the global burden of infectious illnesses and jeopardizes public health initiatives aimed at containing and controlling bacterial infections.

1.2. Pseudomonas aeruginosa as a resilient pathogen

P. aeruginosa stands out among resilient pathogens challenging the current antibiotic treatments. This bacterium has intrinsic resistance mechanisms which include efflux pumps and biofilm formation (Muddassir et al., 2022). The formation of tough biofilm by *P. aeruginosa* imparts another mode of resistance towards antibiotics (Bagge et al., 2004). *P. aeruginosa* is notorious for causing chronic infections in immunocompromised individuals and patients with chronic respiratory conditions (Bassetti et al., 2018). *P. aeruginosa* is largely associated with implant-associated and catheter-associated infections. External otitis, hot tub folliculitis, green nail syndrome, toe web infections, and hot hand-foot infections are the most common infections originating from the skin per se (Spernovasilis et al., 2021). *P. aeruginosa* has been often isolated from chronic wounds and is associated with poor wound healing.

P. aeruginosa possesses a variety of intrinsic as well as acquired resistance mechanisms (El Zowalaty et al., 2015). *P. aeruginosa* is innately resistant to many antibiotics that are widely used. Some types of multidrug-resistant *P. aeruginosa* are resistant to nearly all antibiotics including carbapenems. *P. aeruginosa* has shown to have resistance to most antibiotics because of its restricted outer membrane permeability, drug removal efflux mechanisms, and production of enzymes, like β lactamases that deactivate antibiotics. *P. aeruginosa* is a notorious biofilm producer and exhibits biofilm-mediated antibiotic resistance as well (Pang et al., 2019). Another challenge in treating *P. aeruginosa* infections is the emergence of persister cells which are variations that can withstand high doses of antibiotics without genetic resistance (Balaban et al., 2013).

P. aeruginosa strains are resistant to a wide range of antibiotics. The pattern of resistance of *P. aeruginosa* varies widely depending on whether they are hospital or community-acquired

infections. The resistance pattern shows geographical variations as well. Antipseudomonal drugs that have been approved clinically consist of aminoglycosides, fluoroquinolones, and β-lactams. Effective antimicrobial therapy fails when antipseudomonal agents are used inappropriately at sub-inhibitory concentrations, which have detrimental and severe biological effects, increase the selection of multidrug-resistant (MDR) mutants, and induce the formation of biofilms (Morita et al., 2014). To stop this bacteria from spreading, it is vital to find novel antipseudomonal antimicrobial medicines and enhance the effectiveness of those that are already on the market.

1.3. Development of alternatives to antibiotics against P. aeruginosa and the challenges

In recent years there has been a significant focus on the development of novel, effective antibacterial nanoparticles against multidrug-resistant bacteria. Several non-conventional ways of treating *P.aeruginosa* infections have shown promising results in pre-clinical trials and some of them have succeeded in demonstrating very significant results clinically. Many non-antibiotic strategies have been researched to be used as anti-bacterial. Some of the non-antibiotic antibacterials and antibacterial strategies that are currently being explored against *P. aeruginosa* include quorum-sensing inhibitors, lectin inhibitors, iron chelators, efflux pump inhibitors, phage therapy, different types of nanoparticles, traditional medicines, and phytochemicals (Chatterjee et al., 2016).

Smaller than one micrometer in size, nanoparticles have a high surface area-to-volume ratio, high reactivity, and unique interactions with biological systems. The literature has reported on the antimicrobial effectiveness of many nanoparticles, including polymeric nanoparticles, nanoclusters, liposomes, quantum dots, and dendrimers. Among them, metallic and polymeric

nanoparticles loaded with antibiotics have been thoroughly researched for their ability to fend off *P. aeruginosa* infections.

Nanoparticles have demonstrated potential as potent antibacterial agents against infections caused by *P. aeruginosa* (Dakal et al., 2016). The use of nanoparticles as antibacterial agents offers an alternative to conventional antibiotics to which bacteria are becoming increasingly resistant (Rizzello and Pompa., 2014). The small size and large surface area to volume ratio enable them to exert improved activity even at low doses, making them a potential alternative to antibiotics. In addition, nanoparticles can be designed with specialized surface chemistry and topography that can prevent bacterial adhesion and biofilm formation, a key characteristic of *P. aeruginosa* infections.

Silver is a harmless antibacterial metal, it may be used to reduce the amount of biofilm that bacteria produce. It has been demonstrated that silver nanoparticles work well against *P. aeruginosa* biofilm (Bruna et al., 2021). But silver nanoparticles are also known to be slightly cytotoxic to epithelial cells. ZnO/Curcumin nanoparticles were shown to inhibit LasR-RhR QS systems *in P. aeruginosa*. Curcumin-based nanoformulations are widely being explored for their antibacterial therapeutic potential against *P. aeruginosa* because of their ability to inhibit QS and biofilm formation. A detailed literature review of the use of nanoparticles as alternatives to antibiotics is presented in Chapter 2.

1.4. Definition of problem

The promise of GaCurNPs as a viable treatment for *P. aeruginosa* infections is explored in this study. Curcumin, a naturally occurring substance with a variety of medicinal uses, and gallium, which is well-known for its antibacterial qualities (explored for its use as an ant-QS drug also), are formulated in nanoparticle form, providing a fresh approach to combating antibiotic resistance. The use of curcumin is limited owing to its less solubility and stability in physiological pH which is alkaline. The delivery of curcumin is also limited due to poor bioavailability and for the same reasons stated above. Bacteria are less likely to develop resistance against nanoparticles. Nanoparticle exerts their action via mechanisms like disrupting cell membranes, generating reactive oxygen species, and interfering with cellular processes. This makes it difficult for bacteria to adapt quickly to the nanoparticles, unlike antibiotics. Because of their unique properties, nanoparticles may not align with the traditional antibiotic targets, reducing the selective pressure that promotes the emergence of resistance. Another advantage of this nanoparticle conjugate could be its less cytotoxicity.

1.5. Development of hypothesis

To develop a nanoparticle conjugate containing gallium and curcumin that can serve as a potent and innovative alternative to antibiotics for the treatment of *P. aeruginosa* infections. The nanoparticle is hypothesized to have enhanced stability of curcumin, anti-bacterial and antibiofilm activity, and less cytotoxicity in its conjugated form.

1.6. Objectives of the study

In pursuit of addressing the growing challenges posed by antibiotic-resistant *P. aeruginosa* infection, the study is designed with specific objectives. The nanoparticle is hypothesized to have enhanced stability of curcumin, anti-bacterial/anti-biofilm activity, and less cytotoxicity in its

conjugated form. To prove this hypothesis, four major objectives have been laid, which are given below:

***Objective 1*:** Synthesis and characterization of Gallium-curcumin nanoparticle conjugate (GaCurNPs) – To synthesize GaCurNPs and analyze the physicochemical properties, establishing an understanding of their composition and stability.

Objective 2: Evaluation of *in vitro* antibacterial activity of GaCurNPs against *P. aeruginosa* – To evaluate the *in vitro* antibacterial efficacy of GaCurNPs against an ATCC strain and clinical strain of *P. aeruginosa*, by qualitatively and quantitatively evaluating its effectiveness in inhibiting bacterial growth.

Objective 3: Evaluation of *in vitro* anti-biofilm property of GaCurNPs against *P. aeruginosa* – To investigate the potential of GaCurNPs in disrupting *P. aeruginosa* biofilm and its effect on biofilm formation.

Objective 4: Quantitative real-time gene expression study of biofilm genes in *P. aeruginosa* (both planktonic and biofilm) – To quantify the expression levels of key biofilm formation genes like those involved in adhesion, extracellular matrix production, and quorum sensing genes under the influence of GaCurNPs.

The research findings are expected to contribute to the development of novel antimicrobial agents capable of combating *Pseudomonas* infections. GaCurNPs offer a promising avenue for an alternative treatment strategy addressing the current antibiotic resistance. GaCurNPs could be developed into a topical antibacterial agent potentially leading to improved treatment outcomes and reduced healthcare burden associated with *P. aeruginosa*-associated infections.

CHAPTER 2

2. REVIEW OF LITERATURE

Prokaryotic species like bacteria are ubiquitous and essential to preserving our living environment. On Earth, only a tiny fraction of bacteria are known to be pathogenic or infectious. Bacterial infections and illnesses are caused by several variables, including pathogenicity, virulence, and infectivity. These bacterial infections have a major effect on public health. Treating bacterial infections is often simpler than treating viral infections because there is a greater range of antimicrobial medications that are effective against bacteria. The most common antibacterial agents used in modern medicine are antibiotics.

Antibiotic targets include the ribosome, the nucleic acid synthesis pathway, the cell wall, and the cell membrane. Antibiotics are usually byproducts of other microorganisms that have developed to compete with one another for resources and space. Unlike infectious illnesses resulting from viruses and parasites, antibiotic resistance in bacteria is an issue that is expanding quickly and has the potential to be extremely harmful.

2.1. Antibiotic resistance

Antibiotic resistance is one of the major challenges faced by the human race in recent times. Antibiotic resistance is a silent pandemic that spreads without us even knowing its severity or extent of casualty. The overuse and misuse of antibiotics are the major reasons for the resistance globally (Ventola, 2015). The main causes of antibiotic resistance are excessive antibiotic prescriptions, excessive antibiotic usage in livestock and fish farming, inadequate infection control in hospitals and clinics, poor hygiene and sanitation facilities, and lack of new antibiotic development. According to a very comprehensive study published in 2022, the global burden

associated with antibiotic resistance in 2019 was an estimated 4.95 million deaths out of which 1.27 million deaths were directly attributable to drug resistance (Murray et al., 2022).

2.1.1. Antibiotic resistance mechanism of bacteria

Antibiotic resistance is acquired by bacteria via different mechanisms. Bacteria can have natural or acquired resistance. The mechanisms include modification of antibiotics i.e., the addition of specific chemical moieties or destruction of the antibiotic molecules themselves, restricted uptake and efflux, resistance because of the global cell adaptive process, and bypassing of target sites (Munita and Arias, 2016).

Natural/Innate resistance of bacteria is either intrinsic or induced resistance (Reygaert, 2018). Intrinsic resistance is independent of previous antibiotic exposure. The most common intrinsic mechanism of resistance includes reduced outer membrane permeability and activity of efflux pumps. The lipopolysaccharide (LPS) in Gram-negative bacteria contributes to its intrinsic resistance against many antibiotics. For example, *P. aeruginosa* is resistant to many antibiotics like sulfonamides, ampicillin, 1^{st} and 2^{nd} generation cephalosporins, chloramphenicol, and tetracycline because of its low outer membrane permeability.

Mechanisms of acquired resistance can be broadly divided into four major categories which are (a) limited uptake of the drug (b) modification of drug target (c) inactivating drug and (d) active drug efflux. Gram-negative bacteria often make use of all the four mechanisms mentioned above. On the other hand, Gram-positive bacteria less commonly use the limiting uptake of drugs and also certain drug efflux mechanisms. The difference in this mechanism is mainly because of the difference in structure of the bacteria (Chancey et al., 2012; Fajardo et al., 2008).

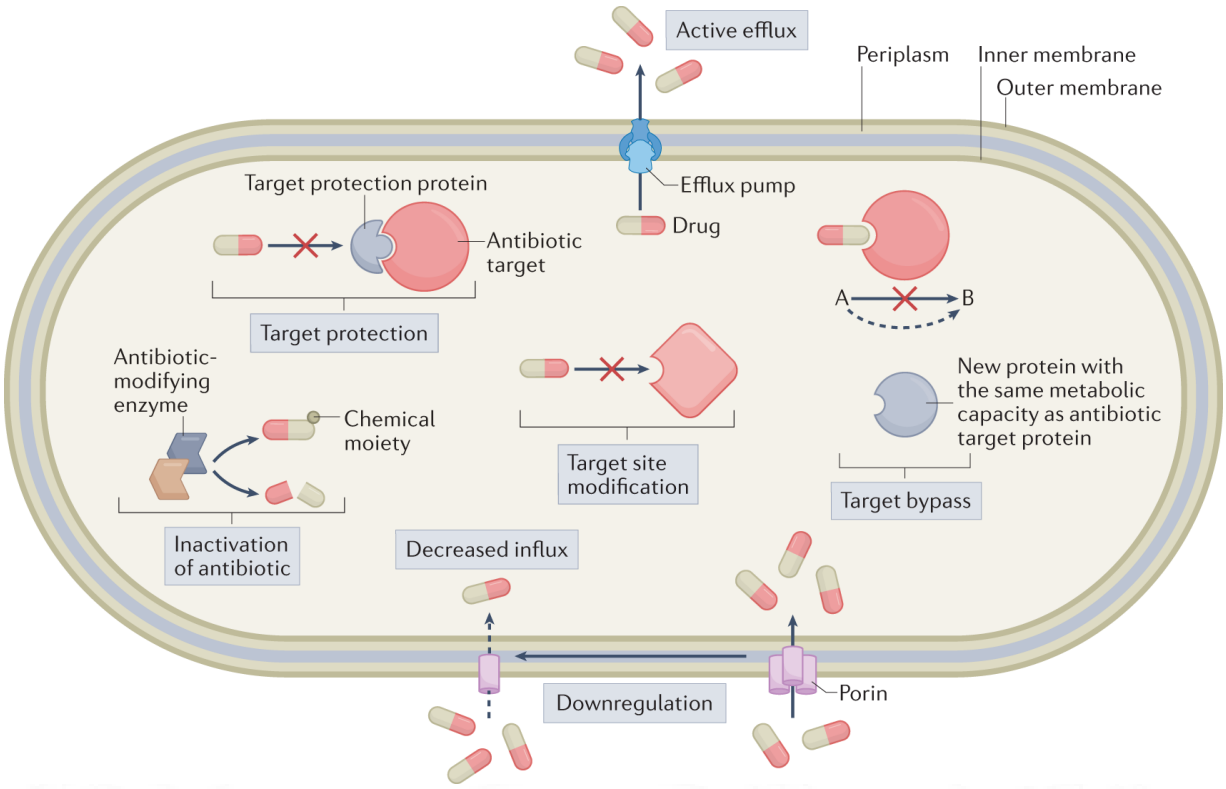

Figure 1: Mechanisms of antibiotic resistance in bacteria (Darby *et al*., 2022)

The antibiotic-resistant ESKAPE pathogens (*Enterococcus faecium*, *Staphylococcus aureus*, *Klebsiella pneumoniae*, *Acinetobacter baumanii*, *Pseudomonas aeruginosa*, and *Enterobacter* species) have tremendously reduced the treatment options for serious infections, increased death rates due to treatment failure, and also increased the burden of disease (Oliveira et al., 2012). Vancomycin-resistant *Enterococcus*, Methicillin-resistant *Staphylococcus aureus*, *K. pneumoniae*, and *Acinetobacter baumanii* resistant to carbapenem and polymixin cause serious infections and cause more than 30% mortality. *P. aeruginosa*, which is innately resistant to numerous antimicrobial agents, is currently resistant to multiple antibiotics that are in use.

2.2. Pseudomonas aeruginosa

2.2.1. General characteristics

P. aeruginosa is a gram-negative, rod-shaped, non-lactose fermenting bacterium that occurs singly, in pairs, or in short chains. *P. aeruginosa* is 1.5–3 µm by 0.5–0.8 µm in size. It is a facultative aerobe that grows well at 37°C and can withstand temperatures ranging from 4°C to 42°C. (Iglewski 1991). It doesn't require organic growth factors and can grow on a wide variety of substrates. *P. aeruginosa* has oxidase activity. Most strains are motile utilizing a single polar flagellum and some of the strains have two or three flagella (Iglewski, 1996). *P. aeruginosa* has a three-layered cell envelope that is comparable to other Gram-negative bacteria's: the peptidoglycan layer, the outer membrane, and the inner, or cytoplasmic, membrane. Lipopolysaccharide (LPS), protein, and phospholipid make up the outer membrane. Comparing *P. aeruginosa*'s LPS to other Gram-negative rods, it is less hazardous. In addition to side-chain and core polysaccharides, the LPS of the majority of *P. aeruginosa* strains contains hydroxy fatty acids, heptose, and 2-keto-3-deoxyoctonic acid. *P.aeruginosa* genome which has a size of 5.5- 7 Mbp, is made up of a single circular chromosome and is known to harbor plasmids that can readily be exchanged. *P. aeruginosa* genome encodes a wide range of enzymes for various metabolic pathways, conferring high nutritional versatility. Around 8% of the genome encodes regulatory genes, which help the bacterium to adapt to harsh and complex growth environments.

Indian Pathogen Priority list was jointly prepared by the WHO India office along with the Department of Science and Technology, Government of India. It categorized pathogens according to the species and resistance into three priority tiers – critical, high, and medium. The priority list was made based on a literature survey on key antibiotic-resistant bacteria in the Indian context and analysis of available data and information on bacterial drug resistance

mechanisms (Figure: 2) *P. aeruginosa* falls in the category of critical priority and calls for immediate action to find alternatives to infection caused by the same. The WHO has listed carbapenem-resistant *P. aeruginosa* as one of the three bacterial species for which there is a critical need for the development of new antibiotics to treat infections.

Table 1: Indian Priority Pathogen list prepared by the WHO office in India in association with the Department of Biotechnology, Govt. of India.

CRITICAL PRIORITY	
Enterobacteriaceae (*Klebsiella pneumoniae* and *Escherichia coli*)	Carbepenem – R Tigecycline – R Colistin – R
Non-fermenting bacteria (*Acinetobacter baumannii* and *Pseudomonas aeruginosa*)	Carbepenem – R Colistin – R
HIGH PRIORITY	
Staphylococcus aureus	MRSA, hVISA Daptomycin – NS Linezolid – R
Enterococcus species	Vancomycin – R Linezolid –R Daptomycin – R
Salmonella species (Typhoidal and Non-typhoidal)	
MEDIUM PRIORITY	
Streptococcus pneumoniae	Cephalosporin – R Fluoroquinolones – R Linezolid – R
Staphylococcus, coagulase-negative	Vancomycin – R Linezolid – R
Haemophilus influenzae	Third-generation cephalosporin – NS Carbepenem – NS
Neisseria meningitidis	Fluoroquinolones – NS Third-generation cephalosporins – NS

2.2.2. Infections caused by **P. aeruginosa**

P.aeruginosa is the most common cause of nosocomial infection, surgical site infections, and bacteremia (Reynolds and Kollef, 2021; Hauser and Rello, 2012). Pneumonia is the most common site of *P.aeruginosa* infection and is the most commonly identified Gram-negative bacteria in nosocomial infection. *P. aeruginosa* is also a common cause of nosocomial urinary tract infections (UTIs), particularly catheter associated UTI. It is closely associated with the lung infections in cystic fibrosis patients. It is an important pathogen in immunocompromised patients, especially patients with neutropenia. *P.aeruginosa* is often isolated from acute and chronic burn wounds and causes severe tissue damage and sepsis (Turner et al., 2014). One of the main organisms that form biofilms in medical devices is *P. aeruginosa* (Mi et al., 2016) (Ribeiro et al., 2012). Skin infestations are also common by *P.aeruginosa*. Green nail syndrome, toe web infection, hot-hand foot infection, hot tub folliculitis, and external otitis are very common skin infections caused by *P.aeruginosa* (Spernovasilis et al., 2021). *P.aeruginosa* forms biofilms in chronic lung infections, chronic wounds, and chronic rhinosinusitis.

2.2.3. Mechanism of antibiotic resistance in P. aeruginosa

P.aeruginosa exhibits resistance toward a variety of antibiotics including aminoglycosides, quinolones, and beta-lactams (Hancock, 1998). The major mechanisms used by *P. aeruginosa* to counter the effect of antibiotics can be divided into intrinsic, acquired, and adaptive resistance.

The intrinsic resistance of *P.aeruginosa* includes low membrane permeability, expression of efflux pumps that expel antibiotics out of the cell, and production of antibiotic-inactivating enzymes. Acquired resistance of *P.aeruginosa* can be either achieved by horizontal gene transfer or mutational changes (Breidenstein et al., 2011). Adaptive resistance involves the formation of biofilm in the lungs of CF patients and also in wounds.

2.2.3.1. Intrinsic resistance

P. aeruginosa has an asymmetric bilayer of phospholipid and LPS contained in porins that create β-barrel protein channels. This outer membrane serves as a selective barrier to inhibit antibiotic penetration (Delcour, 2009). The family of porins can be broadly classified into four classes: gated porins, which are ion-regulated outer membrane proteins responsible for the uptake of ion complexes; non-specific porins, which permit slow diffusion of the majority of small hydrophilic molecules; specific porins, which possess specific sites to bind a particular set of molecules; and efflux porins, which are crucial parts of efflux pumps (Hancock and Brinkman, 2002)). The primary non-specific porin in P. aeruginosa is the OprF protein; OprB, OprD, OprE, OprO, and OprP are certain porins; OprC and OprH are members of the gated porin class. Among the efflux porins are OprM, OprN, and OprJ. The reason for *P. aeruginosa*'s significantly reduced outer membrane permeability in comparison to other bacteria might be attributed to the existence of mainly blocked OprF channels. Furthermore, the lack of *P. aeruginosa* OprF causes an increase in the production of biofilms by upregulating bis-(3′–5′)-cyclic dimeric guanosine monophosphate (c-di-GMP), a crucial messenger for regulating the formation of biofilms.

Efflux system: Five families of bacterial efflux pumps are known to be involved in the removal of toxic compounds from cells: the resistance-nodulation-division (RND) family, the major facilitator superfamily (MFS), the ATP-binding cassette (ABC) superfamily, the small multidrug resistance (SMR) family, and the multidrug and toxic compound extrusion family. *P. aeruginosa*'s antibiotic resistance is mostly caused by proteins that are members of the RND family of efflux pumps (Li and Nikaido, 2009). They are made up of proteins called porin channels, periplasmic linker proteins, and cytoplasmic membrane transporters (Daury et al.,

2016). They are made up of proteins called porin channels, periplasmic linker proteins, and cytoplasmic membrane transporters (Daury et al., 2016). Multidrug efflux (Mex) is the letter-designated term for the cytoplasmic and periplasmic components of *P. aeruginosa* RND pumps, whereas Opr is the letter-designated name for the outer membrane porin. Twelve RND family efflux pumps are expressed by *P. aeruginosa*, four of which are involved in antibiotic resistance: MexAB-OprM, MexCD-OprJ, MexEF-OprN, and MexXY-OprM (Dreier and Ruggerone, 2015)

Antibiotic modifying enzyme: The production of enzymes known as antibiotic-inactivating enzymes, which degrade or alter antibiotics, is one of the main ways that bacteria develop intrinsic resistance. Many antibiotics have chemical bonds, including amides and esters, that can be hydrolyzed (Malloy et al., 2005) by *P.aeruginosa*-produced enzymes like β-lactamases and enzymes that alter aminoglycosides (Poole, 2005; Wolter and Lister, 2013). *P. aeruginosa*, like other Gram-negative bacteria, has an *ampC* gene that may be activated. This gene codes for the hydrolytic enzyme β-lactamase. The β-lactam ring's amide bond can be broken by this enzyme, which renders β-lactam antibiotics inactive (Malloy et al., 2005). Furthermore, based on their amino acid sequences, β-lactamases may be categorized into four classes: A, B, C, and D. β-lactams are hydrolyzed by the enzyme classes A, C, and D via a serine active site. In contrast, the metalloenzymes known as class B β-lactamases need divalent zinc ions to hydrolyze β-lactams (Bush and Jacoby, 2010). It has been demonstrated that *P. aeruginosa*'s class C β-lactamase inhibits the family of β-lactams known as antipseudomonal cephalosporins (Berrazeg et al., 2015). Certain *P. aeruginosa* isolates have been shown to develop extended-spectrum β-lactamases (ESBLs), which give a high level of resistance to the majority of β-lactam antibiotics, including penicillins, cephalosporins, and aztreonam.

2.2.3.2. Acquired resistance

Bacteria can acquire resistance genes by horizontal gene transfer or mutational alterations. Apart from *P.aeruginosa'*s high level of intrinsic antibiotic resistance, acquired resistance plays a significant role in the emergence of multidrug-resistant strains, making it harder to eradicate the microorganism and increasing the number of cases of persistent infections (Henrichfreise et al., 2007)

Resistance by mutation: Due to decreased antibiotic absorption, altered antibiotic targets, overexpression of efflux pumps, and the production of enzymes that inactivate antibiotics, mutations can allow bacteria to persist in the presence of antimicrobial compounds (Munita and Arias, 2016). For instance, a 2009 research by Mandsberg *et al*. showed that increasing mutation frequencies in *P. aeruginosa* due to inactivation of the DNA oxidative repair mechanism results in increased synthesis of β-lactamase and overexpression of the MexCD-OprJ efflux pump. Antibiotic resistance can rise and bacterial membrane permeability can be decreased as a result of spontaneous mutations that alter the expression or function of a particular porin (Hancock and Brinkman, 2002). For example, *P. aeruginosa* with a defect in OprD exhibits strong resistance to carbapenems, particularly imipenem (Fang et al., 2014; H Li et al., 2012; Wolter et al., 2004). Fang *et al.* examined 61 imipenem-resistant *P. aeruginosa* clinical isolates from southern China. They discovered that 50 isolates had mutations that affected OprD expression, 5 isolates had reduced OprD expression, and 6 isolates did not have detectable OprD by PCR. The mutations are caused by frameshift mutations or a premature stop codon. Energy-dependent efflux systems are utilized by bacteria to pump toxic molecules from the cells, thus avoiding their intracellular build-up. Antibiotic susceptibility is therefore reduced in *P. aeruginosa* clinical isolates with overexpressed efflux pumps (Cabot et al., 2011); Cabot et al., 2016 ; (Poonsuk et al., 2014). For

instance, *P. aeruginosa* MexAB-OprM overexpression increased the bacterium's resistance to β-lactams and fluoroquinolones, a family of quinolone, and resulted from gene alterations of transcriptional regulators, mexR, nalB, nalC, or nalD.

Acquisition of resistance genes: Horizontal gene transfer between bacteria of the same or different species can result in the acquisition of antibiotic resistance genes from plasmids, transposons, integrons, and prophages (Breidenstein et al., 2011). The main horizontal gene transfer mechanism involves transformation, transduction, and conjugation. β-lactam resistance gene and aminoglycoside resistance genes are transferred in *P. aeruginosa* (Bonomo and Szabo, 2006; Hong et al., 2015*;* Tseng et al., 2007*;* Poole, 2005). The genes for six different types of metallo-beta-lactamases are carried by genetic elements including integrons and plasmids (Bonomo and Szabo, 2006; Khajuria et al., 2013; Cavalcanti et al., 2015; Tseng et al., 2007). Corneal isolates of *P. aeruginosa* were found to carry fluoroquinolone-resistant genes in the form of transposons (Khan et al., 2020).

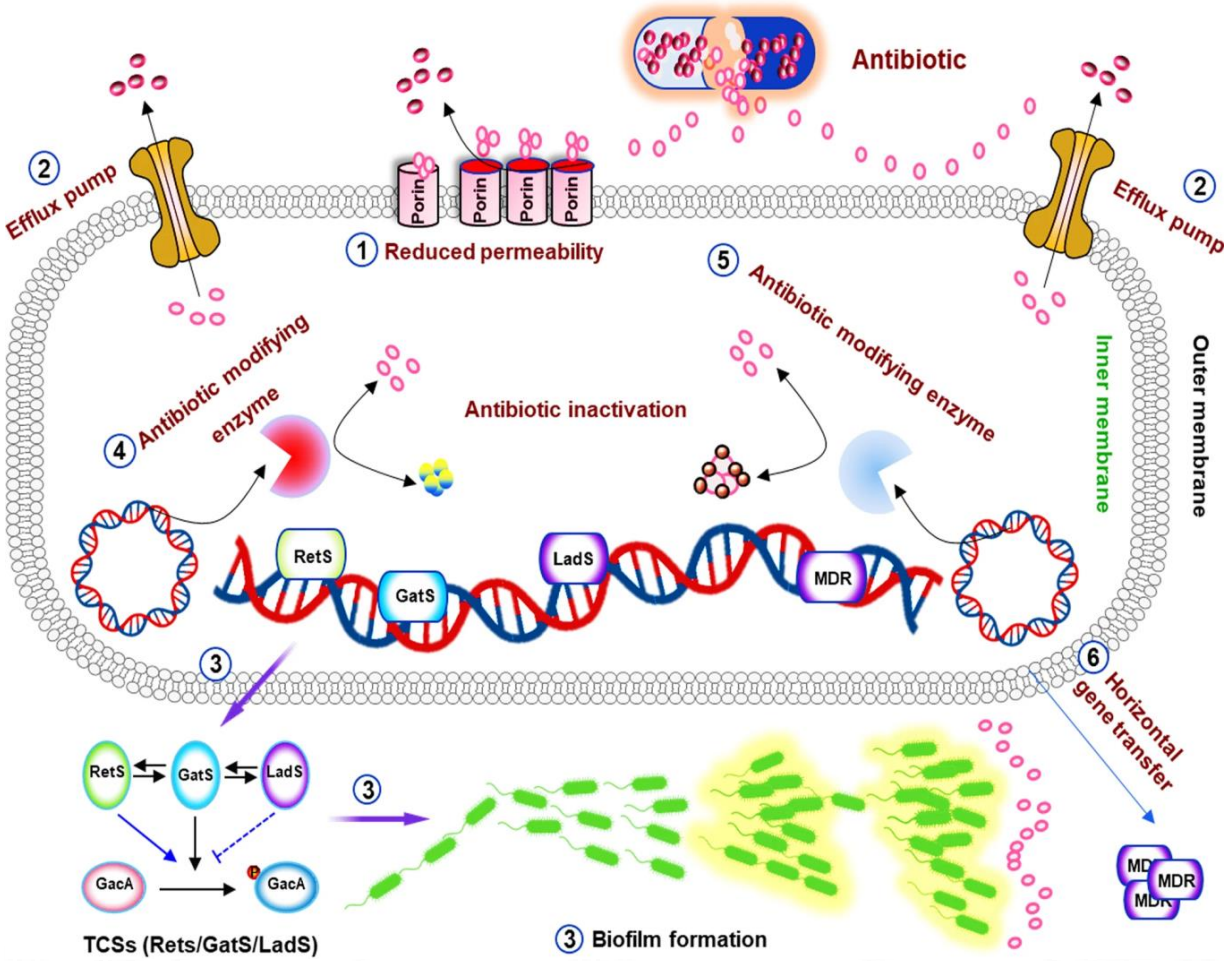

Figure 2: Antibiotic resistance mechanisms of *P. aeruginosa* (Qin *et al*.,2022).

2.2.3.4. Adaptive resistance

Due to brief changes in gene and/or protein expression in response to an environmental stimulus, adaptive resistance boosts a bacterium's capacity to withstand antibiotic treatment and is reversible when the stimulus is withdrawn (Sandoval-Motta and Aldana, 2016). The development of persister cells and biofilm formation in *P. aeruginosa* is the most well-characterized mechanism of adaptive resistance; both processes cause chronic infection and a poor prognosis in CF patients (Taylor et al., 2014). Biofilm-mediated resistance is described in section 2.3.

2.2.4. Virulence factors

Virulence refers to a pathogen's capacity to infect a host and induce clinical symptoms through a variety of mechanisms, including bacterial attachment, colonization, invasion of the host, disruption of host tissue integration, immune response suppression and escape, and host nutrient depletion (Mühlen and Dersch, 2016; Dickey et al., 2017). *P. aeruginosa* virulence factors fall into three basic categories: bacterial surface structure, secreted factors, and bacterial cell-to-cell interactions. Bacterial surface structures consist of five secretion systems (T1SS, T2SS, T3SS, T5SS, and T6SS), lipopolysaccharides, and surface appendages like type IV pili and flagella. Secreted virulence factors include exopolysaccharides (alginate, Pel, Psl), siderophores (pyoverdin, pyochelin), proteases (alkaline protease, elastase A and B, protease IV), and toxins like exotoxinA, pyocyanin, Lipase A, phospholipase C, exolysin, T3SS effectors, etc. (Liao et al., 2022).

2.3. Biofilm formation in P. aeruginosa

Biofilms are three-dimensional structures formed by bacteria that are the toughest to deal with. Since bacterial biofilms may grow in indwelling medical devices like urinary catheters, stents, grafts, etc they pose a serious threat in the hospital environment. Because most bacterial biofilms are intrinsically resistant to antibiotics, it is difficult to eradicate them. The cells are embedded in extracellular polymeric substances which hinder the penetration of antibiotics and thereby fail its activity. Antibiotics are difficult to act on sleeper cells/persister cells which are found in the lowest levels of biofilm and are metabolically inactive. Biofilm is a complex aggregate of bacteria encased in a polymeric matrix that is self-synthesized by bacteria (Thi et al., 2020). Bacteria within the biofilm are protected from high concentrations of antimicrobial treatments

and often escape host immune responses compared to their planktonic counterparts (Lewis, 2001).

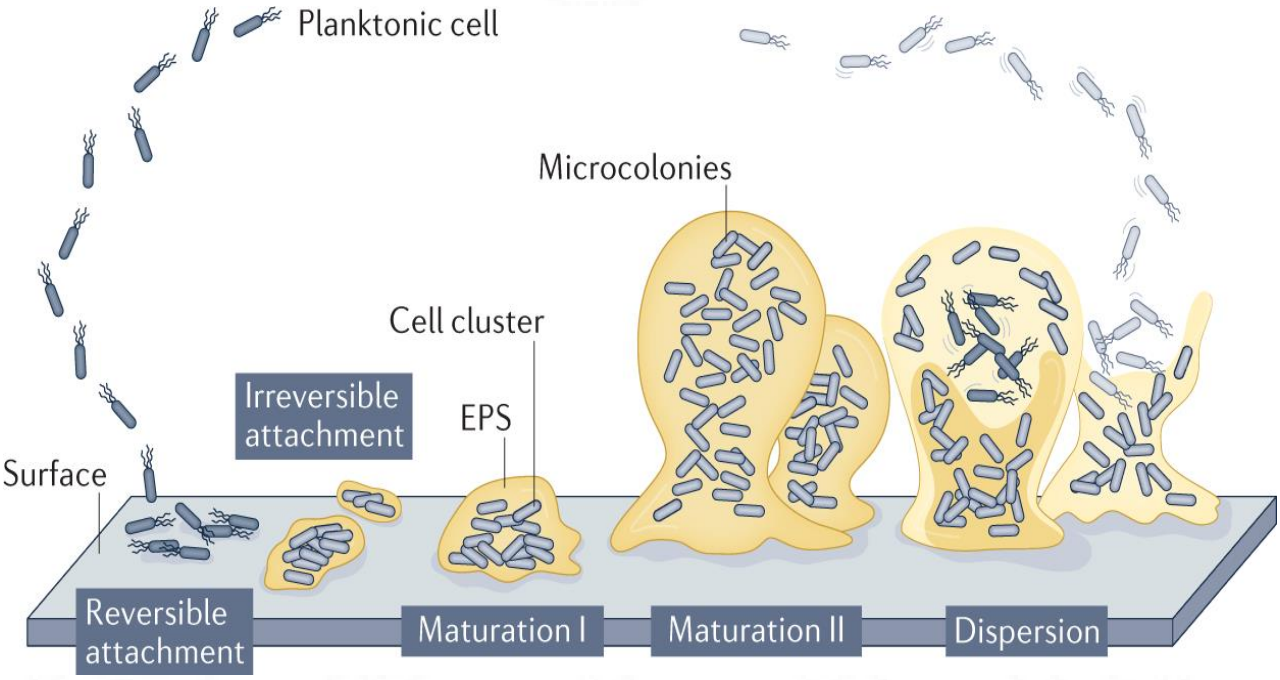

Figure 3: Steps in *P. aeruginosa* biofilm formation (Sauer *et al.*,2022)

P. aeruginosa is a notorious biofilm producer and an excellent model to study biofilm formation. *P.aeruginosa* is known to colonize medical devices (urinary catheters, implants, contact lenses, etc.) (Ghafoor et al., 2011) and human tissues while growing in resistant communities called biofilms. A resilient biofilm is critical for the survival and domination of *P.aeruginosa* in cystic fibrosis and also in wounds. Biofilm also plays a major role in the bacteria's defense against antimicrobial treatment and host defense mechanisms.

2.3.2. Steps in biofilm formation P. aeruginosa

The development of biofilm in *P. aeruginosa* can be divided into five steps. Stage I: Cell appendages like flagella and type IV pili help bacterial cells stick to a surface (O'Toole and

Kolter, 1998) (M et al., 2003). The production of exopolysaccharides needed for surface attachment and twitching motility has been linked to the limited mobility of flagellar filaments (Hickman and Harwood, 2008). This adherence of bacterial cells is reversible. Stage II: Reversible to irreversible adhesion of bacterial cells occurs. Stage III: Attached bacteria gradually multiply into microcolonies, which are more formally organized architectural structures. Stage IV: As a sign of biofilm maturity, these microcolonies continue to grow into large, three-dimensional structures resembling mushrooms. Stage V: Cell autolysis disrupts the matrix cavity at the microcolony's center, releasing scattered cells (Ma et al., 2009). This is followed by Stage VI, when the growth mode switches from sessile to planktonic, allowing uncolonized regions to be seeded and allowing the biofilm cycle to recur.

2.3.3. Components of biofilm

In a biofilm, the bacteria are encased in a self-generated matrix of extracellular polymeric substance (EPS). The EPS is one of the key strategies for the survival of bacteria against unexpected changes in conditions like nutrient availability and temperature (Moradali and Rehm, 2020) (Rollet et al., 2009). *P.aeruginosa* biofilm EPS is composed of polysaccharides, extracellular DNA, proteins, and lipids. More than 90% of the biofilm matrix is the EPS and acts as a scaffold for the attachment of bacteria to abiotic and biotic surfaces and also functions as a shield for bacteria against antibiotics and host immune response. EPS also facilitates cell-to-cell communication (Thi et al., 2020; Jackson et al., 2004; Ryder et al., 2007). Essential nutrients, enzymes, and cytosolic proteins for the biofilm are provided by the EPS.

There are three major exopolysaccharides in *P.aeruginosa* EPS i.e., Psl, Pel, and alginate, which aid in surface attachment, formation of biofilm, and maintaining its stability. Psl is a neutral pentasaccharide composed of D-glucose, D-mannose, and L-rhamnose and is involved in the

adhesion of sessile cells and cell-to-cell interaction during biofilm formation of both mucoid and non-mucoid strains. Psl shields biofilm bacteria from neutrophil phagocytosis (Mishra et al., 2012) and antimicrobials (Billings et al., 2013). Pel is a cationic polysaccharide polymer of N-acetyl D galactosamine and N-acetylD-glucosamine.Psl also shields bacteria from antimicrobials and host defenses. Pel is essentially involved in the surface attachment and maintenance of biofilm integrity of non-mucoid strains. Pellicle biofilm formation in the air-liquid interface is aided by the Pel. Pel imparts tolerance to aminoglycoside antibiotics for biofilm-embedded bacteria (Yang et al., 2011). Alginate is a negatively charged acetylated polymer of mannuronic acid and guluronic acid residues. Alginate is predominantly produced by mucoid strains of *P. aeruginosa*. The mucoid strains have a mutation in the *mucA22* allele. Usually, the mucoid strains are isolated from the lungs of cystic fibrosis patients and the ratio between mannuronic acid and guluronic acid influences the viscoelastic properties of biofilm leading to impairment of cough clearance.

Another significant component of biofilm is eDNA and it is released into the environment during cell lysis. The eDNA is involved in many processes in the biofilm, some of which are: It acts as a nutrient source for bacteria and supports the cellular organization and alignment via twitching motility, acts as a chelator for divalent cation, and it prevents the penetration of antibiotic into the biofilm by making the environment acidic (Chiang et al., 2013) (Wilton et al., 2015) (Wilton et al., 2016) (Gloag et al., 2013) (Fuxman Bass et al., 2010). In *P. aeruginosa* the eDNA secreted influences the inflammatory cascade initiated by the neutrophils.

In addition to polysaccharides and nucleic acids, another important component is the matrix-related protein. Proteins that are present in the biofilm matrix facilitate roles including surface adherence, interaction with other matrix molecules, and matrix stability. Proteins such as CdrA

possess carbohydrate-binding capacity and play a major role in promoting matrix molecule interaction (Borlee et al., 2010). Rhamnolipid is another component present in the biofilm matrix. Rhamnolipids are surface-active glycolipid biosurfactants. During the colonization stage of bacteria, rhamnolipid potentially interacts with the host cells and exhibits cytotoxicity (McClure and Schiller, 1992; Häussler, 2004).

2.3.4. Quorum sensing in P. aeruginosa

P. aeruginosa like numerous microbes employs chemical signals to communicate between cells in a process called Quorum sensing (Miranda et al., 2022). *P. aeruginosa* responds to variations in cell density as well as environmental stimuli or stresses by entering into the QS mode (Mukherjee and Bassler, 2019). QS is characterized by the synthesis, secretion, and accumulation of signaling molecules known as autoinducers (AI), whose concentration and specificity are detected by transcriptional regulators (Fuqua et al., 1994), leading to the expression of particular gene sets across the population. Apart from the generation of biofilms, QS has been associated with the control of several physiological processes such as the synthesis of virulence factors, stress tolerance, metabolic adaptation, and host-microbe interactions.

QS involves the production, release, and detection of signaling molecules called autoinducers. There are two major QS systems in *P. aeruginosa*. The two main systems are the Las and Rhl systems. The Las system comprises two components: LasI and LasR. The autoinducer molecule is N-(3-oxo-dodeconoyl)- homoserine lactone (3-oxo-C12 HSL). LasR is the transcriptional activator and LasI directs the synthesis of the signal molecule 3-oxo-C12 HSL. The LasR-autoinducer complex activates the expression of many genes which includes those involved in the production of virulence factors such as elastase, alkaline protease, and exotoxin (Thi et al., 2020).

In the Rhl system, the autoinducer molecule is N-butanoyl homoserine lactone and consists of two components: RhlI and RhlR. RhlR receptor binds to the autoinducer when the concentration reaches a critical level. The RhlR-autoinducer complex acts as a transcription factor and leads to the production of secondary virulence factors such as pyocyanin, rhamnolipids, and lectins (Liao et al., 2022).

Another QS system is also present in *P.aeruginosa* which is the PQS (Pseudomonas quinolone signal) system. The PqsR–PQS complex in the PQS system feeds back to stimulate the production of the rhlRI gene and activates the pqsABCDH genes. RhlR can suppress the expression of both the *pqsR* and *pqsABCDH* genes, which has been proposed as a means of regulating the proper ratio between 3-oxo-C12-HSL and C4-HSL and, therefore, the activation of the PQS pathway (Iglewski, 1996). The above-mentioned QS system allows *P. aeruginosa* to regulate the expression of various virulence factors and coordinate the behavior of the bacteria as a population.

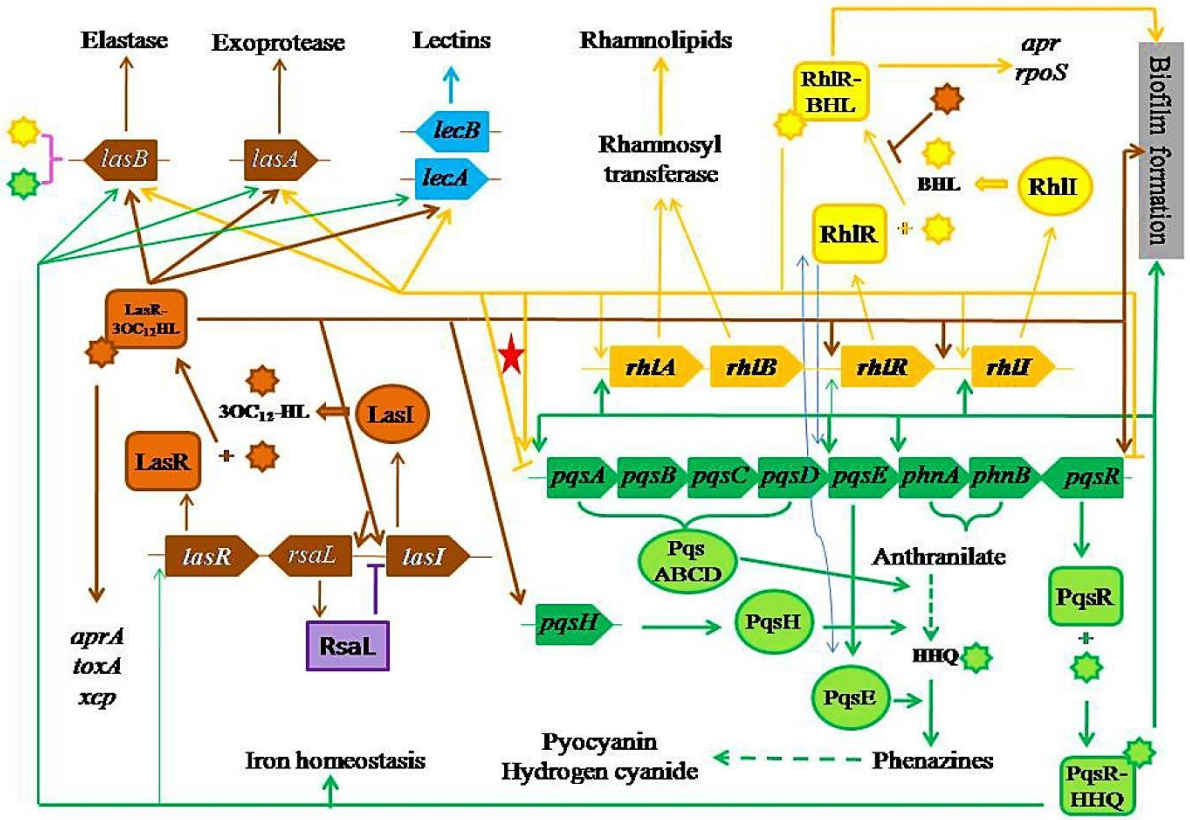

Figure 4: Quorum sensing network in *P. aeruginosa* (Yan *et al*.,2019)

2.3.5. Tolerance and resistance of P. aeruginosa biofilm towards antibiotics

The mechanism of biofilm-associated antibiotic tolerance is described in brief in this section. The physical tolerance or restricted penetration is the major tolerance elicited by *P.aerugnosa* biofilm. Antibiotics must penetrate the extracellular biofilm matrix to reach the embedded bacteria while treating biofilm infections. Numerous studies have indicated that although biofilm matrices do not generally prevent antibiotics from diffusing, there may be limited antibiotic penetration through biofilms in situations where the antibiotics bind to the bacterial membranes or biofilm matrix components (Walters et al., 2003; Tseng et al., 2013). Tseng et al. (2013) directly demonstrated that neutral ciprofloxacin easily enters *P. aeruginosa* biofilms, but

positively charged tobramycin is sequestered in the biofilm's periphery by the use of fluorescently labeled antibiotics. The antibiotics that attach to the biofilm matrix can get saturated with it, thus the antimicrobial tolerance brought on by reduced penetration might only last a short while. But it could provide the bacteria enough time to change into a more tolerant form (Bagge et al., 2004; Pamp et al., 2008). Additionally, the technique could apply to infections in which the biofilm matrix is not saturated by antibiotics due to low antibiotic concentrations at the infection site.

The second level of tolerance involves the physiological tolerance of the biofilm. Bacterial subpopulations with a broad range of metabolic activity are seen in biofilms. High physiological activity is exhibited by subpopulations along the biofilm's edge, whereas little or no physiological activity is exhibited by subpopulations inside the biofilm (Pamp et al., 2008; Stewart et al., 2016). The reason for this heterogeneity is that the metabolically active bacteria near the biofilm's perimeter consume oxygen and nutrients, leaving little to no oxygen and nutrients for the bacteria in the biofilm's center (Stewart et al., 2016). The main antibiotic targets become inactive as a direct result of poor metabolic rates for antibiotic tolerance, which influences the effectiveness of all bactericidal antibiotics to varying degrees. For instance, poor peptidoglycan formation influences the action of beta-lactams, low DNA synthesis influences the impact of quinolones, and low protein synthesis changes the efficiency of inhibitors of protein synthesis, such as aminoglycosides. Antibiotics have a limited effect on low-metabolism bacteria because they trigger adaptive stress responses such the stringent response (Nguyen et al., 2016) and SOS (Bernier et al., 2013), in addition to target inactivity. It has been demonstrated that the stringent response, an adaptive response to nutrition and iron shortages that may occur in biofilms in specific settings, is crucial to the biofilms' ability to withstand antibiotics (Nguyen et

al., 2011). Nutrient limitation and oxygen deprivation are rapidly sensed by the bacterial cells in the biofilm and become metabolically inactive. Bacterial growth rates are decreased in anoxic or hypoxic environments (Williamson et al., 2012). According to research using an *in vitro* colony biofilm model, oxygen restriction under these circumstances may account for 70% (62% ciprofloxacin, 69% tobramycin, and 110% ceftazidime) of the antibiotic tolerance (Borriello et al., 2004). The deeper layer of the biofilm's cells' reduced metabolic activity due to oxygen scarcity changed the way beta-lactam, fluoroquinolone, and aminoglycoside worked. The development of so-called persister cells is another factor that can lead to antibiotic tolerance. When antibiotic therapy is stopped, persister cells, which are slowly or non-dividing bacteria that are less susceptible to antibiotics than the majority of the bacterial population, can go into a vegetative state and resurrect illnesses (Lewis, 2010). The proportion of persister cells in biofilms is often minimal (~0.01%), and they should be differentiated from the mostly nutrient-deficient, spatially limited minority of tolerant, metabolically dormant bacteria that make up the biofilm.

Biofilm tolerance is also caused by the expression of specific genes in the biofilm which are not generally expressed in the planktonic species. Gupta *et al*., presented evidence for the involvement of the messenger molecule c-di-GMP in the antibiotic tolerance of *P. aeruginosa* biofilms (Gupta et al., 2016). Planktonic cells have a lower amount of c-di-GMP than biofilm cells. It was discovered that boosting the c-di-GMP level artificially to "biofilm" levels in planktonic cultures increased the bacterial cells' resistance to antibiotics. Diguanylate cyclase (DGC) PA3177 was shown to be active; upon inactivation, biofilm cells became tobramycin-sensitive (Poudyal and Sauer, 2018).

Biofilms are very resistant to the beta-lactam group of antibiotics and the minimum biofilm inhibitory concentration is around 1000-fold higher concentration than that of planktonic MIC. Beta-lactam antibiotics often have a weak anti-biofilm impact. This is because beta-lactam antibiotics only work on cells that are actively growing and dividing, and their method of action is focused on peptidoglycan formation. Therefore, the sluggish growth of bacteria in biofilms is linked to the basic mechanism of biofilm resistance to beta-lactams.

Fluoroquinolones are found to be more active against biofilm bacteria than beta-lactams and the MBIc for *P. aeruginosa* is almost close to planktonic MICs (Moskowitz et al., 2004; Macià et al., 2014). Since quinolones are uncharged molecules, they permeate the biofilm matrix with ease. Quinolones have shown strong bactericidal efficacy in an in vitro investigation conducted on P. aeruginosa that was either non-growing or growing suboptimally (Eng et al., 1991). However, the bactericidal action of quinolones is affected by low oxygen concentration in biofilms, most likely as a result of ROS production occurring at inadequate levels to provide bactericidal impact. Along with adaptive responses like SOS and the stringent response, the low oxygen level appears to be the main mechanism allowing biofilms to withstand quinolones (Stewart, 2015).

The resistance of *P. aeruginosa* biofilms to aminoglycoside antibiotics appears to be influenced by a multitude of pathways. These processes include the expression of certain genes that confer biofilm-associated aminoglycoside tolerance, as well as the binding of the aminoglycosides by different biofilm matrix components. When *P. aeruginosa* strains that overproduce alginate create biofilms, alginate may function as a defense against aminoglycoside drugs. As a result, it was demonstrated that biofilms made by a *P. aeruginosa* strain that produced excessive amounts of alginate were noticeably more resistant to tobramycin than biofilms made by an isogenic, non-mucoid strain (Hentzer et al., 2001). In *P. aeruginosa* biofilms, the Pel exopolysaccharide can

also offer defense against aminoglycosides. As a result, it was shown that mutant biofilms missing Pel were more sensitive to gentamycin and tobramycin than their wild-type counterparts (Colvin et al., 2011). Furthermore, aminoglycosides may be prevented from penetrating *P. aeruginosa* biofilms by eDNA. Since DNA can bind positively charged antibiotics like aminoglycosides, biofilms formed by a *P. aeruginosa* quorum-sensing mutant lacking DNA release were found to be susceptible to tobramycin. However, biofilms that were supplied with DNA that was incorporated into the biofilm were found to be tobramycin tolerant. As aminoglycosides require an active, oxygen-dependent uptake through the cytoplasmic membrane to reach their ribosomal target, and lack of oxygen impairs the membrane potential and the transport of these molecules into the cytoplasm, both factors contribute to the biofilms' resistance to aminoglycosides (Stewart, 2015).

2.4. Alternatives to antibiotics for treating bacterial infections

Antibiotics are used in conventional antimicrobial therapy to either stop infectious pathogens from growing or kill them. However, the current scenario of increased antimicrobial resistance calls for the development of new antibiotics as well as alternative therapies to treat bacterial infections. Various alternatives have been experimented with by researchers as an alternative to antibiotics. Alternatives to antibiotics include targeting AMR enzymes or targeting AMR bacteria using different approaches. Enzyme inhibitors, phytochemicals, small molecules, RNA silencing, and CRISPR-Cas9 system are some of the strategies that target the enzymes involved in the AMR. Monoclonal antibodies, bacteriophage therapy, antimicrobial peptides, and nanoparticle-based therapy are some of the promising areas of alternatives to antibiotics. Nanoparticles are preferred because it is less likely for bacteria to develop resistance against nanoparticles.

2.4.1. Nanoparticles as anti-bacterial agents

Nanoparticles are usually 100 nm or less in size but certain particles that are 500 nm or smaller are also referred to as nanomaterials (Vert et al., 2012). Nanoparticles can take on various shapes, some of which are nanoparticles, nanowires, and nanorods. Nanomaterials may take on a variety of morphologies and shapes which include rods, spheres, pyramids, fibrous networks, and hollow or solid interiors, with smooth or rough surfaces. When compared to their bulk counterparts, materials in the nanoscale range have unique physicochemical properties, such as shape, size, and surface (Natan and Banin, 2017). Nanomaterials are similar in size to biomolecules as well as bacterial intracellular structure, they can be engineered as new therapeutic modalities (Soenen et al., 2011). Representatives of nanomaterials for antimicrobial application include carbon-based nanoparticles, metal-based nanoparticles, polymers, liposomes, nanoemulsions, and certain smart nanomaterials.

Silver, iron, gold, and other pure metals or their oxides, make up metal-based nanoparticles. According to Lemire *et al* and Miller *et al*, the generation of reactive oxygen species and impairment of membrane function is the main mechanism of action of nanoparticles (Lemire et al.,2013; Miller et al.,2015). It has been demonstrated that multi-drug-resistant bacteria respond well to nanoparticles (Li et al., 2014; Guzman et al., 2012). Silver-based metal nanoparticles are the most well-established type of nanomaterials. Although the exact method of action of silver nanoparticles is uncertain, leached silver disruption of the membrane and ion-mediated death are two possible mechanisms of action.

Carbon-based nanomaterials comprise graphene, carbon quantum dots (Dong et al., 2020), and nanotubes (Mu et al., 2016; Abdelghany et al., 2012). They cause both chemical and physical harm in their bactericidal activity, while the precise mechanism is still unknown. Multiwalled carbon nanotubes inhibited bacterial adhesion in one investigation, preventing the development of biofilms

including *Klebsiella oxytoca, P. aeruginosa,* and *Staphylococcus epidermidis*. Natural or manufactured polymeric nanoparticles are also possible. Catalytic and pH-switchable antimicrobials are made from natural polymers (Kalhapure et al., 2017) (Omwenga et al., 2018). Antimicrobial peptide action can be replicated by synthetic polymers (Palermo and Kuroda, 2010). Additionally, polymeric micelles are employed as nanocarriers to enhance the pharmacokinetic profiles and boost the solubility, stability, and effectiveness of medications (Palermo and Kuroda, 2010). Dendrimers are regular polymeric molecules with an exterior surface containing functional groups, a central core, and branch-like structures extending from the center. It has been demonstrated that *P. aeruginosa* biofilms are inhibited by glycopeptide dendrimers (Reymond et al., 2013). Inorganic and organic nanoparticle combinations are known as nanocomposites.

For instance, the addition of silver nanoparticles to the cationic polymer poly(2-dimethylamino)ethyl methacrylate resulted in synergistic antibacterial activity against *P. aeruginosa* and *Staphylococcus aureus.* Nanoemulsions are hydrophobic and aqueous emulsions at the nanoscale, composed of dispersed layers. They are often used to encapsulate bioactive materials, such as essential oils, and medicine, to increase their stability and solubility (Jaiswal et al., 2015; Kumari et al., 2018).

Liposomes are vesicles having an aqueous inner core made up of one or more phospholipid bilayers. According to Chang and Yeh, these membrane-based structures are highly compatible and efficient antimicrobial delivery vehicles (Chang and Yeh, 2012). They possess the ability to trap hydrophobic pharmaceuticals in their phospholipid membrane and/or encapsulate hydrophilic medications in their aqueous interior (Bandara et al., 2016; Forier et al., 2014).

Smart materials can change their characteristics and function as antimicrobial agents in response to both endogenous stimuli such as pH and bacterial toxins and external stimuli such as light,

temperature, or ultrasound (Baptista et al., 2018; Chen et al., 2019). Hybrid micelles consisting of polyethylene glycol, poly(aspartamide), 2-(diisopropylamonio) ethylamine, azithromycin, and cis-aconityl-d-tyrosine may shrink in size, reverse surface charge, and release drug cargo. The interactions between bacteria and nanomaterials are influenced by van der Waals forces, receptor-ligand interactions, hydrophobic interactions, and electrostatic attractions.

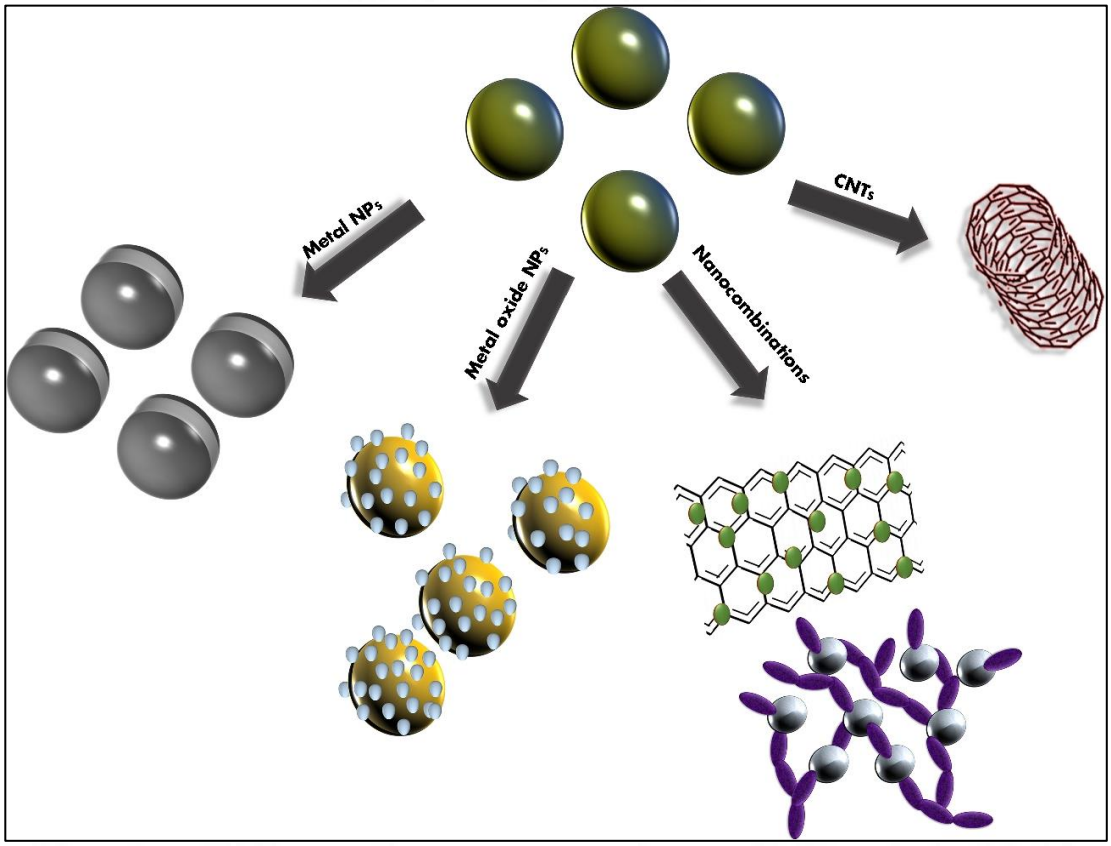

Figure 5: Anti-bacterial nanoparticles that are studied widely (Natan *et al*., 2017)

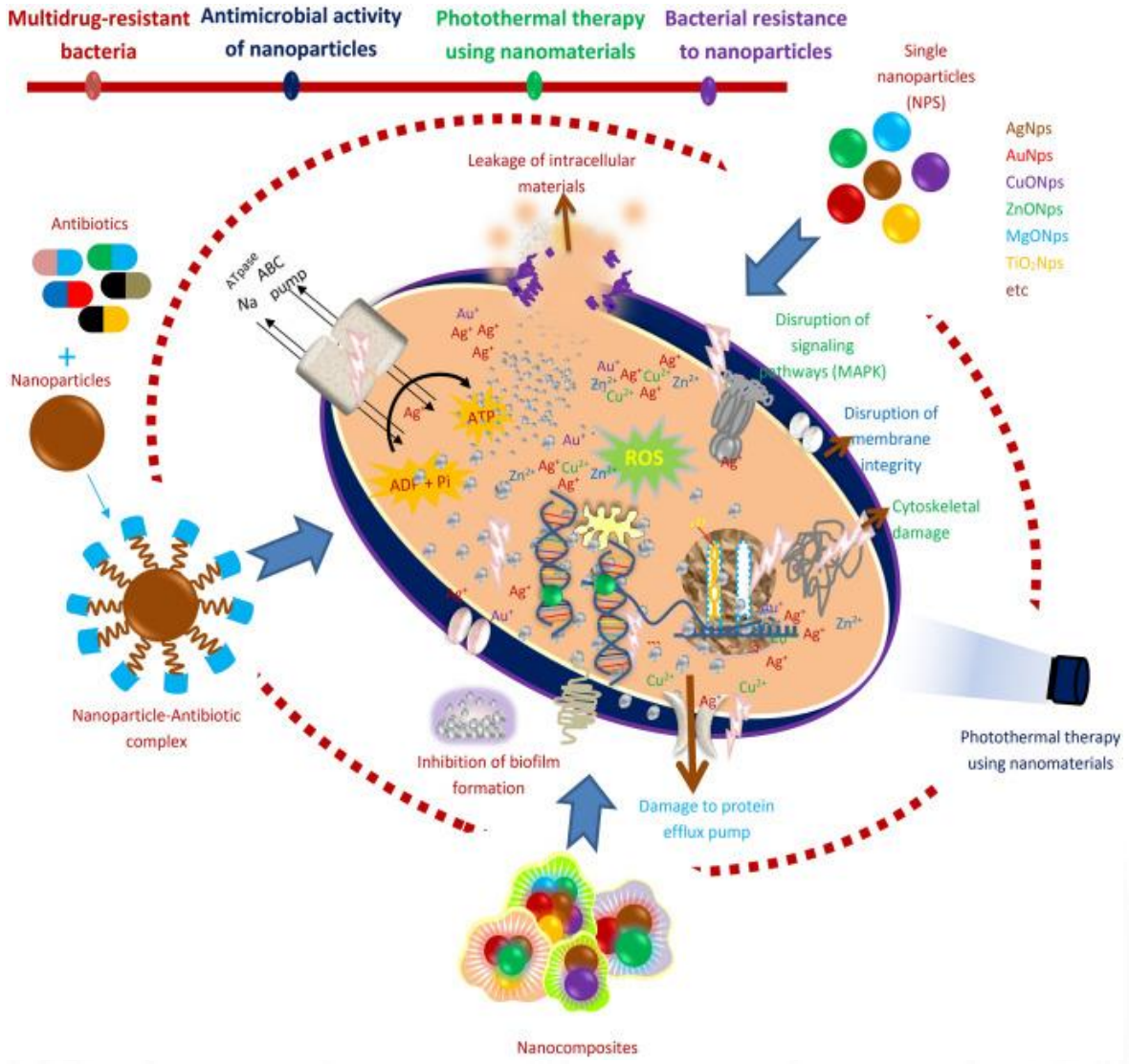

Figure 5: Mechanism of action of various nanoparticles on bacteria (Mba et al., 2021)

2.5. Curcumin

Curcumin is a polyphenolic compound isolated from the rhizome of *Curcuma longa*. Curcumin has been used to treat a wide range of illnesses since ancient times. Over time, scientists have discovered unique features and medical advantages. Curcumin tolerance levels up to 12,000 mg/day, according to Lao et al., make it incredibly safe for human use (Lao et al., 2006).

Curcumin exhibits antibacterial, antiviral, anti-inflammatory, and anti-Alzheimer's activity (Negi et al., 1999; Kuttan et al., 1985; Srimal and Dhawan, 1973; Zhang et al., 2006).

The spectral and photochemical properties of curcumin have been extensively studied by various groups. Curcumin exhibits absorbance maximum at different wavelengths depending on the solvent. In ethanol, curcumin exhibits maximum absorbance at 420 nm and a shoulder at 265 nm. The λ_{max} of curcumin in acetonitrile and methanol are 418 nm and 420 nm respectively. The emission spectrum of curcumin also varies depending on the solvent nature. Curcumin fluorescence is a broad band in ethanol with λ_{max} of 549 nm. Curcumin fluoresces at different wavelength (λ_{max}) in different solvents. The λ_{max} of curcumin in acetonitrile is 524 nm and 549 nm in ethanol (Priyadarsini, 2014a) (Chignell et al., 1994).

There are three major curcuminoids - curcumin, demethoxy curcumin and bis demethoxy curcumin can be identified and separated by High Performance Liquid Chromatography (Anderson et al., 2000). The components can be separated by HPLC as the 3 components have different retention times. The retention time for the three components differs depending on the solvent used for the chromatography. An improved method for the identification and separation of curcuminoids was developed by Jayaprakasha *et al* using a solvent mixture of methanol, 2% acetic acid, and acetonitrile with UV detection at 425 nm. The retention time of curcumin, demethoxy curcumin, and bis demethoxy curcumin in the solvent system is 6.75, 6.4, and 6 minutes respectively (Jayaprakasha et al., 2002). Another group, Wichitnithad, and co-workers developed reverse-phase chromatography on a C-18 column. The solvent system used was acetonitrile and 2% v/v acetic acid in the ratio 40:60. The wavelength for detection was 425 nm. The retention time for curcumin, demethoxy curcumin, and bis demethoxy curcumin is 13.6, 12.1, and 10.8 minutes respectively (Wichitnithad et al., 2009).

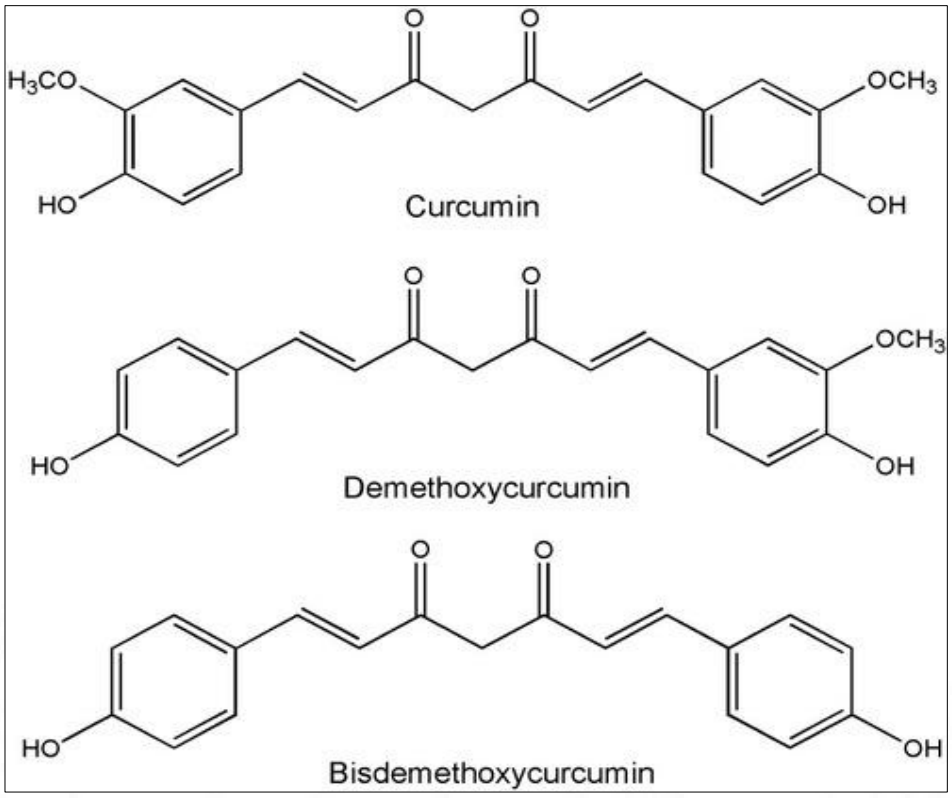

Figure 7: Structure of three curcuminoids (Peng *et al.*, 2021)

2.5.1. Solubility and stability of curcumin in various conditions – pH, temperature, and light

Solubility is one of the major issues concerned with curcumin. Curcumin is insoluble in water in acidic and neutral conditions. It dissolves when the pH is alkaline but tends to degrade rapidly in alkaline pH. Curcumin is soluble in polar solvents like methanol and ethanol and is readily soluble in DMSO (Priyadarsini, 2014).

The major degradation product of curcumin was identified as trans-6-(4'-hydroxy-3'-methoxyphenyl)-2,4-dioxo-5-hexenal whereas vanillin, ferulic acid, and feruloylmethane are the minor products when incubated in 0.1M phosphate buffer, pH 7.2 at 37°C (Wang et al., 1997a). Bicyclopentadione is the major auto-oxidation product of curcumin in physiological conditions

as proved by Griessner and co-workers (Griesser et al., 2011). Light-induced degradation of curcumin in organic solvents results in cleavage of the heptadienone chain, and the most abundant products have been identified as vanillin, ferulic aldehyde, ferulic acid, and feruloylmethane (Tønnesen et al., 1986).

Lee *et al* studied the effect of UV radiation on the chemical stability and bioactivities of curcumin. The degradation rate of curcumin in the presence of UV (254 nm) in water and PBS was found to be accelerated (BH Lee et al., 2013). The effect of pH, storage temperature, and molecular environment on the chemical and physical stability of curcumin in aqueous solution was detailed by Kharat *et al*. They performed a comparative study of the stability of curcumin in aqueous solution and curcumin incorporated in oil-in-water emulsion. The study established that the incorporation of curcumin into oil-in-water emulsions (30% MCT, 1 mg curcumin/g MCT, d32 ≈ 298 nm) improved its water dispersibility and chemical stability (Kharat et al., 2017).

Many approaches have been developed for improving the solubility and stability of curcumin. The complexation of curcumin with cyclodextrins has been found to increase its solubility in aqueous media. Water soluble complexes of curcumin with hydroxyl propyl derivatives of cyclodextrin were synthesized in the mole ratio 2:1 as well as 1:1 (CD: curcumin) (Mohan et al., 2012). Curcumin complexes with divalent cations have been synthesized and characterized by many groups. The synthesis is however done under a high-temperature reflux method like reflux at 100°C under nitrogen gas for 3 hours. Gallium curcumin complexes were synthesized by Mohammadi *et al* by refluxing gallium nitrate and curcumin with methanol as a solvent in the presence of triethylamine followed by cooling and filtration of the solid product (Mohammadi et al., 2005). Curcumin complexes with divalent cations Zn2+, Cu2+, Se2+, and Mg2+ were successfully prepared by Zebeib *et al.* The metal-curcumin complexes were found to be twenty-

fold more stable when complexed with metal ions and the degradation rate of curcumin was below 5% (Zebib et al., 2010).

Another approach to improve stability and solubility is the incorporation of curcumin into liposomes and nanomicelles. In one such approach, nanomicelle curcumin was formulated which was found to have excellent stability in vivo and anti-inflammatory properties (Li et al., 2017). Hasan *et al* have formulated curcumin-incorporated nanoliposome with increased bioavailability and exhibited anti-proliferative activity against MCF-7 cells (Hasan et al., 2014). Curcumin-loaded liposomes using phospholipids were synthesized and evaluated for their anti-cancer activity *in vitro.* Out of the three curcumin-loaded liposomes synthesized the one that used soybean phospholipid was found to have an excellent anti-melanoma effect when compared to curcumin (Chen et al., 2012). Spherical curcumin-loaded PLGA nanospheres of mean particle size 45 nm with an excellent encapsulation efficiency of 90% were synthesized by Mukherjee *et al* (Mukerjee and Vishwanatha, 2009).

2.5.2. Curcumin nanoparticles/nanoformulations

Curcumin in nanoparticle form was formulated by many groups to improve its stability, solubility, bioavailability, antibacterial and anticancer activity. Solid lipid nanoparticles (SLN), polymeric nanoparticles, silver and gold nanoparticles, nanocapsules, liposomal and micellar delivery systems, cyclodextrins, dendrimers, and niosomes are the main nanoformulations (Gera et al., 2017; Karthikeyan et al., 2020). Given curcumin's limited bioavailability, pharmacokinetic profile with fast metabolism, photodegradation, and aqueous solubility (Sharifi-Rad et al., 2020; Tiyaboonchai, Tungpradit, & Plianbangchang, 2007), these practical and effective systems can both facilitate and enhance the biological activity of curcumin. In curcumin nanoformulations, the molecule is embedded in a variety of substances, including polyethylene glycol (PEG)

monoacrylate, gelatin-based nanofibers, (Bisht et al., 2007; Chereddy et al., 2013; Flora et al., 2013; Gopinath et al., 2004; Krausz et al., 2015) collagen, also known as polylactic-co-glycolic acid (PLGA).

Dendrimer-based nanoparticles enhanced the solubility of curcumin in a formulation containing polyamidoamine dendrimer (Falconieri et al., 2017). Enhanced oral bioavailability of curcumin was observed in silica-coated flexible liposomes and the increase in bioavailability was 7.76-fold higher compared to native curcumin solution (C Li et al., 2012). Curcumin (1 h mean half-life) in PLGA and PLGA-PEG blend nanoparticles increased the curcumin mean half-life in about 4 and 6 h, respectively, and the Cmax increased 2.9 and 7.4 times, respectively (Khalil et al., 2013). Moreover, the use of nanoparticles-carrier, specifically PLGA-PEG nanoparticles, was associated with a decrease in both curcumin distribution and metabolism.

Metal nanoparticles conjugated curcumin were also reported to have improved stability and solubility. Silver-curcumin NPs, Gold-silver nanoparticles, curcumin-stabilized zinc nanoparticles, and copper nanoparticles have been reported by various groups for enhanced antibacterial and anticancer activity compared to native curcumin. The antibacterial properties of such nanoparticles are described in section 2.5.3. Metal oxides reported to have been used as drug carriers for curcumin include TiO_2, CuO, ZnO, $Fe3O_4$, and CeO_2. Anti-cancer activity of curcumin was found to be enhanced when curcumin was conjugated with iron oxide nanoparticles against hepatocellular carcinoma (Darwesh and Elbialy, 2021). Curcumin is utilized in the synthesis of gold quantum clusters as a capping and reducing agent which has considerably reduced the cytotoxicity to normal cells but remained toxic to cancer cells (Mahmoudi et al., 2022).

2.5.3. Anti-bacterial activity of curcumin and curcumin nanoformulations

The anti-microbial activity of nanocurcumin was studied by Basniwal *et al*. The nanoparticles were prepared by wet-milling technique and the size range was 2- 40 nm. The particle was found to be effective against *Staphylococcus aureus, Bacillus subtilis, E coli, Pseudomonas aeruginosa, Penicillium notatum and Aspergillus niger* (Bhawana et al., 2011).

In a green approach to nanoparticle synthesis, curcumin was used for the synthesis of gold nanoparticles. Curcumin acts as both a reducing agent and a capping agent. These nanoparticles showed hemocompatibility and is less cytotoxic (Sindhu et al., 2014). A similar approach has been successful in the synthesis of silver nanoparticles also. Recently silver-curcumin nanoparticle was reported to have anti-biofilm activity against clinically important strains by Jaiswal *et al.* They reported that these silver curcumin nanoparticles low in silver content were more effective against both Gram-positive and Gram-negative bacteria and less toxic to human keratinocytes (Jaiswal and Mishra, 2018a). Antibacterial properties of silver nanoparticles were found to be enhanced when cyclodextrin was used as a capping agent. The group reported that the increased activity may be due to a Trojan horse mechanism of increased affinity of bacteria for carbohydrates which delays its growth increasing the silver ion absorption (Jaiswal et al., 2010).

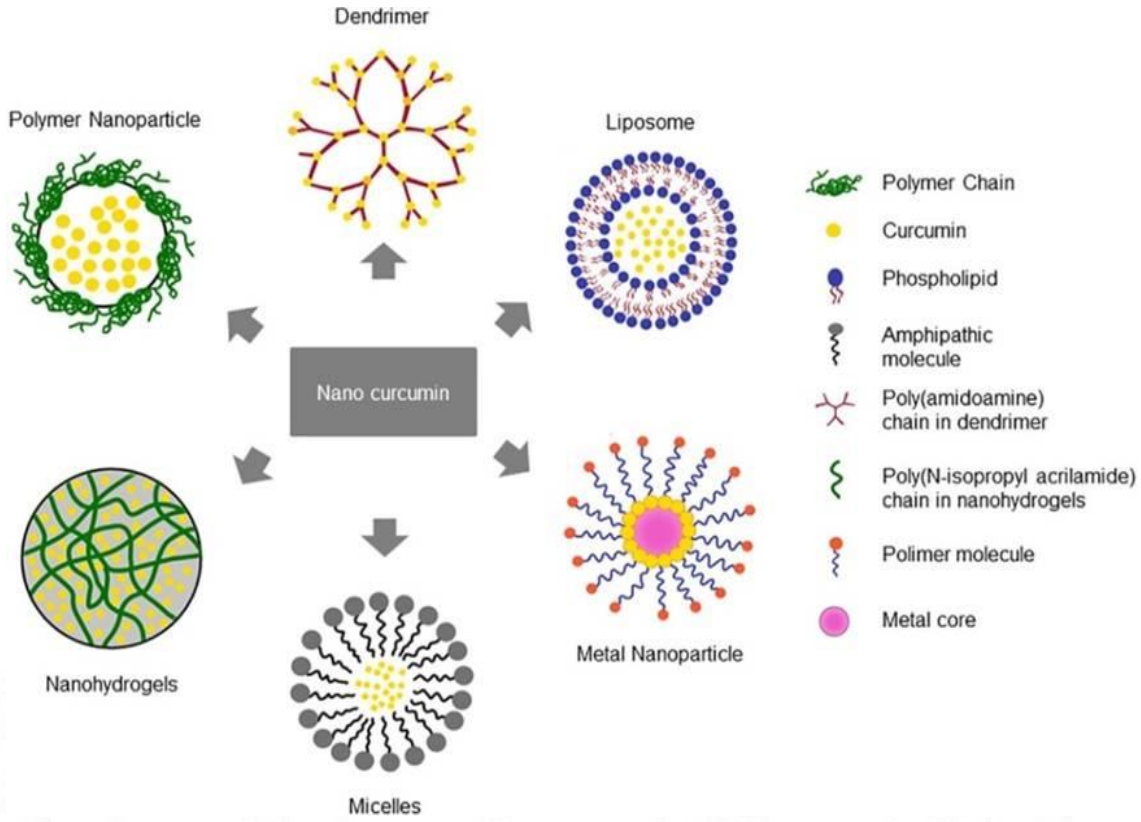

Figure 8: Different nanoformulations of curcumin (Praditya *et al.*, 2019)

The broad spectrum anti-bacterial nature of curcumin is attributed to its membrane-damaging properties. A comprehensive study by Tyagi *et al* proved that the bactericidal activity of curcumin is brought about by membrane leakage. Curcumin acts on both Gram-positive and Gram-negative bacteria which confirms its broad-spectrum nature (Tyagi et al., 2015a). The MIC of curcumin for 7 clinically important strains including MRSA, MSSA, *Pseudomonas aeruginosa*, and *Klebsiella pneumoniae* were determined and evaluated as 219 µg/mL, 217 µg/mL, 175 µg/mL, and 216 µg/mL respectively (Gunes et al., 2016).

Starch-stabilized nanoparticles were reported to be biofilm disrupting and exhibit better antibacterial activity than human cationic antimicrobial peptide LL-37 (Mohanty et al., 2012). Silver-curcumin NPs (Cur-SNPs) combination showed better and increased activity against

Pseudomonas aeruginosa as well as *Staphylococcus aureus* in comparison with CurNPs. The Cur-SNPs disrupted 50% of established biofilm formed on microtitre plates (Loo et al., 2016).

Curcumin inhibits the infectivity of enveloped viruses. Anti-viral effects of curcumin against enveloped viruses Zika and chikungunya were proved by Mounce *et al.* It was shown that the infectivity of the virus reduced in a time and dose-dependent manner. Even though the integrity of the genetic material (RNA) was maintained curcumin interrupted with the binding of these viruses to the host cell (Mounce et al., 2017) . Human Immunodeficiency virus infection was inhibited by the action of curcumin via its anti-integrase activity. Curcumin interacts with the core catalytic domain of the integrase enzyme of HIV (Mazumder et al., 1995). Curcumin-modified silver nanoparticles are reported to be highly efficient in inhibiting respiratory syncytial virus infection. (Yang et al., 2016)

Shlar et al compared the anti-microbial action of two curcumin formulations – methyl b-cyclodextrin supramolecular inclusion complex and poly electrolyte-coated monolithic nanoparticles. The study showed that the cyclodextrin-curcumin inclusion complex exhibits bactericidal activity whereas curcumin nanoparticles showed bacteriostatic activity against *E. coli* (Shlar et al., 2017).

The synergistic effects of curcumin along with antibiotics have been studied by various groups. The synergistic antibacterial activity of curcumin along with each of the antibiotics oxacillin, ampicillin, ciprofloxacin, and norfloxacin was studied by Mun *et al*. The group conducted the study on 10 different methicillin-sensitive as well as methicillin-resistant *Staphylococcus aureus* strains. The MIC of curcumin against these strains ranges from 125ug/mL to 250ug/mL. Curcumin showed excellent synergistic activity against ATCC 25923 along with oxacillin.

Curcumin also showed synergy along with ampicillin against the above-mentioned strain of methicillin-resistant *Staphylococcus aureus*. (Mun et al., 2013). In an independent study, it was reported that curcumin reduces the antimicrobial activity of ciprofloxacin towards specific strains of bacteria. When treated with ciprofloxacin and curcumin together, curcumin inhibited the activity of ciprofloxacin against *Salmonella typhi* and *Salmonella typhimurium* because of its antioxidant action against the oxidative burst induced by ciprofloxacin (Marathe et al., 2013).

The antifungal activity of curcumin has also been widely studied. Martin *et al* studied the anti-fungal activity of curcumin against 23 fungal strains and also demonstrated the anti-adhesive effect of curcumin against Candida species on human buccal epithelial cells (Martins et al., 2008). The study concluded that curcumin was able to inhibit the growth of clinical isolates of *Candida dupliniensis* Cd22 and Cd28 at a lower concentration of 32 µg/mL. *Candida albicans* was more susceptible to curcumin than the non-albicans species.

2.5.4. Anti-biofilm activity of curcumin against biofilm-forming bacteria

It has been shown that curcumin inhibits the QS system, which can diminish P. aeruginosa pathogenicity and biofilm formation (Abdulrahman et al., 2020; Sethupathy et al., 2016). Through an *in silico* study, curcumin was found to be a QS inhibitor of LasR, leading to the reduction of biofilm formation and other virulence factors (Shukla et al., 2021). Curcumin was shown to be a QS inhibitor in this investigation against both the LuxS/AI-2 QS system and the LasI/LasR QS system. Curcumin (at 200 µg/mL) reduced *P. aeruginosa* PA14's synthesis of 3-oxo-C12-HSL by 21% in the LasI/LasR QS system. This behavior was also verified by that achieved a 25% reduction of 3-oxo-C12-HSL production by *P. aeruginosa* PAO1 exposed to a sub-inhibitory concentration of curcumin (at 1 µg/mL) (Rudrappa and Bais, 2008). Inhibition of biofilm formation and diverse virulence factors, like pyocyanin biosynthesis and

elastase/protease activity, were also observed. The same authors reported a MIC value for curcumin of 30 µg/mL instead of the 200 µg/mL found in this study. These differences in concentrations could be related to the bacterial strains used and the purity/availability of curcumin. Curcumin inhibited the LasI/LasR QS system by 21% at 200 µg/mL (Fernandes et al., 2023). Anti-biofilm activity of curcumin-loaded electrospun fiber against *P. aeruginosa* PAO1 was demonstrated by Salle *et al* (Di Salle et al., 2021). The initial steps of biofilm formation were significantly inhibited by curcumin-loaded fiber.

2.5.5. Choice of metal for conjugation of curcumin

In our study, we have chosen Gallium for conjugating curcumin. Gallium is a non-toxic metal belonging to group 13. Gallium finds its application in various fields including medicinal applications. Gallium nitrate and radioactive gallium find their use as diagnostic and therapeutic agents respectively. Citrate-buffered Gallium nitrate (Ganite®) is an FDA-approved drug and is used for the treatment of hypercalcemia post-chemotherapy (Warrell et al., 1986). To create therapeutic complexation, gallium was studied in relation to chelating with a variety of binding ligands, including nitrate, maltolate, citrate, chloride, quinolinolato, naphthoquinone, and heme analog ligands. Additionally, the primary areas of research on gallium coordination compounds are antibacterial and anticancer. Gallium salts have been extensively explored for their antibacterial and anti-biofilm activities. The antibacterial activity of gallium is due to its similarity with Fe^{3+}. Ga^{3+} mimics Fe^{3+} and is thus actively absorbed by bacteria. But unlike Fe^{3+}, Ga^{3+} is unable to undergo a reduction cycle thus repressing the activity iron containing enzymes involved in DNA synthesis and repair, metabolism, respiration, and even oxidative stress (Bernstein, 1998). Singh *et al* have demonstrated the activity of Gallium against *Pseudomonas aeruginosa* both in planktonic form and biofilm form. They reported that the antibacterial effect

is brought about by the disruption of iron metabolism in the bacteria. Gallium nitrate was found to be effective against multi-drug resistant *Acinetobacter baumanii* both *in vitro* and *in vivo.* Gallium nitrate in a concentration ranging from 4 to 64 uM delayed the entry of *Acinetobacter baumanii* into the exponential phase and depleted the growth of bacteria in human serum (Antunes et al., 2012).

Gallium-protoporphyrin complex was found to inhibit the growth of *P. aeruginosa* in iron-depleted conditions. They also demonstrated that gallium-protoporphyrin enters the bacterial cells via the heme-uptake system primarily through PhuR receptor and inhibits the aerobic growth of bacteria by inhibiting cellular respiration (Hijazi et al., 2017). Gallium (III) - citrate was found to be inhibitory against *P. aeruginosa* with IC_{90} values ranging from 20 to 40 µM whereas the inhibitory concentration for *S aureus* was in the millimolar range (Rzhepishevska et al., 2011) (Baldoni et al., 2010). Gallium nitrate was shown to be effective against bacteria encountered in burn wound infection with a MIC of 512 µg/mL against *P. aeruginosa, K. pneumonia, E. cloacae, A. baumannii, S. maltophilia, S. aureus* and *S. epidermidis* (Xu et al., 2017). Gallium-curcumin and Cu-curcumin were found to exhibit remarkable antiviral activity against Herpes simplex virus (HSV-1 in Vero cell line (Zandi et al., 2010)

Gallium-doped phosphate-based glasses (PBGS) are reported to have antibacterial activity. Gallium release from the phosphate-based glass was found to be a controlled release. The gallium ion release and anti-microbial activity against *P. aeruginosa* are directly proportional to the calcium content in the PBG (Valappil et al., 2009). The anti-bacterial activity of gallium nitrate against 9 bacterial strains has been evaluated by Xu *et al*. The MIC of gallium nitrate against Gram-positive *Staphylococcus aureus, Staphylococcus epidermidis,* and Enterococcus *faecalis* is 512, 512, and 256 µg/mL respectively whereas the MIC against Gram-negative *E. coli, P.*

aeruginosa, Klebsiella pneumoniae, Acinetobacter baumanii, and *S. maltophilia* are 256 and 512 µg/mL respectively.

2.6. Raman spectroscopy as a tool for identification of bacteria and studying the effects of anti-bacterial agents

Raman spectroscopy and Confocal Raman microscopy are now widely being exploited as a tool for the identification of bacteria as well as studying the effect of anti-bacterial agents on bacteria and bacterial biofilms. This fast, non-invasive, and label-free technique is gaining wide acceptance in the field of bacteriology. This nondestructive spectroscopic method known as Raman microscopy uses the spatial resolution of an optical microscope to produce fingerprint spectra through the Raman scattering of monochromatic laser light. Raman spectroscopy and a microscope are commonly integrated, allowing for spectrum analysis with a spatial resolution of micrometers.

Raman microscopy was used as a tool to distinguish between planktonic and biofilm forms of *Pseudomonas* sp. using the fingerprint region of Raman spectra (Henry et al., 2017). Biofilm formation by different strains of *Pseudomonas aeruginosa* has been studied by various groups using confocal Raman microscopy. Sandt *et al* used confocal Raman microscopy to study the distribution of components in fully hydrated *Pseudomonas aeruginosa* biofilm (Sandt et al., 2007). Ag nanoparticle-mediated SERS and PCA analysis was used to map the major virulence factor pyocyanin in the *P.aeruginosa* strain (Polisetti et al., 2017). Confocal Raman imaging along with secondary ion mass spectrometry was employed for *in situ* characterization of the distribution of quinolone. Confocal Raman imaging was used as a tool for imaging by many groups complementary with FISH and other techniques (Kniggendorf et al., 2016). Feng *et al* employed confocal Raman microscopy in combination with CLSM to study the growth of

biofilm with respect to time and for differentiating stages of biofilm development (Feng et al., 2015). Confocal Raman microspectroscopy was used for studying the structure and composition of biofilm and the formation of *Pseudomonas aeruginosa* biofilm. (Beier et al., 2012) Chemical characterization of the biofilm matrix was done by Raman microscopy of microbial components as well as extracellular polymeric substances (Ivleva et al., 2009). Raman microscopy was used as a tool to distinguish between planktonic and biofilm forms of Pseudomonas sp. using the fingerprint region of Raman spectra (Henry et al., 2017). The effect and mode of action of various antibiotics on *P. aeruginosa* biofilm was studied by Jung *et al* using Raman spectroscopy and multivariate analysis (Jung et al., 2014). Fiber probe-based Raman spectroscopy along with chemommetric analysis was used for the identification of different species of bacteria involved in biofilm-related infection (Shen et al., 2022).

According to Janissen *et al*. (2015), Raman microscopy can reveal the structure and chemical makeup of EPS at various phases of biofilm development. In particular, symmetrical modes of molecular motion of the analyte molecule, which are not detected by conventional infrared spectroscopy, represent a huge benefit of Raman microscopy (Neugebauer *et al*., 2002). Raman microscopy may successfully augment CLSM analysis, as demonstrated by the use of RM by Ivleva *et al* and Wagner *et al* to monitor the chemical composition of various EPS types during the biofilm development process at specific Raman bands (Ivleva et al., 2009; Wagner et al., 2009). It can consistently identify alterations in the biofilm matrix's chemical makeup, even ones that CLSM is unable to pick up on. It provides information on the label-free EPS components of completely hydrated biofilms *in situ* with little to no sample preparation needed. Furthermore, in contrast to CLSM, RM does not require an adjustable excitation source as it may be excited at a set laser wavelength to gather the whole spectrum (Ivleva et al. 2008).

2.6.1. Raman spectroscopy to study the effect of antibacterial agents on *P. aeruginosa*

P. aeruginosa biofilm has been studied and the effect of various antibiotics on *P. aeruginosa* was deduced in detail using Raman spectroscopy and Principal component analysis (PCA) (Jung et al., 2014). The effect of UV irradiation on *E.coli, Serratia marcescens,* and *Micrococcus luteus* was studied using Raman spectroscopy. All the bacteria studied were irradiated with UV rays for a period ranging from 0 minutes to 20 minutes and the Raman spectra were recorded using a 638 nm laser. An increase in thymine dimer formation was observed in the Raman spectra with an increase in time of irradiation.(Li et al., 2019). Anti-bacterial mechanism of graphene oxide on *E. coli* and *E. faecalis* was evaluated using Raman spectroscopy (Nanda et al., 2016). The membrane lysing activity of graphene oxide on these bacteria was proved by taking Raman spectra after treatment with different concentrations of GO. Other biochemical assays were also conducted to prove the membrane lysing evidence of bacterial cells obtained from Raman spectroscopy. Munchberg *et al* concluded that differences in bacteria treated with antibiotics can be identified. Two strains of *E.coli* and two species of *Pseudomonas* were treated with four antibiotics having different mechanisms of action and were used for the study (Münchberg et al., 2014).

Ag nanoparticle-mediated SERS and PCA analysis were used to map the major virulence factor pyocyanin in *P. aeruginosa* strain (Polisetti et al., 2017). Confocal Raman imaging along with secondary ion mass spectrometry was employed for *in situ* characterization of the distribution of quinolone. Confocal Raman imaging was used as a tool for imaging by many groups complementary with FISH and other techniques (Kniggendorf et al., 2016). Feng *et al* employed confocal Raman microscopy in combination with CLSM for studying the growth of biofilm with respect to time and for differentiating stages of biofilm development (Feng et al., 2015). Confocal Raman microspectroscopy was used for studying the structure and composition of

biofilm and the formation of *P. aeruginosa* biofilm (Beier et al., 2012). Chemical characterization of the biofilm matrix was done by Raman microscopy of microbial components as well as extracellular polymeric substances (Ivleva et al., 2009).

The effect and mode of action of various antibiotics on *P. aeruginosa* biofilm were studied by Jung *et al* using Raman spectroscopy and multivariate analysis (Jung et al., 2014). Fiber probe-based Raman spectroscopy along with chemometric analysis was used for the identification of different species of bacteria involved in biofilm-related infection (Shen et al., 2022). Estevez *et al* studied the effect and mechanism of action of biogenic silver nanoparticles using confocal Raman microscopy along with ESEM and SEM (Estevez et al., 2020).

2.7. Gap area, Relevance of the current study, and Hypothesis

P. aeruginosa is an intrinsically antibiotic-resistant microorganism that plays a very important role in hospital-based infections. *P. aeruginosa* is also involved in various skin infections and is often isolated from burn wounds. *P. aeruginosa* biofilms were isolated from almost all medical devices ranging from hip prostheses to catheters. Often these isolates are resistant to various antibiotics due to adaptive resistance as well. Finding alternative antibacterial agents that can effectively control the growth of these resistant bacteria has become a clinical necessity. Curcumin is known for its antibacterial as well as antibiofilm properties but is known to have poor stability in physiological pH. After reviewing the literature, we hypothesized that conjugating curcumin with a metal can considerably improve its stability without compromising its anti-bacterial properties. Gallium was chosen owing to its non-toxic nature. Also, nanoparticle formulations have improved antibacterial properties compared to their bulk counterparts. Gallium-curcumin complexes reported by Mohammadi *et al* exhibited negligible antibacterial

activity (Mohammadi et al., 2005). In this work, we synthesized gallium-curcumin nanoparticles (GaCurNPs) that possess antibacterial activity against the notorious pathogen *P. aeruginosa*. Curcumin bound to the particle also exhibited improved stability with a very low rate of degradation at physiological pH. We have also utilized Raman spectroscopy as a tool for studying the effect of GaCurNPs on *P. aeruginosa*. This work also contributes to the scope of utilizing Raman spectroscopy as a tool for studying the effect of antibacterial compounds on different bacteria within a very short period.

CHAPTER 3

3. MATERIALS AND METHODS

3.1. Materials

The chemicals and bacterial strains used in the study are listed in the tables below.

Table 2: Chemicals used for the experiments

Name of the chemical	Source	Purity
Acetonitrile	Merck Millipore, Germany	≥ 99.9% Gradient grade for liquid chromatography
Chloroform	Sisco Research Laboratories Pvt. Ltd., India	99.5%, Extrapure, AR grade
Citric acid	Central Drug House Pvt. Ltd., New Delhi	99.0%, LR grade
Curcumin (trade named Biocurcumin)	Arjuna Natural Extracts Ltd., Aluva, India	Contains 95% curcuminoids
2,7- dichloroflourescin diacetate	Sigma Aldrich, USA	≥ 97% HPLC grade
Ethanol	SD Fine chemicals, Mumbai	99.9% ACS reagent
Formic acid	Merck Millipore, Germany	98- 100% Ph. Eur. Grade
Gallium (III) chloride	Sigma Aldrich, USA	≥ 99.999% anhydrous
Gluteraldehyde	Sigma Aldrich, USA	Grade 1, 25% in water
Hydrochloric acid	Sigma Aldrich, USA	37% ACS reagent
Sodium chloride	Central Drug House Pvt. Ltd., New Delhi	99.9% ACS reagent
Tetrahydrofuran	Spectrochem Pvt. Ltd., Mumbai	99.9% HPLC Grade

The table given below tabulates the media and chemicals used for the bacteriology work.

Table 3: Media/Chemicals used for bacteriology work

Media/chemical	Source	Purity/Grade
Agar	Himedia Laboratories Pvt. Ltd., Mumbai	Bacteriological
Ciprofloxacin hydrochloride monohydrate	Himedia Laboratories Pvt. Ltd., Mumbai	98.00% - 102.00%
Dextrose	Himedia Laboratories Pvt. Ltd., Mumbai	99.00%
Luria-Bertani broth	Himedia Laboratories Pvt. Ltd., Mumbai	
Mueller-Hinton broth No.2 control cation	Himedia Laboratories Pvt. Ltd., Mumbai	
Nutrient broth	Himedia Laboratories Pvt. Ltd., Mumbai	
Peptone	Himedia Laboratories Pvt. Ltd., Mumbai	Bacteriological
Tryptone	Sigma Aldrich, USA	Microbiologically tested
Yeast extract	Himedia Laboratories Pvt. Ltd., Mumbai	Bacteriological

The following table (Table 4) lists the kits used for live dead assay and qPCR.

Table 4: Kits used for live dead assay and qPCR experiments

Name of the kit	Source
Baclight® cell viability assay kit	Invitrogen (Thermo Fisher Scientifc Inc.)
Primescript RT-PCR kit	Takara Bio Inc.
TB Green Premix Ex Taq II	Takara Bio Inc.

The following table tabulates the bacterial strains used in the anti-bacterial study. For studying the anti-bacterial effect of GaCurNPs in clinical strains of bacteria, IEC approval was obtained from the Institutional Ethics Committee (**IEC/1928**).

Table 5: Bacterial strains used for anti-bacterial studies

Bacterial strain	Source	Remarks
Pseudomonas aeruginosa ATCC 27853	ATCC	Procured from ATCC
P. aeruginosa clinical strain 1	Urine	Isolated from urine sample of a patient
P. aeruginosa clinical strain 2	ET	Isolated from the endotracheal tube of a patient
P. aeruginosa clinical strain 3	ET	Isolated from the endotracheal tube of a patient
P. aeruginosa clinical strain 4	ET	Isolated from the endotracheal tube of a patient
P. aeruginosa clinical strain 5	Blood	Isolated from the blood sample

For Raman spectral library preparation strains of the following bacteria were used.

Table 6: Bacterial strains used for Raman spectral library preparation

Bacterial strain	Source	Remarks
Acinetobacter baumannii ATCC 19606	ATCC	Procured from ATCC
Escherichia coli ATCC 25922	ATCC	Procured from ATCC
Pseudomonas aeruginosa ATCC 27853	ATCC	Procured from ATCC
Pseudomonas aeruginosa	Blood/ET	Clinical isolate
Staphylococcus aureus ATCC 25923	ATCC	Procured from ATCC
Methicillin-resistant *Staphylococcus aureus*	Blood	Clinical isolate

MilliQ water was used in all experiments conducted.

3.2. Methods

3.2.1. Synthesis and Characterization of Gallium-curcumin nanoparticles (GaCurNPs)

3.2.1.1. Characterization of raw material

Curcumin used for the synthesis of GaCurNPs was checked for its purity using reverse-phase high-performance liquid chromatography (HPLC, LC-2010A, HT, Shimadzu, Japan). A stock solution of 5mg/mL of curcumin was prepared in ethanol. A working solution of 500 μg/mL was prepared in ethanol. The analysis was done using the C-18 column. 1% citric acid and THF (60:40) was used as the solvent system with an isocratic flow rate of 0.7 mL/minute at an oven temperature of 30°C (Wang et al., 1997b). 20 μL was fixed as the injection volume and the curcuminoids were detected at a wavelength of 420 nm.

Curcumin was further characterized using FT-IR spectroscopy as well as Raman spectroscopy. The FT-IR spectra were obtained from Nicolet 5700 (Thermo Fisher Scientific, USA) spectrophotometer with a scan range of 400 – 4000 cm^{-1}. Raman spectra of curcumin were recorded using a Confocal Raman Microscope, with an excitation wavelength of 785 nm using Alpha300 RA, WITec, GmbH.

3.2.1.2. Synthesis of GaCurNPs

Synthesis of GaCurNPs was done by a simple procedure devoid of the addition of a reducing agent or any toxic solvent. Different concentrations of Gallium chloride and curcumin combinations were made to react and finally, the following concentrations were optimized. 0.2 mM Gallium chloride in an aqueous solution was made to react with 4mg/mL curcumin in ethanol at room temperature. The solution was stirred at 200 rpm for an initial 1 hour and then kept in the dark for 48 hours. The reaction mixture turns greenish yellow on the formation of the GaCurNPs. The unreacted curcumin was removed by pressure filtration through a 100 kDa filter.

The resultant solution was lyophilized. The lyophilized powder was used for chemical characterization.

3.2.2. Characterization of GaCurNPs

3.2.2.1. Determination of Size and Zeta Potential

The hydrodynamic diameter and the zeta potential of GaCurNPs in the suspension were measured using Malvern Zetasizer Nano, Malvern Instruments, UK. The temperature was kept constant at 25°C during the measurement. The nanoparticle suspension was kept at room temperature (25-28°C) for 365 days and the size and zeta potential were measured using the same equipment mentioned above.

3.2.2.2. TEM Analysis

Transmission Electron microscopy (TEM, Hitachi H-7650) was used to study the morphological features of the GaCurNPs. A drop of the nanoparticle suspension was air-dried on a carbon-coated copper grid. High-resolution TEM images of GaCurNPs were obtained using JOEL, JEM-2100.

3.2.2.3. X-Ray Diffraction

The crystalline structure of GaCurNPs and curcumin was examined by XRD analyses. Rigaku DmaxC model with CuKα radiation (λ = 1.5418 Å) was used for the study. The analysis was done at 25°C.

3.2.2.4. UV spectroscopy and fluorescence spectroscopy

The absorbance of the synthesized GaCurNPs and curcumin was recorded using a UV-1800 Shimadzu spectrophotometer. The scan wavelength was from 200 nm to 800 nm.

Emission spectra of curcumin and GaCurNPs were measured using a fluorimeter. Curcumin and GaCurNPs were excited at wavelength of 420 nm and emission spectra were recorded from 400 to 800 nm.

3.2.2.5. FT-IR Spectroscopy

GaCurNPs were characterized by FT-IR spectroscopy using Nicolet 5700 (Thermo Fisher Scientific, USA) spectrophotometer. The scanning range was 400 – 4000 cm^{-1} and the KBr pellet method was employed.

3.2.2.6. Raman spectroscopy

Raman spectra of Curcumin and GaCurNPs were recorded using a Confocal Raman Microscope, with an excitation wavelength of 785 nm using Alpha300 RA, WITec, GmbH. The lyophilized powder of GaCurNPs was placed on a glass slide and the spectra were recorded.

3.2.2.7. X-ray Photoelectron Spectroscopy

The elemental analysis of GaCurNPs was performed using X-ray photoelectron spectroscopy. PH1500 Versa Probe II (ULVA-PHI Inc., USA) equipped with micro-focused (200um, 15 KV) monochromatic Al-Kα X-ray source ($h\nu$ =148.6eV) was used to record the spectra. First survey scans were acquired on the sample and for the major detected elements, high-resolution spectra were recorded. These spectra were used for estimating elemental composition (% At) and chemical state assignment by curve fitting software. Survey scans were recorded with X-ray source power of 23.7 W and pass energy of 187.85eV. High-resolution spectra of the major elements were recorded at 46.95eV pass energy.

3.2.3. Quantification of curcumin content in GaCurNPs by RP- HPLC

The concentration of curcumin per milligram of GaCurNPs was quantified using RP- HPLC (HPLC, LC-2010A, HT, Shimadzu, Japan). The analysis was done using the C-18 column. 1% citric acid and THF (60:40) was used as the solvent system with an isocratic flow rate of 0.7 mL/minute at an oven temperature of 30°C (Wang et al., 1997b). 20 µL was fixed as the injection volume and the curcuminoids were detected at a wavelength of 420 nm. The data analysis was done using LC-solution software. The standard curve of curcumin was plotted with different concentrations of curcumin against the area under the peak. The concentrations of curcumin are 3.125, 6.25, 12.5, 25, 50, and 100 µg/mL with $R^2 = 0.994$.

3.2.4. Quantification of Gallium by Inductively Coupled Plasma- Optical Emission Spectrometry (ICP-OES)

Gallium in GaCurNPs was estimated using ICP-OES. Curcumin solution containing 200 µg/mL was used as control. A known quantity of the sample was acidified and analyzed as per the work procedure for ICP-OES analysis (AOAC: Official Methods of Analysis (Volume 1), n.d.). The concentration of the element in the solution was determined from the calibration plot obtained by analyzing standard solutions. The results were recorded and processed using Win Lab 32 software.

3.2.5. Stability of curcumin in GaCurNPs

3.2.5.1. Stability of Curcumin by Reverse Phase- High Pressure Liquid Chromatography

The degradation of curcuminoids bound to GaCurNPs was analyzed using RP-HPLC. GaCurNPs and bare curcumin were incubated in PBS for 24 hours at 37°C in a shaker incubator with 80 rpm. Samples were collected every hour till the 6^{th} hour and then at 24 hours of incubation. Curcuminoids in GaCurNPs were extracted using ethanol and then the samples were loaded into

HPLC. The parameters were the same as mentioned in section 3.3. The percentage of degradation was calculated as:

$$\%\ Degradation\ of\ curcumin = \frac{Ao-An}{Ao} \times 100$$ **(**Equation 1**)**

A_0 = Area under the curve at 0 hour; A_n= Area under the curve at n^{th} hour

3.2.5.2. Stability of curcumin by Liquid Chromatography-Mass spectrometry

Tandem mass spectroscopy (LC-MS/MS) was employed to understand the degradation of native curcumin and GaCurNPs in a phosphate buffer medium. In this experiment, equal weights of curcumin and GaCurNPs were incubated in tubes containing 20 mL of phosphate buffer (pH 7.4) maintained at 37°C and 80 rpm in a shaker incubator. For the analysis, 500 µL of the incubating solution was pipetted out of the tube into a vial and mixed with 500 µL of HPLC-grade ethyl acetate for liquid-liquid extraction. The tube was vortexed well and after the complete separation of the two phases, the upper ethyl acetate layer (containing the curcumin) was transferred to amber-colored LC vials. The vial was evaporated to dryness and the sample solution was reconstituted with a 1:1 mixture of acetonitrile and 0.1% formic acid, the mobile phase. Sample solutions corresponding to curcumin and GaCurNPs were prepared for every hour starting from 0 hours till the 6^{th} hour and then at 24 hours by taking 500 µL aliquots from different tubes incubated under the same conditions.

The procedure followed for this experiment was a slightly modified protocol reported by Ramalingam *et al.* (Ramalingam and Ko, 2014). Chromatographic separation of curcumin was done using Symmetry® C18 3.5 µm column with a dimension of 2.1 X 50 mm. The column temperature was maintained at 30˚C. 20 µL of the samples were injected into the column and curcumin was separated using acetonitrile: 0.1% formic acid in a 1:1 ratio pumped at a flow rate

of 0.2 mL/min. The run time was 6 minutes. Curcumin was detected using multiple reaction monitoring (MRM) mode and the precursor-to-product ion transition was 369 > 285. Mass data was analyzed using Masslynx software.

3.2.6. Cytotoxcity of GaCurNPs on L929 cell line

3.2.6.1. Phase contrast microscopy

L929 cells were grown in a 25 cm^2 tissue culture flask in DMEM medium supplemented with 10% FBS and sodium bicarbonate. An antibiotic solution containing penicillin (100 I.U./mL), streptomycin (100 μg/mL), and amphotericin B (2.5 μg/mL). Cultured cell lines were incubated in a humidified 5% CO_2 incubator at 37°C (NBS Eppendorf, Germany). A confluent monolayer of cells was trypsinized and was then suspended in a 10% growth medium. 100 μL of the cell suspension (5 X 10^3 cells/well) was seeded in a 96-well tissue culture plate and incubated at 37°C in a 5% CO_2 incubator for 24 hours. Nontreated cells were kept as control. Experiments were done in triplicates. Phase contrast images were captured for control and treated samples.

3.2.6.2. Alamar Blue assay

Alamar blue assay was performed to assess the cytotoxicity of GaCurNPs on L929 cell lines. A two-day-old confluent monolayer was trypsinized and the cells were suspended in 10% FBS DMEM medium. A 2-day-old confluent monolayer of cells was trypsinized and the cells were resuspended in a 10% growth medium. 100 uL of the cell suspension (5 X 10^3 cells/well) was seeded onto a 96-well plate and incubated at 37C in a humidified 5% CO_2 incubator. After 24 hours of incubation, the growth media was removed and the cells were treated with different concentrations of curcumin and GaCurNPs (50,100,150,200,250,300,350 μg/mL). After treatment for 24 hours, 10μL of Alamar blue reagent was added to treated cells along with the media. The cells were incubated for 4 hours at 37°C in 5% CO_2 incubator. Fluorescence was

measured using a fluorimeter, an excitation wavelength of 530-560 nm, and an emission wavelength of 590 nm was used. The viability of the cells was calculated using the following formula:

$$Cell\ viability(\%) = \frac{Mean\ flourescence\ intensity\ of\ tretaed\ sample}{Mean\ flourescence\ intensity\ of\ control} \text{ X } 100 \quad \textbf{(}\text{Equation 2}\textbf{)}$$

3.2.7. *In vitro* antibacterial activity of GaCurNPs against *Pseudomonas aeruginosa*

3.2.7.1. Identification and confirmation of bacterial strains

Two *P. aeruginosa* strains were used for this study – an ATCC strain and a clinical strain. The strains were confirmed as *P. aeruginosa* by manually conducted biochemical tests or by an automated method (Vitek 2C 60, Biomeriux Inc, France). Antibiotic sensitivity tests were also conducted for both strains by the disc diffusion method. All the anti-bacterial studies of GaCurNPs were conducted in both *P. aeruginosa* ATCC strain as well as clinical strain 1 which is the urine isolate.

3.2.7.2. Determination of Minimum Inhibitory Concentration (MIC) by micro-broth dilution

The *in vitro* anti-bacterial activity of GaCurNPs and curcumin against *P. aeruginosa* (ATCC 27853) was evaluated by micro-broth dilution method. The broth dilution assay was done in 96-well microtiter plates. Bacteria were cultured in Mueller-Hinton broth and the growth was adjusted to 0.5 McFarlands standard (5 X 10^8 CFU/mL). 200 µL of the stock solution of both curcumin and GaCurNPs was added to the first well and then serially diluted. The concentrations tested were 662 µg, 331 µg, 165.5 µg, 82.75 µg, 41.37 µg, 20.68 µg and 10.34 µg. 100 µl of microbial inoculum (5 X 10^8 CFU/mL) was added to each well. Drug and organism controls were kept for each drug concentration. The plates were incubated at 37°C for 24 hours.

Minimum inhibitory concentration was determined. MIC is the concentration at which there is no visible growth of bacteria in the wells.

3.2.7.3. Determination of MIC of GaCurNPs against clinical isolates by microbroth dilution

Additionally, the MIC of GaCurNPs and curcumin against certain clinical strains of *P. aeruginosa* was also determined. The susceptibility and resistance of these strains to antibiotics were tested by VITEK 2 C system (Biomeriux, France). In the case of clinical strains, the concentrations starting from 400 to 25μg/mL were tested. About 100 μL of microbial inoculum (5×10^6 CFU/mL) was added to each well. Drug and organism controls were kept for each of the drug concentrations in triplicates. The plates were incubated at 37 °C for 24 h. MIC was determined as per the Clinical and Laboratory Standards Institute (CLSI) guidelines. MIC was the concentration at which the wells were clear, i.e., no visible turbidity. MBC was determined as the lowest concentration at which there was no appearance of colonies when transferred from broth to agar plates.

3.2.7.4. Effect of GaCurNPs on growth curve

Bacteria were treated with MIC and 2MIC of GaCurNPs and curcumin and the volume was adjusted to 2.5 mL in LB broth. 50 μL of 0.1 OD bacterial inoculum (freshly grown in 3 - 4 mL LB broth) was added to these test tubes. Tubes were kept in incubator at 37 °C. The OD_{600} readings were taken every hour for 6 hours starting from 0 hour. Untreated *P.aeruginosa* was also kept as control along with the treated bacteria. Data were plotted with OD_{600} values on the Y-axis and time on the X-axis.

3.2.7.5. Effect of GaCurNPs on viability – Live-dead assay

The activity of GaCurNPs was assessed using BacLight® Live/dead assay kit. Bacterial cells were treated with MIC of GaCurNPs and curcumin for 3 hours. Cells were collected by centrifugation at 10,000 rpm for 5 minutes. The cells were washed with saline 3-4 times. The cells were then resuspended in 250 µL saline. Cells were then stained with SYTO and propidium iodide by adding 3 µL of the staining solution freshly prepared (equal volumes of SYTO 9 and propidium iodide were mixed and vortexed). Cells were incubated in the dark for 15 minutes. 5 µL of the solution was added onto a glass slide and a cover slip was mounted on top. Using an inverted fluorescence microscope, images were taken. The bacterial cells were then observed and imaged. Live cells appeared green and dead cells were seen as red. The number of live cells and dead cells were counted for control as well as the treated groups and the percentage of live cells and dead cells was calculated as shown below:

$$Perentage\ of\ live\ cells\ or\ dead\ cells = \frac{Number\ of\ live\ or\ dead\ cells}{Total\ number\ of\ cells}\ X\ 100$$ **(**Equation 3**)**

3.2.7.6. Effect of GaCurNPs on swarming motility

P. aeruginosa was grown in LB broth for 24 hours. Bacteria containing 10^8 CFU/mL were treated with MIC and 2MIC concentration of curcumin and GaCurNPs for 3 hours. 10 µL from the treated samples were inoculated on the center of the swarming plate. (Swarming media is composed of yeast extract, peptone, dextrose, and agar). The plates were incubated overnight at 30°C without inversion. The diameter of swarming by bacteria was measured in millimeters. The experiment was done in triplicates (Norizan et al., 2013).

3.2.7.7. Effect of GaCurNPs on pyocyanin production

P. aeruginosa was grown in LB broth overnight at 37°C. The overnight culture was then inoculated in LB broth till the growth reached the exponential phase or OD reached 0.5. The bacteria were then treated with different concentrations of GaCurNPs (MIC and 2MIC) and incubated for 48 hours. After incubation, the samples were centrifuged at 10,000 rpm for 10 minutes. The supernatant was collected and passed through a filter of pore size 0.22 µm. 3 mL of chloroform and added to 5 ml of filtered supernatant and vortexed thoroughly. The tubes were then centrifuged for 10 minutes at 10,000 rpm. The blue layer was then transferred to a new tube and then acidified with 1 mL of 0.2 N HCl. The pink layer was then transferred to the cuvette and then OD was measured at 520 nm. The concentration of pyocyanin was calculated by the following equation:

$$\text{Concentration of pyocyanin (µg per ml)} = \text{OD 520 X } 17.072 \quad \text{(Equation 4)}$$

3.2.7.8. ROS production using DCFDA (2'-7'- dichlorodihydroflourescien diacetate) assay

P. aeruginosa ATCC 27853 and clinical strain were treated with different concentrations of GaCurNPs and curcumin to estimate ROS production by DCFDA method. 0.5 McFarland exponential phase culture was treated with MIC, 2MIC, and 4MIC of GaCurNPs and curcumin. The treated bacteria were kept at 37°C for 3 hours. The tubes were then centrifuged at 10,000 rpm for 5 minutes. The pelleted cells were resuspended in 1.8 mL PBS and 200 uL of DCFDA. The cells were harvested, washed to remove unreacted DCFDA, and resuspended in PBS. Fluorescence was measured using a fluorimeter.

3.2.7.9. Anti-bacterial activity of GaCurNPs: Raman spectroscopy evidence

The effect of GaCurNPs on *P. aeruginosa* was further investigated using Raman spectroscopy. *P. aeruginosa* culture grown for 16 hours was freshly inoculated into Luria broth. Cells were collected by centrifuging at 10,000 rpm for 5 minutes and then diluted to reach 0.5 OD. Bacteria were treated with MIC concentration of GaCurNPs, curcumin, and ciprofloxacin for 3 hours. Untreated bacteria were kept as control. Bacterial cells were centrifuged at 10,000 rpm for 5 minutes after incubation re-suspended in 3 µL MilliQ water and then dropped on a calcium fluoride slide. Raman spectra were obtained after drying. Raman spectra were acquired using Confocal Raman Microscope, Alpha300 RA, WITec GmbH, Germany equipped with 600 g/mm grating. Excitation was provided by a diode (DPSS) 532 nm laser with a power of 30mW shined on the sample. An acquisition time of 5 seconds was used. 20X objective was used throughout the acquisition of spectra.

3.2.7.10. Effect of GaCurNPs on bacterial cell morphology - FESEM evidence

FESEM was used to further investigate the antibacterial activity of GaCurNPs against *P. aeruginosa* ATCC 27853. 16-hour culture of *P.aeruginosa* was inoculated into Luria broth. Cells were collected by centrifuging at 10,000 rpm for 5 minutes. After that, the cells were diluted to 0.5 OD. For three hours, ciprofloxacin, curcumin, and the MIC concentration of GaCurNPs were incubated with the bacteria. Untreated microorganisms were kept as control. At the end of the incubation period, the bacterial cells were centrifuged at 10,000 rpm for five minutes. Bacterial cells were resuspended in 1mL of PBS. A drop was put on a coverslip and air-dried. Nova NanoSEM 450 was used to obtain images of the gold-sputter-coated samples.

3.2.8. In *vitro* anti-biofilm activity of GaCurNPs

3.2.8.1. Crystal violet assay

Bacteria were inoculated in LB broth (~ 5 mL) and grown till stationary phase and diluted in 1:100 ratio. The assay was done on a 96-well microtiter plate. 100 µl of the diluted culture was added to each well. Bacteria were then treated with MIC and 2MIC of GaCurNPs and curcumin. Non-treated cells served as control. The plates were kept undisturbed for 48 hours for the biofilm to form. The plate was then taken out and planktonic cells were washed and removed. Cells were heat-fixed for 1 hour at 60°C. 100 µL of crystal violet dye was added to each well and kept at room temperature for 15 minutes. The biofilm thus got stained and excess dye was washed with water and the plate was allowed to dry. 200 µl of 30% acetic acid was added to each well and the dye was dissolved. The OD values were measured at 570 nm in a microplate reader (Biotek 800 TS, VT, USA). The inhibition (%) of biofilm was calculated using the following formula:

$$Biofilm\ inhibiton\ (\%) = \frac{OD\ (Control)\ at\ 570\ nm - OD\ (Treated)\ at\ 570\ nm}{OD\ (Control)\ at\ 570\ nm} \times 100 \quad \text{(Equation 5)}$$

3.2.8.2. Effect of GaCurNPs on biofilm – Live/dead assay

P. aeruginosa was inoculated in LB broth and incubated overnight. The culture was then diluted 1:100 and 100 uL was added to each well of 6 well plate in which sterilized coverslips were placed. Biofilm was allowed to form for 24 hours. Plates were then taken out of the incubator and the biofilm was treated with 2MIC and 4MIC of curcumin and GaCurNPs. After 24 hours of treatment, the wells were washed with PBS twice to remove planktonic bacteria. About 3 µL SYTO 9 and 3 uL propidium iodide were added to 1 mL filter-sterilized water. A volume of 200 uL of the staining solution was added to the biofilm sample gently without disturbing it. Biofilm was stained for 20-30 minutes at room temperature protected from light. Excess stain was

removed by rinsing with filter-sterilized water. Imaging was done using a fluorescence microscope in oil immersion.

3.2.8.3. Effect of GaCurNPs on biofilm- FESEM evidence

A loopful of bacteria was inoculated in LB broth and incubated overnight at 37°C. The culture was diluted 1:100 in LB broth. Sterile 6 well plates were used for growing biofilms. Coverslips were dropped into the wells after sterilizing by dipping in 70% ethanol overnight followed by exposure to UV radiation for 30 minutes. The diluted bacterial culture was added into the wells and incubated at 37°C for 24 hours for bacteria to form biofilm. The biofilm was then treated with different concentrations of GaCurNPs and curcumin (2MIC and 4MIC). After 24 hours of incubation, the biofilm was washed with saline twice or thrice to remove unattached cells. The washed biofilm was then fixed on the coverslips using 2.5% gluteraldehyde at 4°C for 4 hours. The samples were then dehydrated using increasing concentrations (10%, 30%, 50%, 70%, 90%) of ethanol. The samples were then dried and sputter-coated with gold. SEM images were taken using Nova NanoSEM 450.

3.2.9. Raman spectroscopy as a tool to study the effects of GaCurNPs on *P. aeruginosa* biofilm

Raman spectroscopy and Confocal Raman microscopy are now widely being exploited as a tool for the identification of bacteria as well as the detection of bacteria and bacterial biofilms. This fast, non-invasive, and label-free technique is gaining wide acceptance in the field of bacteriology. Confocal Raman microspectroscopy was used for studying the structure and composition of biofilm and the formation of *P. aeruginosa* biofilm. The effect and mode of action of various antibiotics on *P. aeruginosa* biofilm were studied by Jung *et al.* using Raman spectroscopy and multivariate analysis (Jung et al., 2014). Fiber probe-based Raman

spectroscopy along with chemometric analysis was used for the identification of different species of bacteria involved in biofilm-related infection (Shen et al., 2022).

Here, the utility of Raman spectroscopy along with PCA for the differentiation of different bacterial species based on their unique spectra was tested. And following that the same technique was employed to study the effect of GaCurNPs on *P. aeruginosa* biofilm.

3.2.9.1. Bacterial Raman spectra library preparation

The following standard strains were obtained from the American Type Culture Collection (ATCC): One Gram-positive and three Gram-negative- *Staphylococcus aureus* ATCC 25923, *Escherichia coli* ATCC 25922, *Pseudomonas aeruginosa* ATCC 27853 and *Acinetobacter baumannii* ATCC 19606.

Raman spectroscopy: Bacteria grown for 16 hours were freshly inoculated into Luria broth. Cells were collected by centrifuging at 10,000 rpm for 5 minutes and diluted to obtain 0.5 OD. Bacterial cells were collected by centrifuging at 10,000 rpm for 5 minutes. The cells were re-suspended in 5 µL MilliQ water and dropped on a calcium fluoride slide and dried. Raman spectra were acquired using a confocal Raman microscope (Alpha300 RA, WITec GmbH, Germany) equipped with a 600 g/mm grating. Sample excitation was performed using a 30 mW, 532 nm diode laser (DPSS). The integration time was set to 5s with an objective magnification of 50X, throughout the spectra acquisition. Spectra were recorded from ten different spots from the bacterial suspension to acquire the spectra from many cells for each strain. Further, fifty accumulations were done from each of these spots. The spectra were individually background corrected. The averaged spectrum from ten different spots of each studied strain was used for principal component analysis.

Library preparation and principal component analysis*:* Baseline correction and normalization of the spectra were performed using Witec Projectplus (Version 2) software. Baseline correction was performed using sixth-order polynomials, and normalization of the spectra was performed with respect to the 2920 cm^{-1} Raman peak. The spectra were truncated to the range from 400 to 1800 cm^{-1}. All the processed spectra were saved into a single file folder as the spectral library.

3.2.9.2. Study of the effect of GaCurNPs on P.aeruginosa biofilm by Confocal Raman microscopy

Data collection: *P. aeruginosa* biofilm was grown on glass coverslips. Coverslips were sterilized by placing them in ethanol and exposed to UV radiation for 30 minutes. The coverslips were then dried inside the laminar flow. Bacteria were grown in LB broth for 16 hours were diluted 1:100. 1 mL of this diluted culture was added to 6-well plates with coverslips in them. *P. aeruginosa* biofilm was grown in coverslips for 24 hours at 37°C without disturbing. Untreated biofilm grown for 24 hours was kept as control. For GaCurNP-treated biofilms, the biofilms grown for 24 hours were treated with MIC, 2MIC, and 4MIC of GaCurNPs for the next 24 hours. Biofilm was also treated with MIC of ciprofloxacin for 24 hours. Biofilm was then washed with PBS twice to remove unattached cells.

Raman spectroscopy data acquisition: Confocal Raman spectral imaging was done at room temperature using Confocal Raman Microscope (Alpha 300R WITec, GmbH, Germany) equipped with an excitation laser of 532 nm and a 50x objective. The used grating had 600 lines per mm. The hyper spectral mapping was performed on an XY plane 5 µm above the surface of the coverslip to avoid the spectral peaks from the glass. A 50 µm x 50 µm (250 μm^2) area was mapped with a resolution of 150 points x 150 lines and an integration time of 0.5s. Ten spectra

from 10 different points, uniformly distributed on this chemical map, were extracted to carry out the PCA.

***Processing of collected data*:** The spectral image processing was done using Witec Projectplus (Version 2) software. Baseline correction was done using sixth-order polynomial and the normalization of spectra was done using the 2922 cm^{-1} (-CH deformation) Raman peak. All the spectra after processing were saved into a folder.

Principal Component Analysis: PCA was performed on the spectral data of the untreated biofilm and biofilm treated with the above-mentioned concentrations of GaCurNPs. Spectral data of *P. aeruginosa* biofilm treated with MIC of ciprofloxacin was also included for PCA.

3.2.10. Gene expression study of biofilm formation genes and quorum sensing genes in *P. aeruginosa* by Real-Time qPCR

3.2.10.1 Effect of GaCurNPs on biofilm formation genes and quorum sensing genes in planktonic P. aeruginosa

The expression of genes involved in virulence, biofilm formation, and quorum sensing of *P. aeruginosa* was studied using Real-time quantitative PCR. The expression of the following genes on treatment with GaCurNPs was studied: algD, rpoS, lecA, proC, pelA, exoS, lasR, lasI, rhlR, and rhlI. OprL gene was used as the control.

***RNA isolation from bacterial cells*:** *P. aeruginosa* ATCC 27853 and clinical strain were grown overnight in LB broth in a conical flask at 37°C. The cells were then collected by centrifuging at 10,000 rpm for 5 minutes. Bacteria cells were then incubated at 37°C with and without GaCurNPs. Untreated *P. aeruginosa* biofilm was kept as the control. The concentrations used were half MIC, MIC and 2MIC concentration of GaCurNPs. The treatment was done for 3 hours to correlate it with other results. After incubation, the cells were collected by centrifugation at

10000 rpm for 5 minutes. The cells were then washed twice with saline. RNA from the bacterial cells was isolated using Pathkits RNA isolation kit. 400 µl of lysis buffer was added to the cells and mixed thoroughly by pipetting. 400 µl of isopropanol was then added and vortexed well. 400 µl of the total solution was added to the spin column and centrifuged at 8000 rpm for 1 minute. This step was repeated for the remaining volume of solution. The spin column was carefully opened and 500 µl of wash buffer was added and centrifuged at 8000 rpm for 1 minute. The filtrate was discarded and the column was washed again with 500 µl of wash buffer. The column was then dry spun at maximum speed for 1 minute. The column was then placed on a 1.5 ml tube followed by the addition of 60 µl of elution buffer and then centrifuged at 8000 rpm for 1 minute. The concentration of RNA was measured using a Nanodrop spectrophotometer. The isolated RNA was stored at – 80° C till further use.

***cDNA synthesis*:** RNA was converted to cDNA using Takara Prime script 1st strand cDNA synthesis kit. 100 ng of RNA was used for the synthesis of cDNA per 20 µl reaction. 100 pmol of random 6-mers were used as primers for the synthesis. The reaction for the first step is listed in Table 7.

Table 7: Reaction mixture for the first step of cDNA synthesis

Template RNA (100ng)	4 µl
Random 6-mer (50 uM)	1 µl
dNTP mixture (10mM each)	1 µl
RNase free water	4 µl
Total volume	10 µl

The above mixture was incubated for 5 minutes at 65°C and then immediately cooled in ice to 4°C. The template RNA primer mixture was then added to the following reaction mixture to a total volume of 20 µl (Table 8).

Table 8: Reaction mixture for step 2 of cDNA synthesis

Template RNA mixture	10 µl
5X Primescript buffer	4 µl
RNase inhibitor (40 U/ul)	0.5 µl (20 U)
PrimeScript RTase (200 U/mL)	0.5 µl (200 U)
RNase free water	5 µl
Total volume	20 µl

The PCR steps for cDNA synthesis are as follows:

- 30°C for 10 minutes
- 42°C for 30 minutes
- 95°C for 5 minutes
- 4°C

The concentration of cDNA was checked using Thermoscientific NanoDrop One, USA. The quantified cDNA was used for quantitative real-time PCR.

Real-time quantitative gene expression analysis: The cDNA samples were then subjected to quantitative real-time PCR analysis. Real-time PCR was done using TB Green Premix Ex Taq II (Tli RNase H Plus) by Takara Bio Inc. PCR was performed in a CFX96 Real-time PCR detection system by Bio-Rad Laboratories, Inc. 50 ng cDNA was used for the reaction. A PCR mixture was prepared according to the manufacturer's instructions as given in table 9. The PCR steps are listed in Table 10.

Table 9: Reaction mixture for real-time PCR

Reagent	Volume (µl)	Final concentration
TB Green Premix ExTaq II (Tli RNaseH Plus) (2X)	12.5	1X
PCR forward primer (10 µM)	1	0.4 µM
PCR revere primer (10 µM)	1	0.4 µM
Template cDNA	2	50 ng
Sterile purified water	8.5	
Total volume	25	

Table 10: Steps in real-time qPCR

Step 1: Initial denaturation – 95 C for 30 secs	1 cycle
Step 2: PCR 95° C for 5 secs 60° C for 30 secs	40 cycles
Step3: Melt curve analysis	

The primer used for the real-time qPCR is as follows:

Table 11: *P. aeruginosa* primers used for gene expression analysis

Gene	Forward primer (5'-3')	Reverse primer (5'-3')
oprL(control)	5' AACAGCGGTGCCGTTGAC 3'	5' GTCGGAGCTGTCGTACTCGAA 3'
algD	5' GCGACCTGGACCTGGGCT 3'	5' TCCTCGATCAGCGGGATC 3'
rpoS	5' CGGCGAGTTGGTCATCATCAAACA 3'	5'ATCGATTGCCCTACCTTGACCTGT 3'

lecA	5´CACCATTGTGTTTCCTGGCGTTCA-3′	5´-AGAAGGCAACGTCGACTCGTTGAT-3′
proC	5´CAGGCCGGGCAGTTGCTGTC-3´	5´-GGTCAGGCGCGAGGCTGTCT-3′
pelA	5' AAGAACGGATGGCTGAAGG 3'	5' TTCCTCACCTCGGTCTCG 3'
exoS	5' GGCGGATGCGGAAAAGTAC 3'	5' CTGACGCAGAGCGCGATT 3'
lasR	5' GGCGGATGCGGAAAAGTAC 3'	5' AACTGGTCTTGCCGATGG 3'
lasI	5' GCTTCTGCACGGCAAGGA 3'	5' ATGGCGAAACGGCTGAGTT 3'
rhlR	5' GCCAGCGTCTTGTTCGG 3'	5' CGGTCTGCCTGAGCCATC 3'
rhlI	5' GTAGCGGGTTTGCGGATG 3'	5' CGGCATCAGGTCTTCATCG 3'

The relative expression of each gene with respect to control was quantified using the $2^{-\Delta\Delta CT}$ method. With respect to the ΔΔCT of the $2^{-\Delta\Delta CT}$ method, the first ΔCT is the difference in the threshold cycle between the target and reference genes is $\Delta CT = CT\,(target\ gene) - CT\,(Reference\ gene)$.

The ΔΔCT is the difference in the ΔCT as in the above-mentioned formula between the target and the reference samples, which is as follows:

$\Delta\Delta\mathrm{CT} = \Delta CT(target\ sample) - \Delta CT(reference\ sample)$. The relative gene expression for the reference sample is usually set to 1 because ΔΔCT is 0 and therefore 2^0 is equal to 1.

3.2.10.2. Effect of GaCurNPs on biofilm formation genes and quorum sensing genes in P. aeruginosa biofilm

P. aeruginosa biofilm was grown in sterilized coverslips placed in 6-well plates. The bacterial cell density was kept the same for control and treated samples. The biofilm was then treated with different concentrations of GaCurNPs for 24 hours. RNA isolation, cDNA synthesis, and RT-PCR were done using the same procedure as detailed in section **3.11.1**. The relative

expression of each gene was measured by the $2^{-\Delta\Delta CT}$ method. The percentage reduction in gene expression was calculated as:

$$Percentage\ reduction = \frac{fold\ chage\ of\ control - fold\ change\ of\ test}{fold\ change\ of\ control}\ X\ 100$$

3.2.11. Statistical analysis

For quantitative experiments, three replicates were kept in a single experiment and three independent experiments were conducted. The values were then averaged and expressed as mean ± standard deviation (SD). Statistical analysis wherever required was done using *paired t-test* on triplicate data values. Statistical significance was reported using the p-values and are given in figure legends wherever applicable.

CHAPTER 4

4. RESULTS AND DISCUSSION

4.1. Characterization of raw material

Characterization of raw material i.e., curcumin was checked for its purity and characterized by RP-HPLC. Curcumin was also characterized using FT-IR spectroscopy and Raman spectroscopy. The purity of curcuminoid peaks can be assessed based on their resolution, symmetry, and absence of impurities or interfering peaks. The presence of well-defined and symmetrical peaks with good resolution indicates the purity of the curcuminoids and the absence of contaminants or degradation products. RP-HPLC showed three distinct peaks that correspond to curcumin, demethoxy curcumin, and bisdemethoxy curcumin with retention times 23.6, 27.1, and 31.5 mins respectively (Figure 9). The ratio of three curcuminoids was found to be 79:18:3 (Dhanya et al., 2021).

Curcumin showed characteristic FT-IR and Raman peaks as shown in Figures 10a and b (Mohan et al., 2012). The FT-IR and Raman peaks of curcumin are shown in Table 12 and Table 13 respectively.

In all the studies presented in this thesis, the term 'curcumin' has been used to collectively refer to curcuminoids, despite the presence of analogs- demethoxy curcumin and bisdemethoxy curcumin, as indicated in the chromatogram (Figure 9). This generalization was applied to simplify the discussion, although the active components include a mixture of curcuminoids.

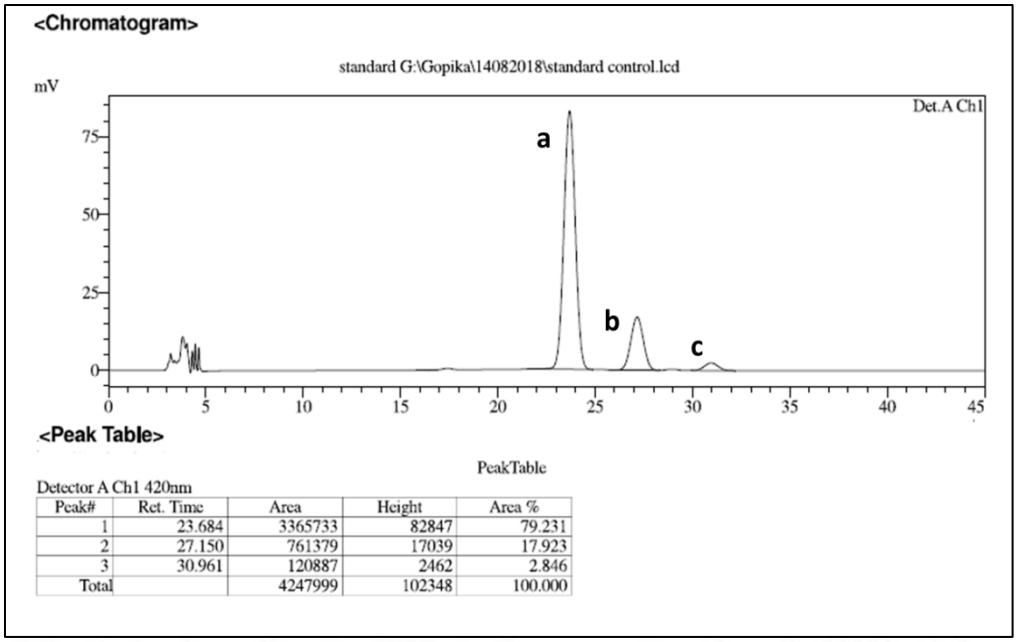

Peak#	Ret. Time	Area	Height	Area %
1	23.684	3365733	82847	79.231
2	27.150	761379	17039	17.923
3	30.961	120887	2462	2.846
Total		4247999	102348	100.000

Figure 9: Chromatogram of curcumin: Chromatogram of curcumin showing three distinct peaks of: a) curcumin, b) demethoxycurcumin, and c) bisdemethoxycurcumin.

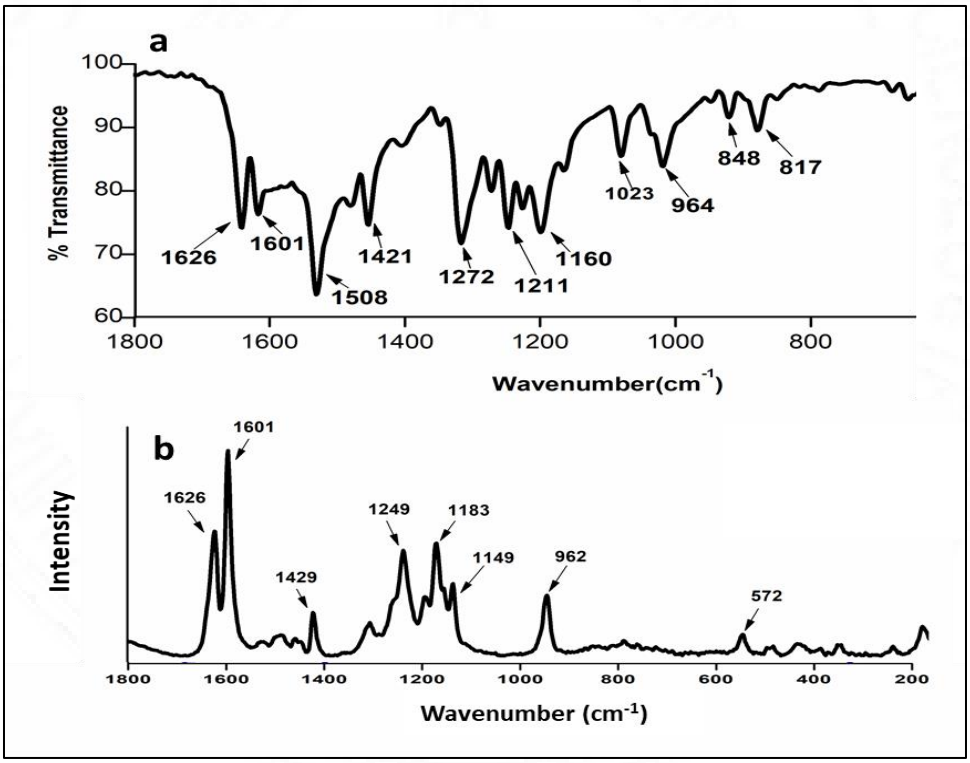

Figure 10: Characterization of curcumin by FT-IR and Raman spectroscopy: a) FT-IR spectra and b) Raman spectra of curcumin used in the study.

Table 12: Characteristic FT-IR peaks of curcumin

Wavenumber (cm^{-1})	Peak assignment
1626	Mixed vibration of carbonyl C=O and C=C
1600	symmetric aromatic stretching vibrations ν(C=C
1506	C−O stretching, C−C−C bending, and C−C−O bending
1427	In-plane C−OH bending of the enolic group
1272	Enol ν(C−O)
1153,1025	skeletal C−C−H and methyl group deformations
962	out-of-plane bending vibrations of C−C−H
855, 806	out-of-plane bending vibrations of C−C−H moieties

Table 13: Characteristic Raman peaks of curcumin

Wavenumber (cm^{-1})	Peak assignment
1626	C=O str. vibration
1601	ν(C=O), ν(C=Cring)
1429	Phenolic ν(C-O)
1149, 1183	Enolic ν(C-O)

4.2. Characterization of GaCurNPs

4.2.1. Size and zeta potential

Particle size assessment by dynamic light scattering (DLS) method revealed that the size of GaCurNPs was 79.5 nm (Figure 11b). DLS measures the hydrodynamic diameter and subsequently, the size will be slightly greater than the actual particle size. The zeta potential of

GaCurNPs was estimated as +22.1 mV which demonstrated that the particles were moderately stable (Figure 11c).

Figure 11: Size and Zeta potential of GaCurNPs measured by Dynamic Light Scattering: a) Images of curcumin and GaCurNPs, b) Particle size distribution of GaCurNPs, and c) Zeta potential of GaCurNPs.

4.2.2. TEM and XRD analysis

Transmission electron microscopy uncovered that the particles were spherical and the size was measured as 25 - 35 nm (Figure 12a and 12b). High-resolution TEM uncovered the crystalline

fringes of GaCurNPs. The perfect crystalline pattern revealed the incorporation of gallium in GaCurNPs. This was additionally confirmed by the powder XRD examination of GaCurNPs and curcumin. Native curcumin has a characteristic crystalline pattern as previously reported in the literature (Rajasekar and Devasena., 2015). The crystalline pattern of curcumin was replaced by the typical ordering of Gallium oxides (Figure 13). JCPDS indexing of the crystalline pattern proposed the existence of Ga as GaO(OH) in the GaCurNPs. The absence of crystalline fringes of curcumin and the presence of a halo in the lower angle region implies the self-assembly of curcumin molecules around the GaO(OH) nanoparticles. HRTEM micrograph of GaCurNPs showed lattice fringes separated by 0.43 nm which is in agreement with the d-spacing of 110 planes of GaO(OH) (Figure 12e).

The formation of GaO(OH) nanoparticles from the aqueous solution of Ga^{3+} was reported before by Gedankan *et al* (Avivi et al., 1999). The stability of Ga-containing oxides like Ga_2O_3 and GaO(OH) can be worked on by the functionalization with ligands, particularly with acidic functionalities. By functionalization with acidic functionalities, the stability of Ga_2O_3 and GaO(OH) can be improved (Adams and Ivanisevic, 2019). Thus, the enolic form of curcumin interacts with the in situ-shaped GaO(OH) to form GaCurNPs.

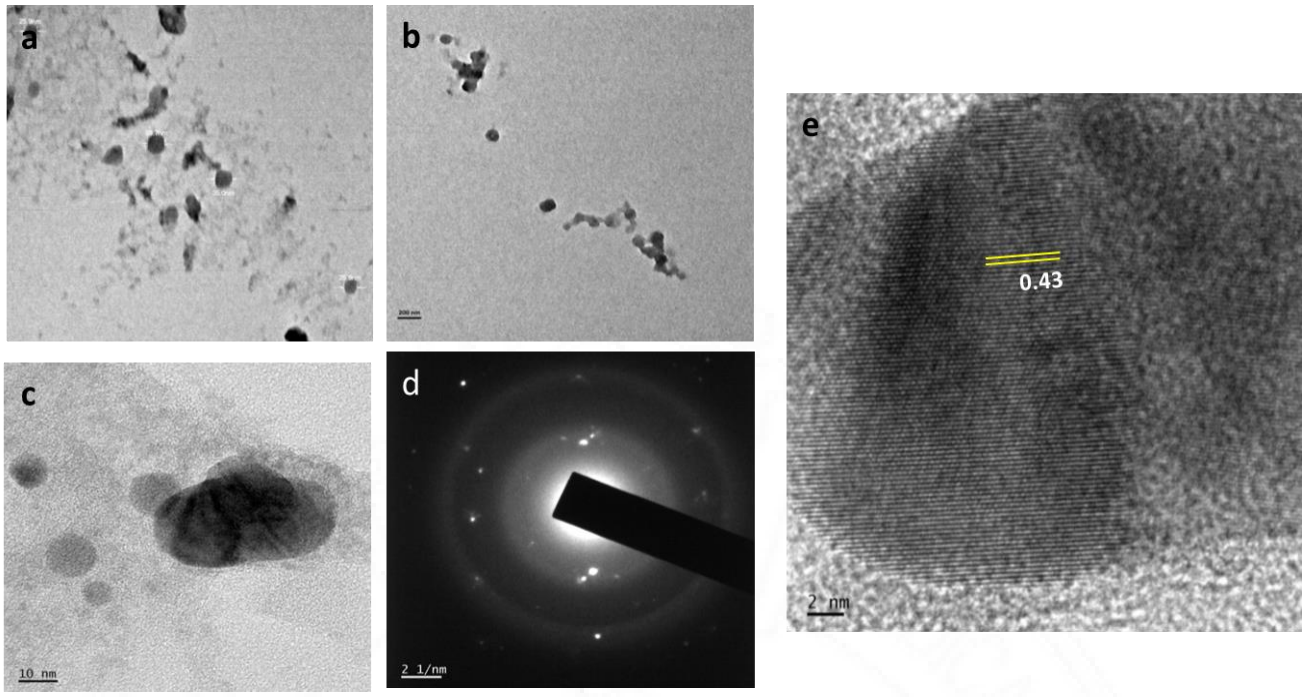

Figure 12: Transmission Electron Micrography images of GaCurNPs. (a) and (b) Transmission Electron Microscopy (TEM) image of GaCurNPs; (c) and (e) High-resolution TEM; (d) Selected area diffraction pattern of GaCurNPs.

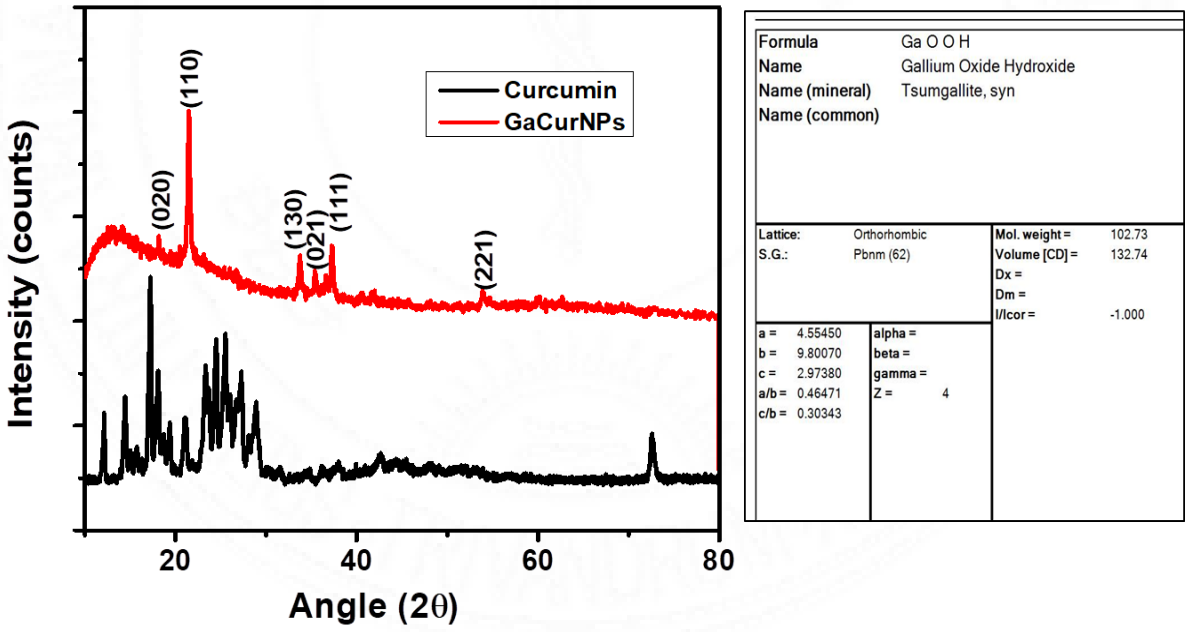

Figure 13: XRD of curcumin and GaCurNPs. The peaks in GaCurNPs correspond to GaO(OH).

4.2.3. UV spectroscopy and fluorescence spectroscopy

The absorbance and emission spectra of curcumin and GaCurNPs are represented in Figure 14. Curcumin exhibited maximum absorbance at 423 nm as reported in the literature (Mondal and Ghosh, 2012). The absorbance maximum of GaCurNPs was recorded to be 405 nm indicating a blue shift. This could be possibly due to the interaction of curcumin with the GaO(OH).

The emission of curcumin was recorded as 564 nm. The emission maxima for GaCurNPs was 558 nm. The intensity of fluorescence emission of GaCurNPs was found to be decreased. This suggested that there is quenching of curcumin fluorescence on conjugation with GaO(OH) and there is a shift (blue shifted) in the emission maxima from 564 nm to 558 nm. It has been reported that curcumin on conjugation with liposomes or metals, fluorescence gets quenched and also the emission maxima gets blue-shifted (Dhanya et al., 2021).

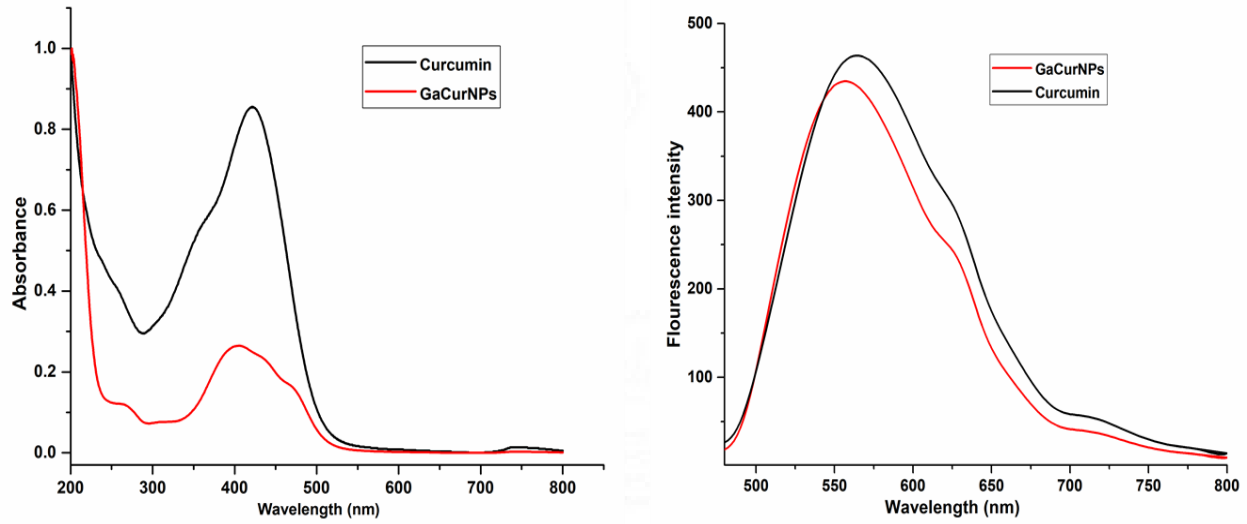

Figure 14: Absorption spectra and Emission spectra of GaCurNPs: (a) Absorption spectra of curcumin and GaCurNPs, (b) Emission spectra of curcumin and GaCurNPs.

4.2.4. FT-IR spectroscopy

Detailed vibrational spectra of curcumin and GaCurNPs were recorded. The vibrational spectrum of curcumin was reported by Kolev and coworkers (Kolev et al., 2005). Figure 15 shows the FT-IR spectra of curcumin and GaCurNPs. Detailed vibrational spectra of curcumin and GaCurNPs were recorded. A sharp peak at 3508 cm^{-1} indicates the hydroxyl group. The peak at 1626 cm^{-1} is a mixed vibration of carbonyl C=O and C=C. The strong peak at 1601 cm^{-1} is indicative of the symmetric aromatic stretching vibrations ν(C=C). The peak at 1508 cm^{-1} is attributed to the ν(C=O) while the enol ν(C-O) peak is obtained at 1272 cm^{-1}. The peak at 1023 cm^{-1} accounts for the presence of C-O-C bond. The benzoate *trans* -CH vibration is at 959 cm^{-1} and the *cis* vibration of the aromatic ring was obtained at 713 cm^{-1}. A shift in 1626 cm^{-1} in the carbonyl group in curcumin to 1617 cm^{-1} in GaCurNPs indicates the interaction of gallium with the carbonyl group of curcumin. This suggests the formation of GaCurNPs. There is also a broadening and decrease in intensity of peak at 1272 cm^{-1} (enol C-O) in GaCurNPs. The peaks at 1428 cm^{-1}, and 964 cm^{-1} are evident in GaCurNPs which indicates that curcumin is intact.

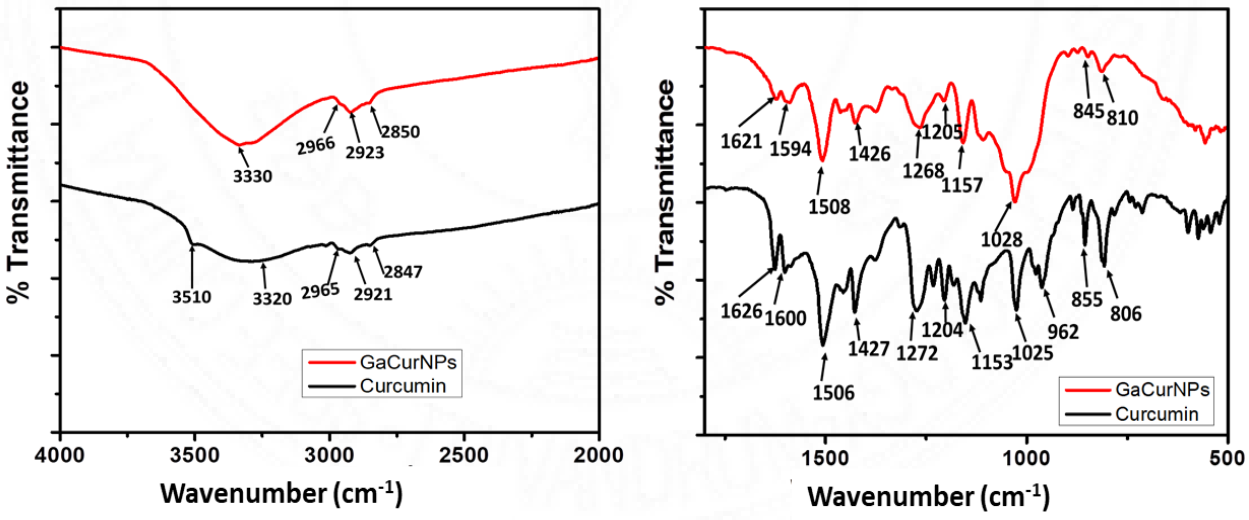

Figure 15: FT-IR spectrum of curcumin and GaCurNPs.

4.2.5. Raman spectroscopy

The Raman spectrum of curcumin obtained suggests the existence of curcumin in enol form (Figure 16). No peak was observed in the region of 1800 cm^{-1} to 1650 cm^{-1}. The peak at 1626 cm^{-1} corresponds to *ν*(C=O) and *ν*(C=C). The strong peak at 1601 cm^{-1} is characteristic of the aromatic vibrations of the C-C_{ring}. The peak at 1429 cm^{-1} indicates the presence of phenolic *ν*(C-O). The enolic *ν*(C-O) vibrations are marked as 1149 cm^{-1} and 1183 cm^{-1}. The ~ 10 cm^{-1} shift of carbonyl peak from 1626 cm^{-1} in curcumin to 1631 cm^{-1} in GaCurNPs can be inferred as the interaction of gallium with carbonyl oxygen and the formation of GaCurNPs. The broadening and decrease in intensity of the C-O (enol) peak at 1272 cm^{-1} also confirms the formation of GaCurNPs. A change in the relative intensity of the peaks at 1631 cm^{-1} and 1599 cm^{-1} was observed.

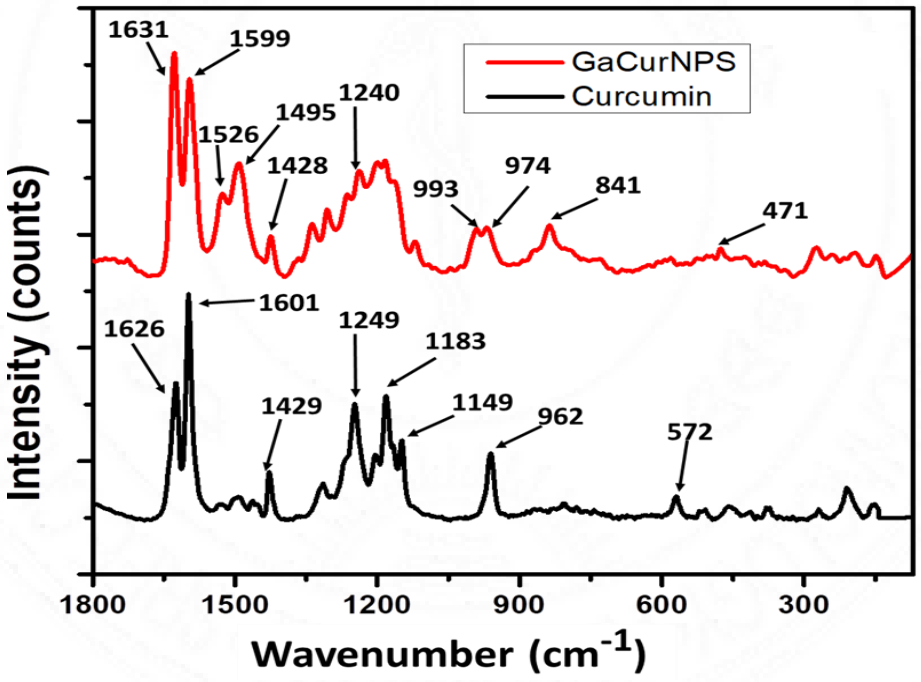

Figure 16: Raman spectra of curcumin and GaCurNPs.

4.2.6. X-ray photoelectron spectroscopy

X-ray photoelectron spectroscopy (XPS) was used to investigate the type of binding interactions and the chemical identities of the constituents. The existence of curcumin and GaO(OH) in the nanoparticles is confirmed by the XPS spectra of GaCurNPs, which show their distinctive peaks. Per the literature report, characteristic transitions of Ga are found at 1146.51 (Ga 2p1/2), 1119.61 (Ga 2p3/2), 22.42 (Ga 3d3/2), and 20.51 eV (Ga 3d5/2) (Lee et al., 2013; Bourque et al., 2016) (Figure 17c and 17d). Curcumin's carbon (C 1s) and oxygen (O 1s) atoms are responsible for the peaks that were seen at around 284 and 532 eV. Significant peak widening is seen when comparing the C1s and O1s peaks of GaCurNPs with those of bare curcumin; this phenomenon may be related to the interaction between GaO(OH) and curcumin. Further information on the mechanism of interactions can be obtained by deconvolution of the peaks. Curcumin's C1s peak deconvolutes into three main peaks: C–O (286.23 eV), C=O (288.28 eV), and sp3 carbon (284.72 eV). It's interesting to note that the deconvolution of GaCurNPs' wide C1s peak produces four peaks in addition to a little movement in peak locations (Figure 9a). The sp2-hybridized carbon atom is the location of the fourth peak, which was detected at 283.94 eV, indicating that curcumin is present in the complex in the enolic form. Pure curcumin's oxygen peak (O 1s) is deconvoluted into peaks that are C–O (531.18 eV) and C=O (532.77 eV) (Figure 17b). The O1s spectra in GaCurNPs have the same peaks, but the Ga-curcumin interactions cause the peak to enlarge. According to a study, the binding energy of the GaO(OH) O 1s peaks (Ga–OH and Ga^{3+}–O) is likewise located in this area (Feng et al., 2019). Thus, it is probable that the O 1s peaks of GaCurNPs will overlap.

Based on the spectroscopic evidence and evidence gathered from XRD and TEM analysis, the schematic representation of GaCurNPs is depicted in Figure 18.

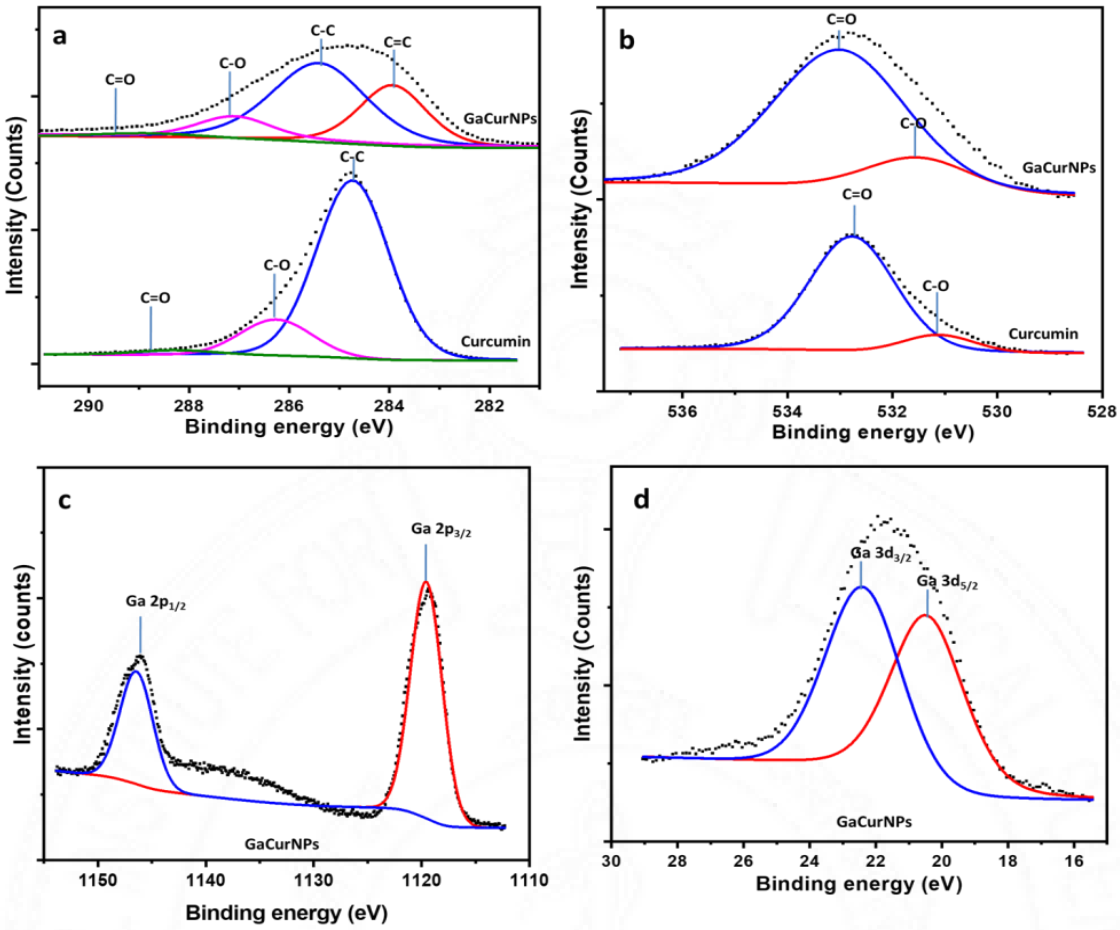

Figure 17: XPS spectra of GaCurNPs and curcumin: (a) C1s peaks (b) O1s peaks (c) Ga 2p peaks and (d) Ga3d peaks of GaCurNPs.

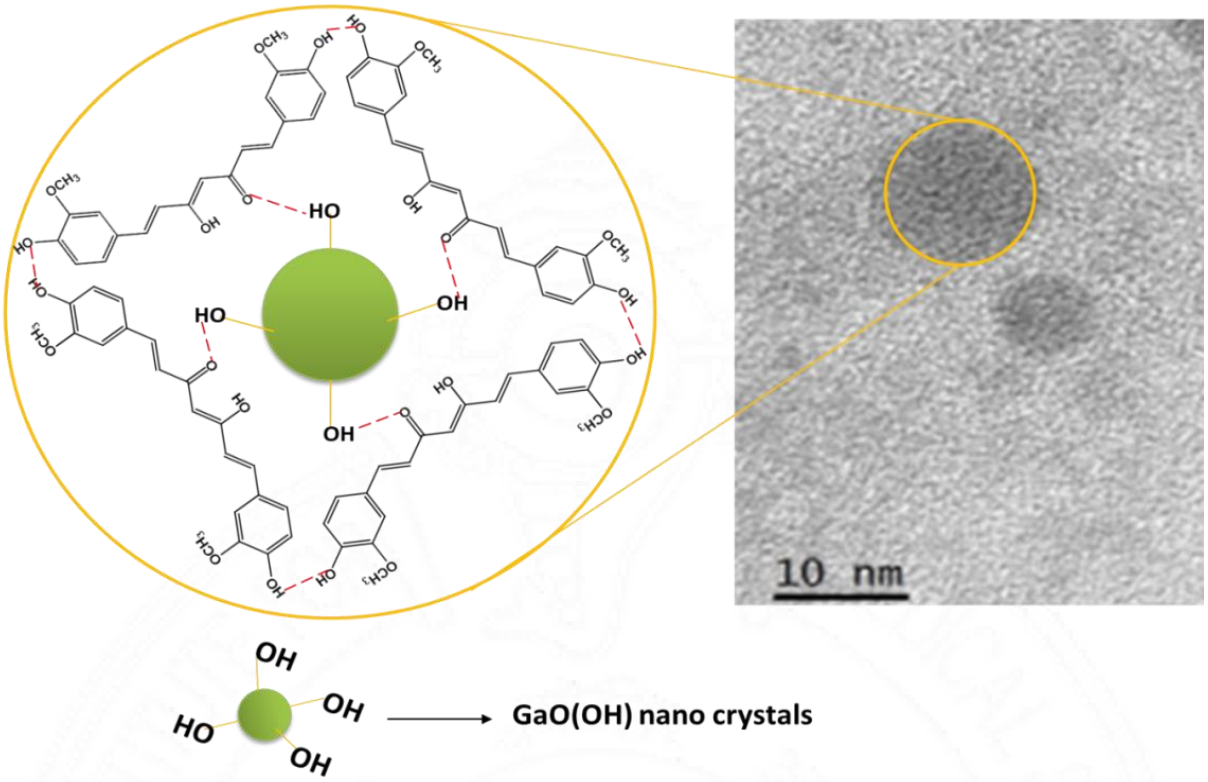

Figure 18: Schematic representation of the proposed structure of GaCurNPs.

4.3. Quantification of curcumin by RP-HPLC and gallium by ICP-OES

The amount of curcumin per milligram of GaCurNPs was estimated by RP-HPLC. Curcumin is a mixture of three active components - curcumin, demethoxycurcumin, and bisdemethoxycurcumin and their ratio was found to be 79:18:3. The retention time of the components was 23.6, 27.6, and 31.5 minutes. The curcumin bound to the particle was extracted in ethanol and quantified. It was estimated that one milligram of GaCurNPs contains 200 ± 3.7 µg of curcumin per mg of GaCurNPs (n=3).

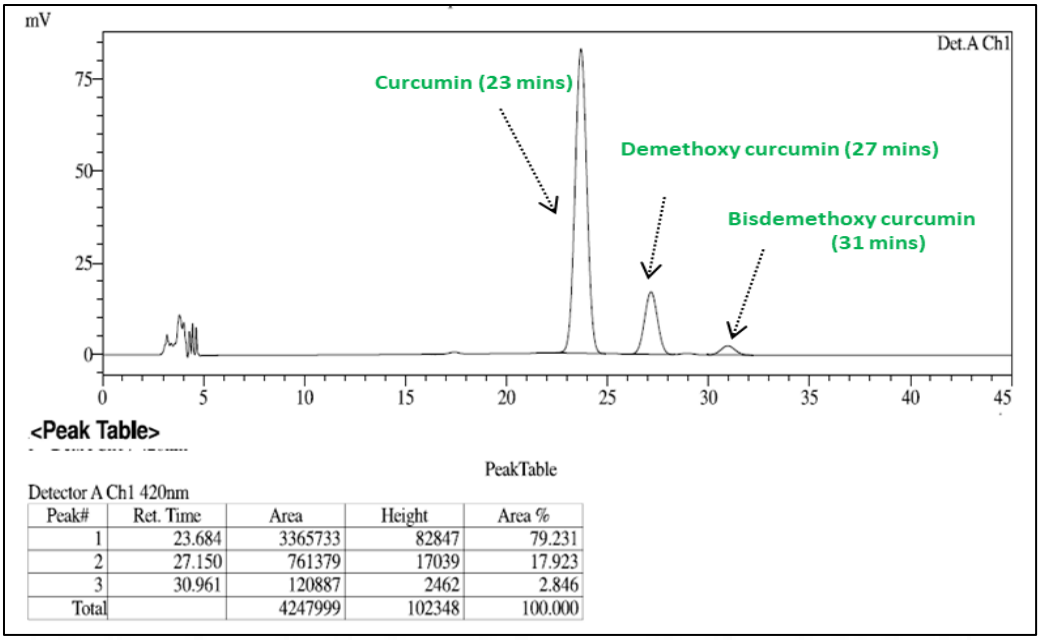

Peak#	Ret. Time	Area	Height	Area %
1	23.684	3365733	82847	79.231
2	27.150	761379	17039	17.923
3	30.961	120887	2462	2.846
Total		4247999	102348	100.000

Figure 19: **Chromatogram of curcuminod showing retention peaks of curcumin, demethoxycurcumin, and bisdemethoxycurcumin.**

The concentration of gallium per milliliter of GaCurNPs was estimated by ICP-OES. It was estimated that the concentration of gallium is 16 ppm.

4.4. Stability study of curcumin in GaCurNPs

4.4.1. Stability of curcumin by RP-HPLC

According to D Kumavat *et al.*, curcumin breaks down rapidly at physiological pH (7.4) with a degradation constant of 0.0145 min^{-1} or 0.924 hr^{-1} (Kumavat et al., 2013). Bisdemethoxycurcumin, curcumin, and demethoxycurcumin are the three components that constitute curcumin. Both curcumin and GaCurNPs were incubated in conditions mimicking physiological conditions as described in section 3.2.5.1. Curcumin was extracted in ethanol and loaded into the column. When compared to bare curcumin, the results showed that the curcumin bound to the GaCurNPs remained stable in physiological conditions. Under physiological conditions, bare curcumin showed 95% degradation whereas curcumin extracted from

GaCurNPs degraded very slowly with only 23.4 % degradation at 24 hours (Figure 20a). Curcumin attached to GaCurNPs showed 15.5% degradation at 6 hours and 61% degradation for bare curcumin. At 24 hours, demethoxycurcumin in bare curcumin exhibited a degradation of 49.5 % whereas the degradation was 29% for curcumin bound to GaCurNPs. Degradation of bisdemethoxycurcumin is the lowest among the three curcuminoids and a similar trend in degradation pattern was reported by Esatbeyoglu *et al* (Esatbeyoglu et al., 2012).

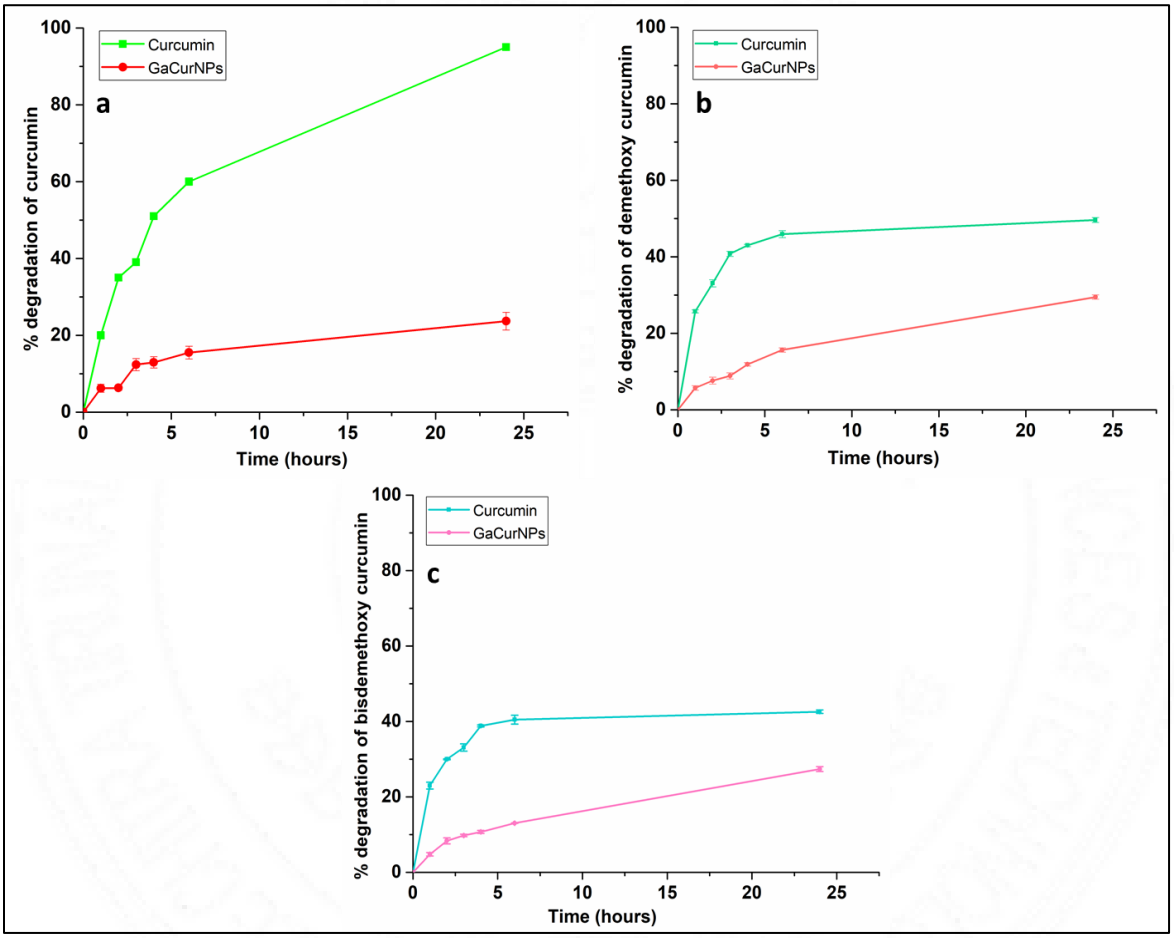

Figure 20: Stability of curcuminoids in physiological pH. Curve showing the degradation of: (a) curcumin, (b) demethoxycurcumin, and (c) bisdemethoxycurcumin attached to GaCurNPs in pH 7.4 and temperature 37°C.

4.4.2. Stability of curcumin by LC-MS

The product ion spectrum of curcumin is represented in Figure 21. Curcumin standards were prepared by diluting curcumin stock solution with a concentration of 0.56 mg/mL prepared in the mobile phase. The calibration curve of curcumin was obtained by plotting peak areas corresponding to the MRM transition 369 > 285 vs. concentration of standards ranging from 280 ng/mL - 280 µg/mL and was used for quantifying the amount of curcumin in the sample solutions. Representative total ion chromatograms of GaCurNPs samples corresponding to the MRM transition of curcumin are given in Figure 22. Native curcumin and GaCurNPs displayed a lowering of peak intensity with time suggesting the degradation of curcumin with time. The relative lowering of peak area/concentration of curcumin with time was estimated as given in Figure 22b. It's obvious from Figure 14a that the native curcumin degrades faster with time in comparison with the GaCurNPs whose degradation was considerably low. Bare curcumin showed 61.5 % degradation at 6 hours whereas curcumin attached to GaCurNPs exhibited 15.7 % degradation. At 24 hours, the degradation of curcumin was 25% and 93.8% for bare curcumin and curcumin bound to GaCurNPs respectively. The result was in good agreement with the degradation pattern obtained in RP-HPLC. This observation underlines the fact that the formation of nanoconjugates with gallium nanoparticles improves the stability of curcumin and resulted in a suitable reservoir to deliver the action of curcumin *in vitro*.

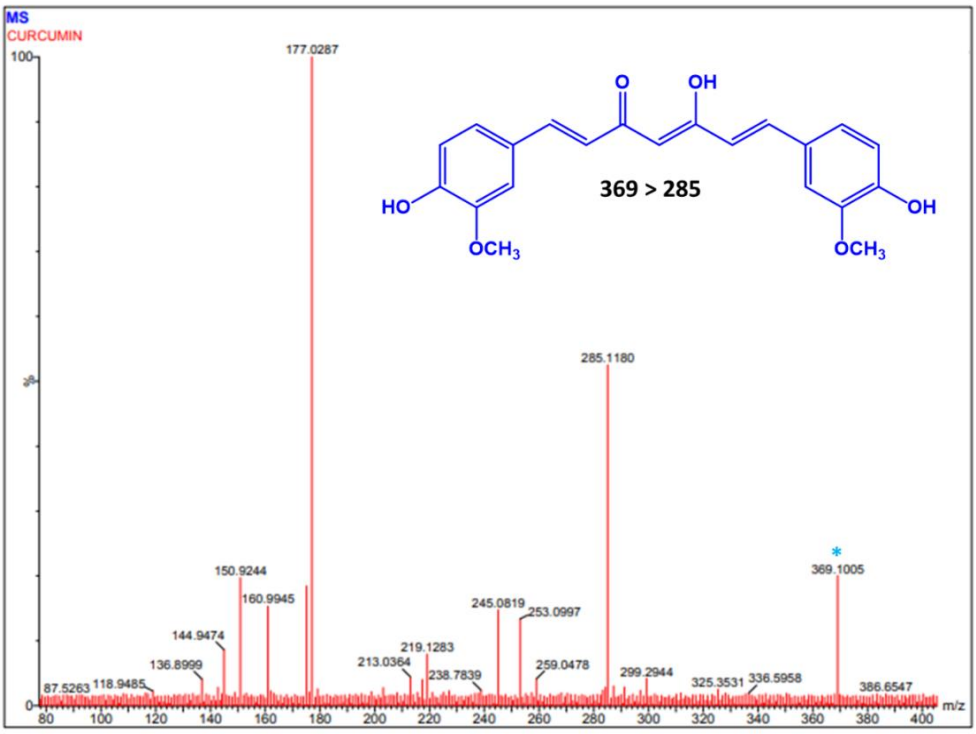

Figure 21: Product ion spectrum of curcumin. The parent ion peak is marked with an asterisk (*).

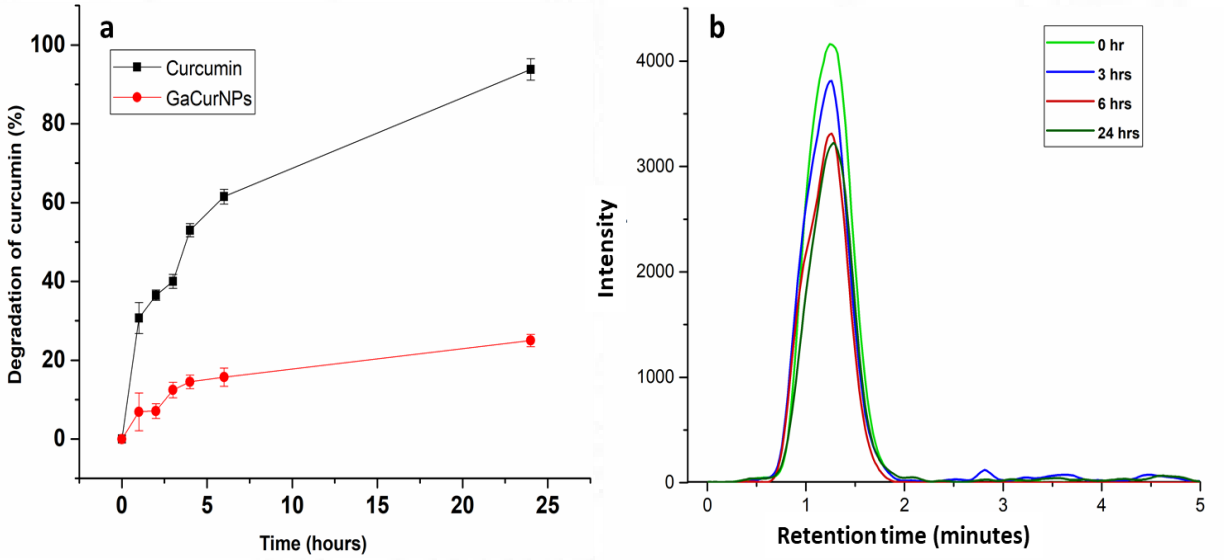

Figure 22: Stability of curcumin in physiological pH: (a) Degradation profile of curcumin and GaCurNPs, (b) chromatogram of curcumin extracted from GaCurNPs.

4.5. Cytotoxicity of GaCurNPs

4.5.1. Phase contrast microscopy

Cytotoxicity of GaCurNPs was first studied using phase contrast microscopy till a concentration of 150 µg/mL. After 24 hours of incubation with the L929 cell line, curcumin as well as GaCurNPs showed no toxicity at 50 µg/mL concentration. At 100 µg/mL of curcumin concentration, the morphology of cells changed owing to the toxicity. GaCurNPs didn't show any significant change in the cell morphology at 100 µg/mL concentration. The cells were in normal morphology on treatment with 150 µg/mL of GaCurNP and fewer cells were seen to be dead (Figure 23h). GaCurNPs were found to be non-cytotoxic even at concentrations greater than MIC concentrations. This suggests that GaCurNPs are found to be less toxic than free curcumin at higher concentrations. The results obtained for curcumin's cytotoxicity coincide with the IC_{50} value of curcumin as reported by Adahoun *et al* which is 458.14 µM (Adahoun et al., 2017).

4.5.2. Alamar blue assay

Using the Alamar blue test, GaCurNPs' cytotoxicity was evaluated in further detail. Alamar blue is a blue non fluorescent dye that may be used to monitor the reducing environment of live cells. It can be reduced to a pink, highly fluorescent resorufin. There is a correlation between the reduction in fluorescence intensity and the cells' reduced capacity to convert resazurin to resorufin due to the increased number of dead cells. Figure 23i shows the impact of varying curcumin and GaCurNPs concentrations on the viability of L929 cell lines. At a dosage of 250 µg/mL, GaCurNPs were shown to increase cell viability to 76.9 %, which was more than that of cells treated with the same amount of curcumin. At 350 µg/mL of GaCurNPs, the cells showed 68.9 % vitality, but at the same dose of curcumin, the cells showed 45.7 % viability. About 90% of the cells were still viable at a dose of 100 µg/mL, which is near the GaCurNPs' minimum

inhibitory concentration (82.75 µg/mL). GaCurNPs were less cytotoxic than curcumin at all tested concentrations. The material is safe to use at large dosages as evidenced by the cell viability of around 70% even at 4MIC concentration.

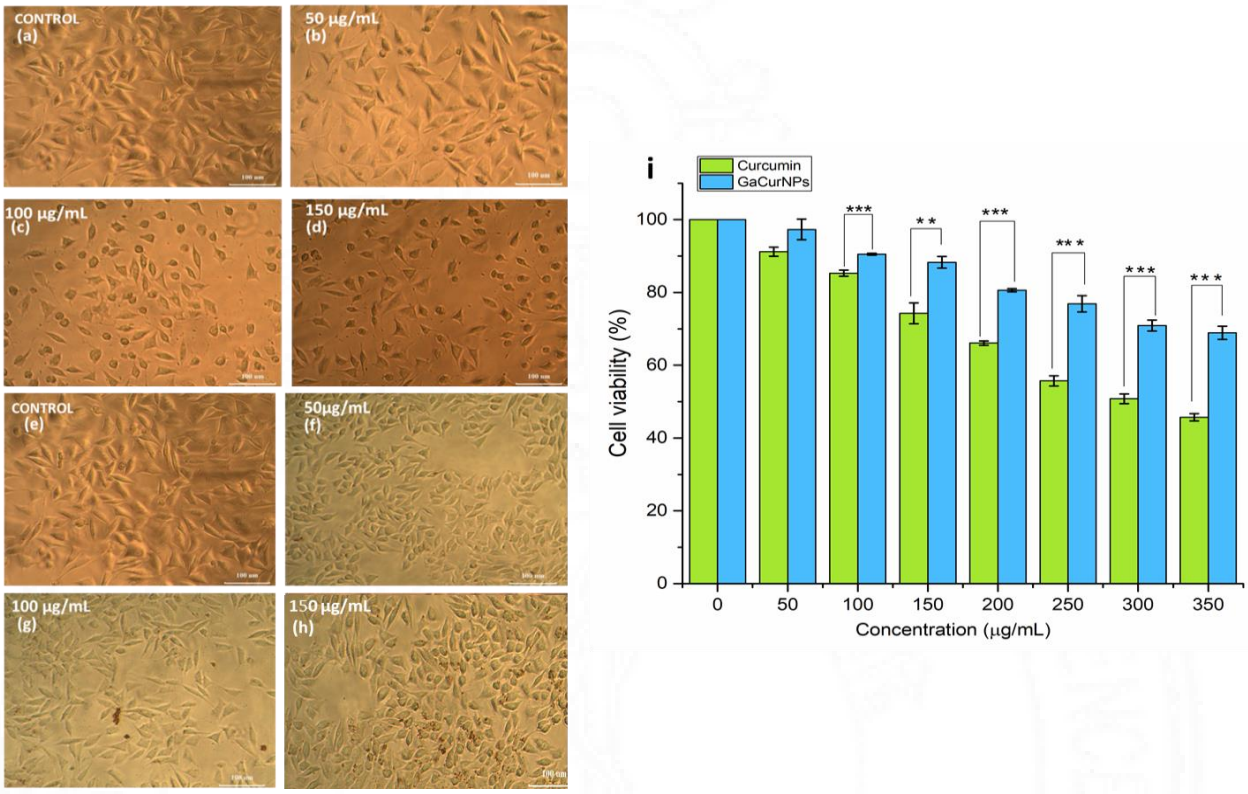

Figure 23: Phase contrast images and Alamar blue assay showing the effect of GaCurNPs and curcumin on L929 cell lines. (a) and (e) control untreated L929cells; (b−d) L929 cells treated with curcumin with concentrations 50, 100, and 150 µg/mL for 24 h, respectively; (f−h) L929 cells treated with GaCurNPs having curcumin concentrations 50,100, and 150 µg/mL; and (i) effect of different concentrations of curcumin and GaCurNPs on the viability of L929 cell lines quantified by the AlamarBlue assay. Values represent Mean±SD and were obtained from three experiments. Statistically significant with $p<0.01$(**) and $p<0.001$(***).

4.6. In vitro antibacterial activity of GaCurNPs against P. aeruginosa

4.6.1 Antibiotic sensitivity of *P. aeruginosa* ATCC 27853 strain and clinical strain

The strains were confirmed as *P. aeruginosa* by conventional biochemical testing as well as by an automated VITEK 2C system (Biomerieux, France). The antimicrobial susceptibility pattern of the two strains is given in the table (Table 14) below:

Table 14: Antibiotic sensitivity of ATCC strain and clinical strain used in the study

Antibiotics	Susceptibility	
	ATCC strain	Clinical strain
Amikacin	S	S
Cefepime	S	S
Aztreonam	R	R
Gentamycin	S	S
Ceftazidime	R	R
Cefperazone + sulbactum	R	R
Piperacillin + Tazobactum	R	R
Ciprofloxacin	S	S
Piperacillin	R	R
Imipenem, Meropenem	S	S
Colistin	S	S

S - susceptible; R - resistant

4.6.2. Determination of MIC by micro-broth dilution method

The MICs of curcumin and GaCurNPs against *P. aeruginosa* were determined using a range of concentrations. Curcumin and GaCurNPs had MIC values of 41.37 μg/mL and 82.75 μg/mL respectively, against *P. aeruginosa* ATCC 27853 at the tested concentrations of 662 μg/mL, 331 μg/mL, 165.5 μg/mL, 82.75 μg/mL, 41.375 μg/mL, 20.68 μg/mL, and 10.34 μg/mL. The results were confirmed by two independent experiments done in triplicates. MIC was the concentration where no turbidity was observed in broth but colonies were formed when transferred from broth to agar plates. In earlier studies, Gunes et al. found curcumin's MIC against *P. aeruginosa* ATCC 27853 to be 175 μg/mL (Gunes et al., 2016) Shivangi *et al.* estimated it to be 512 μg/mL against *P. aeruginosa* ATCC 25619. Another study reported the sub-inhibitory curcumin concentration against *P. aeruginosa* PAO1 to be 125 g/mL (Roudashti et al., 2017). In the present study, the MIC values for four clinical *P. aeruginosa* isolates ranged from 50 μg/mL to 400 μg/mL. The MIC values for all of the strains that were tested in this study are shown in Table 15.

4.6.3. Determination of MIC against clinical isolates by micro-broth dilution method

As per the MIC values detected by the automated VITEK 2 C system (Biomerieux, France), the clinical isolates had varying susceptibilities to well-established antimicrobials including Carbapenems and Colistin. While clinical strain 3 was a highly susceptible strain with susceptibility to even lower antibiotics like amikacin and ceftazidime, clinical strain 2 was an MDR strain with resistance to higher drugs including Colistin, a drug which is frequently used as a last resort for treating MDR infections. The promising MIC values against *P. aeruginosa* merit additional investigations to confirm their antibacterial viability and *in vivo* efficacy against its clinical strains.

Table 15: MIC of curcumin and GaCurNPs against *P. aeruginosa* ATCC 27853 and various clinical strains.

***P. aeruginosa* strain**	**MIC (µg/mL)**		**MBC (µg/mL)**		**Susceptbility to carbepenems and colistin**
	Curcumin	GaCurNPs	Curcumin	GaCurNPs	
ATCC 27853	41.37	82.75	82.75	165	Susceptible
Clinical strain 1	50	100	100	200	Susceptible
Clinical strain 2	100	200	200	400	Resistant
Clinical strain 3	100	200	200	200	Susceptible
Clinical strain 4	50	100	100	200	Susceptible
Clinical strain 5	50	100	100	200	Susceptible

4.6.4. Effect of GaCurNPs on the growth curve

GaCurNPs and curcumin were used in MIC and 2MIC treatments of *P. aeruginosa* ATCC 27853. For six hours, beginning with the 0th hour, the hourly OD values were recorded. The typical growth curve obtained is depicted in Figure 24a. As the data shows, the bacteria treated with GaCurNPs and curcumin recorded a drop in OD values, whereas the untreated *P. aeruginosa* displayed an exponential rise. When *P. aeruginosa* was treated with MIC of GaCurNPs, the bacterial growth was reflected by an initial increase in OD, followed by decreased values, suggesting the antibacterial action of the nanoparticle. A similar trend was observed in the case of curcumin treated cells as well. This increase in OD may be explained as the initial growth period of the bacteria during the period before the entry of the curcumin or nanoparticles into the cells, before initiating cell lysis. The data shows a quicker lysis on treatment with nanoparticles. Curcumin treatment had a 3-hour period before a demonstrable

effect. Bacterial cells when exposed to the 2MIC of curcumin did not show any growth (Figure 24a).

The decrease in OD values of *P.aeruginosa* clinical strain treated with the MIC and 2MIC of GaCurNPs over a period of 0 to 6 hours could indicate that GaCurNPs effectively inhibit the growth of *P. aeruginosa* over time (Figure 24b). The MIC and 2MIC concentrations could exert a bacteriostatic or bactericidal effect, resulting in reduced bacterial proliferation compared to the untreated control. The increased inhibitory effect observed at 2MIC compared to MIC suggests a concentration-dependent response to GaCurNPs treatment i.e., the higher concentrations of GaCurNPs result in greater inhibition of bacterial growth.

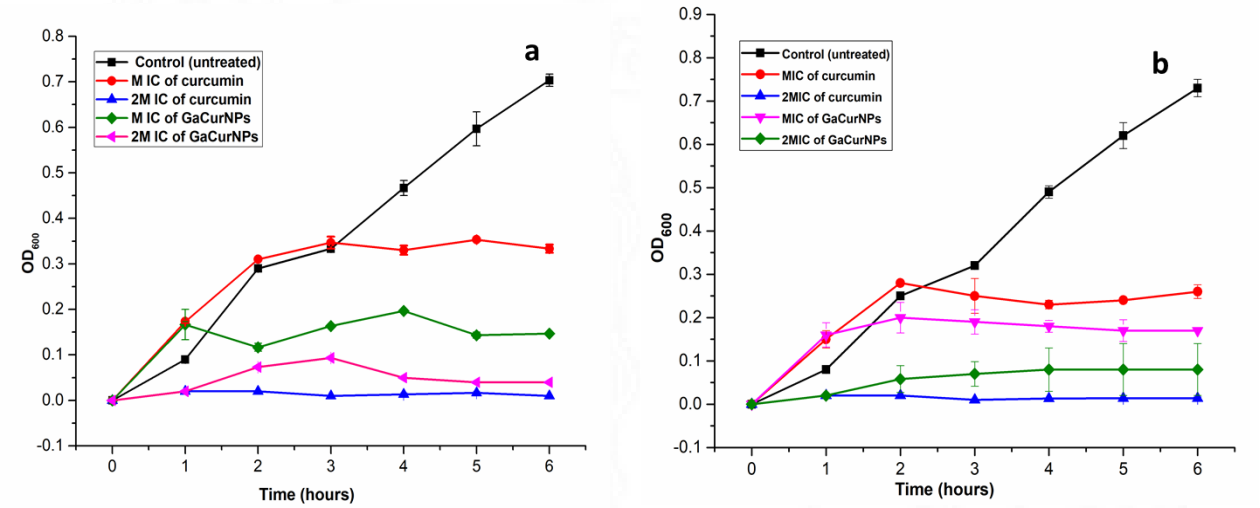

Figure 24: Growth curves of *P. aeruginosa* on treatment with GaCurNPS and curcumin: (a) ATCC strain treated with MIC and 2MIC of curcumin and GaCurNPs and (b) clinical strain treated with MIC and 2MIC of curcumin and GaCurNPs.

4.6.5. Effect of GaCurNPs on viability - Live/dead assay

P. aeruginosa ATCC 27853 was treated with the MIC of GaCurNPs and curcumin for 3 hours, after which the live/dead experiment was conducted. Bacterial cells treated with GaCurNPs and curcumin were labeled with SYTO9/ PI stain to study the percentage of live/dead cells. The

untreated control of ATCC strain showed 100% live cells stained by SYTO9 and exhibited green color with motility when viewed under microscope. Images from fluorescence microscopy demonstrated that *P. aeruginosa* bacteria were live and viable in the control and untreated conditions (Figure 25a). PI staining caused the cells treated with the MIC of GaCurNPs to appear red, indicating disruption of the cell membrane integrity (Figure 25c). At MIC, GaCurNPs caused bacterial cell death by cell membrane rupture. These findings show strong correlations with the findings from Raman and SEM investigations as well as growth curve estimates (described later in sections 4.6.8 and 4.6.9). When compared to GaCurNPs, bacterial cells treated with the MIC of curcumin displayed fewer dead cells (Figure 25b), suggesting a slower bactericidal action by curcumin.

P. aeruginosa clinical strain treated with MIC of GaCurNPs showed around 80% bacterial cell death (Figure 26c). Cells had lost their motility and were observed in orange color indicating imminent cell death. Cells treated with GaCurNPs showed an increased number of dead cells in comparison with what was obtained after treatment with curcumin. This points to the increased activity of GaCurNPs on *P. aeruginosa*.

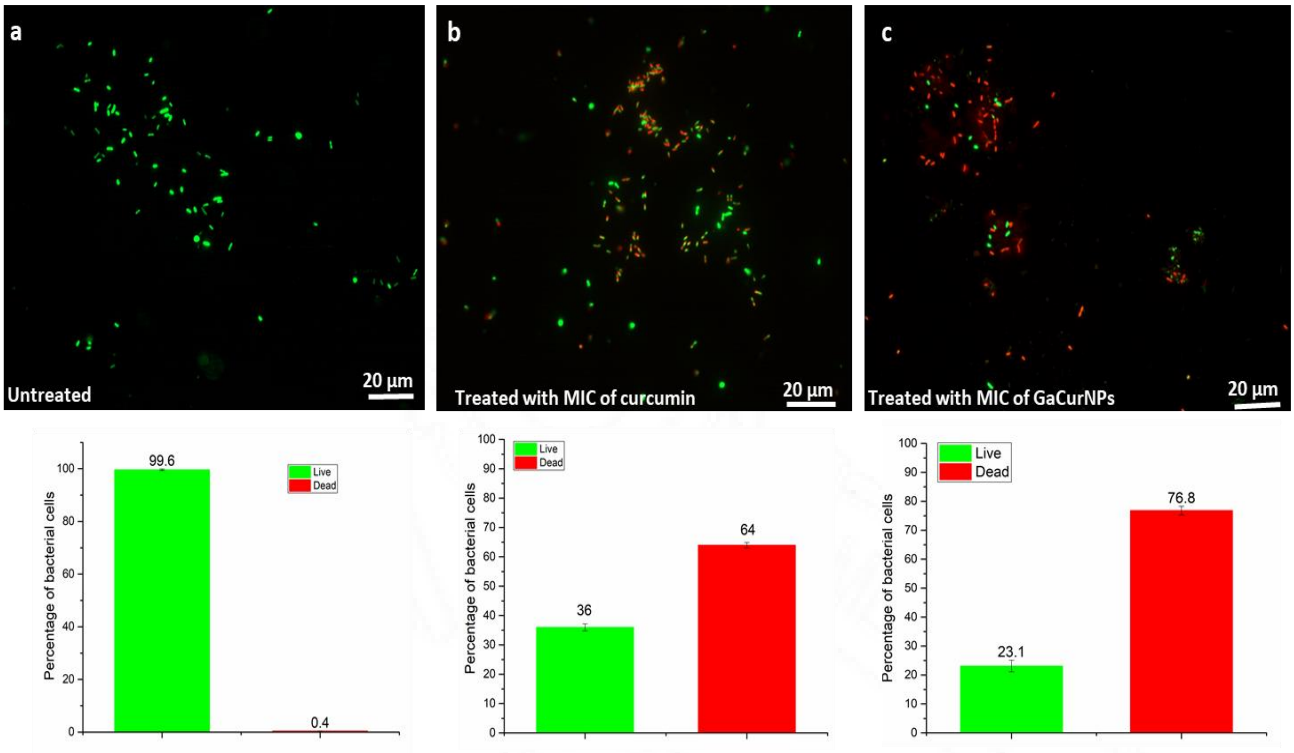

Figure 25: Fluorescence microscopy images of *P. aeruginosa* ATCC 27853 strain treated with GaCurNPs. (a) untreated control (b) treated with MIC of curcumin (c) treated with MIC of GaCurNPs.

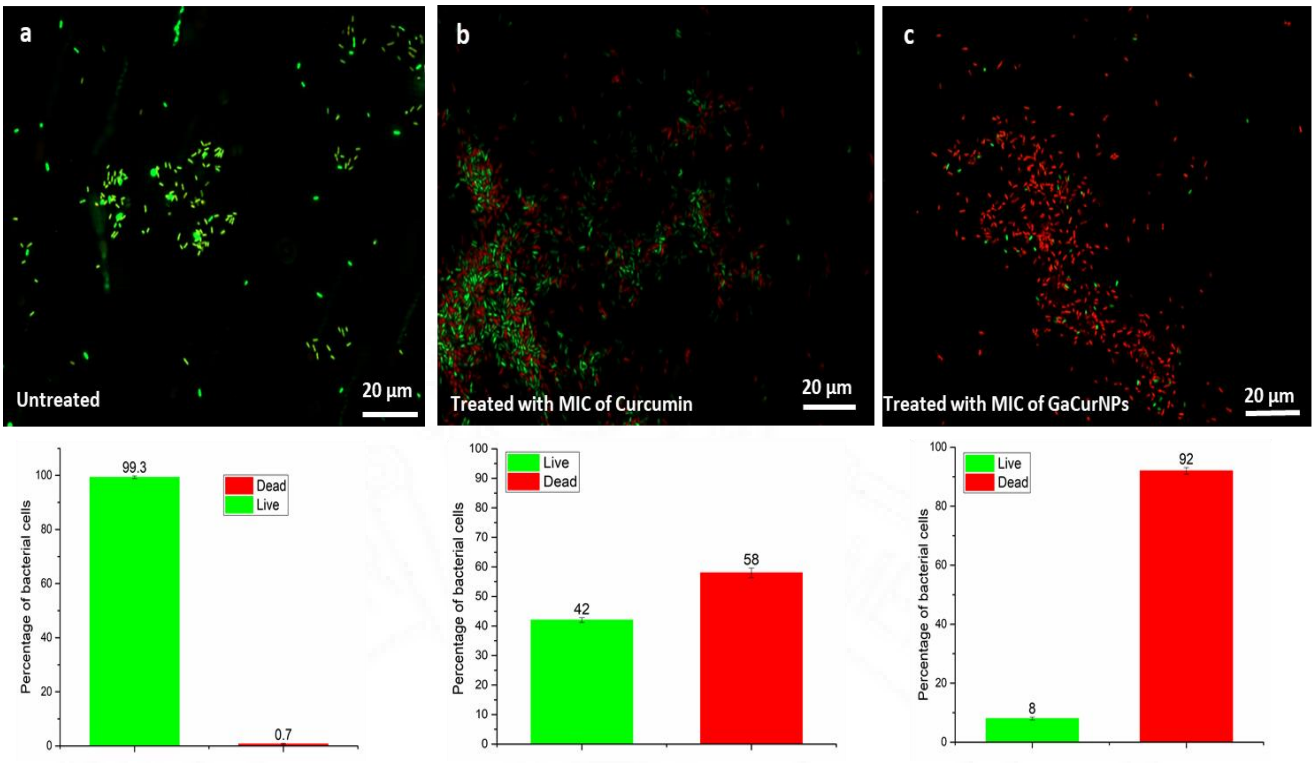

Figure 26: Fluorescence microscopy images of *P. aeruginosa* clinical strain treated with GaCurNPs. (a) untreated control (b) treated with MIC of curcumin (c) treated with MIC of GaCurNPs.

4.6.6. Effect of GaCurNPs on the swarming motility

Swarming is more than just a way of locomotion. It represents a complicated adaptation that results in changes in the expression of genes associated with virulence and antibiotic resistance (Köhler et al., 2000). Swarming motility is closely associated with quorum sensing in *P. aeruginosa*. Curcumin has been reported to inhibit the swarming motility of *Serratia marsescens* completely (Santos et al., 2021). Higher concentrations of curcumin (100 µg/mL, 200 µg/mL, and 300µg/mL) were known to sharply decrease the swarming motility of *P.aeruginosa* 24-hour culture (Modi et al., 2023). On treatment with MIC and 2MIC of curcumin and GaCurNPs, the swarming motility of both *P. aeruginosa* ATCC 27853 and the clinical strain was found to be reduced. In the ATCC strain, the swarming motility of untreated bacteria was represented by a

diameter of 14 mm (Figure 27a). On treatment with MIC of GaCurNPs, the motility was reduced and the diameter was 7.5 mm. This implies that the motility was reduced almost by half on 3 hours of treatment with MIC of GaCurNPs when compared to untreated bacteria. Similarly, treatment with MIC of curcumin also reduced the motility of the ATCC strain to a diameter of 8.5 mm. On treatment with 2MIC of GaCurNPs and curcumin, the diameter was reduced to 3.1 mm and 3.5 mm, respectively, in ATCC strain. So, higher concentrations of GaCurNPs and curcumin effectively inhibited the swarming motility of *P. aeruginosa* with a 77.8% decrease on treatment with 2MIC of GaCurNPs.

The swarming motility of the clinical strain was comparatively lower than that of the ATCC strain (Figure 28a). The untreated clinical strain showed 7.4 mm diameter in the swarming plate. On treatment with 2MIC of GaCurNPs, the diameter observed was 1.75 mm ie., there was a 76.3% decrease in the swarming motility of bacteria. The treatment of bacteria with the MIC of GaCurNPs also reduced the motility by 33.3%. MIC and 2MIC of curcumin showed a decrease in motility by 59.4% and 72.9% respectively. This could indicate the anti-QS effect of GaCurNPs.

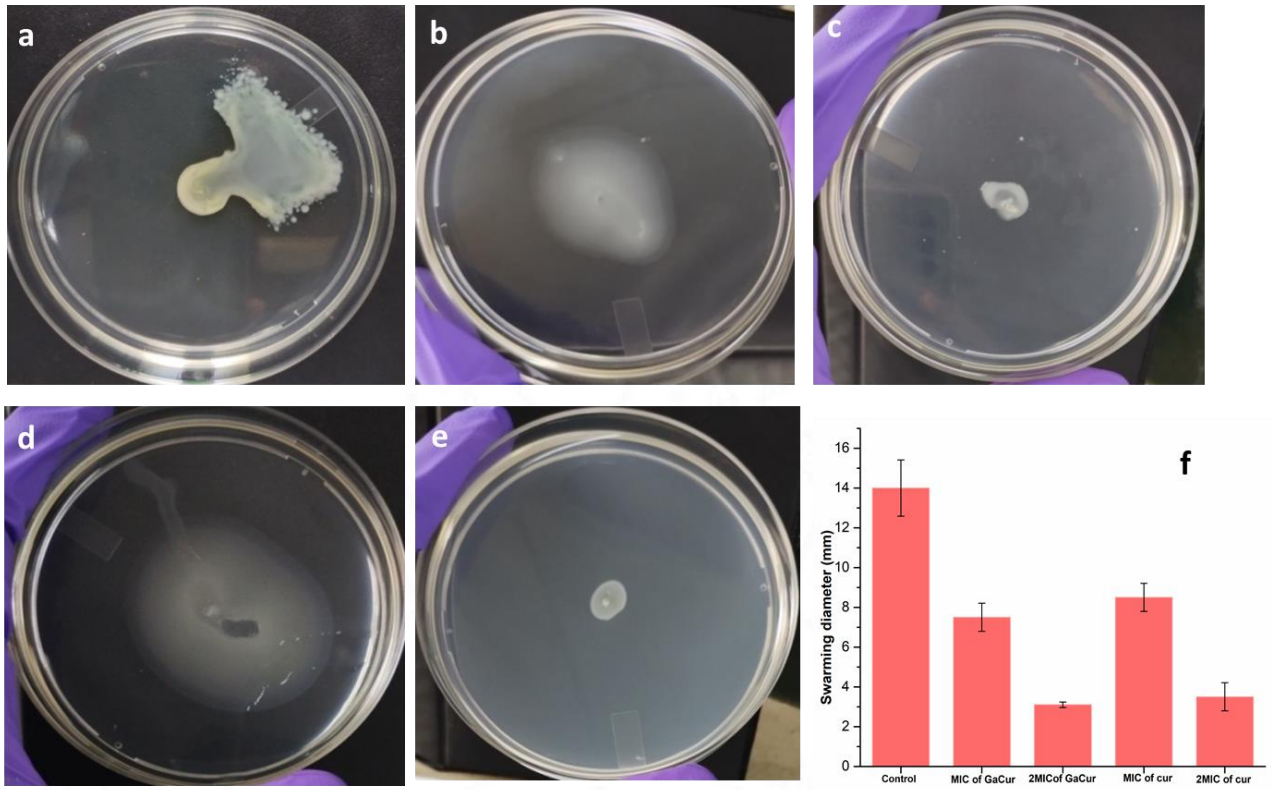

Figure 27: Effect of GaCurNPs on the swarming motility of *P. aeruginosa* ATCC 27853 strain. (a) Untreated control, (b) treated with MIC, and (c) 2MIC of GaCurNPs, (d) treated with (e) MIC, and (e) 2MIC of curcumin.

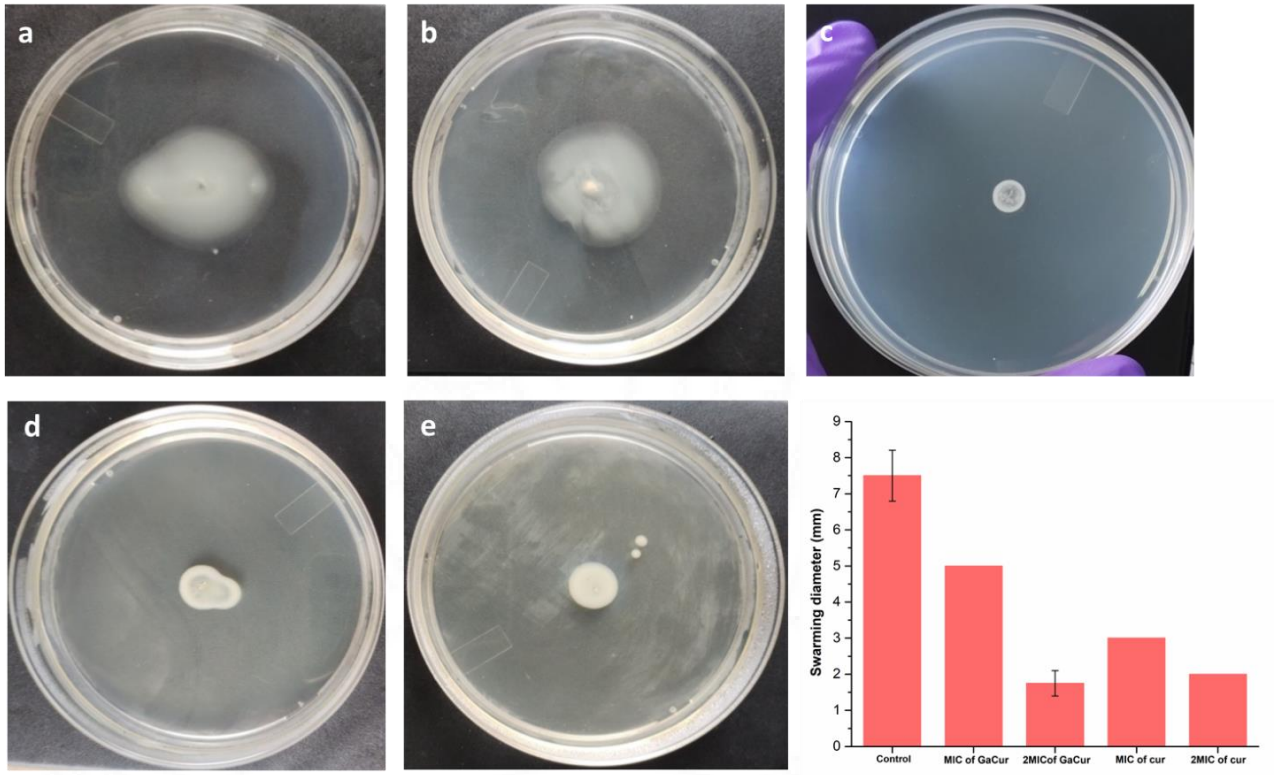

Figure 28: Effect of GaCurNPs on the swarming motility of *P. aeruginosa* clinical strain. (a) Untreated control (b) treated with MIC and (c) 2MIC of GaCurNPs (d) treated with MIC and (e) 2MIC of curcumin.

4.6.7. Effect of GaCurNPs on pyocyanin production

Production of pyocyanin by both *P. aeruginosa* ATCC 27853 and clinical strain in the presence of different concentrations of GaCurNPs and curcumin was studied. An increase in the concentration of curcumin and GaCurNPs reduced the production of pyocyanin by *P. aeruginosa* in both strains. Previous reports have proven that curcumin reduces pyocyanin production in *P. aeruginosa* (Rudrappa and Bais, 2008). Studies have also shown that sub-inhibitory concentrations of metal-curcumin complexes reduced pyocyanin production in *P. aeruginosa* PAO1 (Gholami et al., 2020). In the ATCC strain, the untreated bacteria produced 3.5 µg/mL pyocyanin. This pyocyanin production drastically reduced on treatment with 2MIC of GaCurNPs

to 0.46 µg/mL, an 86.85% reduction, whereas with treatment with 2MIC curcumin, it reduced by 86.28%. On treatment with MICs of curcumin and GaCurNPs, a 51.4% and 78.5% respective reduction in pyocyanin production was observed. In clinical strain, bacteria without treatment showed pyocyanin production of 1.79 µg/mL. On treatment with 2MIC of curcumin and GaCurNPs, the pyocyanin production decreased to 0.31 µg/mL and 0.41 µg/mL, respectively. There is a significant statistical difference in the decrease in bacterial pyocyanin production when treated with MIC of curcumin and GaCurNPs in both ATCC and clinical strains. In *P. aeruginosa*, the formation of biofilm is intricately linked with pyocyanin production, which is involved in maintaining the stability and structural integrity of the biofilms (Das et al., 2016) (Chimi et al., 2024). The observed reduction in pyocyanin production implies that GaCurNPs may hinder the development of biofilms by disrupting mechanisms mediated by pyocyanin. In clinical settings, disrupting the production of *P. aeruginosa* biofilms is especially important since these biofilms are linked to antibiotic resistance and persistent infections and are notoriously difficult to eliminate. QS processes govern *P. aeruginosa'*s synthesis of pyocyanins, and bacterial coordination and communication are essential for controlling the expression of virulence factors and biofilm formation. The observed decrease in pyocyanin levels could be a result of GaCurNPs interfering with QS signaling pathways, which in turn would disrupt the communication network and reduce the expression of the genes involved in pyocyanin production.

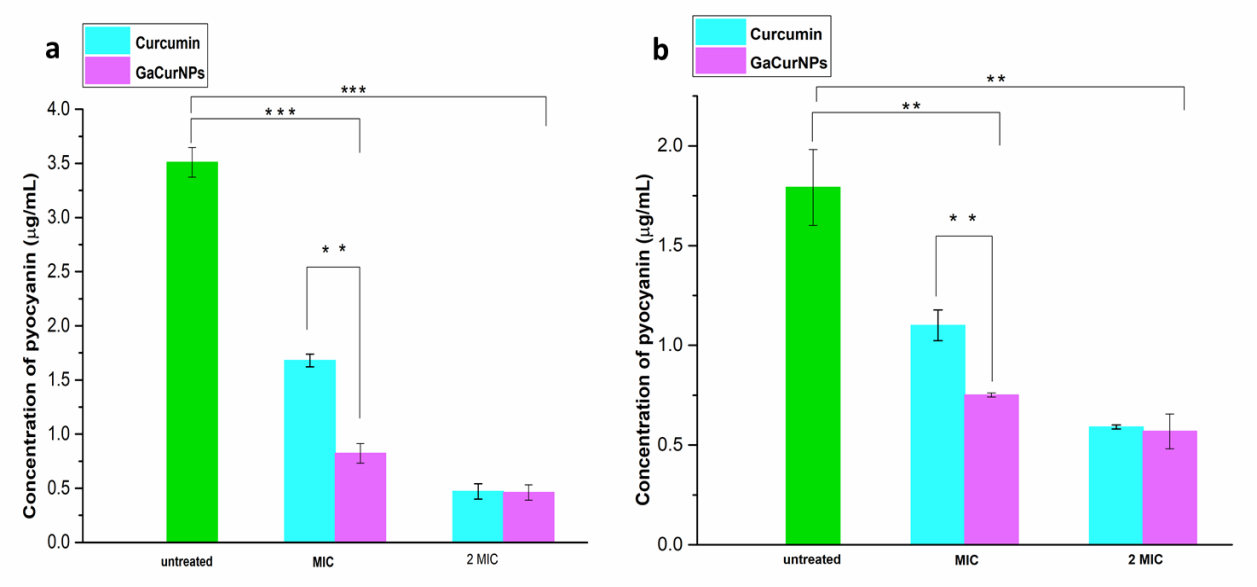

Figure 29: Effect of different concentrations of curcumin and GaCurNPs on Pyocyanin production by *P. aeruginosa.* (a) Pyocyanin production by *P. aeruginosa* ATCC 27853 and (b) *P. aeruginosa* clinical strain. Values represent Mean ± SD obtained from three experiments. Statistically significant with $p < 0.01$(**) and $p < 0.001$(***).

4.6.8. ROS production by DCFDA assay

ROS production in both *P. aeruginosa* ATCC 27853 and clinical strain was studied using DCFDA assay (Figure 30). Curcumin is known to have increased ROS production in bacteria as well, and it is one of the mechanisms by which nanoparticles bring about its antibacterial effect (Yu et al., 2020; Dai et al., 2022; Zheng et al., 2020; Yun and Lee, 2016). ROS production causes membrane peroxidation, DNA damage, and inactivation of several enzymes crucial for the survival of bacteria. On treatment with MIC of curcumin and GaCurNPs, ATCC strain showed an increase in ROS production compared to untreated control. 2MIC treatment increased ROS production to a much higher level. As evident from the SEM images, the membranes were damaged and this may be possibly due to the membrane peroxidation caused by the production of ROS in the bacterial cell.

In the clinical strain, a similar observation was made. MIC treatment considerably increased ROS production, which almost doubled when treated with 2MIC of GaCurNPs. This increase is statistically significant as well when compared to untreated and curcumin-treated. The results obtained from SEM showed membrane damage that may be co-related with this GaCurNPs-induced ROS production during treatment. The potential of GaCurNPs as antimicrobial agents with oxidative stress-mediated modes of action is highlighted by the statistically significant increase in ROS generation in *P. aeruginosa* treated with MIC and 2MIC of GaCurNPs. It was comparable to the effect of curcumin on the strains. GaCurNPs' ability to induce the formation of ROS points to a possible mechanism of action for their antibacterial activity against *P. aeruginosa*. GaCurNPs may interact with bacterial cells, setting off a series of biological events, including oxidative processes that ultimately lead to bacterial cytotoxicity. The additional antimicrobial actions of GaCurNPs, such as membrane rupture, decrease in pyocyanin production, or reduction in swarming motility may be supplemented by this oxidative stress-mediated approach.

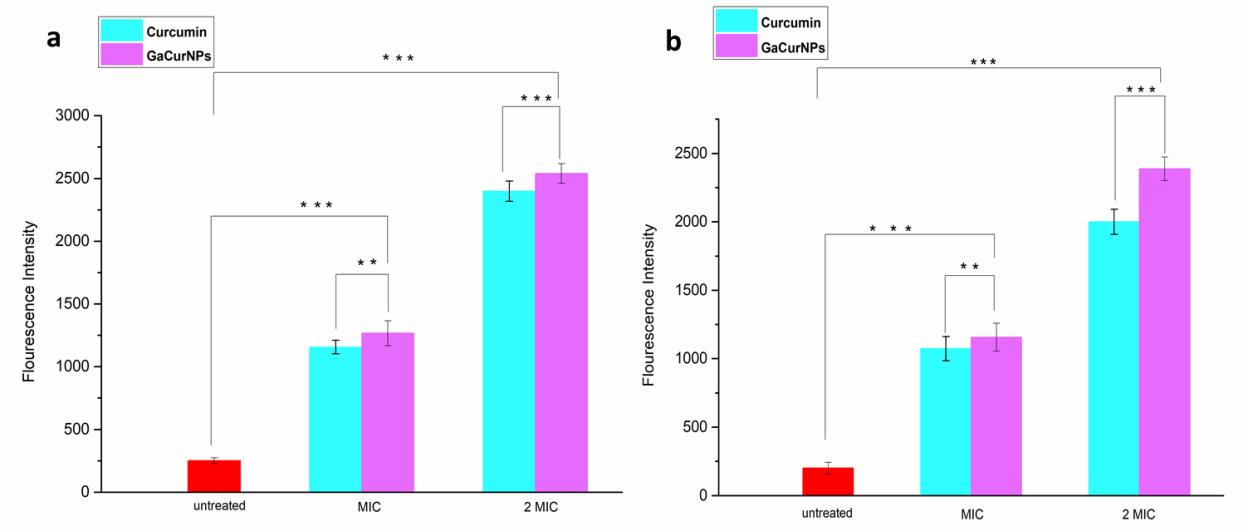

Figure 30: ROS production in *P. aeruginosa* on treatment with different concentrations of curcumin and GaCurNPs. (a) *P. aeruginosa* ATCC 27853 and (b) clinical strain. Values represent Mean ± SD and were obtained from three experiments. Statistically significant with $p<0.01$(**); $p<0.001$(***).

4.6.9. Antibacterial activity of GaCurNPs: Raman spectroscopy evidence

Anti-bacterial activity of GaCurNPs against *P. aeruginosa* was studied using Raman spectroscopy. Proteins, nucleic acids, lipids, and polysaccharides are among the biochemical components found in bacterial cells that may be identified by their distinctive molecular fingerprints using Raman spectroscopy. Following treatment with GaCurNPs and curcumin, changes in the Raman spectra were detected, indicating modifications in the composition or conformation of these biomolecules and the effect of the antimicrobial drugs on bacterial physiology. Untreated *P. aeruginosa* was used as control, and the Raman peaks were assigned as in Table 5. The Raman peaks were scattered between 500 and 1700 cm^{-1}. The hydrophobic amino acid valine was indicated by the peak at 671 cm^{-1}, whereas the strong peak at 744 cm^{-1} represented a wagging vibration of tryptophan. At 778 cm^{-1}, the peak for uracil, cytosine, and

thymine ring breathing was obtained. Wavenumber 1000 cm^{-1} was associated with phenylalanine and the C−C stretching of glycosidic linkage, whereas the peak at 1120 cm^{-1} was attributed to C−O−C skeletal stretching. The amide II and I peaks were obtained at 1582 and 1660 cm^{-1}, respectively. A strong peak at 744 cm^{-1} suggested tryptophan, a hydrophobic amino acid. The peak at 671 cm^{-1} referred to the valine stretching vibration. The spectra of *P. aeruginosa* treated with curcumin and GaCurNP show notable variations when compared to the control. It was reported that curcumin's antibacterial activity against *P.aeruginosa* PA01 was caused by the downregulation of the biofilm initiation gene (Rudrappa and Bais, 2008). The difference in the 1125 cm^{-1} peak, which is contributed by the C-O stretching of saccharide, correlates with the earlier findings reported by Rudrappa *et al*. Curcumin may act on *P. aeruginosa* by downregulating genes associated with biofilm formation, which may have resulted in the decreased production of polysaccharides. In contrast to the GaCurNP- treated system, the curcumin-treated system exhibited more resolved peaks. The weak and indistinct/unresolved peaks in GaCurNPs could indicate the enhanced activity of GaCurNPs. Independent research groups have shown that curcumin appears to have strain-specific antibacterial action. The action of curcumin is known to be associated with membrane disruption in *S. aureus*, *E. coli*, *P. aeruginosa*, and *Enterococcus faecalis* (Tyagi et al., 2015b). In an earlier study silver-curcumin nanoparticles were shown to interact with the cell membrane of bacteria and cause its disruption resulting in the leakage of the cell contents (Bhawana et al., 2011). In both the curcumin-treated and GaCurNP-treated systems, there is a significant decrease in the 2927 cm^{-1} ($-CH_2$ peak), indicating the disintegration and rupture of the cell membrane. Also, the peaks at 1309 cm^{-1}, contributed by the -CH groups, were indistinguishable indicating severe damage to the bacterial membrane (Figure 31b).

As described earlier, one of the major mechanisms of action of nanoparticles in bacteria is the formation of reactive oxygen species (ROS) (Wang et al.,2017). The diminished peaks related to DNA and protein could be due to the interaction of this ROS with these intracellular components which resulted in the leaking of cells. Ciprofloxacin, a fluoroquinolone antibiotic, binds covalently to DNA gyrase and topoisomerase IV (Hooper.,1999). The Raman spectral characteristics in the ciprofloxacin-treated (0.5 and 1μg/mL) sample were similar to those of control bacteria (Figure 31c). Following a 24-hour treatment with ciprofloxacin, we observed a significant alteration in the spectrum characteristics of the bacteria, suggesting that their cell structure had been destroyed (Figure 31d). This suggests that GaCurNPs were able to bring about the antibacterial activity within 3 hours of contact with the bacteria.

In the case of *P. aeruginosa* clinical strain also, there was a significant change in the Raman spectra after treatment with GaCurNPs. The clinical strain exhibited Raman peaks characteristic of the species (Table 5). On treatment with GaCurNPs for 3 hours, major peaks in the fingerprint region (400- 1800 cm^{-1}) of Raman spectra were diminished and also found to be unresolved (Figure 32c). On 3-hour treatment with ciprofloxacin itself, a significant change in the Raman spectra was observed. On 24-hour treatment, no Raman peaks were observed pointing to the destruction of bacterial cells. The peaks at 2927 cm^{-1}, 1309 $cm^{-1,}$ and 1125 cm^{-1} were reduced in GaCurNPs and curcumin-treated bacteria similar to the observations made for the *P. aeruginosa* ATCC 27853 strain. The alterations noticed in Raman spectra offered insights into the mechanisms of action underlying curcumin and GaCurNP's antibacterial properties. Changes in the vibrational modes of proteins, for example, might be a sign of protein denaturation or aggregation, which would interfere with crucial enzymatic processes necessary for the survival

of bacteria. Alterations in lipid composition or membrane characteristics might compromise membrane integrity, resulting in cell leakage or reduced absorption of nutrients.

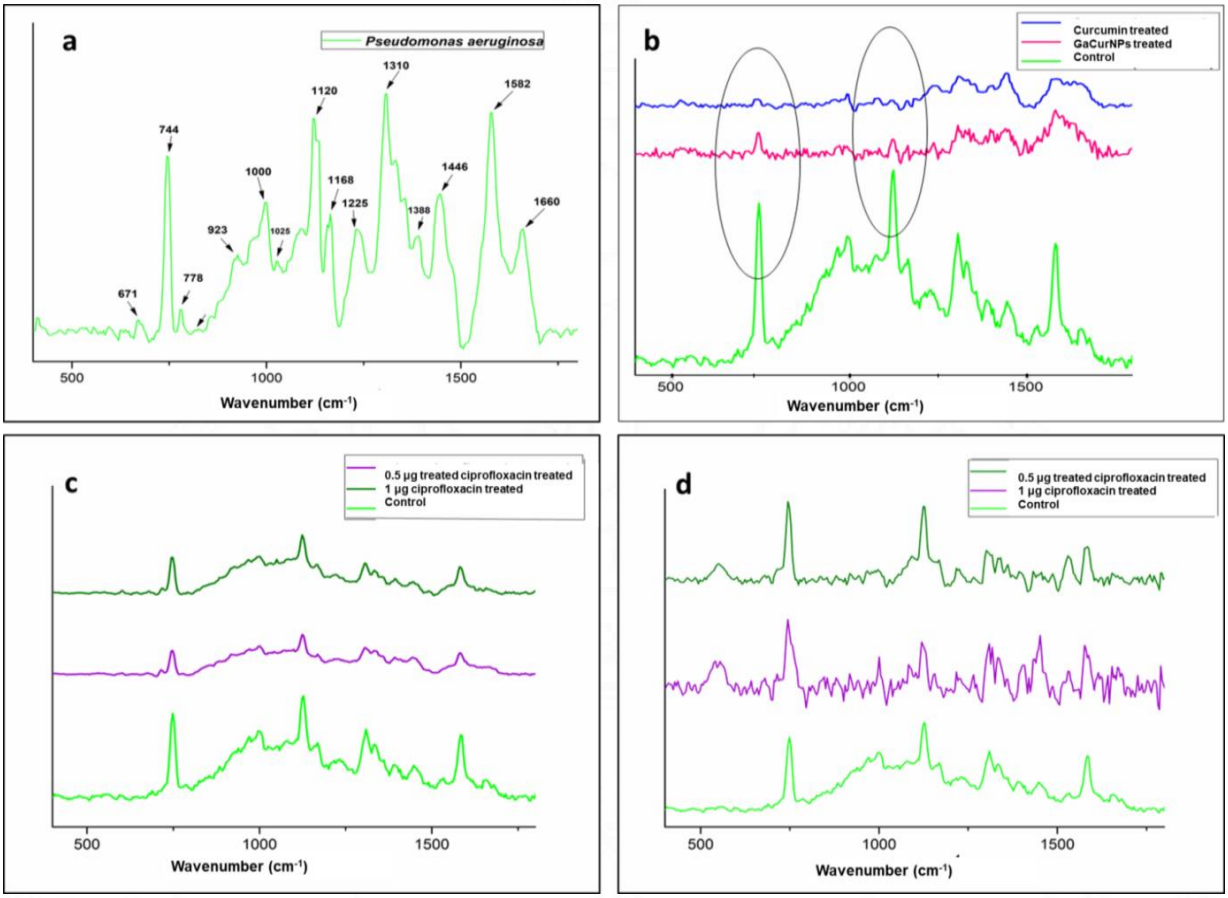

Figure 31: Effect of GaCurNPs on Raman spectra of *P. aeruginosa* ATCC 27853. (a) untreated control (b) treated with MIC of curcumin and GaCurNPs for 3 hours (c) treated with different concentrations of ciprofloxacin for 3 hours (d) treated with different concentrations of ciprofloxacin for 24 hours.

Table 15: Peak assignment of wavenumber

Wavenumber (cm^{-1})	Peak assignment
671	Valine, $CN^{+}(CH_3)_3$ stretching (De Gelder et al., 2007)
744	Wagging l-tryptophan (Freire et al., 2017)
778	Uracil, Cytosine, Thymine ring breathing (Jung et al., 2014)
829	O-P-O symmetric stretching, Ring br. Tyrosine
923	Stretching vibration of C-C
1000	Symmetric ring breathing of Phenylalanine (Jung et al., 2014)
1029	-CH in-plane vibration of Phenylalanine (Jung et al., 2014)
1120	C-C stretching, C-O-C skeletal stretching - glycosidic linkage of saccharides, C-C stretching - glycosidic linkage of saccharides (Jung et al., 2014)
1168	Guanine, Cytosine, C-H Tyrosine, Phenylalanine, *ν*(C-O-C) (Jung et al., 2014)
1310	-CH deformation vibration
1446	Guanine, Adenine, CH deformation vibration (Jung et al., 2014)
1582	Guanine, Adenine, Amide II (Jung et al., 2014)
1660	Amide I

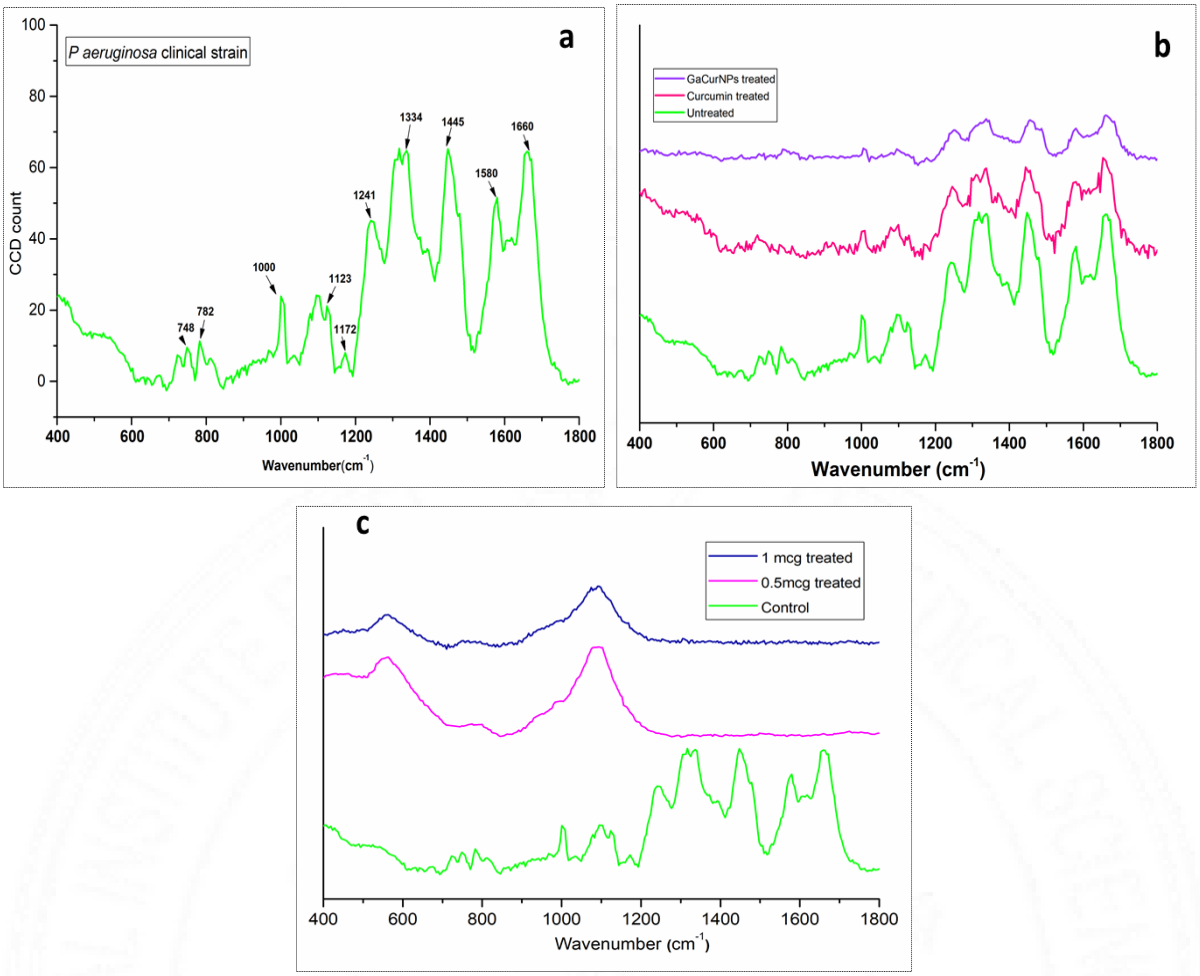

Figure 32: Effect of GaCurNPs on Raman spectra of *P. aeruginosa* clinical strain. (a) untreated (b) treated with MIC of curcumin and GaCurNPs for 3 hours (c) treated with different concentrations of ciprofloxacin for 3 hours.

4.6.10. Effect of GaCurNPs on bacterial cell morphology - Scanning electron microscopy evidence

SEM provided additional evidence of bacterial cell wall damage. *P. aeruginosa*, both ATCC and clinical strains, treated with MICs of GaCurNPs, curcumin, and ciprofloxacin, were imaged using FESEM to the results obtained by Raman spectroscopy. Untreated *P. aeruginosa* ATCC 27853 was used as control (Figure 33a). From the FESEM images, it is evident that GaCurNPs have membrane-damaging properties (Figure 33d). It has been established from earlier studies

that the size of the nanoparticles plays a key role in its antibacterial activity, i.e., smaller nanoparticles elicit better antibacterial activity (De Gelder et al., 2007). Curcumin nanoparticles of size ~ 110 nm in size is known to penetrate bacterial cells and cause membrane lysis (Pandit et al., 2015). 2-40 nm-sized curcumin nanoparticles were also shown to cause membrane damage in bacterial cells (Bhawana et al., 2011). Nanoparticles greater than 10 nm in size have been observed to get wrapped by the bacterial membrane, in an *in vitro* study, regardless of the surface chemistry. The same study, however, showed that the adhesion of large nanoparticles (>10 nm) on the bacterial lipid membrane resulted in cell deformation or crumbling (Linklater et al., 2020). The particle size observed in our study for GaCurNPs was 25-35 nm, and therefore, these particles may possess significant penetration capability causing cell membrane damage leading to oozing out of cell contents.

In the case of GaCurNPs, the activity elicited may be a combined activity of nanoparticles and curcumin. Crater/dent formation was also observed in GaCurNP-treated bacteria. Notably, the activity of GaCurNPs was elicited within 3 hours of incubation. The bacterial membrane damaging property of curcumin (termed curcumin I) was reported by Tyagi *et al* with supporting SEM images (Tyagi et al., 2015b). The surface dent/ craters formation that resulted when the bacterial cells were treated with curcumin (Figure 33c), suggests membrane destruction. In the case of ciprofloxacin-treated bacteria (Figure 33b), the bacterial morphological features were different from those caused by nanoparticle and curcumin treatment. As evident from Fig. 33b, some cells were observed to be in a transitional phase to become 'Ovoid cells' and some exhibited close to spherical shape characteristic of bacteria treated with ciprofloxacin. It has been reported that ciprofloxacin treatment results in pleated cell walls and shrinkage of cells which was observed in the present study as well (Figure 33b) (Rai et al., 2008). GaCurNPs exhibited a

rapid and superior cell-damaging effect on *P. aeruginosa* and destroyed the cells within 3 hours of treatment, in comparison with ciprofloxacin.

Similar results were observed for *P. aeruginosa* clinical strain also. Bacteria treated with GaCurNPs showed severe membrane damage within 3 hours of exposure (Figure 34d). Clinical strain treated with ciprofloxacin showed pleated cell membrane (Figure 34b). The observed damage to the cell membrane indicates that GaCurNPs disrupt the lipid bilayer structure of the bacterial cell membrane. The nanoparticles interact with the lipids in the membrane to cause lipid peroxidation, pore development, or membrane destabilization (Ozdal and Gurkok, 2022; Niu and Zhang, 2023; Hettiarachchi et al., 2021). Bacterial cell death results from these membrane-disruptive actions, which impair membrane integrity and function.

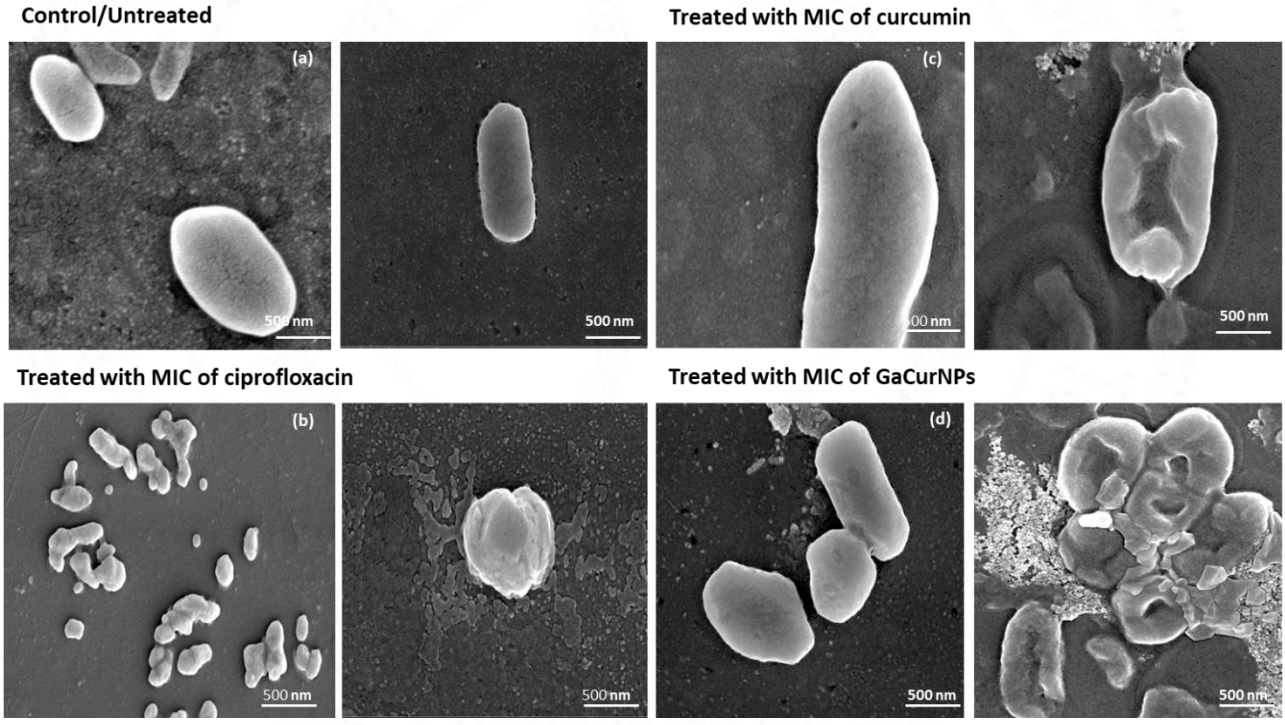

Figure 33: Scanning electron micrographs of *P. aeruginosa* ATCC 27853 showing the effect of GaCurNPs. (a) untreated (b) treated with MIC of ciprofloxacin (c) treated with MIC of curcumin (d) treated with MIC of GaCurNPs.

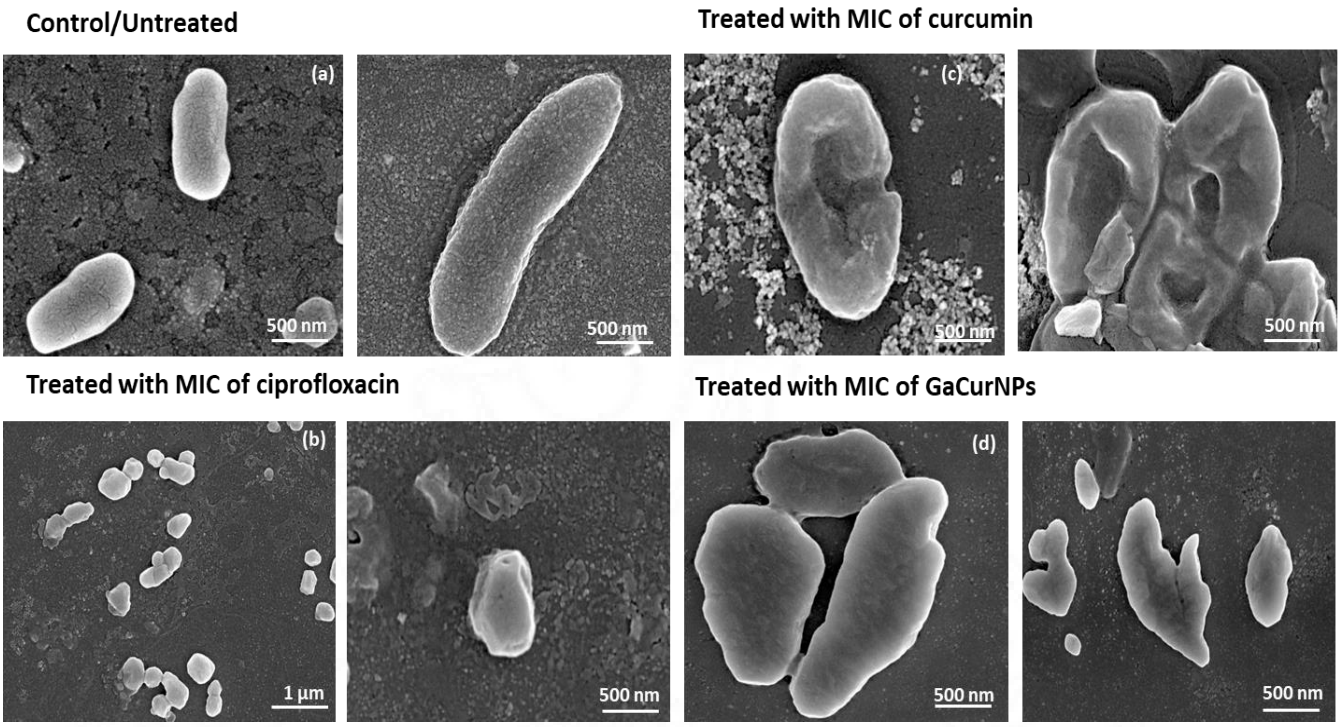

Figure 34: SEM images of *P. aeruginosa* clinical strain showing the effect of GaCurNPs: (a) control/untreated (b) Treated with ciprofloxacin (c) treated with MIC of curcumin (d) treated with MIC of GaCurNPs.

4.7. In vitro anti - biofilm activity of GaCurNPs

4.7.1. Crystal violet assay

4.7.1.1. Effect of GaCurNPs on P. aeruginosa ATCC 27853 biofilm

The effect of GaCurNPs on *P. aeruginosa* ATCC 27853 and clinical strain biofilm formation was evaluated using crystal violet assay. Bacteria were inoculated with different concentrations of bare curcumin and GaCurNPs to initiate the formation of a biofilm. The control, without the particles, showed satisfactory biofilm formation. However, inhibition of biofilm formation was noted in the treated cases. The 4MIC concentration of GaCurNPs inhibited biofilm formation by 93.95% while the same of curcumin inhibited biofilm formation by 84.08%. A 33.8% reduction in biofilm formation was observed when 2MIC concentration of GaCurNPs was used and a

slightly higher reduction in biofilm formation was exhibited by 2MIC GaCurNPs which is 28.7% A 15.36% reduction in biofilm formation was observed when bacteria were inoculated with the MIC of GaCurNPs. The results indicated that GaCurNPs at an increasing concentration have the potential to inhibit biofilm formation in *P. aeruginosa* ATCC 27853.

P. aeruginosa ATCC 27853 biofilm grown for 24 hours was treated with MIC, 2MIC, and 4MIC concentrations of bare curcumin and GaCurNPs to study the effect on mature biofilm. The biofilm grown for 24 hours was treated with MIC, 2MIC and 4MIC of curcumin. 2MIC of curcumin disrupted biofilm by 33.41% whereas the 2MIC concentration of GaCurNPs reduced the biofilm by 41.97%. 4MIC concentration of GaCurNPs showed 89% disruption of the 24-hour-old biofilm.

4.7.1.2. Effect of GaCurNPs on P. aeruginosa clinical strain biofilm

It was shown in section 4.7.1.1. that GaCurNPs can inhibit biofilm formation. A similar pattern of biofilm inhibition by GaCurNPs was observed with the clinical strain as well. On treatment with MIC and 2MIC of GaCurNPs, the inhibition of biofilm formation was found to be slightly lower than that elicited by curcumin, resulting in 12.03% and 50.83% inhibition respectively. However, at higher concentrations i.e., 4MIC of GaCurNPs brought about 98.95% inhibition resulting in a more significant impact compared to curcumin.

In 24-hour mature biofilm, GaCurNPs caused 14.36% and 26.23% disruption at MIC and 2MIC concentrations (Figure 35b). At 4MIC concentration, GaCurNPs elicited a 97.13% reduction in the biofilm.

Higher concentrations of GaCurNPs resulted in more extensive disruption of biofilm structure, indicating a direct relationship between GaCurNPs concentration and biofilm disruption efficacy.

The observation of dose-dependent inhibition of biofilm formation with progressive concentrations of GaCurNPs highlights the potency of GaCurNPs in disrupting biofilm development by *P. aeruginosa*. This finding is consistent with previous studies demonstrating the dose-dependent antimicrobial effects of curcumin nanoparticles against biofilms (Loo et al., 2016) (Palanisamy et al., 2023). A similar finding was also made by Sharifian *et al* where nano curcumin inhibited biofilm formation in a dose-dependent manner (Sharifian et al., 2020). GaCurNPs may involve several factors, including physical disruption of biofilm structure, inhibition of extracellular matrix production, and induction of bacterial cell death. GaCurNPs may be physically disrupting biofilm architecture by penetrating the biofilm matrix and destabilizing the interactions between bacterial cells and extracellular polymeric substances (EPS). Additionally, GaCurNPs could potentially interfere with the production of EPS components critical for biofilm integrity, leading to the disintegration of the biofilm structure. Further investigations are needed to elucidate the exact mechanism by which GaCurNPs inhibit biofilm formation in *P. aeruginosa*.

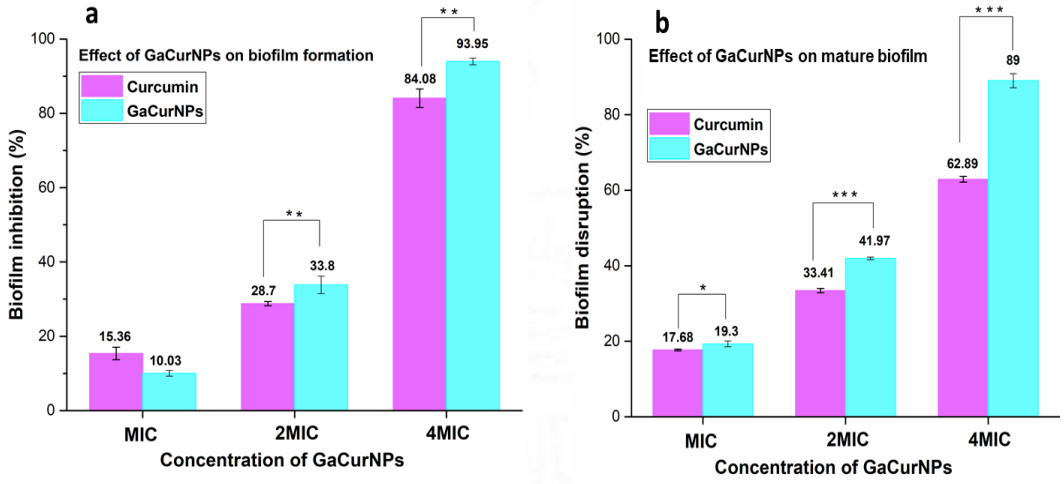

Figure 35: Effect of GaCurNPs on *P. aeruginosa* ATCC 27853 biofilm: (a) Effect of GaCurNPs on *P. aeruginosa* ATCC 27853 biofilm formation and (b) effect of GaCurNPs on mature biofilm.

The values represent mean ± SD and from triplicate experiments. Statistically significant with p<0.01(**); p<0.001(***).

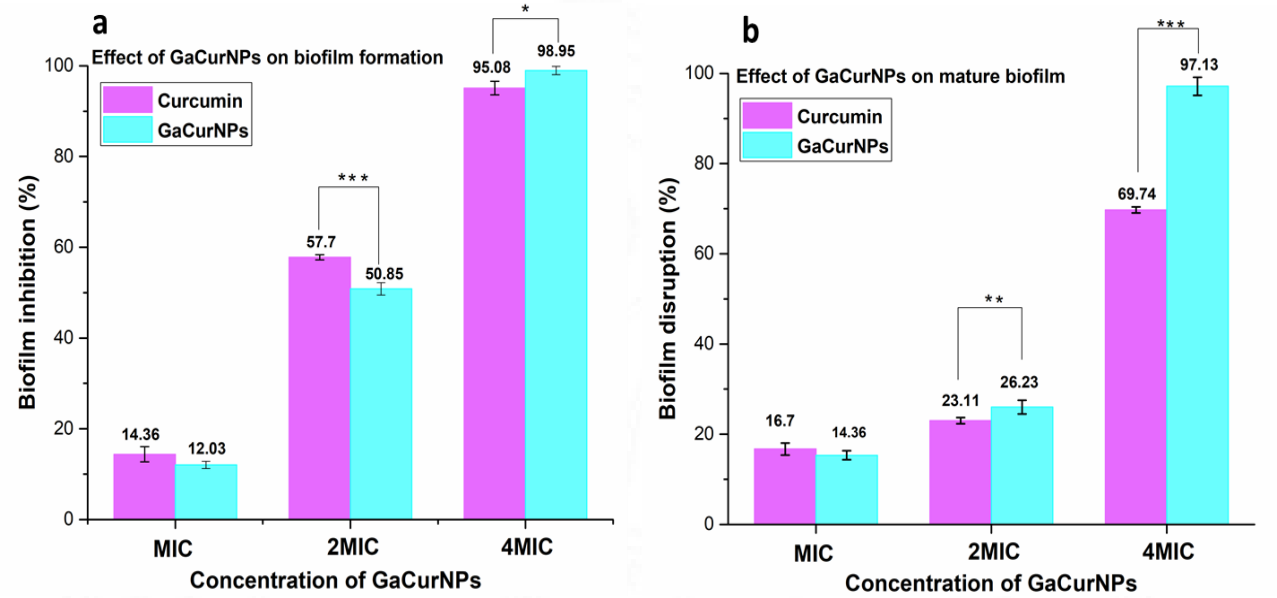

Figure 36: Effect of GaCurNPs on *P. aeruginosa* clinical strain biofilm. (a) Effect of curcumin and GaCurNPs on *P. aeruginosa* clinical strain biofilm formation and (b) effect of GaCurNPs on 24-hour mature biofilm. The values represent mean ± SD and from triplicate experiments. Statistically significant with p<0.01(**); p<0.001(***).

4.7.2. Effect of GaCurNPs on biofilm - live/dead assay

The use of fluorescence microscopy live/dead assay with SYTO9 and propidium iodide (PI) allows for the visualization of live and dead bacterial cells within mature biofilms. Live cells are stained green with SYTO9, whereas dead cells with compromised membranes are stained red with PI. The observed increase in red fluorescence intensity with increasing concentrations of GaCurNPs indicates a higher proportion of dead cells within the biofilm, confirming the biofilm disruption activity of GaCurNPs.

P. aeruginosa ATCC 27853 strain, when treated with MIC of GaCurNPs, showed fewer observable live cells (green) compared to the control. However, when the concentration

increased to 2MIC and 4MIC, the number of non-viable/dead (red) cells increased significantly (Figure 37a). The observed dose-dependent disruption of mature biofilms by GaCurNPs, with a progressive increase from MIC to 4MIC, highlights their efficacy in eradicating established biofilms formed by *P. aeruginosa*. Very similar results were observed for the *P. aeruginosa* clinical strain where treatment with 4MIC of GaCurNPs caused almost complete disruption of biofilm (Figure 38d). Untreated control showed healthy live bacterial cells representative of a stable biofilm (Figure 38a).

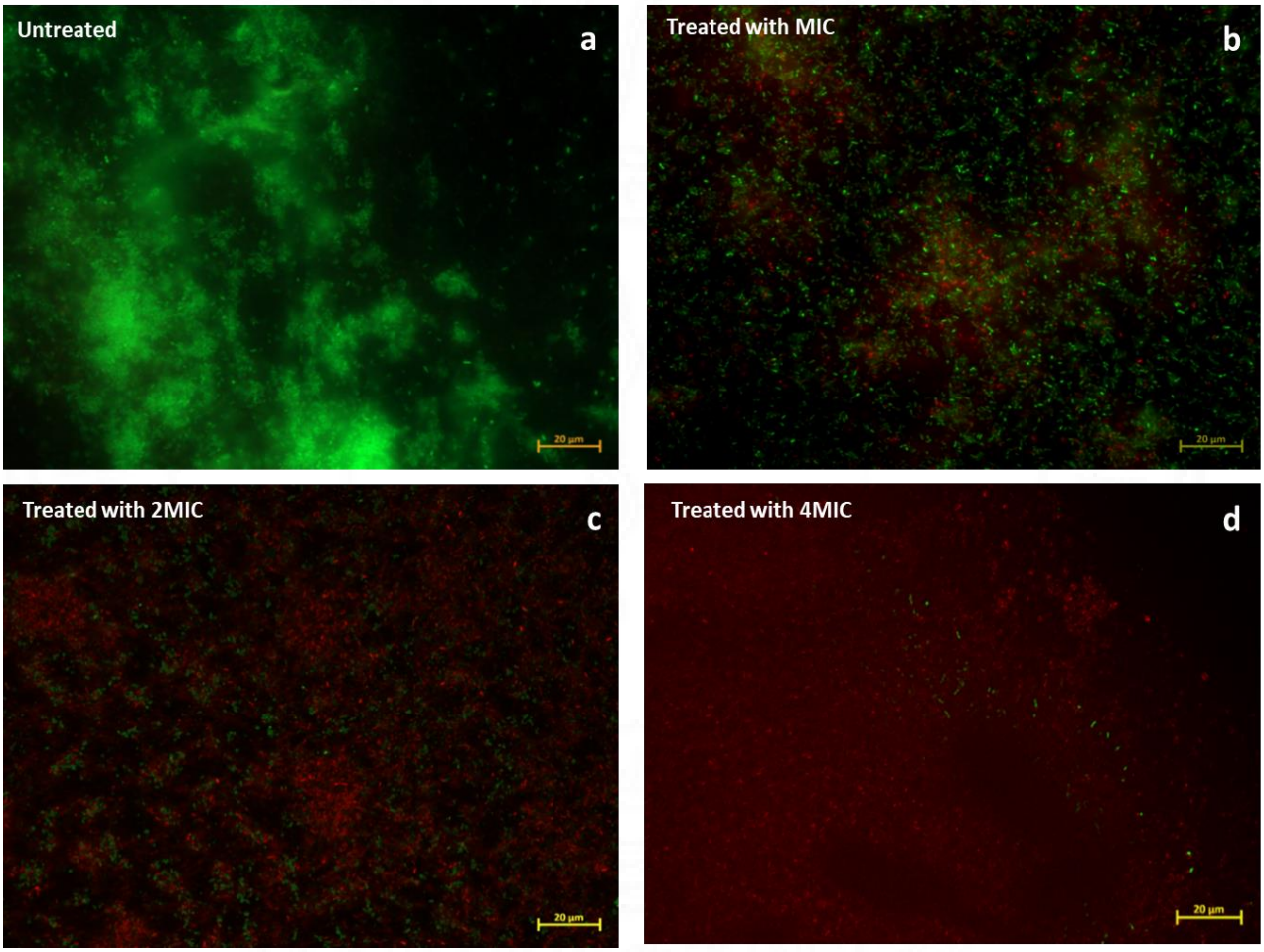

Figure 37: Fluorescence microscopy images of *P. aeruginosa* ATCC 27853 biofilm treated with GaCurNPs. (a) untreated control (b) treated with MIC of GaCurNPs (c) treated with 2MIC of GaCurNPs (d) treated with 4MIC of GaCurNPs.

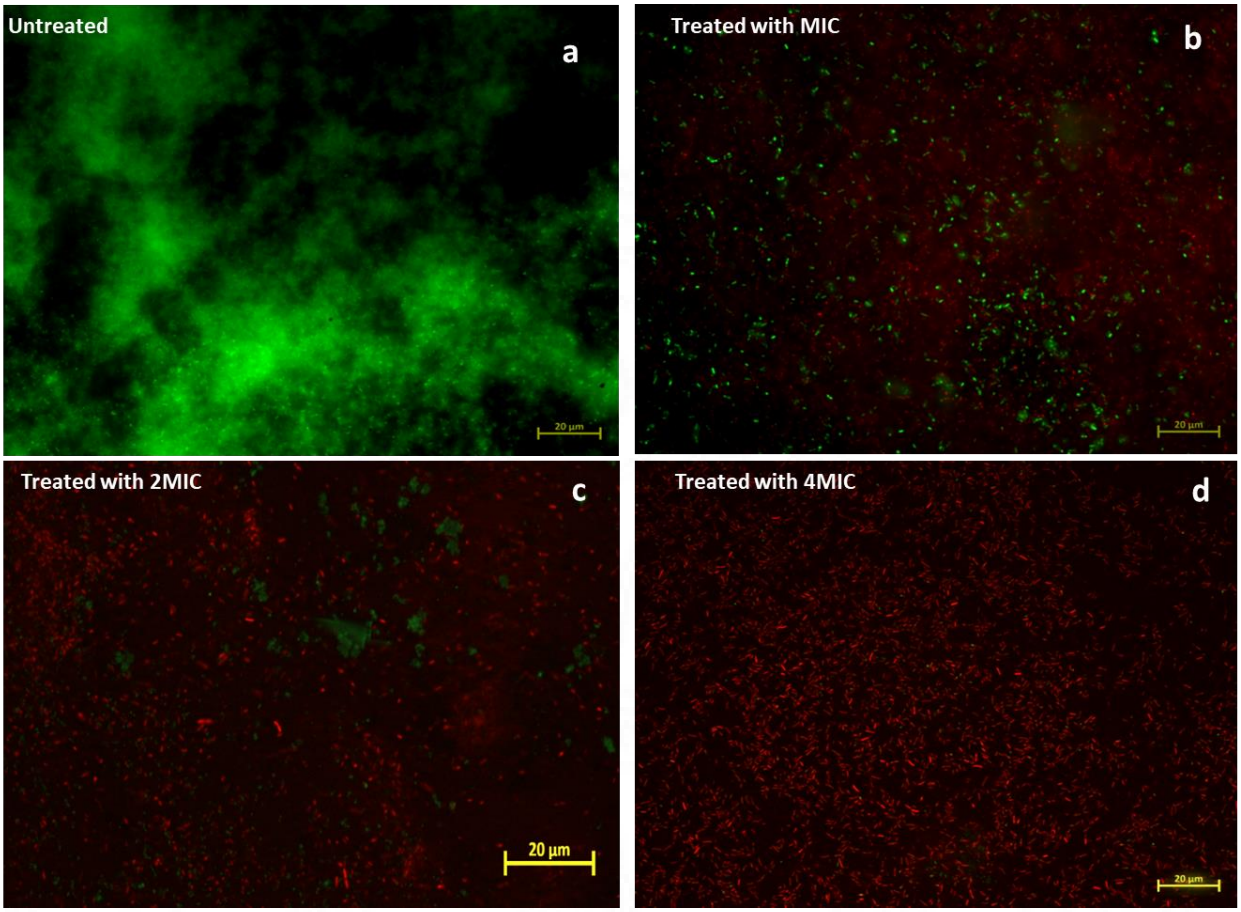

Figure 38: Fluorescence microscopy images of *P. aeruginosa* clinical strain biofilm treated with GaCurNPs: (a) untreated control (b) treated with MIC of GaCurNPs (c) treated with 2MIC of GaCurNPs (d) treated with 4MIC of GaCurNPs.

4.7.3. Effect of GaCurNPs on biofilm: FESEM evidence

Further investigation into the anti-biofilm activity was done by scanning electron microscopy. Biofilm grown on glass coverslips for 24 hours was treated with different concentrations of GaCurNPs. On treatment with MIC and 2MIC of GaCurNPs, the ATCC 27853 strain biofilm showed changes in the biofilm structure compared to untreated biofilm. The cell morphology can be seen altered with craters and holes on the surface of the cell membrane. ATCC strain, when treated with 4MIC of GaCurNPs, showed almost complete destruction of biofilm (Figure 39d). The bacterial cells that are seen on the biofilm were destroyed and the morphology was impaired.

For clinical strain at MIC, there may be initial signs of biofilm disruption, such as alterations in biofilm architecture, irregularities in cell morphology, and localized areas of cell detachment (Figure 40 b). As the concentration of GaCurNPs increases to 2MIC and 4MIC (Fig: 40c and d), these morphological changes become more pronounced, with extensive disruption of biofilm structure, loss of cellular integrity, and widespread cell death observed. Clinical strain biofilm, when treated with 4MIC, destroyed the biofilm structure. Punctures and dents can be seen on the surface of the bacterial cells. Curcumin nanoformulations are known to have similar effects on various bacterial biofilms as reported by various groups (Jaiswal and Mishra, 2018b); (Ma et al., 2020). The dose-dependent disruption of mature biofilms by GaCurNPs highlights the potency of GaCurNPs in eradicating biofilms formed by *P. aeruginosa*. The increasing concentration of GaCurNPs corresponds to a progressive increase in the extent of biofilm disruption, indicating a direct relationship between GaCurNPs concentration and biofilm disruption efficacy. This reiterates the potential effectiveness of GaCurNPs as antimicrobial agents against *P. aeruginosa* biofilm-associated infections.

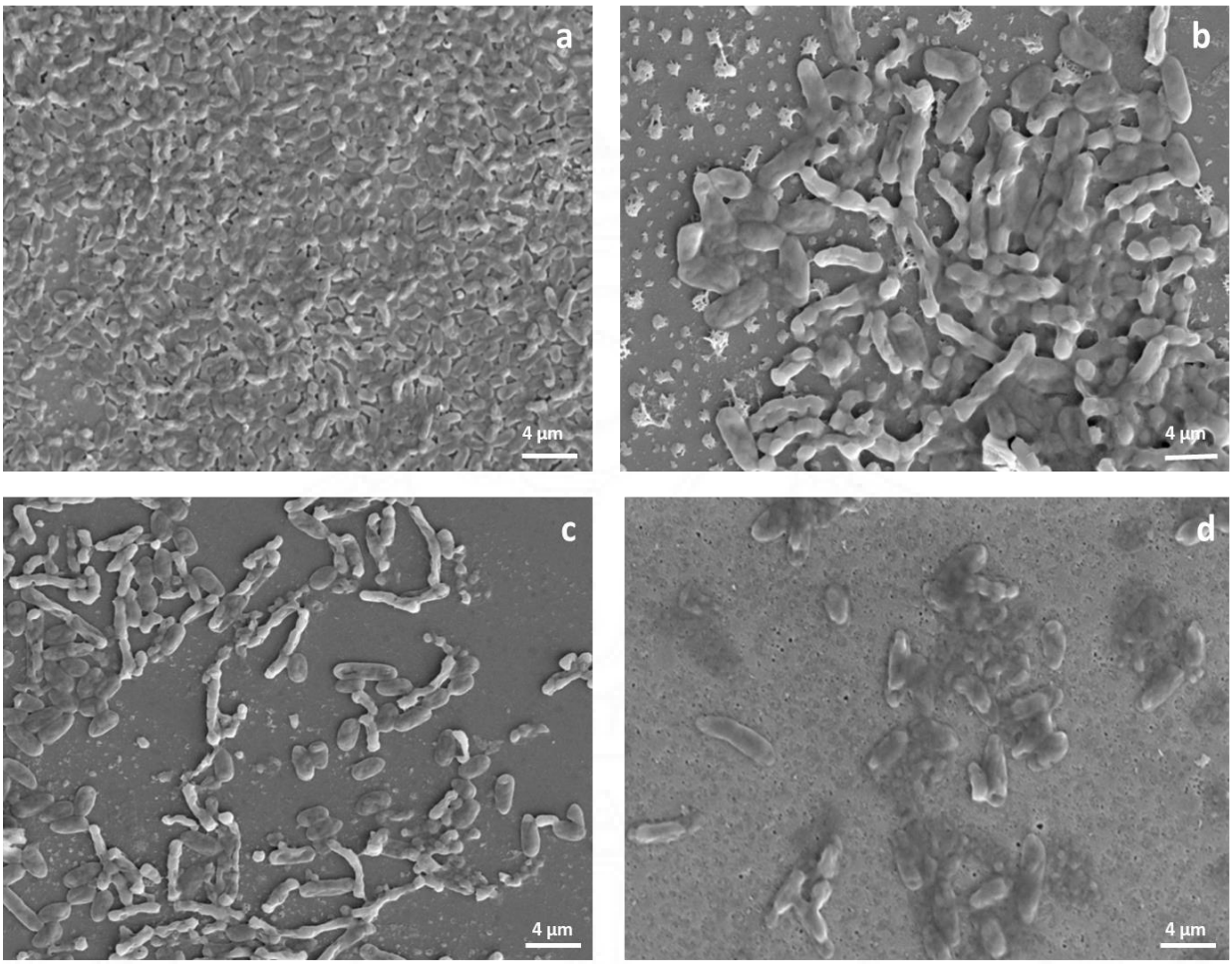

Figure 39: FESEM images of *P. aeruginosa* ATCC 27853 biofilm treated with GaCurNPs: (a) untreated control (b) treated with MIC of GaCurNPs (c) treated with 2MIC of GaCurNPs (d) treated with 4MIC of GaCurNPs.

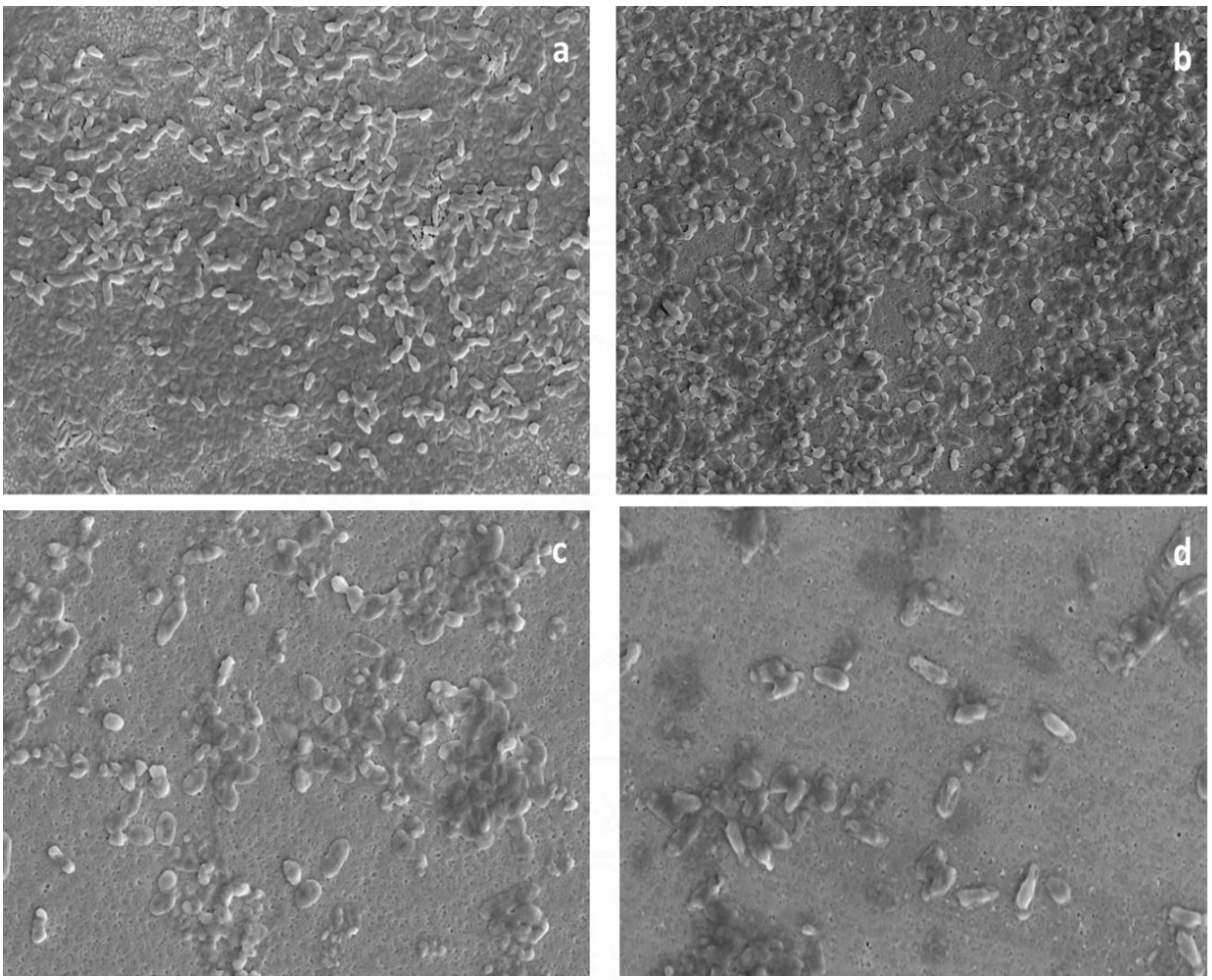

Figure 40: FESEM images of *P. aeruginosa* clinical strain treated with GaCurNPs: (a) untreated control (b) treated with MIC of GaCurNPs (c) treated with 2MIC of GaCurNPs (d) treated with 4MIC of GaCurNPs.

4.8. Raman spectroscopy as a tool to study the effect of GaCurNPs on P. aeruginosa biofilm

4.8.1. Bacterial Raman spectra library preparation

The study revealed unique spectral outputs for each species of bacteria studied. The spectral library included the spectra of gram-positive and gram-negative bacteria (Figure 41). Table 17 lists the peak assignments of the bacterial spectra of *P. aeruginosa* and other bacteria obtained during the study. One of the most important findings about the peaks was that the capsular

polysaccharide - corresponding peak at 497 cm^{-1} was only seen in the *S. aureus* instance. In addition, *P. aeruginosa* showed a peak at 598 cm^{-1}, which corresponds to pyocyanin.

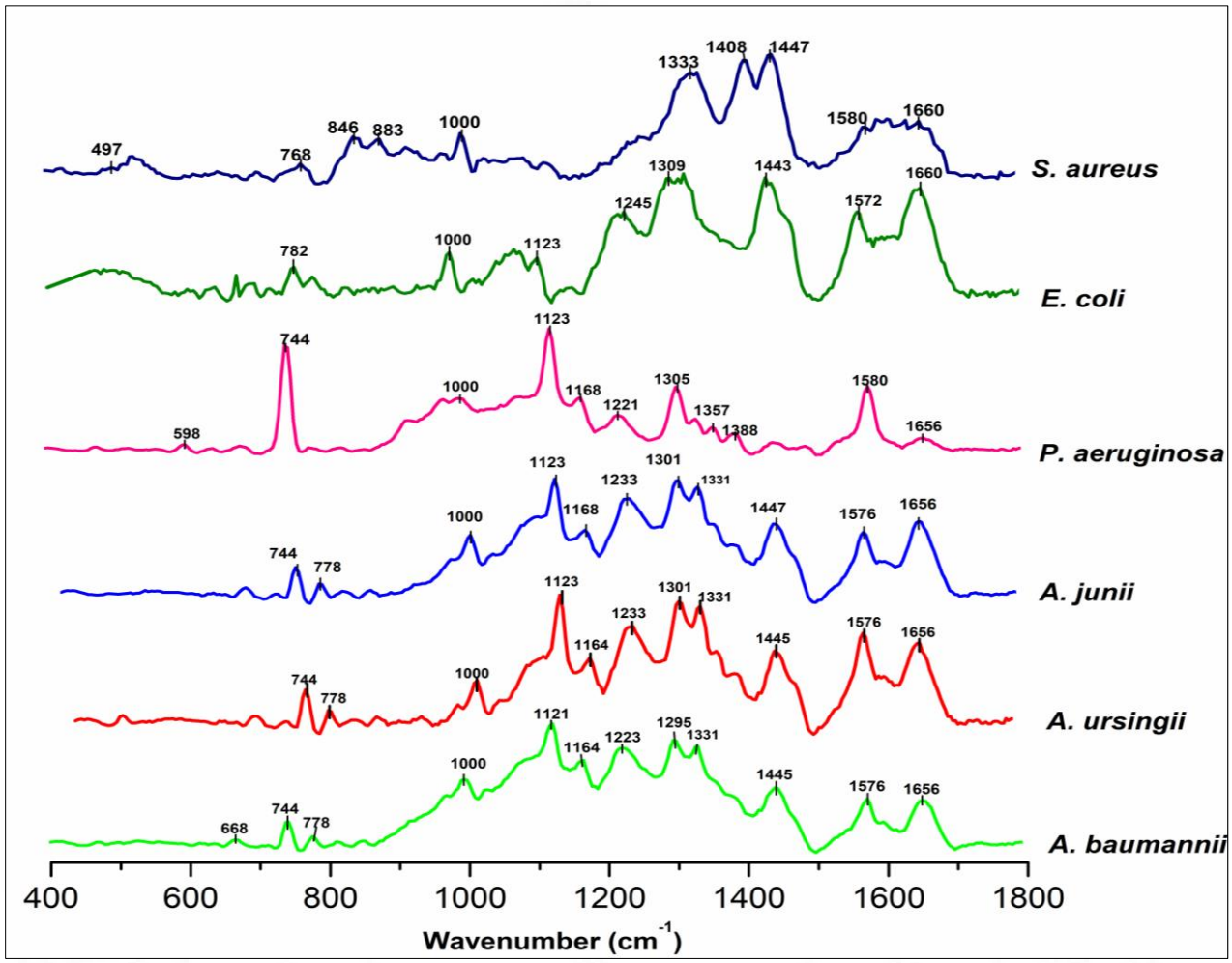

Figure 41: Annotated Raman spectra of gram-positive and gram-negative strains of bacteria.

Table 17: Peak assignment of gram-positive and gram-negative bacteria

Bacteria (wavenumber, cm^{-1})				Peak assignment
E coli	***Pseudomonas aeruginosa***	***Acinetobacter baumannii***	***Staphylococcus aureus***	
-	-	-	497	Capsular polysaccharide of Gram-positive bacteria
-	598	-	-	Pyocyanin
671	680	668	-	Guanine
748	744	744	744	Wagging *l*-tryptophan
782	-	778	768	Uracil, Cytosine, Thymine ring breathing
1000	1000	1000	1000	Symmetric ring breathing of Phenylalanine
1123	1123	1121	1120	C–C stretching, C–O–C skeletal stretching- glycosidic linkage of saccharides C–C stretching corresponding to glycosidic linkage of saccharides
-	1221	1223	1229	Symmetric or asymmetric phosphate stretching vibration
1305	1305	1294	-	$–CH_2$ fatty acid deformation; Cytosine
1323	1330	1330	1330	Adenine, Guanine
1443	1443	1445	1446	Guanine, Adenine, CH deformity
1573	1581	1576	1580	Guanine, Uracil ring stretching, Amide II, –COO stretching
1660	1656	1656	1660	Amide I, C=C stretching

4.8.2. Study of the effect of GaCurNPs on *P. aeruginosa* biofilm by Confocal Raman microscopy

Confocal Raman microscopy along with PCA, was used as a tool to study the effect of GaCurNPs on *P. aeruginosa* biofilm (Jung et al., 2014). The assignment of Raman peaks of *P. aeruginosa* biofilm is given in Table 18. The alteration of *P. aeruginosa* ATCC 27853 and clinical biofilm spectra upon treatment with 2MIC and 4MIC concentrations of GaCuNPs as observed through confocal Raman microscopy implies significant changes in the biochemical composition and structural organization of the biofilm matrix (Figure 42 and 43). The observed alterations in the Raman spectra of treated *P. aeruginosa* biofilms, coupled with a reduction in the area of bacterial spectra, suggest perturbations in the biochemical composition and structural integrity of the biofilm matrix upon GaCuNPs treatment. These changes may reflect disruptions in cellular components, such as proteins, lipids, and nucleic acids, indicative of bacterial damage or metabolic alterations induced by GaCuNPs. Also, 24-hour- mature *P. aeruginosa* biofilm on treatment with GaCurNPs exhibited noticeable alterations in the spectrum. The –CH deformation peak at 2922 cm^{-1}, contributed by the outer membrane lipids, was reduced in 4MIC GaCurNPs treated biofilm The reduction in the intensity of the lipid and other peaks in the fingerprint region upon GaCurNPs treatment suggests alterations in the lipid content and overall biochemical composition of *P. aeruginosa* biofilms affecting their membrane integrity.

Ciprofloxacin is one of the most active antibiotics against biofilm because it is neutral in charge (MIC same as MBIC) (Fernández-Olmos et al., 2012). Therefore, ciprofloxacin was used as control to demonstrate biofilm disruption (Figure 44). In ciprofloxacin-treated biofilm, all major Raman peaks were disrupted. The biofilms of both the ATCC strain and clinical strain also showed the same results.

Table 18: Raman peaks assignments of *P. aeruginosa* biofilm.

Wavenumber (cm^{-1})	Peak assignment
552	Pyocyanin
752	Wagging l-tryptophan
1000	Phenylalanine
1088	Glycosidic ring, C-C strc., C-O-C, pyocyanin
1112	C-C skeletal str..-glycosidic linkage of saccharides
1168	Guanine, Cytosine, C-H Tyrosine, Phenylalanine, *v*(C-O-C)
1449	Guanine, Adenine, -CH deformation vibration
1576	Guanine, Adenine, Amide II, COO- str, asymmetric
1660	Amide I
2922	-CH deformation (mainly contributed by lipids of the intact cell membrane)

PCA is a commonly used dimensionality reduction technique to reduce the number of significant variables based on data variability. It reduces the data complexity and retains the key features of the data. PCA transforms the data into components called principle components (PC) orthogonal to each other and captures the variance of the dataset in decreasing order. PC 1 represents the direction of maximum variance and PC 2 represents an orthogonal direction with the next higher variance. The relevance of the PC 1 vs 2 plot is the visualization of the plot between the two most significant principle components of the dataset, which enables us to examine whether these features are enough to distinguish between the data types in our dataset. The plot elucidates the

inherent patterns among the groups in our dataset that are captured in principle components 1 and 2.

There is a clustering of observations in the dataset that have similar spectra. The same bacterial species have similar spectra with clustering among them, as this similarity is being captured in PC 1 and 2. In the plot (Figure 45), clustering can be attributed to the fact that bacterial strains with comparable biochemical makeup have similar vibrational modes for functional groups. This results in the clustering of data points. *P. aeruginosa* biofilm treated with GaCurNPs, both the ATCC strain and clinical strain have clustered together which suggests that the changes happening at the molecular level are the same for both strains.

The distinct clustering of untreated and treated biofilms in PCA further supports the notion that GaCurNPs treatment induces substantial alterations in the biofilm composition and structure. PCA analysis allows for the discrimination of spectral patterns associated with different experimental conditions, highlighting the discriminative power of Raman spectroscopy in detecting subtle biochemical changes in bacterial biofilms.

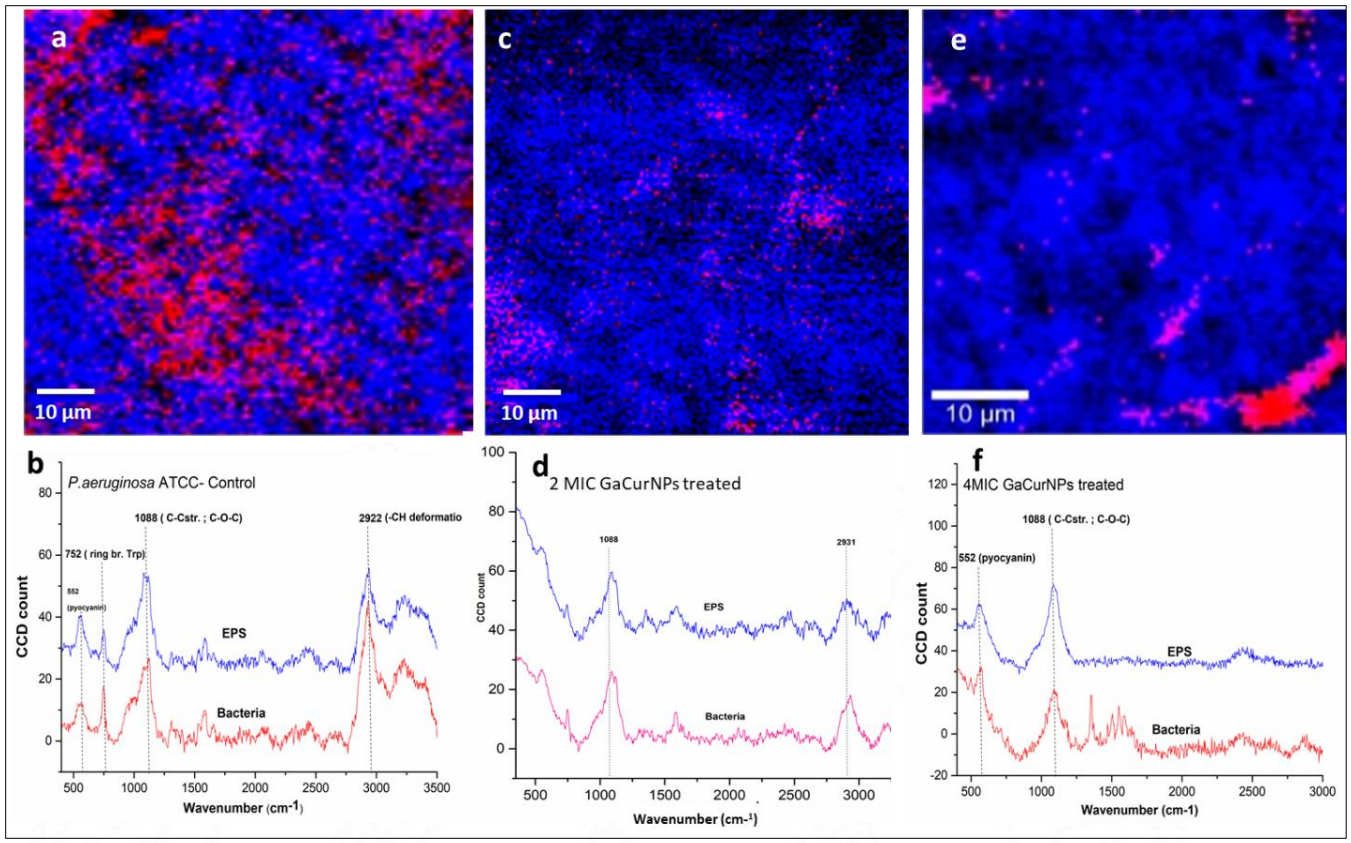

Figure 42: Confocal Raman image and cluster spectra of 24-hour mature *P. aeruginosa* ATCC 27853 biofilm treated with different concentrations of GaCurNPs: (a) and (b) untreated control (c) and (d) treated with 2MIC of GaCurNPs (e) and (f) treated with 4MIC of GaCurNPs.

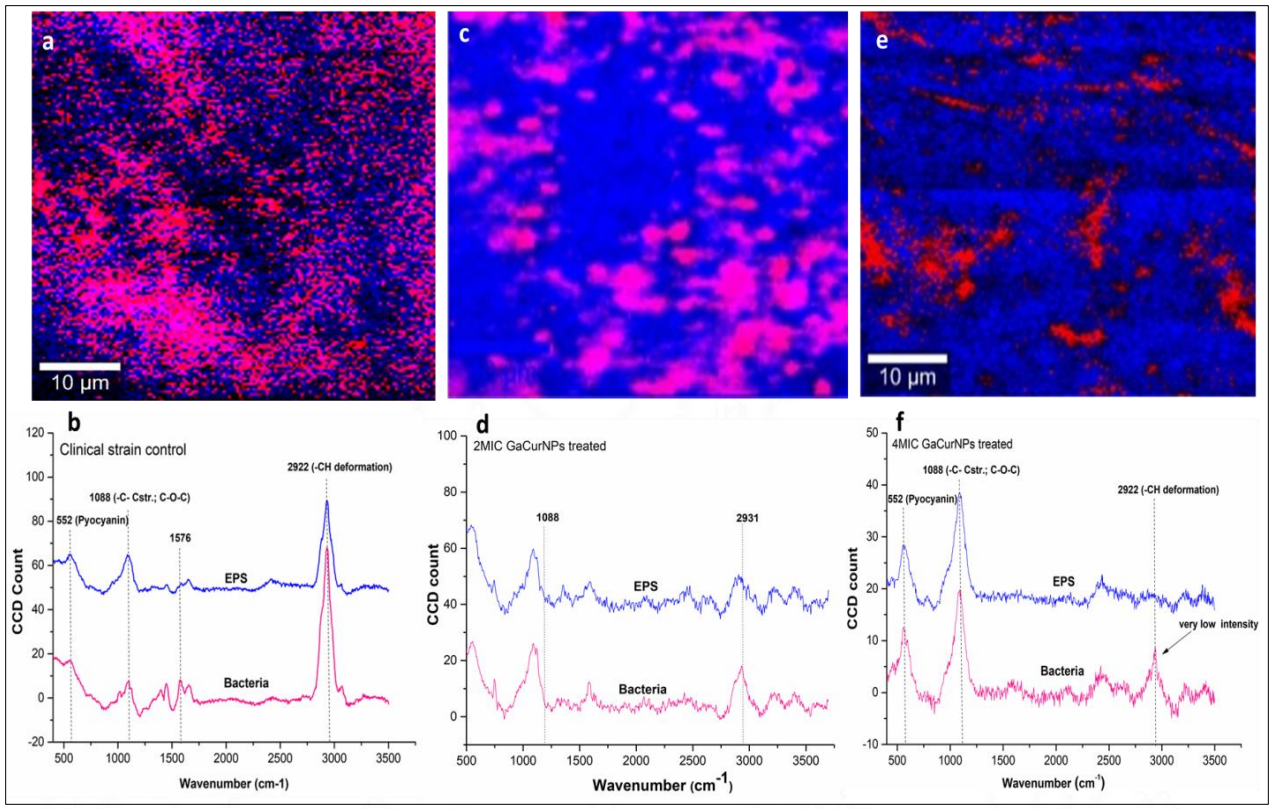

Figure 43: Confocal Raman image and cluster spectra of 24-hour mature *P. aeruginosa* clinical strain biofilm treated with different concentrations of GaCurNPs: (a) and (b) untreated control (c) and (d) treated with 2MIC of GaCurNPs (e) and (f) treated with 4MIC of GaCurNPs.

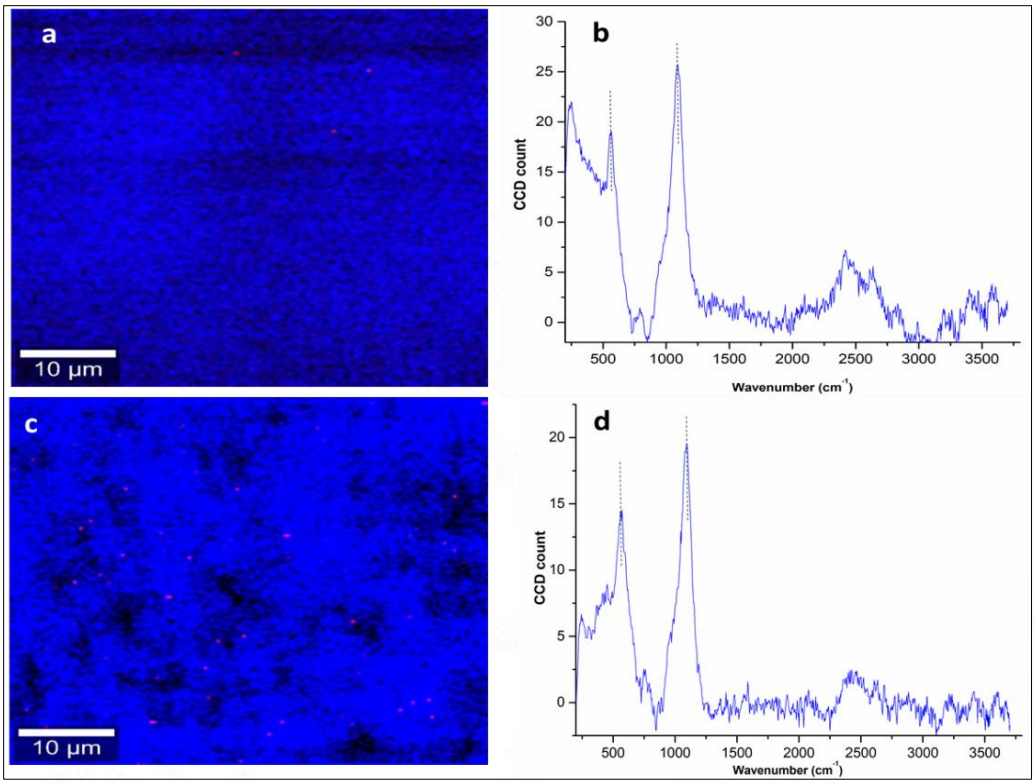

Figure 44: Confocal Raman image and cluster spectra of 24-hour mature *P. aeruginosa* ATCC 27853 biofilm and clinical strain biofilm treated with 2MIC of ciprofloxacin: (a) and (b) *P. aeruginosa* ATCC 27853 treated with 2MIC of ciprofloxacin (c) and (d) *P. aeruginosa* clinical strain treated with 2MIC of ciprofloxacin.

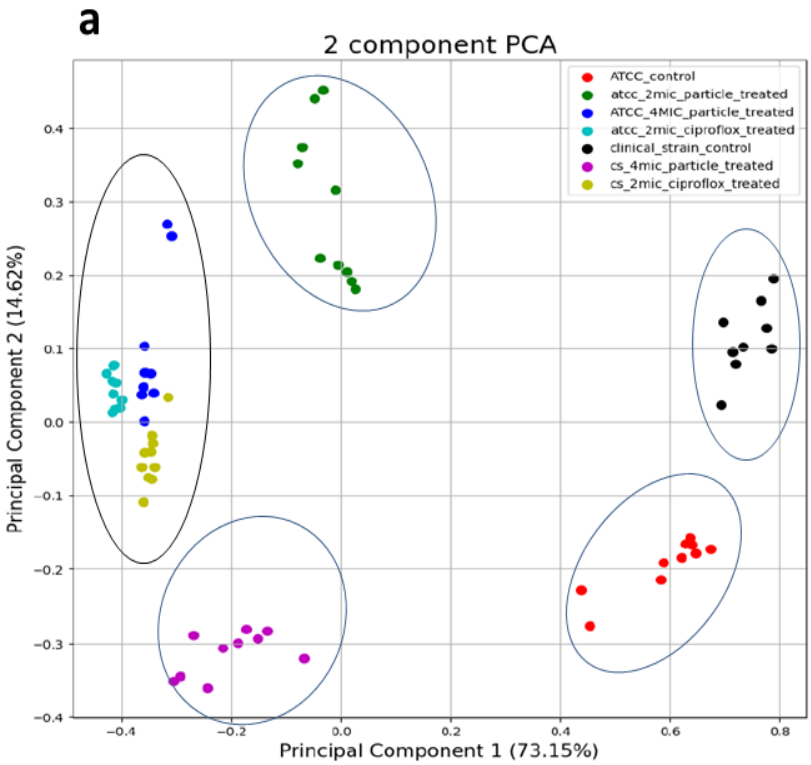

Figure 45: PCA plot illustrating the clustering of untreated and treated *P. aeruginosa.*

4.9. Gene expression study of biofilm genes and quorum sensing genes in P. aeruginosa biofilm by Real - Time qPCR

A resilient biofilm formation by *P. aeruginosa* is essential and critical for its survival. Utilizing 3-oxo-C12-HSL and C4-HSL, respectively, the LasI/R and RhlI/R systems control the expression of approximately 10% of *P. aeruginosa* genes. Key virulence factors including protease, elastase, lipase, pyocyanin, pyoverdine, rhamnolipid, hydrogen cyanide, swarming, and biofilm- formation are regulated by those genes. Curcumin has been shown to downregulate QS genes involved in the production of QS signaling molecules (autoinducers) and the expression of QS-regulated virulence factors in *P. aeruginosa*. Curcumin is also known to downregulate many genes involved in biofilm formation and survival. The use of curcumin as an anti-QS drug was

earlier reported by Abdulrahman *et al.*, and Sethupathy *et al.*, (Abdulrahman et al., 2020) (Sethupathy et al., 2016). In our study, oprL which codes for an outer membrane protein was chosen as the housekeeping gene owing to its high sensitivity and specificity (Qin et al., 2003); (Thi et al., 2020). Studying the effect of GaCurNPs on quorum-sensing (QS) genes in *P. aeruginosa* is crucial for addressing antibiotic resistance. *P. aeruginosa* uses quorum sensing to control virulence, biofilm formation, and antibiotic resistance. By targeting QS genes, GaCurNPs can disrupt bacterial communication, reduce biofilm formation, and lower pathogenicity without directly killing the bacteria, helping to avoid resistance development.

The effect of sub-inhibitory 1/2 MIC, MIC, and 2MIC concentrations of GaCurNPs on the biofilm, virulence, and quorum sensing genes was studied. The effect of GaCurNPs on the expression of 10 genes involved in biofilm formation and quorum sensing of *P. aeruginosa* was evaluated. The observation of concentration-dependent downregulation of various genes in planktonic *P.aeruginosa* upon treatment with sub-MIC (1/2MIC), MIC, and supra-MIC (2MIC) concentrations of GaCurNPs suggests a complex regulatory effect of GaCurNPs on gene expression *in P. aeruginosa*. This inhibition of gene expression plays a key role in inhibiting biofilm formation. The mechanism involves the generation of ROS which contributes to the reducing biofilm thickness and extracellular polysaccharide production.

4.9.1. Effect of GaCurNPs on the expression of biofilm and quorum sensing genes in planktonic *P. aeruginosa* ATCC 27853

The untreated control *P. aeruginosa* showed expression of all the ten genes studied, in its planktonic form. The planktonic bacteria were treated with ½ MIC, MIC, and 2MIC. GaCurNPs treatment caused a reduction in the gene expression of all tested biofilm and virulence genes. Higher concentrations (MIC and 2MIC) lead to more pronounced changes in gene expression

compared to sub-MIC concentrations, reflecting a dose-response relationship. Exposure to GaCurNPs significantly reduced proC, lecA, pelA, and algD expressions at 1/2 MIC (31.42%, 40.56%, 53.7%, and 79.3% reduction respectively), MIC (87.33%, 94.3%, 96.6%, and 92% reduction respectively) and 2MIC (98.09%, 97.4%, 96.4% and 93% reduction respectively).

RpoS, a master stress response regulator that affects the expression of more than 40% of all QS genes, production of extracellular alginate, exotoxin A, and biofilm formation was also seen to be downregulated on treatment with different concentrations of GaCurNPs. RpoS on treatment with ½ MIC, MIC, and 2MIC was downregulated by 50%, 71.4%, and 73% respectively. ExoS was also downregulated in a dose-dependent fashion on treatment with GaCurNPs. The percentage downregulation of exoS was 47.5%, 93.7%, and 97.2% on treatment with ½ MIC, MIC, and 2MIC respectively. Figure 46 a-f depicts the downregulation of genes proC, lecA, pelA, algD, rpoS, and exoS on treatment with the progressive GaCurNPs concentrations.

GaCurNPs also caused a reduction in gene expression of all the QS genes studied, namely lasI, lasR, rhlI, and rhlR, in a dose-dependent manner. The reduction observed for 1/2 MIC (20.6%, 18.7%, 72.3%, and 79% reduction respectively), MIC (87.3%, 68.7%, 97.1%, and 98.2% reduction respectively), and 2MIC (96.9%, 97.7%, 93.2%, and 98.6% reduction respectively) were significant when compared to untreated control.

The downregulation of virulence genes (e.g., rpoS,exoS, lecA), biofilm-related genes (e.g., pelA, algD, proC), and quorum sensing genes (e.g., lasI, lasR, rhlI, rhlR) indicate a broad impact of GaCurNPs on various cellular processes and regulatory pathways including a potential attenuation of pathogenicity and biofilm formation in *P. aeruginosa*. It may also be involved in the establishment and persistence of infection. LecA, a virulence gene involved in adhesion and

biofilm formation, was found to be downregulated in MDR strains of *P. aeruginosa* on nanocurcumin treatment (Shariati et al., 2019), similar to the results of this study. The reduction observed in the downregulation of rpoS genes also could in turn be influencing the expression of the other QS genes.

These observations from our study concur with the results by Rudrappa *et al* who reported the downregulation of QS genes by curcumin (Rudrappa and Bais., 2008). LasI/LasR and RhlI/RhlR genes were dose-dependently downregulated by GaCurNPs. Another study also reported similar effects for ZnO/curcumin nanocomposites in the repression of lasI/lasR and several other biofilm genes in *P. aeruginosa* (Prateeksha et al., 2019).

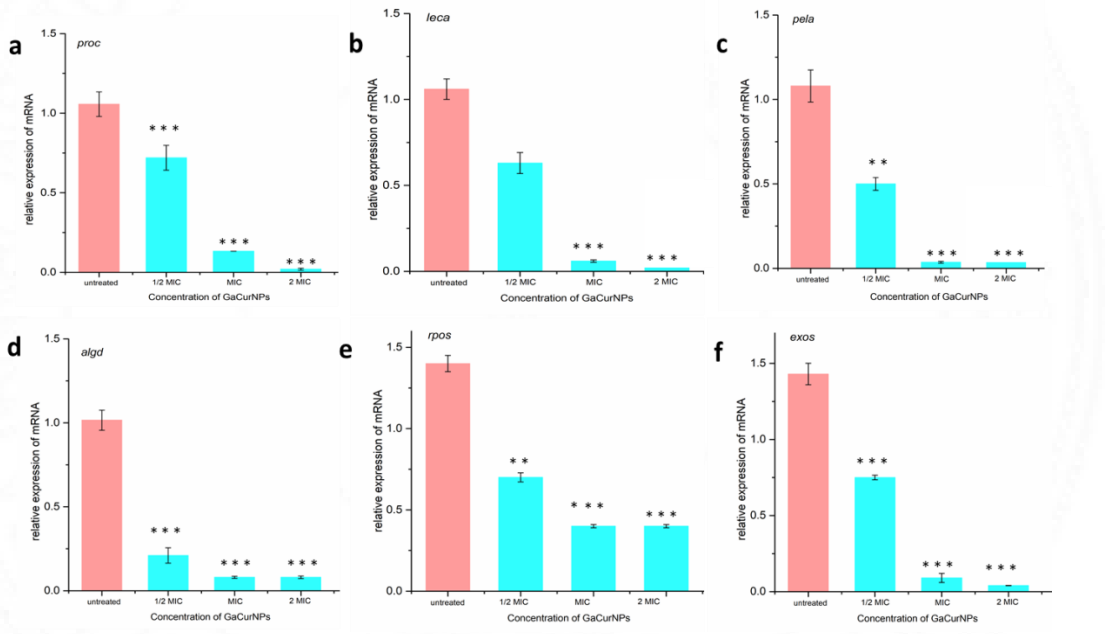

Figure 46: Relative gene expression of biofilm genes in planktonic *P. aeruginosa* ATCC 27853 on treatment with different concentrations of GaCurNPs. Relative gene expression of (a) proC (b) lecA (c) pelA(d) algD (e) rpoS (f) exoS on treatment with ½ MIC, MIC and 2MIC of GaCurNPs. The results are represented as mean ± SD. Significant difference between the test and control was measured as **p<0.01 and ***p<0.001.

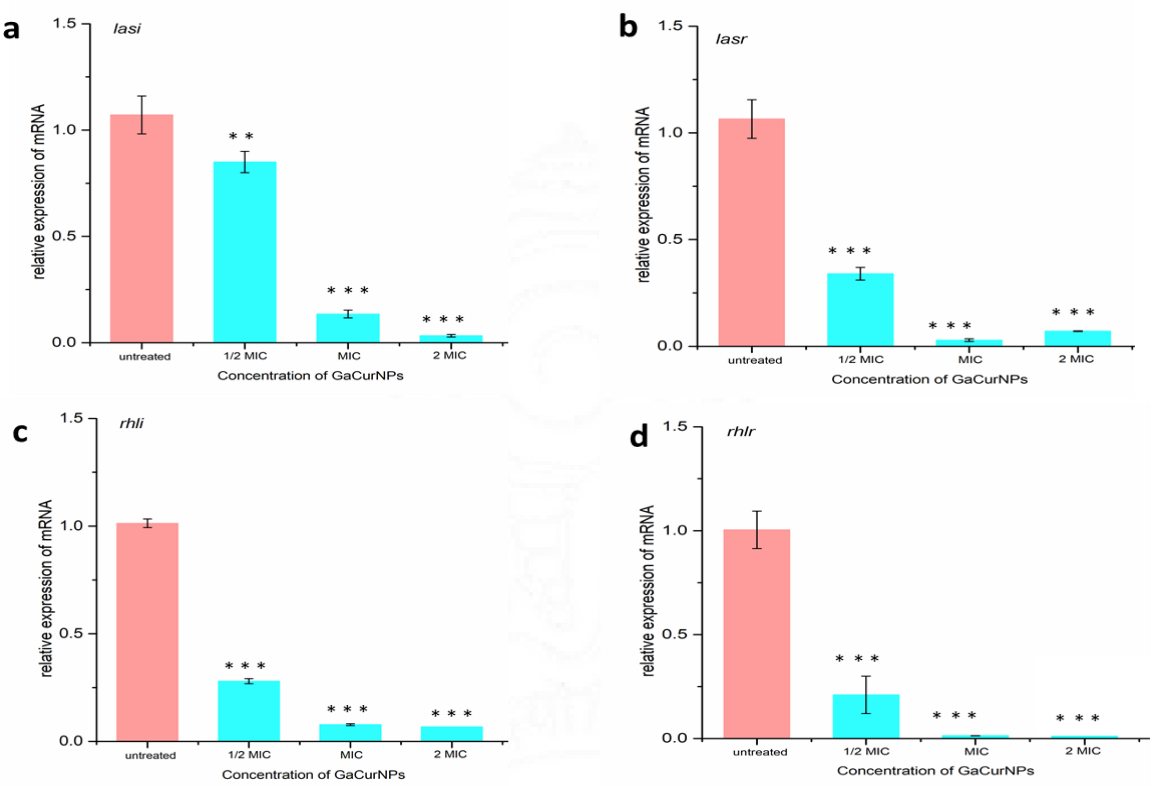

Figure 47: Relative gene expression of QS genes in planktonic *P. aeruginosa* ATCC 27853 on treatment with GaCurNPs. Relative gene expression of (a) lasI (b) lasR (c) rhlI (d) rhlR on treatment with ½ MIC, MIC and 2MIC of GaCurNPs. The results are represented as mean ± SD. Significant difference between the test and control was measured as **p<0.01 and ***p<0.001.

4.9.2. Effect of GaCurNPs on the expression of biofilm and quorum sensing genes in planktonic *P. aeruginosa* clinical strain

Further, a reduction in the expression of biofilm and QS genes was observed in the clinical strain of *P. aeruginosa* as well. The reduction in gene expression was similar to that observed in the ATCC strain. GaCurNPs caused a reduction in gene expression of all the genes studied in a dose-dependent manner that was statistically significant. GaCurNPs reduced proC, lecA, pelA, and algD expression at 1/2 MIC (7.14%, 62.2%, 42.3%, and 10.2% reduction respectively), MIC (50.89%, 92.9%, 55.9%, and 86.3% reduction respectively) and 2MIC (52.67%, 91%, 61% and

98.1% reduction respectively). RpoS on treatment with 1/2MIC, MIC, and 2MIC caused downregulation of 24.07%, 62.9%, and 73.1% respectively. ExoS exhibited downregulation of 1.8%, 55.04%, and 78.9% on treatment with ½ MIC, MIC, and 2MIC respectively. GaCurNPs significantly reduced lasI, laR, rhlI, and rhlR expression at 1/2 MIC (31.4%, 29%, 21.7%, and 80.4% reduction respectively), MIC (68.5%, 58.9%, 46.1%, and 87.2% reduction) and 2MIC (78.7%, 96.4%, 90.2%, and 90.6% reduction). The results suggest that GaCurNPs can modulate the expression of biofilm and virulence genes in the planktonic form of *P. aeruginosa* clinical strain also.

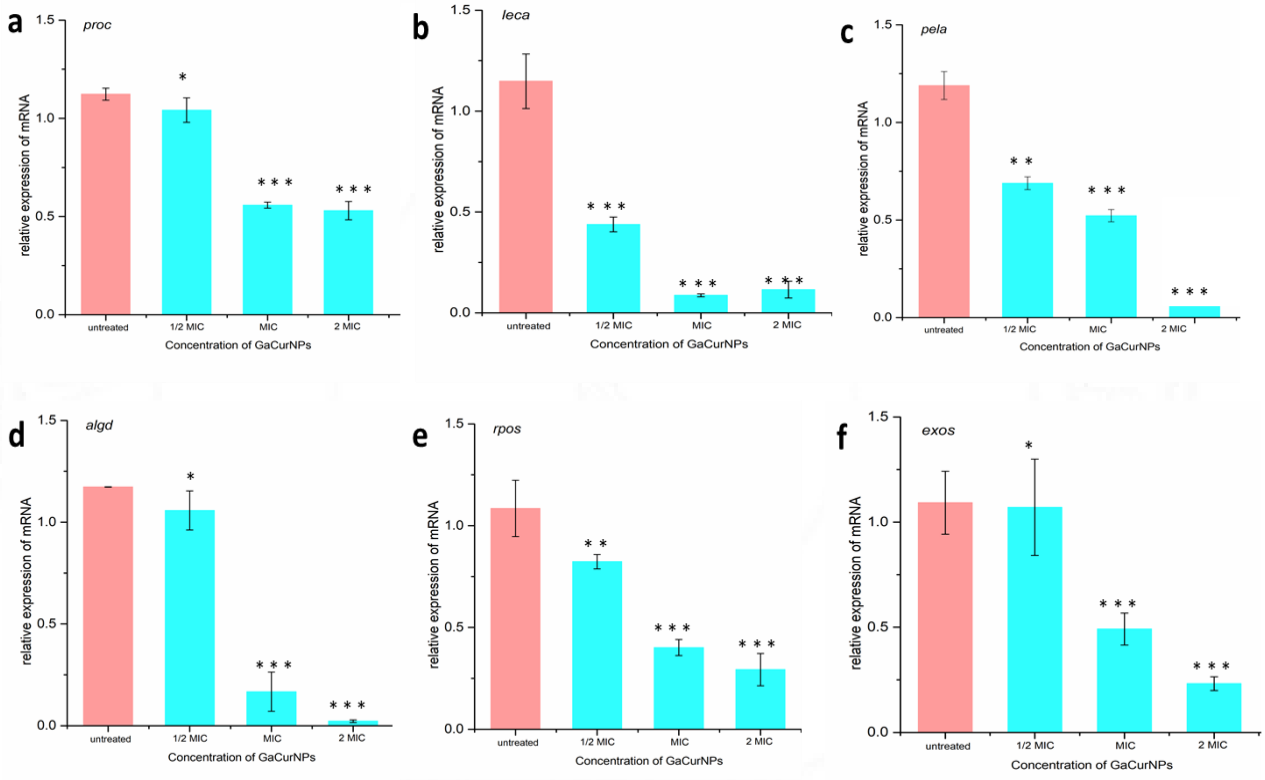

Figure 48: Relative gene expression of biofilm genes in planktonic *P. aeruginosa* clinical strain on treatment with GaCurNPs. Relative gene expression of (a) proC (b) lecA (c) pelA(d) algD (e) rpoS (f) exoS on treatment with ½ MIC, MIC and 2MIC of GaCurNPs. The results are

represented as mean ± SD. Significant difference between the test and control was measured as **p<0.01 and ***p<0.001.

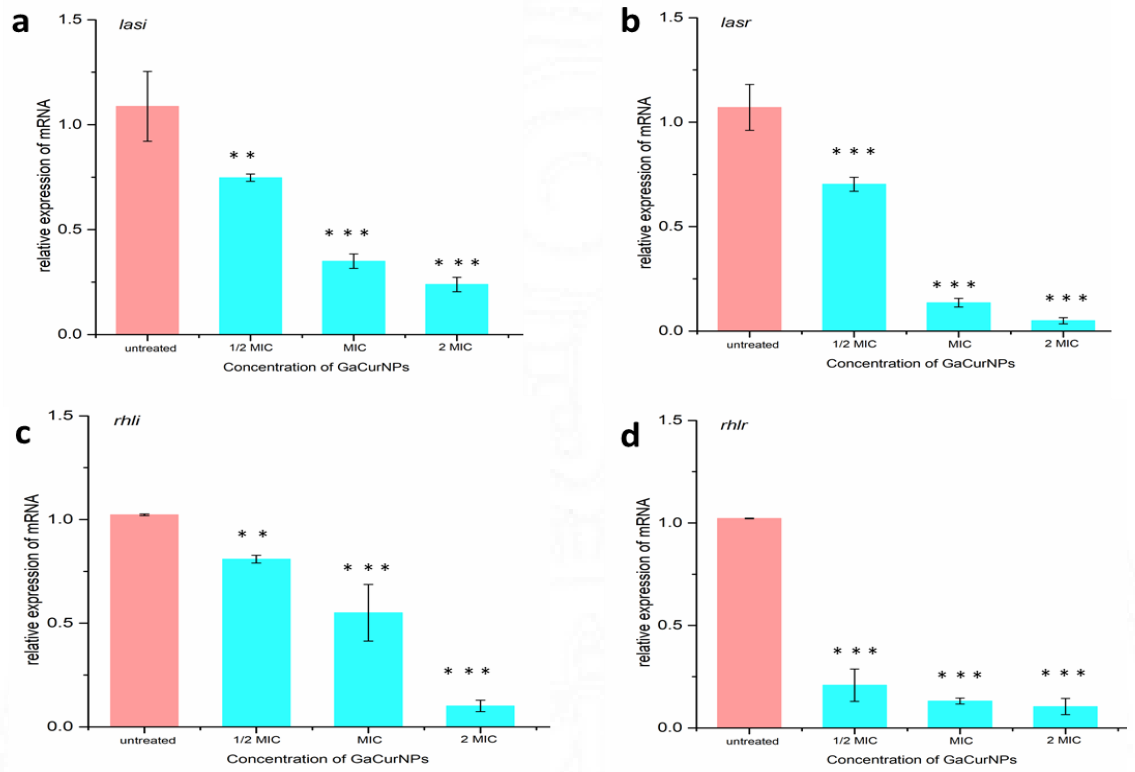

Figure 49: Relative gene expression of QS genes in planktonic *P. aeruginosa* clinical strain on treatment with GaCurNPs. Relative gene expression of: (a) lasI (b) lasR (c) rhlI (d) rhlR on treatment with ½ MIC, MIC and 2MIC of GaCurNPs. The results are represented as mean ± SD. Significant difference between the test and control was measured as **p<0.01 and ***p<0.001

4.9.3. Effect of GaCurNPs on the expression of biofilm and quorum sensing in *P. aeruginosa* ATCC 27853 biofilm

GaCurNPs caused a dose-dependent reduction in gene expression of all the biofilm and QS genes. GaCurNPs significantly reduced proC, lecA, pelA, and algD expression at 1/2 MIC (2.25%, 9.7%, 60.86%, and 3% reduction), MIC (55.6%, 55.2%, 81.88%, and 55.6% reduction) and 2MIC (81.2%, 91.04%, 88.4% and 81.9% reduction). RpoS and exoS were found to be

significantly downregulated by GaCurNPs at 1/2 MIC (55.03% and 31.4% reduction respectively), MIC (60.4% and 53.5% reduction respectively), 2MIC (79.86% and 88.5% reduction respectively). The QS genes lasI, lasR, rhlI, and rhlR also showed a dose-dependent downregulation in gene expression when compared to untreated control. GaCurNPs significantly reduced lasI, laR, rhlI, rhlR expression at 1/2 MIC (40.7%, 36%, 57%, and 52% reduction), MIC (67.5%, 75%, 74%, and 73% reduction) and 2MIC (86.11%, 93%, 89% and 87% reduction).

At ½ MIC, a slight decrease in gene expression was observed, indicating an initial inhibitory effect on biofilm formation and quorum sensing. Subsequently, at MIC concentration a more effective reduction in gene expression was noted, exhibiting a dose-dependent and more pronounced disruption of biofilm and QS mechanism. Remarkably on treatment with 2MIC concentration, a more significant downregulation of biofilm and QS genes was observed indicating a potent inhibitory effect on *P. aeruginosa* biofilm development and QS-related virulence.

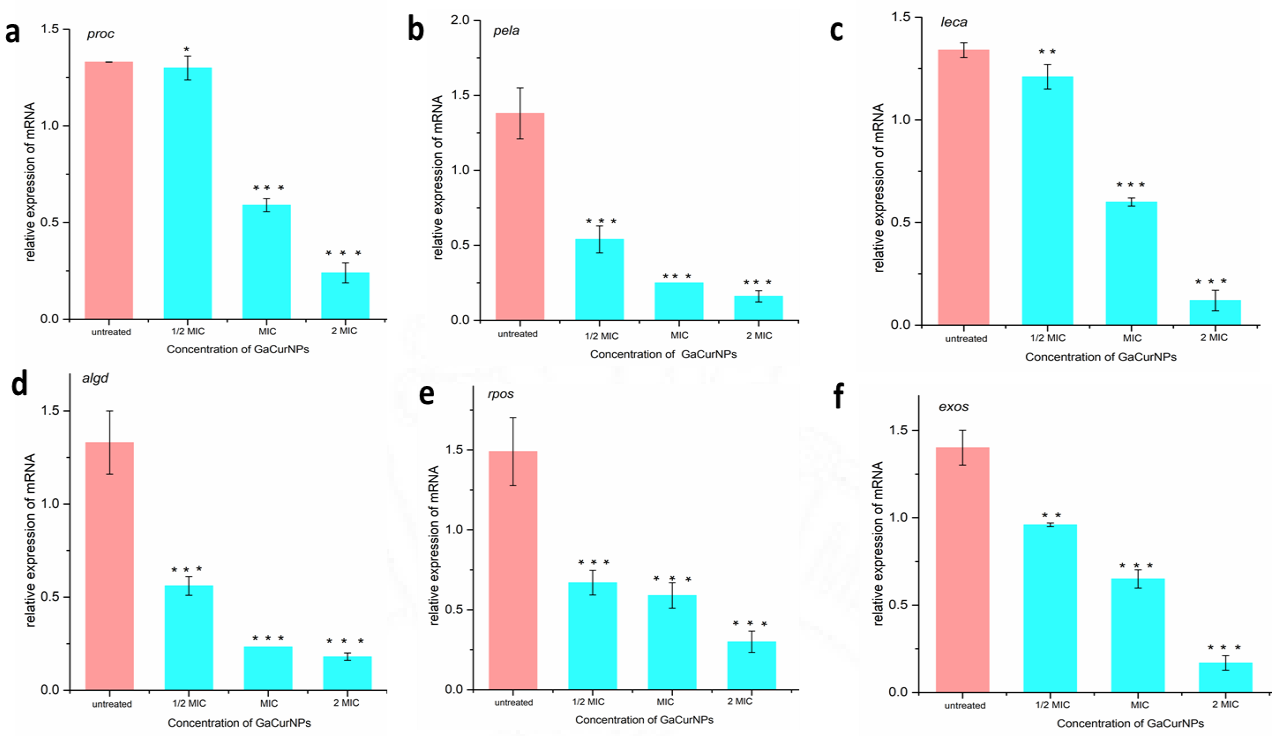

Figure 50: Relative gene expression of biofilm formation genes in *P. aeruginosa* ATCC 27853 biofilm on treatment with GaCurNPs. Relative gene expression of (a) proC (b) lecA (c) pelA(d) algD (e) rpoS (f) exoS on treatment with ½ MIC, MIC and 2MIC of GaCurNPs. The results are represented as mean ± SD. Significant difference between the test and control was measured as **p<0.01 and ***p<0.001.

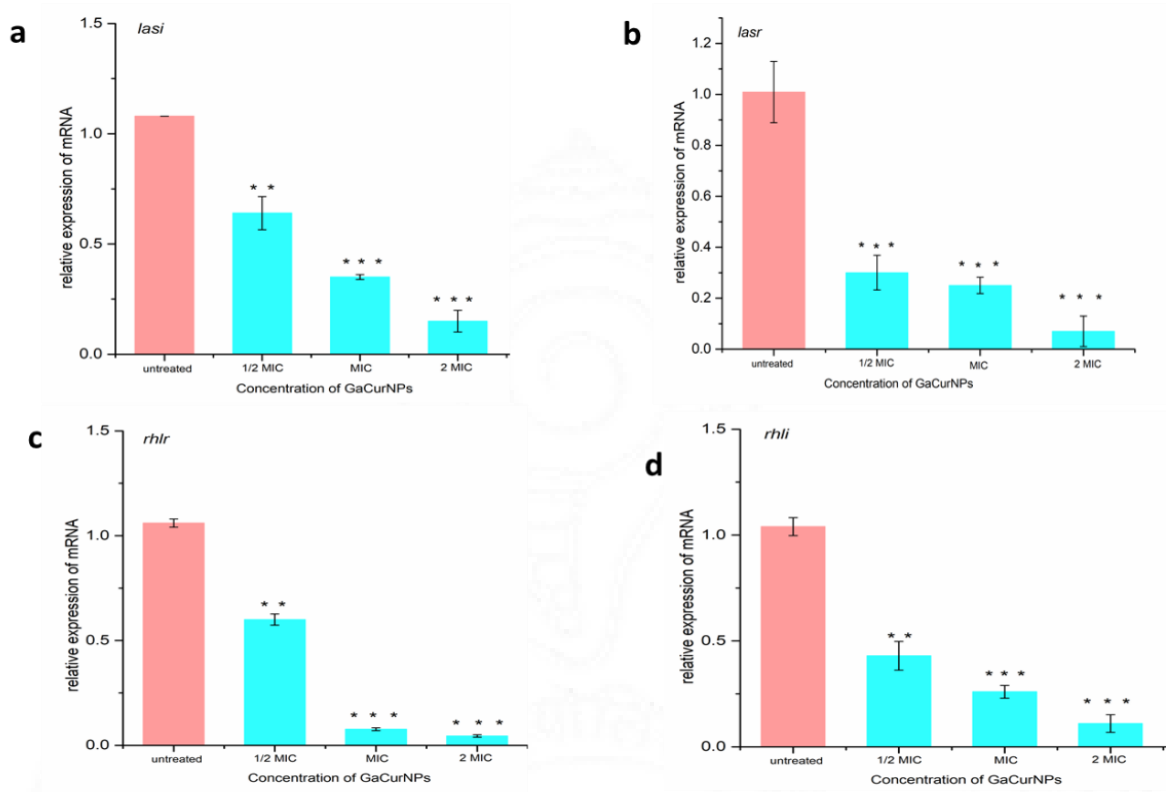

Figure 51: Relative gene expression of QS genes in *P. aeruginosa* ATCC 27853 biofilm on treatment with GaCurNPs. Relative gene expression of (a) lasI (b) lasR (c) rhlI (d) rhlR on treatment with ½ MIC, MIC and 2MIC of GaCurNPs. The results are represented as mean ± SD. Significant difference between the test and control was measured as **p<0.01 and ***p<0.001.

4.9.4. Effect of GaCurNPs on the expression of biofilm and quorum sensing in *P. aeruginosa* genes in clinical strain biofilm

Further, a statistically significant was observed in the clinical strain of *P. aeruginosa* as well. And the decrease in expression was statistically significant as well. GaCurNPs caused a reduction in gene expression in a dose-dependent manner. GaCurNPs significantly reduced proC, lecA, pelA, and algD expression at 1/2 MIC (30%, 13%, 61.9%, and 47% reduction), MIC (41%, 51%, 65.7%, and 73% reduction) and 2MIC (61%, 56.3%, 67% and 74% reduction). Further, the expression of RpoS and exoS was significantly suppressed by GaCurNPs at 1/2MIC (reduction, 33%, and 31%), MIC (reduction, 85%, and 57%) and 2MIC (reduction, 90% and 97%). The

quorum sensing genes under study lasI, lasR, rhlI, and rhlR also showed a reduction in gene expression when compared to untreated control.

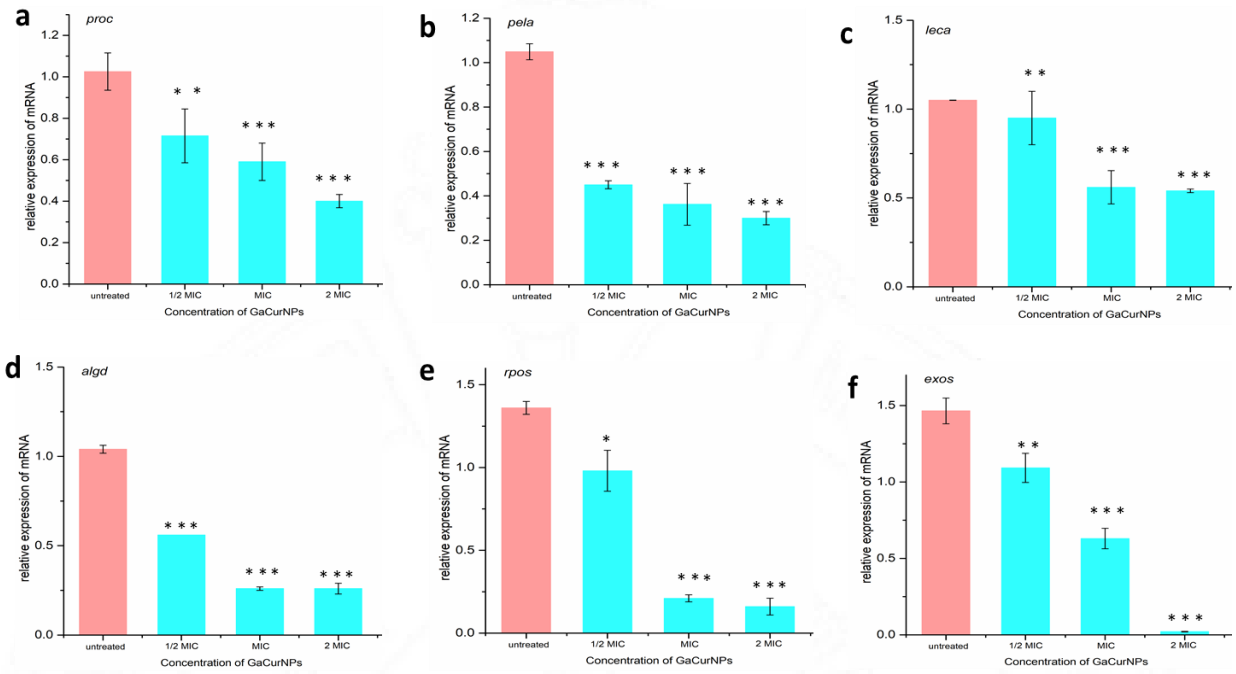

Figure 52: Relative gene expression of biofilm formation genes in *P. aeruginosa* clinical strain biofilm on treatment with GaCurNPs. Relative gene expression of (a) proC (b) lecA (c) pelA(d) algD (e) rpoS (f) exoS on treatment with ½ MIC, MIC and 2MIC of GaCurNPs. The results are represented as mean ± SD. Significant difference between test and control was measured as **p<0.01 and ***p<0.001.

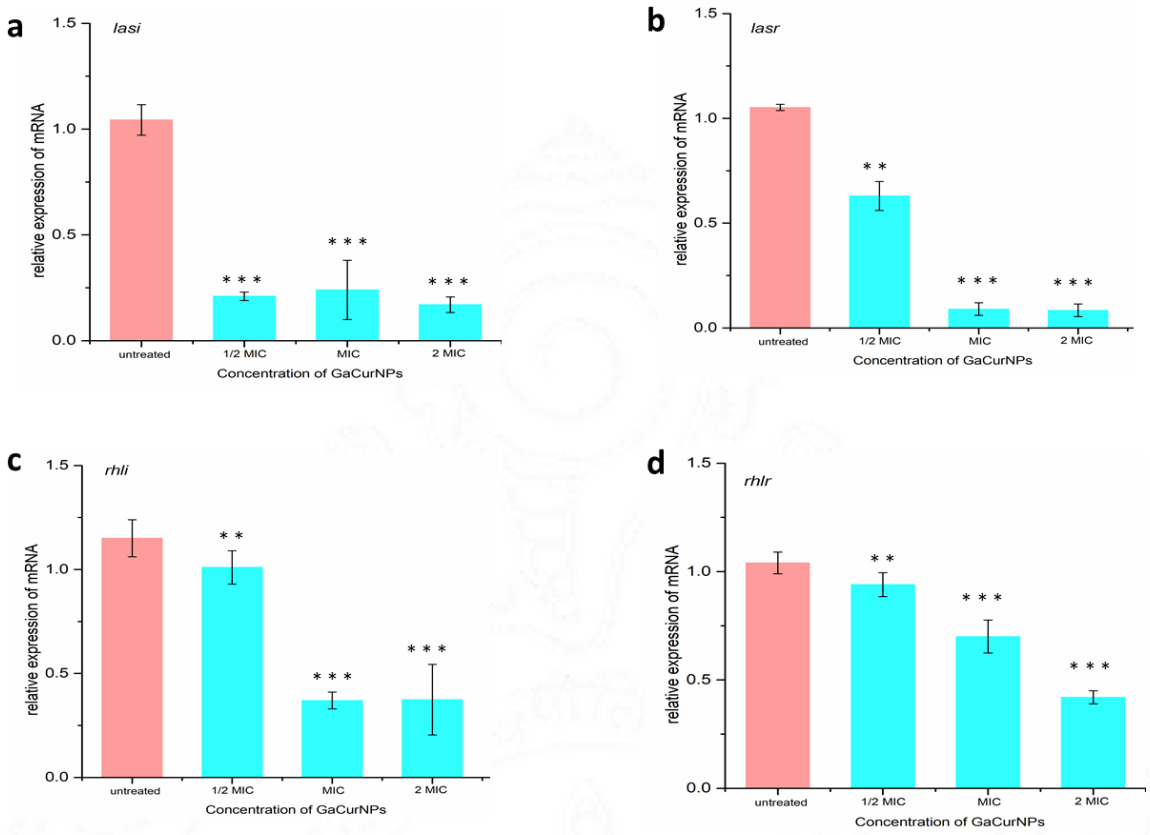

Figure 53: Relative gene expression of QS genes in *P. aeruginosa* clinical strain biofilm on treatment with GaCurNPs. Relative gene expression of (a) lasI (b) lasR (c) rhlI (d) rhlR on treatment with ½ MIC, MIC and 2MIC of GaCurNPs. The results are represented as mean ± SD. Significant difference between test and control was measured as **p<0.01 and ***p<0.001.

The results indicate that GaCurNPs exhibit activity against both planktonic and biofilm forms of bacteria, showing significant inhibition of bacterial growth and biofilm formation. This provides a foundation for exploring the mechanisms by which GaCurNPs disrupt bacterial processes and enhance antimicrobial efficacy at the molecular level. The key bacterial killing mechanisms of nanoparticles include disruption of the bacterial cell membrane, generation of reactive oxygen species (ROS), interaction with intracellular components, biofilm disruption, quorum sensing inhibition, induction of bacterial apoptosis-like pathways or electrostatic interactions (Wang et

al., 2017). The antibacterial mechanisms of GaCurNPs based on experimental findings are as follows:

1. ***Electrostatic interactions***: As evidenced in the literature, positively charged nanoparticles interact with negatively charged bacterial cell membranes and bring about cell membrane damage (Neal, 2008). GaCurNPs are positively charged, allowing them to interact with the negatively charged bacterial cell membrane. This electrostatic interaction can lead to membrane disruption and lysis. As observed from the SEM images, holes and craters were observed on the surface of the *P. aeruginosa* cell membrane. Some bacterial cells were observed to be completely lysed. The electrostatic interactions might have contributed to this damage. The nanoparticles attach to the bacterial surface, destabilizing the membrane structure by disrupting its lipid layer. This weakens the membrane, leading to pores or cracks and causes the leakage of vital intracellular components (Linklater et al., 2020; de Macedo et al., 2022). The damage caused by the GaCurNPs might compromise the integrity of the bacterial cell membrane, causing lysis and eventually cell death.
2. ***Reactive Oxygen Species (ROS) Production***: Our study showed that GaCurNPs induce ROS production in bacterial cells. ROS can cause oxidative stress, DNA damage, protein denaturation, and lipid peroxidation (Vaishampayan and Grohmann, 2022). Further, Raman spectroscopy analysis revealed a significant reduction in the characteristic peaks corresponding to DNA, proteins, and lipids following treatment with the MIC of GaCurNPs. This could be attributed to the ROS-mediated damage of cellular components. The membrane damage, as evident from the SEM could also be due to lipid peroxidation and denaturation of membrane proteins. This experimental evidence points towards potential

inhibition of replication and transcription, functional impairment of proteins, and membrane integrity loss, leading to bacterial cell death.

3. ***Reduction in Pyocyanin production***: Pyocyanin is a virulence factor produced by *P. aeruginosa*, and its production is regulated by bacterial quorum sensing (Morkunas et al., 2012). In our study, we found that there was a decrease in pyocyanin production on treatment with GaCurNPs. The decreased pyocyanin production by GaCurNPs can undercut the virulence and biofilm formation of *P. aeruginosa*. This can make the bacterial cells more sensitive to membrane disruption, ROS generation, and biofilm damage. Furthermore, studies have shown that a decrease in pyocyanin production can make bacteria more sensitive to antibacterials (Jiang et al., 2023). Therefore, by targeting pyocyanin, GaCurNPs not only mediate direct antibacterial effects but also help with increased susceptibility toward conventional antibacterial agents like ethanol.
4. ***Biofilm disruption***: GaCurNPs disrupt biofilm formation, weakening the protective matrix around bacteria and increasing bacterial susceptibility. As evident from the crystal violet assay, GaCurNPs disrupted biofilm, and further evidence from Raman spectroscopy, SEM and live dead assay supported this observation.

Therefore, we may conclude that bacterial killing could be caused by one or more of the mechanisms described above.

CHAPTER 5

5. SUMMARY AND CONCLUSION

5.1. Summary

P. aeruginosa is a resilient pathogen that is innately resistant to many antibiotics. The resistance of this bacterium to antibacterial agents has become alarmingly more. The frequent, sustained, and unchecked use of antibiotics is one of the main causes of the rise in resistant bacterial strains, especially multidrug-resistant variants. Fewer newer antibiotic classes are being created to combat *P. aeruginosa*. A wide variety of alternatives have been explored for controlling antibiotic - *P. aeruginosa* ranging from nanotechnology to antipseudomonal vaccines. Because of their small size, high surface reactivity, and diverse modes of action, nanoparticles have demonstrated themselves to be effective antimicrobials. The most widely used nanoparticles are silver nanoparticles then followed by antimicrobial peptides, chitosan, zinc, titanium, and copper. Silver nanoparticles are found to be cytotoxic and so are the other nanoparticles. A decrease in toxicity and enhancement in antibacterial properties are observed when these nanoparticles are conjugated with polymers or phytochemicals.

This study is focused on developing an alternative to antibiotics for *P. aeruginosa* which can potentially be used for topical applications. Here, curcumin was chosen for the synthesis of nanoparticles along with gallium. Curcumin has excellent antibacterial properties but its solubility and degradation physiological pH limits its use. Gallium also has excellent antibacterial and antibiofilm properties. An additional advantage is the non-toxicity of gallium and the tolerance of gallium by humans. This study exploits the use of curcumin in conjugation with gallium in a nanoformulation for its antibacterial and antibiofilm properties. This process of

conjugation of curcumin with gallium is known to impart improved stability to curcumin thereby enhancing its antibacterial properties. Firstly, our study highlights the excellent stability of curcumin bound to GaCurNPs in physiological pH and temperature, which is crucial for its application in biological systems. In addition, the nanoparticles exhibited a size of less than 50 nm which enhances the capabilities of penetration and improved activity, thus improving the therapeutic potential. The observed antibacterial and antibiofilm activity against *P. aeruginosa,* a notorious opportunistic pathogen is noteworthy and has significant clinical translational value. GaCurNPs demonstrate the ability to mitigate virulence factors as evidenced by the reduction in swarming motility and pyocyanin production. ROS production and cell membrane rupture also indicate the capacity of GaCurNPs to inhibit the ability of *P. aeruginosa* to establish and propagate infections. The study also highlights the ability of GaCurNPs to interfere with the molecular-level mechanism of biofilm formation, virulence, and quorum sensing. Biofilm, virulence, and QS genes are effectively downregulated by GaCurNPs in *P. aeruginosa* thereby underlining the interference of these nanoparticles in the gene expression levels. In addition to the therapeutic potential, a novel strategy of using Raman spectroscopy/ Confocal Raman microscopy in combination with PCA as a tool to study the effect of GaCurNPs was used. This approach provides insights into the interaction of nanoparticles with biofilm and a comparatively less time-consuming and label-free technique for studying the effect of nanoparticles/compounds on *P. aeruginosa* biofilm. In summary, the findings of this study project the immense promise of GaCurNPs as an alternative effective strategy for combating *P. aeruginosa* infections. The contributions of this study possess significant implications for the development of alternative therapeutic agents aimed at addressing infections caused by bacterial biofilms in clinical settings.

GaCurNPs could be a versatile tool in combating bacterial resistance against *P. aeruginosa*. Given the potentials and limitations of GaCurNPs, their application in clinical settings can be strategically focused on specific areas. The administration of nanoparticles orally or parenterally in the current form is not possible and therefore thorough *in vivo* studies have to be conducted to unravel the best route of administration.

GaCurNPs can be a promising topical antibacterial agent and may be used as a coating for medical devices, particularly against *P. aeruginosa* in skin and soft tissue infections (SSTIs) and biofilm-associated infections. Further details on these potential applications are given below:

- Topical Application for Skin and Soft Tissue Infections (SSTIs)

GaCurNPs have shown efficacy in disrupting bacterial biofilms, which are a significant problem in chronic skin infections caused by *P. aeruginosa*. The ability of GaCurNPs to produce reactive oxygen species (ROS) and damage bacterial cell membranes makes them effective in preventing and treating SSTIs. However, it cannot be directly applied on to the infected areas, since that will limit its bioavailability. Additionally, sustained release of the GaCurNPs is necessary for optimum antibacterial activity. Therefore, an effective way of delivering GaCurNPs would be to incorporate GaCurNPs into a gel/or a polymer matrix that allows for a controlled release of GaCurNPs at the infected site. The gel can maintain a moist environment and ensure sustained nanoparticle action against bacteria.

- Coatings on Medical Devices

GaCurNPs may be coated onto medical devices, such as catheters, wound dressings, or implants, to prevent biofilm formation. This is crucial as biofilm-associated infections are often resistant to antibiotics and can lead to device failure. The positive charge of GaCurNPs aids in disrupting

bacterial membranes, providing an antimicrobial surface that actively prevents bacterial colonization. This could reduce the risk of infection in patients using medical devices.

5.2. Conclusions

1. Gallium metal was identified for the conjugation of curcumin owing to its non-toxicity and antibacterial properties.

2. GaCurNPs were synthesized successfully after optimizing the reactants gallium chloride and curcumin.

3. Size determination and zeta potential of GaCurNPs were determined. The size was less than 100 nm and the nanoparticles were moderately stable.

4. Spectroscopic evidence unveiled the oxidation state of gallium to be +3 and the interaction between gallium and curcumin as non-covalent in nature.

5. The stability of curcumin attached to GaCurNPs was found to be greatly increased in physiological pH in comparison with bare curcumin.

6. The cytotoxicity of GaCurNPs on L929 cells was significantly less when compared to bare curcumin.

7. The MIC of GaCurNPs on *P. aeruginosa* ATCC 27853 and some clinical strains were calculated and the growth inhibition of *P. aeruginosa* ATCC 27853 strain and a clinical strain was recorded for various concentrations of curcumin and GaCurNPs. GaCurNPs were observed to bring about greater inhibition at MIC and 2MIC concentrations compared to bare curcumin.

8. Swarming motility and pyocyanin production of *P. aeruginosa* strains were compromised on treatment with GaCurNPs. A dose-dependent decrease in swarming motility and pyocyanin

production was observed in both the strains under study. ROS production and membrane damage were also observed in *P. aeruginosa* strains treated with GaCurNPs.

10. GaCurNPs in concentrations MIC, 2MIC, and 4MIC were tested for its antibiofilm activity. GaCurNPs have been shown to inhibit biofilm formation and also the destruction of mature biofilm in a dose-dependent fashion. The higher the treatment concentration, the higher the inhibition and disruption.

11. The viability of bacterial cells in biofilm was reduced greatly on treatment with a high concentration of GaCurNPs (4MIC).

12. FESEM evidence showed the disruption of biofilm by GaCurNPs. SEM analysis showed that GaCurNPs disrupted biofilm by causing lysis of bacterial cells and disruption of EPS.

13. Confocal Raman microscopy along with PCA was used as a tool to study the effect of GaCurNPs on *P. aeruginosa.* The distinct clustering of untreated and treated biofilms in PCA further supports the notion that GaCurNPs treatment induces substantial alterations in the biofilm composition and structure.`

14. A dose-dependent downregulation of biofilm formation genes and QS genes was observed in both planktonic and biofilm forms of *P. aeruginosa.* The results were suggestive of GaCurNPs capable of modulating the expression of biofilm formation and virulence genes in the planktonic as well as biofilm form of *P. aeruginosa.*

5.3. Future perspectives of the study

1. To validate the activity of GaCurNPs in more multidrug resistant strains of *P. aeruginosa.*

2. Since GaCurNPs show promising antibacterial and antibiofilm properties, the nanoparticles may be incorporated into a suitable gel matrix for topical applications.

3. Transitioning from *in vitro* studies to *ex vivo* models is crucial to validate the actual potential of the nanoparticles. *In vivo* studies in a suitable infected animal model to study the biodistribution and therapeutical efficiency are required for clinical translation.

4. Given the potential of GaCurNPs to serve as a topical treatment for *Pseudomonas* skin and wound infections, the optimization of formulations and delivery systems has to be validated.

In conclusion, the future perspectives for the study on GaCurNPs as a potent alternative to antibiotics against *Pseudomonas* infection include a wide range of research directions including *in vivo* validation, topical application studies, mechanistic investigations, and translational efforts towards clinical applications. By addressing these key areas, this research has the potential to advance our understanding as a promising therapeutic option for combating *Pseudomonas* infections and improving patient outcomes.

REFERENCES

Abdelghany SM, Quinn DJ, Ingram RJ, et al. (2012) Gentamicin-loaded nanoparticles show improved antimicrobial effects towards Pseudomonas aeruginosa infection. *International Journal of Nanomedicine* 7: 4053–4063.

Abdulrahman H, Misba L, Ahmad S, et al. (2020) Curcumin induced photodynamic therapy mediated suppression of quorum sensing pathway of Pseudomonas aeruginosa: An approach to inhibit biofilm in vitro. *Photodiagnosis and Photodynamic Therapy* 30: 101645.

Adahoun MA, Al-Akhras M-AH, Jaafar MS, et al. (2017) Enhanced anti-cancer and antimicrobial activities of curcumin nanoparticles. *Artificial Cells, Nanomedicine, and Biotechnology* 45(1). Taylor & Francis: 98–107.

Adams WT and Ivanisevic A (2019) Nanostructured Oxides Containing Ga: Materials with Unique Properties for Aqueous-Based Applications. *ACS Omega* 4(4). American Chemical Society: 6876–6882.

Anderson AM, Mitchell MS and Mohan RS (2000) Isolation of Curcumin from Turmeric. *Journal of Chemical Education* 77(3): 359.

Antunes LCS, Imperi F, Minandri F, et al. (2012) In Vitro and In Vivo Antimicrobial Activities of Gallium Nitrate against Multidrug-Resistant Acinetobacter baumannii. *Antimicrobial Agents and Chemotherapy* 56(11): 5961–5970.

AOAC: Official Methods of Analysis (Volume 1) (n.d.).

Avivi S, Mastai Y, Hodes G, et al. (1999) Sonochemical Hydrolysis of Ga3+ Ions: Synthesis of Scroll-like Cylindrical Nanoparticles of Gallium Oxide Hydroxide. *Journal of the American Chemical Society* 121(17). American Chemical Society: 4196–4199.

Bagge N, Schuster M, Hentzer M, et al. (2004) Pseudomonas aeruginosa biofilms exposed to imipenem exhibit changes in global gene expression and beta-lactamase and alginate production. *Antimicrobial Agents and Chemotherapy* 48(4): 1175–1187.

Balaban NQ, Gerdes K, Lewis K, et al. (2013) A problem of persistence: still more questions than answers? *Nature Reviews Microbiology* 11(8). Nature Publishing Group: 587–591.

Baldoni D, Steinhuber A, Zimmerli W, et al. (2010) In Vitro Activity of Gallium Maltolate against Staphylococci in Logarithmic, Stationary, and Biofilm Growth Phases: Comparison of Conventional and Calorimetric Susceptibility Testing Methods. *Antimicrobial Agents and Chemotherapy* 54(1): 157–163.

Bandara HMHN, Herpin MJ, Kolacny DJr, et al. (2016) Incorporation of Farnesol Significantly Increases the Efficacy of Liposomal Ciprofloxacin against Pseudomonas aeruginosa

Biofilms in Vitro. *Molecular Pharmaceutics* 13(8). American Chemical Society: 2760–2770.

Baptista PV, McCusker MP, Carvalho A, et al. (2018) Nano-Strategies to Fight Multidrug Resistant Bacteria—"A Battle of the Titans". *Frontiers in Microbiology* 9. Frontiers: 381070.

Bassetti M, Vena A, Croxatto A, et al. (2018) How to manage Pseudomonas aeruginosa infections. *Drugs in Context* 7: 212527.

Beier BD, Quivey RG and Berger AJ (2012) Raman microspectroscopy for species identification and mapping within bacterial biofilms. *AMB Express* 2(1): 35.

Bernier SP, Lebeaux D, DeFrancesco AS, et al. (2013) Starvation, together with the SOS response, mediates high biofilm-specific tolerance to the fluoroquinolone ofloxacin. *PLoS genetics* 9(1): e1003144.

Bernstein LR (1998) Mechanisms of Therapeutic Activity for Gallium. *Pharmacological Reviews* 50(4): 665–682.

Berrazeg M, Jeannot K, Ntsogo Enguéné VY, et al. (2015) Mutations in β-Lactamase AmpC Increase Resistance of Pseudomonas aeruginosa Isolates to Antipseudomonal Cephalosporins. *Antimicrobial Agents and Chemotherapy* 59(10): 6248–6255.

Bhawana, Basniwal RK and Buttar HS (2011) Curcumin Nanoparticles: Preparation, Characterization, and Antimicrobial Study. *Journal of Agricultural and Food Chemistry* 59(5): 2056–2061.

Billings N, Millan M, Caldara M, et al. (2013) The extracellular matrix Component Psl provides fast-acting antibiotic defense in Pseudomonas aeruginosa biofilms. *PLoS pathogens* 9(8): e1003526.

Bisht S, Feldmann G, Soni S, et al. (2007) Polymeric nanoparticle-encapsulated curcumin ('nanocurcumin'): a novel strategy for human cancer therapy. *Journal of Nanobiotechnology* 5: 3.

Bonomo RA and Szabo D (2006) Mechanisms of Multidrug Resistance in Acinetobacter Species and Pseudomonas aeruginosa. *Clinical Infectious Diseases* 43(Supplement_2): S49–S56.

Borlee BR, Goldman AD, Murakami K, et al. (2010) Pseudomonas aeruginosa uses a cyclic-di-GMP-regulated adhesin to reinforce the biofilm extracellular matrix. *Molecular Microbiology* 75(4): 827–842.

Borriello G, Werner E, Roe F, et al. (2004) Oxygen limitation contributes to antibiotic tolerance of Pseudomonas aeruginosa in biofilms. *Antimicrobial Agents and Chemotherapy* 48(7): 2659–2664.

Bourque JL, Biesinger MC and Baines KM (2016) Chemical state determination of molecular gallium compounds using XPS. *Dalton Transactions* 45(18): 7678–7696.

Breidenstein EBM, de la Fuente-Núñez C and Hancock REW (2011) Pseudomonas aeruginosa: all roads lead to resistance. *Trends in Microbiology* 19(8): 419–426.

Bruna T, Maldonado-Bravo F, Jara P, et al. (2021) Silver Nanoparticles and Their Antibacterial Applications. *International Journal of Molecular Sciences* 22(13): 7202.

Bush K and Jacoby GA (2010) Updated functional classification of beta-lactamases. *Antimicrobial Agents and Chemotherapy* 54(3): 969–976.

Cabot G, Ocampo-Sosa AA, Tubau F, et al. (2011) Overexpression of AmpC and Efflux Pumps in Pseudomonas aeruginosa Isolates from Bloodstream Infections: Prevalence and Impact on Resistance in a Spanish Multicenter Study. *Antimicrobial Agents and Chemotherapy* 55(5). American Society for Microbiology: 1906–1911.

Cabot G, Zamorano L, Moyà B, et al. (2016) Evolution of Pseudomonas aeruginosa Antimicrobial Resistance and Fitness under Low and High Mutation Rates. *Antimicrobial Agents and Chemotherapy* 60(3): 1767–1778.

Cavalcanti FL de S, Mirones CR, Paucar ER, et al. (2015) Mutational and acquired carbapenem resistance mechanisms in multidrug resistant *Pseudomonas aeruginosa* clinical isolates from Recife, Brazil. *Memórias do Instituto Oswaldo Cruz* 110. Instituto Oswaldo Cruz, Ministério da Saúde: 1003–1009.

Chancey ST, Zähner D and Stephens DS (2012) Acquired inducible antimicrobial resistance in Gram-positive bacteria. *Future Microbiology* 7(8): 959–978.

Chang H-I and Yeh M-K (2012) Clinical development of liposome-based drugs: formulation, characterization, and therapeutic efficacy. *International Journal of Nanomedicine* 7: 49–60.

Chatterjee M, Anju CP, Biswas L, et al. (2016) Antibiotic resistance in Pseudomonas aeruginosa and alternative therapeutic options. *International Journal of Medical Microbiology* 306(1): 48–58.

Chen W, Li S, Renick P, et al. (2019) Bacterial acidity-triggered antimicrobial activity of self-assembling peptide nanofibers. *Journal of Materials Chemistry B* 7(18). The Royal Society of Chemistry: 2915–2919.

Chen Y, Wu Q, Zhang Z, et al. (2012) Preparation of Curcumin-Loaded Liposomes and Evaluation of Their Skin Permeation and Pharmacodynamics. *Molecules* 17(5): 5972–5987.

Chereddy KK, Coco R, Memvanga PB, et al. (2013) Combined effect of PLGA and curcumin on wound healing activity. *Journal of Controlled Release: Official Journal of the Controlled Release Society* 171(2): 208–215.

Chiang W-C, Nilsson M, Jensen PØ, et al. (2013) Extracellular DNA Shields against Aminoglycosides in Pseudomonas aeruginosa Biofilms. *Antimicrobial Agents and Chemotherapy* 57(5): 2352–2361.

Chignell CF, Bilskj P, Reszka KJ, et al. (1994) SPECTRAL AND PHOTOCHEMICAL PROPERTIES OF CURCUMIN. *Photochemistry and Photobiology* 59(3): 295–302.

Chimi LY, Noubom M, Bisso BN, et al. (2024) Biofilm Formation, Pyocyanin Production, and Antibiotic Resistance Profile of Pseudomonas aeruginosa Isolates from Wounds. *International Journal of Microbiology* 2024: 1207536.

Colvin KM, Gordon VD, Murakami K, et al. (2011) The pel polysaccharide can serve a structural and protective role in the biofilm matrix of Pseudomonas aeruginosa. *PLoS pathogens* 7(1): e1001264.

Dai C, Lin J, Li H, et al. (2022) The Natural Product Curcumin as an Antibacterial Agent: Current Achievements and Problems. *Antioxidants* 11(3): 459.

Dakal TC, Kumar A, Majumdar RS, et al. (2016) Mechanistic Basis of Antimicrobial Actions of Silver Nanoparticles. *Frontiers in Microbiology* 7. Frontiers.

Darwesh R and Elbialy NS (2021) Iron oxide nanoparticles conjugated curcumin to promote high therapeutic efficacy of curcumin against hepatocellular carcinoma. *Inorganic Chemistry Communications* 126: 108482.

Das T, Ibugo AI, Klare W, et al. (2016) Role of Pyocyanin and Extracellular DNA in Facilitating Pseudomonas aeruginosa Biofilm Formation. In: *Microbial Biofilms - Importance and Applications*. IntechOpen. Available at: https://www.intechopen.com/chapters/50678 (accessed 24 March 2024).

Daury L, Orange F, Taveau J-C, et al. (2016) Tripartite assembly of RND multidrug efflux pumps. *Nature Communications* 7(1). 1. Nature Publishing Group: 10731.

De Gelder J, De Gussem K, Vandenabeele P, et al. (2007) Reference database of Raman spectra of biological molecules. *Journal of Raman Spectroscopy* 38(9): 1133–1147.

de Macedo EF, Santos NS, Nascimento LS, et al. (2022) Interaction between Nanoparticles, Membranes and Proteins: A Surface Plasmon Resonance Study. *International Journal of Molecular Sciences* 24(1): 591.

Delcour AH (2009) Outer membrane permeability and antibiotic resistance. *Biochimica et Biophysica Acta (BBA) - Proteins and Proteomics* 1794(5). Mechanisms of Drug Efflux and Strategies to Combat Them: 808–816.

Dhanya CS, Paul W, Victor SP, et al. (2021) On improving the physiological stability of curcuminoids: Curcumininoid-silver nanoparticle complex as a better and efficient therapeutic agent. *Nano-Structures & Nano-Objects* 25: 100661.

Di Salle A, Viscusi G, Di Cristo F, et al. (2021) Antimicrobial and Antibiofilm Activity of Curcumin-Loaded Electrospun Nanofibers for the Prevention of the Biofilm-Associated Infections. *Molecules* 26(16). 16. Multidisciplinary Digital Publishing Institute: 4866.

Dickey SW, Cheung GYC and Otto M (2017) Different drugs for bad bugs: antivirulence strategies in the age of antibiotic resistance. *Nature Reviews Drug Discovery* 16(7). 7. Nature Publishing Group: 457–471.

Dong X, Liang W, Meziani MJ, et al. (2020) Carbon Dots as Potent Antimicrobial Agents. *Theranostics* 10(2): 671–686.

Dreier J and Ruggerone P (2015) Interaction of antibacterial compounds with RND efflux pumps in Pseudomonas aeruginosa. *Frontiers in Microbiology* 6: 660.

El Zowalaty ME, Al Thani AA, Webster TJ, et al. (2015) Pseudomonas aeruginosa: arsenal of resistance mechanisms, decades of changing resistance profiles, and future antimicrobial therapies. *Future Microbiology* 10(10): 1683–1706.

Esatbeyoglu T, Huebbe P, Ernst IMA, et al. (2012) Curcumin—From Molecule to Biological Function. *Angewandte Chemie International Edition* 51(22): 5308–5332.

Estevez MB, Raffaelli S, Mitchell SG, et al. (2020) Biofilm Eradication Using Biogenic Silver Nanoparticles. *Molecules* 25(9): 2023.

Fajardo A, Martínez-Martín N, Mercadillo M, et al. (2008) The Neglected Intrinsic Resistome of Bacterial Pathogens. *PLOS ONE* 3(2). Public Library of Science: e1619.

Falconieri MC, Adamo M, Monasterolo C, et al. (2017) New Dendrimer-Based Nanoparticles Enhance Curcumin Solubility. *Planta Medica* 83(5): 420–425.

Fang Z, Zhang L, Huang Y, et al. (2014) OprD mutations and inactivation in imipenem-resistant Pseudomonas aeruginosa isolates from China. *Infection, Genetics and Evolution* 21: 124–128.

Feng J, Fuente-Núñez C de la, J. Trimble M, et al. (2015) An in situ Raman spectroscopy-based microfluidic “lab-on-a-chip” platform for non-destructive and continuous characterization of Pseudomonas aeruginosa biofilms. *Chemical Communications* 51(43). Royal Society of Chemistry: 8966–8969.

Feng J, Fu B, Fang L, et al. (2019) Uniform gallium oxyhydroxide nanorod anodes with superior lithium-ion storage. *RSC Advances* 9(60). Royal Society of Chemistry: 34896–34901.

Fernandes S, Borges A, Gomes IB, et al. (2023) Curcumin and 10-undecenoic acid as natural quorum sensing inhibitors of LuxS/AI-2 of Bacillus subtilis and LasI/LasR of Pseudomonas aeruginosa. *Food Research International* 165: 112519.

Fernández-Olmos A, García-Castillo M, Maiz L, et al. (2012) In vitro prevention of Pseudomonas aeruginosa early biofilm formation with antibiotics used in cystic fibrosis patients. *International Journal of Antimicrobial Agents* 40(2): 173–176.

Flora G, Gupta D and Tiwari A (2013) Nanocurcumin: A Promising Therapeutic Advancement over Native Curcumin. *Critical Reviews™ in Therapeutic Drug Carrier Systems* 30(4). Begel House Inc.

Forier K, Raemdonck K, De Smedt SC, et al. (2014) Lipid and polymer nanoparticles for drug delivery to bacterial biofilms. *Journal of Controlled Release: Official Journal of the Controlled Release Society* 190: 607–623.

Freire PTC, Barboza FM, Lima JA, et al. (2017) *Raman Spectroscopy of Amino Acid Crystals*. IntechOpen. Available at: https://www.intechopen.com/chapters/52839 (accessed 1 February 2022).

Fuqua WC, Winans SC and Greenberg EP (1994) Quorum sensing in bacteria: the LuxR-LuxI family of cell density-responsive transcriptional regulators. *Journal of Bacteriology* 176(2): 269–275.

Fuxman Bass JI, Russo DM, Gabelloni ML, et al. (2010) Extracellular DNA: a major proinflammatory component of Pseudomonas aeruginosa biofilms. *Journal of Immunology (Baltimore, Md.: 1950)* 184(11): 6386–6395.

Gera M, Sharma N, Ghosh M, et al. (2017) Nanoformulations of curcumin: an emerging paradigm for improved remedial application. *Oncotarget* 8(39): 66680–66698.

Ghafoor A, Hay ID and Rehm BHA (2011) Role of Exopolysaccharides in Pseudomonas aeruginosa Biofilm Formation and Architecture ▿. *Applied and Environmental Microbiology* 77(15): 5238–5246.

Gholami M, Zeighami H, Bikas R, et al. (2020) Inhibitory activity of metal-curcumin complexes on quorum sensing related virulence factors of Pseudomonas aeruginosa PAO1. *AMB Express* 10(1): 111.

Gloag ES, Turnbull L, Huang A, et al. (2013) Self-organization of bacterial biofilms is facilitated by extracellular DNA. *Proceedings of the National Academy of Sciences of the United States of America* 110(28): 11541–11546.

Griesser M, Pistis V, Suzuki T, et al. (2011) Autoxidative and Cyclooxygenase-2 Catalyzed Transformation of the Dietary Chemopreventive Agent Curcumin. *Journal of Biological Chemistry* 286(2): 1114–1124.

Gunes H, Gulen D, Mutlu R, et al. (2016) Antibacterial effects of curcumin: An in vitro minimum inhibitory concentration study. *Toxicology and Industrial Health* 32(2): 246–250.

Gupta P, Sarkar S, Das B, et al. (2016) Biofilm, pathogenesis and prevention--a journey to break the wall: a review. *Archives of Microbiology* 198(1): 1–15.

Guzman M, Dille J and Godet S (2012) Synthesis and antibacterial activity of silver nanoparticles against gram-positive and gram-negative bacteria. *Nanomedicine: Nanotechnology, Biology, and Medicine* 8(1): 37–45.

Hancock RE (1998) Resistance mechanisms in Pseudomonas aeruginosa and other nonfermentative gram-negative bacteria. *Clinical Infectious Diseases: An Official Publication of the Infectious Diseases Society of America* 27 Suppl 1: S93-99.

Hancock REW and Brinkman FSL (2002) Function of pseudomonas porins in uptake and efflux. *Annual Review of Microbiology* 56: 17–38.

Hasan M, Belhaj N, Benachour H, et al. (2014) Liposome encapsulation of curcumin: Physico-chemical characterizations and effects on MCF7 cancer cell proliferation. *International Journal of Pharmaceutics* 461(1): 519–528.

Hauser AR and Rello J (2012) *Severe Infections Caused by Pseudomonas Aeruginosa*. Springer Science & Business Media.

Häussler S (2004) Biofilm formation by the small colony variant phenotype of Pseudomonas aeruginosa. *Environmental Microbiology* 6(6): 546–551.

Henrichfreise B, Wiegand I, Pfister W, et al. (2007) Resistance Mechanisms of Multiresistant Pseudomonas aeruginosa Strains from Germany and Correlation with Hypermutation. *Antimicrobial Agents and Chemotherapy* 51(11): 4062–4070.

Henry VA, Jessop JLP and Peeples TL (2017) Differentiating Pseudomonas sp. strain ADP cells in suspensions and biofilms using Raman spectroscopy and scanning electron microscopy. *Analytical and Bioanalytical Chemistry* 409(5): 1441–1449.

Hentzer M, Teitzel GM, Balzer GJ, et al. (2001) Alginate Overproduction Affects Pseudomonas aeruginosa Biofilm Structure and Function. *Journal of Bacteriology* 183(18). American Society for Microbiology: 5395–5401.

Hettiarachchi SS, Dunuweera SP, Dunuweera AN, et al. (2021) Synthesis of Curcumin Nanoparticles from Raw Turmeric Rhizome. *ACS Omega* 6(12). American Chemical Society: 8246–8252.

Hickman JW and Harwood CS (2008) Identification of FleQ from Pseudomonas aeruginosa as a c-di-GMP-responsive transcription factor. *Molecular Microbiology* 69(2): 376–389.

Hijazi S, Visca P and Frangipani E (2017) Gallium-Protoporphyrin IX Inhibits Pseudomonas aeruginosa Growth by Targeting Cytochromes. *Frontiers in Cellular and Infection Microbiology* 7.

Hong DJ, Bae IK, Jang I-H, et al. (2015) Epidemiology and Characteristics of Metallo-β-Lactamase-Producing Pseudomonas aeruginosa. *Infection & Chemotherapy* 47(2): 81–97.

Hooper DC (1999) Mode of action of fluoroquinolones. *Drugs* 58 Suppl 2: 6–10.

Iglewski BH (1996) Pseudomonas. In: Baron S (ed.) *Medical Microbiology*. 4th ed. Galveston (TX): University of Texas Medical Branch at Galveston. Available at: http://www.ncbi.nlm.nih.gov/books/NBK8326/ (accessed 12 December 2023).

Ivleva NP, Wagner M, Horn H, et al. (2009) Towards a nondestructive chemical characterization of biofilm matrix by Raman microscopy. *Analytical and Bioanalytical Chemistry* 393(1): 197–206.

Jackson KD, Starkey M, Kremer S, et al. (2004) Identification of psl, a locus encoding a potential exopolysaccharide that is essential for Pseudomonas aeruginosa PAO1 biofilm formation. *Journal of Bacteriology* 186(14): 4466–4475.

Jaiswal M, Dudhe R and Sharma PK (2015) Nanoemulsion: an advanced mode of drug delivery system. *3 Biotech* 5(2): 123–127.

Jaiswal S and Mishra P (2018a) Antimicrobial and antibiofilm activity of curcumin-silver nanoparticles with improved stability and selective toxicity to bacteria over mammalian cells. *Medical Microbiology and Immunology* 207(1). Springer Berlin Heidelberg: 39–53.

Jaiswal S and Mishra P (2018b) Antimicrobial and antibiofilm activity of curcumin-silver nanoparticles with improved stability and selective toxicity to bacteria over mammalian cells. *Medical Microbiology and Immunology* 207(1): 39–53.

Jaiswal S, Duffy B, Jaiswal AK, et al. (2010) Enhancement of the antibacterial properties of silver nanoparticles using β-cyclodextrin as a capping agent. *International Journal of Antimicrobial Agents* 36(3): 280–283.

Jayaprakasha GK, Jagan Mohan Rao L and Sakariah KK (2002) Improved HPLC Method for the Determination of Curcumin, Demethoxycurcumin, and Bisdemethoxycurcumin. *Journal of Agricultural and Food Chemistry* 50(13): 3668–3672.

Jiang S, Deng Y, Long Z, et al. (2023) Reduction of pyocyanin synthesis and antibiotic resistance in Pseudomonas aeruginosa by low concentration ethanol. *FEMS microbiology letters* 370: fnad069.

Jung GB, Nam SW, Choi S, et al. (2014) Evaluation of antibiotic effects on Pseudomonas aeruginosa biofilm using Raman spectroscopy and multivariate analysis. *Biomedical Optics Express* 5(9): 3238.

Kalhapure RS, Jadhav M, Rambharose S, et al. (2017) pH-responsive chitosan nanoparticles from a novel twin-chain anionic amphiphile for controlled and targeted delivery of vancomycin. *Colloids and Surfaces. B, Biointerfaces* 158: 650–657.

Karthikeyan A, Senthil N and Min T (2020) Nanocurcumin: A Promising Candidate for Therapeutic Applications. *Frontiers in Pharmacology* 11: 487.

Khajuria A, Praharaj AK, Kumar M, et al. (2013) Emergence of NDM – 1 in the Clinical Isolates of Pseudomonas aeruginosa in India. *Journal of Clinical and Diagnostic Research : JCDR* 7(7): 1328–1331.

Khalil NM, do Nascimento TCF, Casa DM, et al. (2013) Pharmacokinetics of curcumin-loaded PLGA and PLGA-PEG blend nanoparticles after oral administration in rats. *Colloids and Surfaces. B, Biointerfaces* 101: 353–360.

Khan M, Summers S, Rice SA, et al. (2020) Acquired fluoroquinolone resistance genes in corneal isolates of Pseudomonas aeruginosa. *Infection, Genetics and Evolution* 85: 104574.

Kharat M, Du Z, Zhang G, et al. (2017) Physical and Chemical Stability of Curcumin in Aqueous Solutions and Emulsions: Impact of pH, Temperature, and Molecular Environment. *Journal of Agricultural and Food Chemistry* 65(8): 1525–1532.

Kniggendorf A-K, Nogueira R, Kelb C, et al. (2016) Confocal Raman microscopy and fluorescent in situ hybridization - A complementary approach for biofilm analysis. *Chemosphere* 161: 112–118.

Köhler T, Curty LK, Barja F, et al. (2000) Swarming of Pseudomonas aeruginosa Is Dependent on Cell-to-Cell Signaling and Requires Flagella and Pili. *Journal of Bacteriology* 182(21). American Society for Microbiology: 5990–5996.

Kolev TM, Velcheva EA, Stamboliyska BA, et al. (2005) DFT and experimental studies of the structure and vibrational spectra of curcumin. *International Journal of Quantum Chemistry* 102(6): 1069–1079.

Kumari S, Kumaraswamy RV, Choudhary RC, et al. (2018) Thymol nanoemulsion exhibits potential antibacterial activity against bacterial pustule disease and growth promotory effect on soybean. *Scientific Reports* 8(1). 1. Nature Publishing Group: 6650.

Kumavat S, Chaudhari Y, Borole P, et al. (2013) ENHANCEMENT OF SOLUBILITY AND DISSOLUTION RATE OF CURCUMIN BY SOLID DISPERSION TECHNIQUE. *International Research Journal of Pharmacy* 4(5): 226–232.

Kuttan R, Bhanumathy P, Nirmala K, et al. (1985) Potential anticancer activity of turmeric (Curcuma longa). *Cancer Letters* 29(2): 197–202.

Lao CD, Ruffin MT, Normolle D, et al. (2006) Dose escalation of a curcuminoid formulation. *BMC Complementary and Alternative Medicine* 6(1): 10.

Lee BH, Choi HA, Kim M-R, et al. (2013) Changes in chemical stability and bioactivities of curcumin by ultraviolet radiation. *Food Science and Biotechnology* 22(1): 279–282.

Lee EJ, Hur MG, Son JM, et al. (2013) Effect of Liquid Ga on Metal Surfaces: Characterization of Morphology and Chemical Composition of Metals Heated in Liquid Ga. *Journal of Nanomaterials* 2013. Hindawi: e619682.

Lemire JA, Harrison JJ and Turner RJ (2013) Antimicrobial activity of metals: mechanisms, molecular targets and applications. *Nature Reviews Microbiology* 11(6). 6. Nature Publishing Group: 371–384.

Lewis K (2001) Riddle of Biofilm Resistance. *Antimicrobial Agents and Chemotherapy* 45(4). American Society for Microbiology: 999–1007.

Lewis K (2010) Persister Cells. *Annual Review of Microbiology* 64(1): 357–372.

Li C, Zhang Y, Su T, et al. (2012) Silica-coated flexible liposomes as a nanohybrid delivery system for enhanced oral bioavailability of curcumin. *International Journal of Nanomedicine* 7. Dove Medical Press: 5995–6002.

Li H, Luo Y-F, Williams BJ, et al. (2012) Structure and function of OprD protein in Pseudomonas aeruginosa: from antibiotic resistance to novel therapies. *International journal of medical microbiology: IJMM* 302(2): 63–68.

Li M, Xin M, Guo C, et al. (2017) New nanomicelle curcumin formulation for ocular delivery: improved stability, solubility, and ocular anti-inflammatory treatment. *Drug Development and Industrial Pharmacy* 43(11): 1846–1857.

Li R, Dhankhar D, Chen J, et al. (2019) Identification of Live and Dead Bacteria: A Raman Spectroscopic Study. *IEEE Access* 7: 23549–23559.

Li X, Robinson SM, Gupta A, et al. (2014) Functional Gold Nanoparticles as Potent Antimicrobial Agents against Multi-Drug-Resistant Bacteria. *ACS Nano* 8(10). American Chemical Society: 10682–10686.

Li X-Z and Nikaido H (2009) Efflux-mediated drug resistance in bacteria: an update. *Drugs* 69(12): 1555–1623.

Liao C, Huang X, Wang Q, et al. (2022) Virulence Factors of Pseudomonas Aeruginosa and Antivirulence Strategies to Combat Its Drug Resistance. *Frontiers in Cellular and Infection Microbiology* 12.

Linklater DP, Baulin VA, Le Guével X, et al. (2020) Antibacterial Action of Nanoparticles by Lethal Stretching of Bacterial Cell Membranes. *Advanced Materials* 32(52): 2005679.

Loo C-Y, Rohanizadeh R, Young PM, et al. (2016) Combination of Silver Nanoparticles and Curcumin Nanoparticles for Enhanced Anti-biofilm Activities. *Journal of Agricultural and Food Chemistry* 64(12): 2513–2522.

M K, A A-J, S M, et al. (2003) Involvement of bacterial migration in the development of complex multicellular structures in Pseudomonas aeruginosa biofilms. *Molecular microbiology* 50(1). Mol Microbiol.

Ma L, Conover M, Lu H, et al. (2009) Assembly and development of the Pseudomonas aeruginosa biofilm matrix. *PLoS pathogens* 5(3): e1000354.

Ma S, Moser D, Han F, et al. (2020) Preparation and antibiofilm studies of curcumin loaded chitosan nanoparticles against polymicrobial biofilms of *Candida albicans* and *Staphylococcus aureus*. *Carbohydrate Polymers* 241: 116254.

Macià MD, Rojo-Molinero E and Oliver A (2014) Antimicrobial susceptibility testing in biofilm-growing bacteria. *Clinical Microbiology and Infection: The Official Publication of the European Society of Clinical Microbiology and Infectious Diseases* 20(10): 981–990.

Mahmoudi A, Kesharwani P, Majeed M, et al. (2022) Recent advances in nanogold as a promising nanocarrier for curcumin delivery. *Colloids and Surfaces B: Biointerfaces* 215: 112481.

Malloy JL, Veldhuizen RAW, Thibodeaux BA, et al. (2005) Pseudomonas aeruginosa protease IV degrades surfactant proteins and inhibits surfactant host defense and biophysical functions. *American Journal of Physiology. Lung Cellular and Molecular Physiology* 288(2): L409-418.

Marathe SA, Kumar R, Ajitkumar P, et al. (2013) Curcumin reduces the antimicrobial activity of ciprofloxacin against Salmonella Typhimurium and Salmonella Typhi. *Journal of Antimicrobial Chemotherapy* 68(1). Oxford Academic: 139–152.

Martins C, Silva D, Neres A, et al. (2008) Curcumin as a promising antifungal of clinical interest. *The Journal of antimicrobial chemotherapy* 63: 337–9.

Mazumder A, Raghavan K, Weinstein J, et al. (1995) Inhibition of human immunodeficiency virus type-1 integrase by curcumin. *Biochemical Pharmacology* 49(8): 1165–1170.

McClure CD and Schiller NL (1992) Effects of Pseudomonas aeruginosa rhamnolipids on human monocyte-derived macrophages. *Journal of Leukocyte Biology* 51(2): 97–102.

Mi R, M R, B R, et al. (2016) Susceptibility of metallic magnesium implants to bacterial biofilm infections. *Journal of Biomedical Materials research. Part A* 104(6): 1489–1499.

Miller KP, Wang L, Benicewicz BC, et al. (2015) Inorganic nanoparticles engineered to attack bacteria. *Chemical Society Reviews* 44(21). The Royal Society of Chemistry: 7787–7807.

Miranda SW, Asfahl KL, Dandekar AA, et al. (2022) Pseudomonas aeruginosa Quorum Sensing. *Advances in experimental medicine and biology* 1386: 95–115.

Mishra M, Byrd MS, Sergeant S, et al. (2012) Pseudomonas aeruginosa Psl polysaccharide reduces neutrophil phagocytosis and the oxidative response by limiting complement-mediated opsonization. *Cellular Microbiology* 14(1): 95–106.

Modi B, Bahadur S, Bhowmik P, et al. (2023) Curcumin and Colistin are Synergistic in Inhibiting the Growth and Biofilm Formation of Pseudomonas aeruginosa Isolated from Environmental Sample. *Infectious Diseases Diagnosis & Treatment*. Gavin Publishers. Epub ahead of print 25 May 2023.

Mohammadi K, Thompson KH, Patrick BO, et al. (2005) Synthesis and characterization of dual function vanadyl, gallium and indium curcumin complexes for medicinal applications. *Journal of Inorganic Biochemistry* 99(11): 2217–2225.

Mohan PRK, Sreelakshmi G, Muraleedharan CV, et al. (2012) Water soluble complexes of curcumin with cyclodextrins: Characterization by FT-Raman spectroscopy. *Vibrational Spectroscopy* 62: 77–84.

Mohanty S, Mishra S, Jena P, et al. (2012) An investigation on the antibacterial, cytotoxic, and antibiofilm efficacy of starch-stabilized silver nanoparticles. *Nanomedicine: Nanotechnology, Biology, and Medicine* 8(6). Elsevier Inc.: 916–924.

Mondal S and Ghosh S (2012) Role of curcumin on the determination of the critical micellar concentration by absorbance, fluorescence and fluorescence anisotropy techniques. *Journal of Photochemistry and Photobiology B: Biology* 115: 9–15.

Moradali MF and Rehm BHA (2020) Bacterial biopolymers: from pathogenesis to advanced materials. *Nature Reviews. Microbiology* 18(4): 195–210.

Morita Y, Tomida J and Kawamura Y (2014) Responses of Pseudomonas aeruginosa to antimicrobials. *Frontiers in Microbiology* 4. Frontiers.

Morkunas B, Galloway WRJD, Wright M, et al. (2012) Inhibition of the production of the Pseudomonas aeruginosa virulence factor pyocyanin in wild-type cells by quorum sensing autoinducer-mimics. *Organic & Biomolecular Chemistry* 10(42). The Royal Society of Chemistry: 8452–8464.

Moskowitz SM, Foster JM, Emerson J, et al. (2004) Clinically Feasible Biofilm Susceptibility Assay for Isolates of Pseudomonas aeruginosa from Patients with Cystic Fibrosis. *Journal of Clinical Microbiology* 42(5). American Society for Microbiology: 1915–1922.

Mounce BC, Cesaro T, Carrau L, et al. (2017) Curcumin inhibits Zika and chikungunya virus infection by inhibiting cell binding. *Antiviral Research* 142: 148–157.

Mu H, Tang J, Liu Q, et al. (2016) Potent Antibacterial Nanoparticles against Biofilm and Intracellular Bacteria. *Scientific Reports* 6(1). 1. Nature Publishing Group: 18877.

Muddassir M, Raza A, Munir S, et al. (2022) Antibacterial efficacy of silver nanoparticles (AgNPs) against metallo-β-lactamase and extended spectrum β-lactamase producing

clinically procured isolates of Pseudomonas aeruginosa. *Scientific Reports* 12(1). Nature Publishing Group: 20685.

Mühlen S and Dersch P (2016) Anti-virulence Strategies to Target Bacterial Infections. In: Stadler M and Dersch P (eds) *How to Overcome the Antibiotic Crisis : Facts, Challenges, Technologies and Future Perspectives*. Current Topics in Microbiology and Immunology. Cham: Springer International Publishing, pp. 147–183. Available at: https://doi.org/10.1007/82_2015_490 (accessed 13 December 2023).

Mukerjee A and Vishwanatha JK (2009) Formulation, Characterization and Evaluation of Curcumin-loaded PLGA Nanospheres for Cancer Therapy. *Anticancer Research* 29(10): 3867–3875.

Mukherjee S and Bassler BL (2019) Bacterial quorum sensing in complex and dynamically changing environments. *Nature Reviews. Microbiology* 17(6): 371–382.

Mun S-H, Joung D-K, Kim Y-S, et al. (2013) Synergistic antibacterial effect of curcumin against methicillin-resistant Staphylococcus aureus. *Phytomedicine* 20(8–9): 714–718.

Münchberg U, Rösch P, Bauer M, et al. (2014) Raman spectroscopic identification of single bacterial cells under antibiotic influence. *Analytical and Bioanalytical Chemistry* 406(13): 3041–3050.

Munita JM and Arias CA (2016) Mechanisms of Antibiotic Resistance. In: *Virulence Mechanisms of Bacterial Pathogens*. John Wiley & Sons, Ltd, pp. 481–511. Available at: https://onlinelibrary.wiley.com/doi/abs/10.1128/9781555819286.ch17 (accessed 12 August 2020).

Murray CJ, Ikuta KS, Sharara F, et al. (2022) Global burden of bacterial antimicrobial resistance in 2019: a systematic analysis. *The Lancet* 399(10325). Elsevier: 629–655.

Nanda SS, Yi DK and Kim K (2016) Study of antibacterial mechanism of graphene oxide using Raman spectroscopy. *Scientific Reports* 6(1). 1. Nature Publishing Group: 1–12.

Natan M and Banin E (2017) From Nano to Micro: using nanotechnology to combat microorganisms and their multidrug resistance. *FEMS Microbiology Reviews* 41(3): 302–322.

Neal AL (2008) What can be inferred from bacterium–nanoparticle interactions about the potential consequences of environmental exposure to nanoparticles? *Ecotoxicology* 17(5): 362–371.

Negi PS, Jayaprakasha GK, Jagan Mohan Rao L, et al. (1999) Antibacterial Activity of Turmeric Oil: A Byproduct from Curcumin Manufacture. *Journal of Agricultural and Food Chemistry* 47(10): 4297–4300.

Nguyen D, Joshi-Datar A, Lepine F, et al. (2011) Active starvation responses mediate antibiotic tolerance in biofilms and nutrient-limited bacteria. *Science (New York, N.Y.)* 334(6058): 982–986.

Nguyen TA, Tang QD, Doan DCT, et al. (2016) Micro and nano liposome vesicles containing curcumin for a drug delivery system. *Advances in Natural Sciences: Nanoscience and Nanotechnology* 7(3). IOP Publishing: 035003.

Niu B and Zhang G (2023) Effects of Different Nanoparticles on Microbes. *Microorganisms* 11(3). 3. Multidisciplinary Digital Publishing Institute: 542.

Norizan SNM, Yin W-F and Chan K-G (2013) Caffeine as a Potential Quorum Sensing Inhibitor. *Sensors* 13(4). 4. Multidisciplinary Digital Publishing Institute: 5117–5129.

Oliveira F, Giana H and Silveira L (2012) Discrimination of selected species of pathogenic bacteria using near-infrared Raman spectroscopy and Principal Components Analysis. *Journal of biomedical optics* 17: 107004.

Omwenga EO, Hensel A, Shitandi A, et al. (2018) Chitosan nanoencapsulation of flavonoids enhances their quorum sensing and biofilm formation inhibitory activities against an E.coli Top 10 biosensor. *Colloids and Surfaces. B, Biointerfaces* 164: 125–133.

O'Toole GA and Kolter R (1998) Flagellar and twitching motility are necessary for Pseudomonas aeruginosa biofilm development. *Molecular Microbiology* 30(2): 295–304.

Ozdal M and Gurkok S (2022) Recent advances in nanoparticles as antibacterial agent. *ADMET & DMPK* 10(2): 115–129.

Palanisamy G, Lee J-H and Lee J (2023) Curcumin-loaded hydroxyapatite nanoparticles for enriched removal of organic pollutants and inhibition of dual-species biofilm formation. *Environmental Technology & Innovation* 32: 103364.

Palermo EF and Kuroda K (2010) Structural determinants of antimicrobial activity in polymers which mimic host defense peptides. *Applied Microbiology and Biotechnology* 87(5): 1605–1615.

Pamp SJ, Gjermansen M, Johansen HK, et al. (2008) Tolerance to the antimicrobial peptide colistin in Pseudomonas aeruginosa biofilms is linked to metabolically active cells, and depends on the pmr and mexAB-oprM genes. *Molecular Microbiology* 68(1): 223–240.

Pandit RS, Gaikwad SC, Agarkar GA, et al. (2015) Curcumin nanoparticles: physico-chemical fabrication and its in vitro efficacy against human pathogens. *3 Biotech* 5(6): 991–997.

Pang Z, Raudonis R, Glick BR, et al. (2019) Antibiotic resistance in *Pseudomonas aeruginosa*: mechanisms and alternative therapeutic strategies. *Biotechnology Advances* 37(1): 177–192.

Polisetti S, Baig NF, Morales-Soto N, et al. (2017) Spatial Mapping of Pyocyanin in Pseudomonas aeruginosa Bacterial Communities by Surface Enhanced Raman Scattering. *Applied spectroscopy* 71(2): 215–223.

Poole K (2005) Aminoglycoside resistance in Pseudomonas aeruginosa. *Antimicrobial Agents and Chemotherapy* 49(2): 479–487.

Poonsuk K, Tribuddharat C and Chuanchuen R (2014) Simultaneous overexpression of multidrug efflux pumps in Pseudomonas aeruginosa non-cystic fibrosis clinical isolates. *Canadian Journal of Microbiology* 60(7): 437–443.

Prateeksha, Rao CV, Das AK, et al. (2019) ZnO/Curcumin Nanocomposites for Enhanced Inhibition of Pseudomonas aeruginosa Virulence via LasR-RhlR Quorum Sensing Systems. *Molecular Pharmaceutics* 16(8). American Chemical Society: 3399–3413.

Priyadarsini KI (2014a) The Chemistry of Curcumin: From Extraction to Therapeutic Agent. *Molecules* 19(12): 20091–20112.

Priyadarsini KI (2014b) The chemistry of curcumin: From extraction to therapeutic agent. *Molecules* 19(12): 20091–20112.

Qin X, Emerson J, Stapp J, et al. (2003) Use of Real-Time PCR with Multiple Targets To Identify Pseudomonas aeruginosa and Other Nonfermenting Gram-Negative Bacilli from Patients with Cystic Fibrosis. *Journal of Clinical Microbiology* 41(9): 4312–4317.

Rai D, Singh JK, Roy N, et al. (2008) Curcumin inhibits FtsZ assembly: an attractive mechanism for its antibacterial activity. *Biochemical Journal* 410(1): 147–155.

Rajasekar A and Devasena. T (2015) Facile Synthesis of Curcumin Nanocrystals and Validation of Its Antioxidant Activity Against Circulatory Toxicity in Wistar Rats. *Journal of Nanoscience and Nanotechnology* 15(6): 4119–4125.

Ramalingam P and Ko YT (2014) A validated LC-MS/MS method for quantitative analysis of curcumin in mouse plasma and brain tissue and its application in pharmacokinetic and brain distribution studies. *Journal of Chromatography. B, Analytical Technologies in the Biomedical and Life Sciences* 969: 101–108.

Reygaert WC (2018) An overview of the antimicrobial resistance mechanisms of bacteria. *AIMS Microbiology* 4(3): 482–501.

Reymond J-L, Bergmann M and Darbre T (2013) Glycopeptide dendrimers as Pseudomonas aeruginosa biofilm inhibitors. *Chemical Society Reviews* 42(11). The Royal Society of Chemistry: 4814–4822.

Reynolds D and Kollef M (2021) The Epidemiology and Pathogenesis and Treatment of Pseudomonas aeruginosa Infections: An Update. *Drugs* 81(18): 2117–2131.

Ribeiro M, Monteiro FJ and Ferraz MP (2012) Infection of orthopedic implants with emphasis on bacterial adhesion process and techniques used in studying bacterial-material interactions. *Biomatter* 2(4): 176–194.

Rizzello L and Pompa PP (2014) Nanosilver-based antibacterial drugs and devices: Mechanisms, methodological drawbacks, and guidelines. *Chemical Society Reviews* 43(5). The Royal Society of Chemistry: 1501–1518.

Rollet C, Gal L and Guzzo J (2009) Biofilm-detached cells, a transition from a sessile to a planktonic phenotype: a comparative study of adhesion and physiological characteristics in Pseudomonas aeruginosa. *FEMS microbiology letters* 290(2): 135–142.

Roudashti S, Zeighami H, Mirshahabi H, et al. (2017) Synergistic activity of sub-inhibitory concentrations of curcumin with ceftazidime and ciprofloxacin against Pseudomonas aeruginosa quorum sensing related genes and virulence traits. *World Journal of Microbiology and Biotechnology* 33(3): 50.

Rudrappa T and Bais HP (2008) Curcumin, a Known Phenolic from Curcuma longa, Attenuates the Virulence of Pseudomonas aeruginosa PAO1 in Whole Plant and Animal Pathogenicity Models. *Journal of Agricultural and Food Chemistry* 56(6). American Chemical Society: 1955–1962.

Ryder C, Byrd M and Wozniak DJ (2007) Role of polysaccharides in Pseudomonas aeruginosa biofilm development. *Current opinion in microbiology* 10(6): 644–648.

Rzhepishevska O, Ekstrand-Hammarström B, Popp M, et al. (2011) The antibacterial activity of Ga3+ is influenced by ligand complexation as well as the bacterial carbon source. *Antimicrobial Agents and Chemotherapy* 55(12): 5568–5580.

Sandoval-Motta S and Aldana M (2016) Adaptive resistance to antibiotics in bacteria: a systems biology perspective. *Wiley Interdisciplinary Reviews. Systems Biology and Medicine* 8(3): 253–267.

Sandt C, Smith-Palmer T, Pink J, et al. (2007) Confocal Raman microspectroscopy as a tool for studying the chemical heterogeneities of biofilms in situ. *Journal of Applied Microbiology* 103(5): 1808–1820.

Santos CA, Lima EMF, Franco BDG de M, et al. (2021) Exploring Phenolic Compounds as Quorum Sensing Inhibitors in Foodborne Bacteria. *Frontiers in Microbiology* 12.

Sethupathy S, Prasath KG, Ananthi S, et al. (2016) Proteomic analysis reveals modulation of iron homeostasis and oxidative stress response in Pseudomonas aeruginosa PAO1 by curcumin inhibiting quorum sensing regulated virulence factors and biofilm production. *Journal of Proteomics* 145. Focus on Medical Proteomics and Protein Quantitation: 112–126.

Shariati A, Asadian E, Fallah F, et al. (2019) Evaluation of Nano-curcumin effects on expression levels of virulence genes and biofilm production of multidrug-resistant Pseudomonas

aeruginosa isolated from burn wound infection in Tehran, Iran. *Infection and Drug Resistance* 12: 2223–2235.

Sharifian P, Yaslianifard S, Fallah P, et al. (2020) Investigating the Effect of Nano-Curcumin on the Expression of Biofilm Regulatory Genes of Pseudomonas aeruginosa. *Infection and Drug Resistance* 13: 2477–2484.

Sharifi-Rad J, Rayess YE, Rizk AA, et al. (2020) Turmeric and Its Major Compound Curcumin on Health: Bioactive Effects and Safety Profiles for Food, Pharmaceutical, Biotechnological and Medicinal Applications. *Frontiers in Pharmacology* 11.

Shen H, Rösch P, Pletz MW, et al. (2022) In Vitro Fiber-Probe-Based Identification of Pathogens in Biofilms by Raman Spectroscopy. *Analytical Chemistry* 94(13). American Chemical Society: 5375–5381.

Shlar I, Droby S, Choudhary R, et al. (2017) The mode of antimicrobial action of curcumin depends on the delivery system: monolithic nanoparticles vs. supramolecular inclusion complex. *RSC Advances* 7(67): 42559–42569.

Shukla A, Shukla G, Parmar P, et al. (2021) Exemplifying the next generation of antibiotic susceptibility intensifiers of phytochemicals by LasR-mediated quorum sensing inhibition. *Scientific Reports* 11(1). 1. Nature Publishing Group: 22421.

Sindhu K, Rajaram A, Sreeram KJ, et al. (2014) Curcumin conjugated gold nanoparticle synthesis and its biocompatibility. *RSC Advances* 4(4): 1808–1818.

Soenen SJ, Rivera-Gil P, Montenegro J-M, et al. (2011) Cellular toxicity of inorganic nanoparticles: Common aspects and guidelines for improved nanotoxicity evaluation. *Nano Today* 6(5): 446–465.

Spernovasilis N, Psichogiou M and Poulakou G (2021) Skin manifestations of Pseudomonas aeruginosa infections. *Current Opinion in Infectious Diseases* 34(2): 72.

Srimal RC and Dhawan BN (1973) Pharmacology of diferuloyl methane (curcumin), a non-steroidal anti-inflammatory agent*. *Journal of Pharmacy and Pharmacology* 25(6): 447–452.

Stewart PS (2015) Antimicrobial Tolerance in Biofilms. *Microbiology Spectrum* 3(3). American Society for Microbiology: 10.1128/microbiolspec.mb-0010–2014.

Stewart PS, Zhang T, Xu R, et al. (2016) Reaction–diffusion theory explains hypoxia and heterogeneous growth within microbial biofilms associated with chronic infections. *npj Biofilms and Microbiomes* 2(1). 1. Nature Publishing Group: 1–8.

Taylor PK, Yeung ATY and Hancock REW (2014) Antibiotic resistance in Pseudomonas aeruginosa biofilms: Towards the development of novel anti-biofilm therapies. *Journal of Biotechnology* 191. Special Issue dedicated to Karl-Erich Jaeger on the occasion of his 60th Birthday: 121–130.

Thi MTT, Wibowo D and Rehm BHA (2020) Pseudomonas aeruginosa Biofilms. *International Journal of Molecular Sciences* 21(22): 8671.

Tønnesen HH, Karlsen J and van Henegouwen GB (1986) Studies on curcumin and curcuminoids. VIII. Photochemical stability of curcumin. *Zeitschrift Fur Lebensmittel-Untersuchung Und -Forschung* 183(2): 116–122.

Tseng BS, Zhang W, Harrison JJ, et al. (2013) The extracellular matrix protects Pseudomonas aeruginosa biofilms by limiting the penetration of tobramycin. *Environmental Microbiology* 15(10): 2865–2878.

Tseng S-P, Hsueh P-R, Tsai J-C, et al. (2007) Tn6001, a Transposon-Like Element Containing the blaVIM-3-Harboring Integron In450. *Antimicrobial Agents and Chemotherapy* 51(11): 4187–4190.

Turner KH, Everett J, Trivedi U, et al. (2014) Requirements for Pseudomonas aeruginosa Acute Burn and Chronic Surgical Wound Infection. *PLOS Genetics* 10(7). Public Library of Science: e1004518.

Tyagi P, Singh M, Kumari H, et al. (2015a) Bactericidal activity of curcumin I is associated with damaging of bacterial membrane. *PLoS ONE* 10(3): 1–15.

Tyagi P, Singh M, Kumari H, et al. (2015b) Bactericidal Activity of Curcumin I Is Associated with Damaging of Bacterial Membrane. *PLOS ONE* Zhou D (ed.) 10(3): e0121313.

Vaishampayan A and Grohmann E (2022) Antimicrobials Functioning through ROS-Mediated Mechanisms: Current Insights. *Microorganisms* 10(1). 1. Multidisciplinary Digital Publishing Institute: 61.

Valappil SP, Ready D, Abou Neel EA, et al. (2009) Controlled delivery of antimicrobial gallium ions from phosphate-based glasses. *Acta Biomaterialia* 5(4): 1198–1210.

Ventola CL (2015) The Antibiotic Resistance Crisis. *Pharmacy and Therapeutics* 40(4): 277–283.

Vert M, Doi Y, Hellwich K-H, et al. (2012) Terminology for biorelated polymers and applications (IUPAC Recommendations 2012). *Pure and Applied Chemistry* 84(2): 377–410.

Wagner M, Ivleva NP, Haisch C, et al. (2009) Combined use of confocal laser scanning microscopy (CLSM) and Raman microscopy (RM): Investigations on EPS – Matrix. *Water Research* 43(1): 63–76.

Walters MC, Roe F, Bugnicourt A, et al. (2003) Contributions of antibiotic penetration, oxygen limitation, and low metabolic activity to tolerance of Pseudomonas aeruginosa biofilms to ciprofloxacin and tobramycin. *Antimicrobial Agents and Chemotherapy* 47(1): 317–323.

Wang L, Hu C and Shao L (2017) The antimicrobial activity of nanoparticles: present situation and prospects for the future. *International Journal of Nanomedicine* 12: 1227–1249.

Wang Y-J, Pan M-H, Cheng A-L, et al. (1997a) Stability of curcumin in buffer solutions and characterization of its degradation products. *Journal of Pharmaceutical and Biomedical Analysis* 15(12): 1867–1876.

Wang Y-J, Pan M-H, Cheng A-L, et al. (1997b) Stability of curcumin in buffer solutions and characterization of its degradation products. *Journal of Pharmaceutical and Biomedical Analysis* 15(12): 1867–1876.

Warrell RP, Skelos A, Alcock NW, et al. (1986) Gallium Nitrate for Acute Treatment of Cancer-related Hypercalcemia: Clinicopharmacological and Dose Response Analysis. *Cancer Research* 46(8): 4208–4212.

Wichitnithad W, Jongaroonngamsang N, Pummangura S, et al. (2009) A simple isocratic HPLC method for the simultaneous determination of curcuminoids in commercial turmeric extracts. *Phytochemical Analysis* 20(4): 314–319.

Williamson KS, Richards LA, Perez-Osorio AC, et al. (2012) Heterogeneity in Pseudomonas aeruginosa biofilms includes expression of ribosome hibernation factors in the antibiotic-tolerant subpopulation and hypoxia-induced stress response in the metabolically active population. *Journal of Bacteriology* 194(8): 2062–2073.

Wilton M, Charron-Mazenod L, Moore R, et al. (2015) Extracellular DNA Acidifies Biofilms and Induces Aminoglycoside Resistance in Pseudomonas aeruginosa. *Antimicrobial Agents and Chemotherapy* 60(1): 544–553.

Wilton M, Wong MJQ, Tang L, et al. (2016) Chelation of Membrane-Bound Cations by Extracellular DNA Activates the Type VI Secretion System in Pseudomonas aeruginosa. *Infection and Immunity* 84(8): 2355–2361.

Wolter DJ and Lister PD (2013) Mechanisms of β-lactam resistance among Pseudomonas aeruginosa. *Current Pharmaceutical Design* 19(2): 209–222.

Wolter DJ, Hanson ND and Lister PD (2004) Insertional inactivation of oprD in clinical isolates of Pseudomonas aeruginosa leading to carbapenem resistance. *FEMS Microbiology Letters* 236(1): 137–143.

Xu Z, Zhao X, Chen X, et al. (2017) Antimicrobial effect of gallium nitrate against bacteria encountered in burn wound infections. *RSC Advances* 7(82): 52266–52273.

Yang L, Hu Y, Liu Y, et al. (2011) Distinct roles of extracellular polymeric substances in Pseudomonas aeruginosa biofilm development. *Environmental Microbiology* 13(7): 1705–1717.

Yang XX, Li CM and Huang CZ (2016) Curcumin modified silver nanoparticles for highly efficient inhibition of respiratory syncytial virus infection. *Nanoscale* 8(5): 3040–3048.

Yu Z, Li Q, Wang J, et al. (2020) Reactive Oxygen Species-Related Nanoparticle Toxicity in the Biomedical Field. *Nanoscale Research Letters* 15(1): 115.

Yun DG and Lee DG (2016) Antibacterial activity of curcumin via apoptosis-like response in Escherichia coli. *Applied Microbiology and Biotechnology* 100(12): 5505–5514.

Zandi K, Ramedani E, Mohammadi K, et al. (2010) Evaluation of antiviral activities of curcumin derivatives against HSV-1 in Vero cell line. *Natural Product Communications* 5(12): 1935–1938.

Zebib B, Mouloungui Z and Noirot V (2010) Stabilization of Curcumin by Complexation with Divalent Cations in Glycerol/Water System. Available at: https://www.hindawi.com/journals/bca/2010/292760/abs/ (accessed 9 January 2019).

Zhang L, Fiala M, Cashman J, et al. (2006) Curcuminoids enhance amyloid-β uptake by macrophages of Alzheimer's disease patients. *Journal of Alzheimer's Disease* 10(1): 1–7.

Zheng D, Huang C, Huang H, et al. (2020) Antibacterial Mechanism of Curcumin: A Review. *Chemistry & Biodiversity* 17(8).

LIST OF PUBLICATIONS

1. Ramesh, G.; Kaviyil, J. E.; Paul, W.; Sasi, R.; Joseph, R. Gallium–Curcumin Nanoparticle Conjugates as an Antibacterial Agent against Pseudomonas aeruginosa: Synthesis and Characterization. *ACS Omega* **2022**. https://doi.org/10.1021/acsomega.1c06398. (IF: 4.1)

2. Ramesh, G.; Paul, W.; Valparambil Puthanveetil, V.; Raja, K.; Embekkat Kaviyil, J. Raman Spectroscopy as a Novel Technique for the Identification of Pathogens in a Clinical Microbiology Laboratory. *Spectroscopy Letters*, **2022**, 55(8), 546-551. https://doi.org/10.1080/00387010.2022.2120899. (IF: 1.7)

Manuscript Under Preparation

Gopika Ramesh, Jyothi E.K.,Willi Paul, Roy Joseph. Exploring curcumin nanoparticles as biofilm inhibitors: Insights into *P. aeruginosa* Biofilm Inhibition.

CONFERENCES PRESENTATIONS & PROCEEDINGS

Poster Presentations

1. **Gopika Ramesh**, Willi Paul, Roy Joseph. 'Nanoparticle formulation of curcumin with gallium: for improved solubility and stability of curcumin: synthesis and characterization'. Poster presented at **'Nanobiotek- 2018'** held from October 25- 27, 2018 at All India

Institute of Medical Sciences, New Delhi, organized by the Department of Science and Technology.

2. Jyothi E.K., **Gopika Ramesh**, Willi Paul, Kavita Raja. 'Raman spectroscopy as a tool for diagnosis of *Acinetobacter baumannii'.* E- poster presented at the 30th European Congress on Clinical Microbiology and Infectious Diseases held from April 18-21, 2020 in Paris, France.

3. Jyothi E.K., **Gopika Ramesh**, Willi Paul, Vishal Valparambil, Kavita Raja, Roy Joseph. 'Evaluation of antibacterial properties of a novel nanoparticle conjugate against *Pseudomonas aeruginosa*'. Poster presented at 33rd European Congress on Clinical Microbiology and Infectious Diseases held from April 15- 18, 2023 in Copenhagen, Denmark.

Oral Presentation

1. **Gopika Ramesh**, Jyothi E.K., Willi Paul, Roy Joseph. 'A novel nanoparticle conjugate as an antibacterial agent against *Pseudomonas aeruginosa*'. Paper presented at the International Conference on Biomaterials, Regenerative Medicine and Devices (BioRemedi 2022) held at Indian Institute of Technology Guwahati from December 14-18, 2022.

CURRICULUM VITAE

Gopika Ramesh
M.Sc. Biochemistry and Molecular Biology
Central University of Kerala

Email: gopikaramesh26@gmail.com
Contact: +91 9995160394
Date of birth: August 24, 1991
Nationality: Indian

EDUCATION

2014	M.Sc. Biochemistry and Molecular Biology	Central University of Kerala, India	8.81 CGPA
2012	B.Sc. Industrial Microbiology and Biochemistry	University of Kerala, India	90.7%
2009	All India Senior School Certificate Examination	Central Board of Secondary Education	80%
2007	All India Secondary School Examination	Central Board of Secondary Education	90%

HONOURS

1. Recipient of INSPIRE Fellowship - Department of Science and Technology, Government of India.
2. Qualified and secured All India Rank - 610 for Graduate Aptitude Test in Engineering (GATE) in Life Sciences,2014 - 2015 (Reg no: XL11055S1020).
3. Recipient of Kerala State Council for Science, Technology and Environment (KSCSTE) Research Fellowship in 2015.
4. Awarded University 1st Rank for M.Sc. Biochemistry and Molecular Biology, Central University of Kerala, India (2012 - 2014) on July 18, 2015.

AREAS OF RESEARCH EXPERIENCE

1. **Cell biology:** Cancer cell biology, Adipogenesis (3T3 - L1 Cell biology)
2. **Molecular Biology:** Gene Cloning
3. **Microbiology**: Bacteriology
4. **Material Chemistry**: Synthesis and Characterization (Nanoparticles)

SKILLS AND TECHNIQUES

1. **Animal Cell Culture:** Maintenance of adherent cell lines, Cytotoxicity assays, Maintenance and Differentiation of 3T3 - L1 cell line.
2. **Molecular Biology:** PCR, RT - PCR, Agarose gel electrophoresis, SDS - PAGE, Western blotting.
3. **Analytical Techniques:** Thin - layer Chromatography, FAME Preparation, RP-HPLC.
4. **Material chemistry:** Nanoparticle synthesis and characterization by various spectroscopic techniques like FT-IR spectroscopy, Raman spectroscopy, and X - ray photoelectron spectroscopy.
5. **Microbiology:** Bacteriology, Microbroth dilution assay, anti-bacterial assays, preparation of bacterial samples for SEM, use of Raman spectroscopy for the identification of various clinically relevant pathogens, Confocal Raman microscopy in bacteriology.

RESEARCH EXPERIENCE

1. Research intern at CSIR - CFTRI, Mysore from **May 2015 - July 2016** (Supervisor: Dr. Ajay Tumaney)

2. Ph.D. scholar at Sree Chitra Tirunal Institute for Medical Sciences and Technology, Trivandrum, India, from **January 2017 - till date**.

PUBLICATIONS

1. **Ramesh, G**.; Kaviyil, J. E.; Paul, W.; Sasi, R.; Joseph, R. Gallium–Curcumin Nanoparticle Conjugates as an Antibacterial Agent against Pseudomonas Aeruginosa: Synthesis and Characterization. ACS Omega 2022, 7(8), 6795–6809. https://doi.org/10.1021/acsomega.1c06398

2. **Ramesh, G.;** Paul, W.; Valparambil Puthanveetil, V.; Raja, K.; Embekkat Kaviyil, J. Raman Spectroscopy as a Novel Technique for the Identification of Pathogens in a Clinical Microbiology Laboratory. *Spectroscopy Letters*, 2022, 55(8), 546-551. https://doi.org/10.1080/00387010.2022.2120899

3. Renjith S., S. L. Sreejith, **Gopika Ramesh**, D. R. Sherin, Jyothi E.K., Willi Paul, Roy Joseph., Ionic liquid-based antimicrobial coating on polymeric surface: A green chemistry approach, Results in Surfaces and Interfaces, 2021, 5, 100026. https://doi.org/10.1016/j.rsurfi.2021.1000266

4. 'Slow-growing and biofilm-producing *Pseudomonas aeruginosa* causing cardiac implantable electronic device (CIED) associated infective endocarditis' (Jyothi Embekkat KaviyiL, Dinoop Korol Ponnambath, Narayanan Namboothiri, **Gopika Ramesh**, Anjali Sethumadhavan, Kavita Raja) – manuscript accepted in Malaysian Journal of Microbiology.

CONFERENCE PAPERS

1. **Gopika Ramesh**, Jyothi E.K., Willi Paul, Roy Joseph. 'A novel nanoparticle conjugate as an antibacterial agent against *Pseudomonas aeruginosa*'. Paper presented at the International Conference on Biomaterials, Regenerative Medicine and Devices (BioRemedi 2022) held at Indian Institute of Technology Guwahati from December 14-18, 2022.

2. **Gopika Ramesh**, Willi Paul, Roy Joseph. 'Nanoparticle formulation of curcumin with gallium: for improved solubility and stability of curcumin: synthesis and characterization'. Poster presented at **'Nanobiotek- 2018'** held from October 25- 27, 2018 at All India Institute of Medical Sciences, New Delhi, organized by the Department of Science and Technology.

3. Jyothi E.K., **Gopika Ramesh**, Willi Paul, Kavita Raja. 'Raman spectroscopy as a tool for diagnosis of *Acinetobacter baumannii'.* E- poster presented at the 30th European Congress on Clinical Microbiology and Infectious Diseases held from April 18-21, 2020 in Paris, France.

4. Jyothi E.K., **Gopika Ramesh**, Willi Paul, Vishal Valparambil, Kavita Raja, Roy Joseph. 'Evaluation of antibacterial properties of a novel nanoparticle conjugate against *Pseudomonas aeruginosa*'. Poster presented at 33rd European Congress on Clinical Microbiology and Infectious Diseases held from April 15-18, 2023 in Copenhagen, Denmark.

5. Jyothi E.K., Renjith S, **Gopika Ramesh**, Willi Paul, Kavita Raja**.** 'Evaluation of antibacterial properties of ionic liquid against *E.coli.* Poster presentation at 34th European Congress on clinical microbiology and Infectious diseases **held** from April 27-30, 2024 in Barcelona, Spain.

APPENDIX A

SWARMING MOTILITY AGAR, 100 mL

Glucose	1g
Peptone	0.5 g
Yeast extract	0.2 g
Agar	0.5 g

Added distilled water to a final volume of 100 mL and autoclaved at 121°C, 15 lbs. The agar medium was poured into 90 mm petriplates in molten form.

PBS (1000 mL) pH 7.4

NaCl	8 g
KCl	0.2 g
Na_2HPO_4	1.44 g
KH_2PO_4	0.24g

Added distilled water to a final volume of 1000 mL, the solution is filtered and stored at room temperature.

APPENDIX B

PLAGIARISM REPORT

DrillBit

The Report is Generated by DrillBit Plagiarism Detection Software

Submission Information

Author Name	Gopika Ramesh
Title	Ms.
Paper/Submission ID	1683470
Submitted by	rjoseph@sctimst.ac.in
Submission Date	2024-04-22 23:44:55
Total Pages	118
Document type	Thesis

Result Information

Similarity 7 %

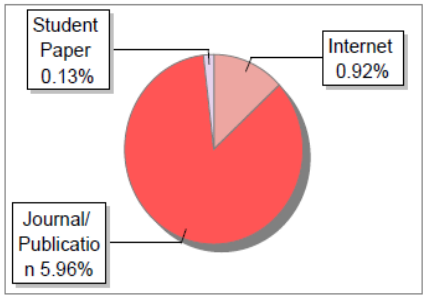

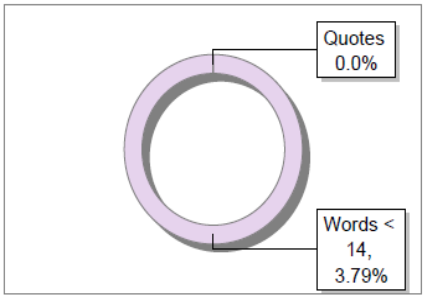

Exclude Information

Quotes	Excluded
References/Bibliography	Excluded
Sources: Less than 14 Words %	Excluded
Excluded Source	0 %
Excluded Phrases	Excluded

Database Selection

Language	English
Student Papers	Yes
Journals & publishers	Yes
Internet or Web	Yes
Institution Repository	Yes

A Unique QR Code use to View/Download/Share Pdf File